Characterization of the Material Properties of Rolled Sections

by

Timothy Kyle Jaquess, B.S.C.E.

Thesis

Presented to the Faculty of the Graduate School of

The University of Texas at Austin

in Partial Fulfillment

of the Requirements

for the Degree of

Master of Science in Engineering

The University of Texas at Austin

December 1998

Characterization of the Material Properties of Rolled Sections

Approved by
Supervising Committee:

Supervisor: Karl H. Frank

Joseph A. Yura

Acknowledgements

Thanks go out to Wayne Fontenot, Mike Bell, Ray Madonna, Blake Stasney, and the rest of the staff at FSEL. Thanks also to Ken Miller, without whom I would still be sitting in front of the milling machine.

And to Mom & Dad: Thank you for everything

September 24, 1998

Abstract

Characterization of the Material Properties of Rolled Sections

Timothy Kyle Jaquess, M.S.E.

The University of Texas at Austin, 1998

Supervisor: Karl H. Frank

Over the last ten years, tremendous changes have occurred in the production methods of rolled structural-steel shapes. This study characterizes the geometric properties, tensile properties, toughness properties, and chemical composition of a set of 17 wide-flange members from four different steel mills that employ modern production methods. These material properties can be used in design and research to model the behavior of structural members. A typical stress-strain curve was calculated, based on the results from the tension testing program. Results show that the yield strength of a flange in a typical wide-flange shape is generally about 95% of the yield strength given in the mill test report.

Table of Contents

List of Tables

List of Figures

Chapter 1: Project Overview

Tremendous changes have occurred in the manufacturing process of rolled structural steel shapes over the past 10 years. Practically every steel mill in the world has made the transition from ingot-casting to continuous casting. In a continuous casting process, the molds are open-ended, allowing the steel to pass directly through the molds in near net shape blooms, whereas the ingot-casting process requires the producers to strip the molds and reheat the ingots before they can be rolled into blooms. Also, most mills have switched completely from an iron ore-based production to using all recycled material. In addition to being a cheaper, more environmentally friendly method of steel production, it produces cleaner steel in terms of the amount of micro-alloys and carbon present.

While these changes in the steel industry have greatly lowered production costs and improved mill efficiency, they have introduced a slightly different chemical composition to the steel. Since scrap automobiles and large appliances are often used in the recycling process, metallic impurities such as copper, lead, tin are more abundant in modern steel than in traditional steel. It is not certain to what extent these metals affect the material properties of the rolled sections. Currently, the ASTM requirements for A36 and A572 Gr. 50 steels do not place limits on the amounts of these elements.

This report characterizes the basic geometric and material properties of modern structural steel rolled sections in an effort to aid in the development of connection and element design procedures. Seventeen wide-flange sections from

shape producers in the U.S., Great Britain, and Luxembourg were used in this project. Many of the sections were rotarized during the milling process, typical of sections used in construction. Table 1.1.1 lists the shape and producer of each rolled section, and includes the labeling convention used in this project to designate specific members.

Table 1.1.1 Shapes and Producers Used in Project

Shape	Mill C	Mill N	Mill B	Mill T
W24x62	C1	N1		
W24x162				T1
W30x211		N2		T2
W36x300		N3	B3	T3
W14x211		N4	B1	T4
W36x150		N5	B4	T5
W14x311		N6	B2	T6

The cross-sectional dimensions of member depth (d), flange width (b_f), flange thickness (t_f), and web thickness (t_w) were measured at various locations in all members. Figure 1.1.1 shows the approximate locations of each of the measurements. A complete tabulation of the data is given in Appendix A.

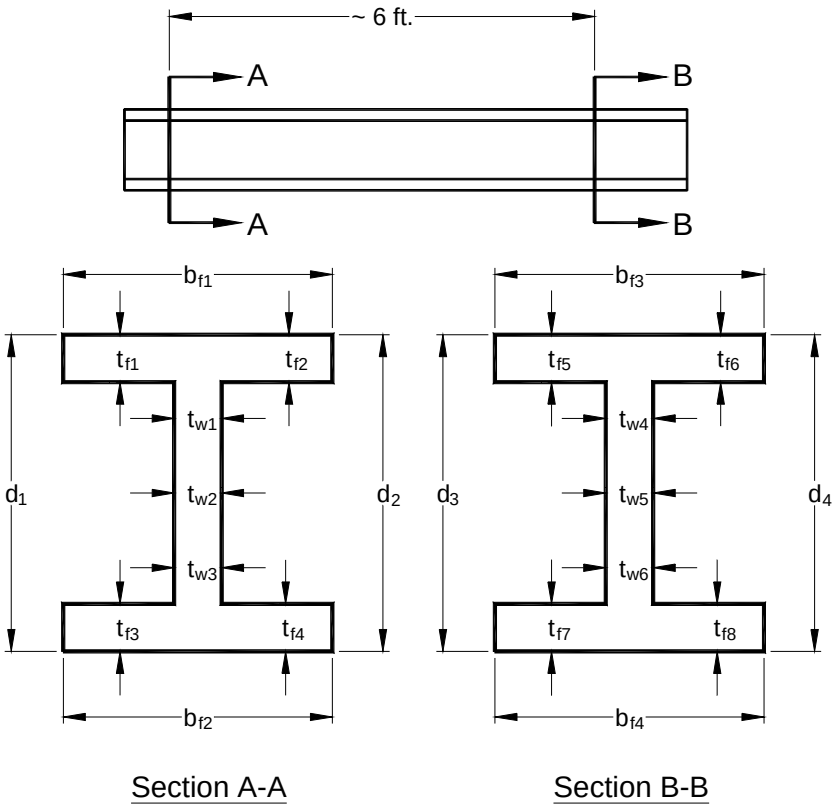

Figure 1.1.1 Locations of Cross-sectional Measurements

In Chapter 2, these measurements are compared to the specified values in ASTM A6 and JIS G3136, the Japanese Industrial Standard. The effect of dimensional variation on flexural behavior is also discussed.

A total of 106 tension tests were performed on coupons taken from the flanges and webs of the members. Figure 1.1.2 shows the location and member from which each coupon was taken. The figure to the right of the table illustrates

the labeling scheme used. The drawings in Appendix B show precisely where on each member the coupons were taken.

	Flange				Web		
	A	B	C	D	E	F	G
C1	X	X	X	X	X	X	X
N1	X	X	X	X	X	X	X
N2	X	X	X	X	X	X	X
N3		X		X		X	
N4		X		X		X	
N5	X	X*	X	X		X	
N6		X		X		X	
B1	X	X	X	X	X	X	X
B2	X	X	X	X	X	X	X
B3	X	X	X	X	X	X	X
B4	X	X	X	X	X	X	X
T1	X	X	X	X	X	X	X
T2	X	X	X	X	X	X	X
T3	X	X	X	X	X	X	X
T4	X	X	X	X	X	X	X
T5	X	X	X	X	X	X	X
T6	X	X	X	X	X	X	X

* = 2 Coupons tested at this location

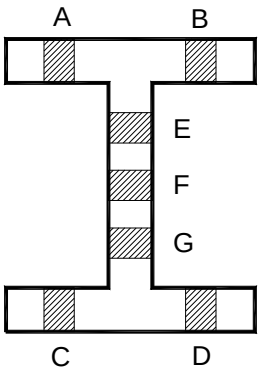

Tension Coupon Layout

Figure 1.1.2 Locations and Producers of Tensile Coupons

Chapter 3 documents the guidelines followed in the tension testing procedure, and Chapter 4 presents the results. These values are compared with the minimum yield strength, tensile strength, and total elongation requirements in ASTM A572 Gr. 50. Based on the test data, typical values of the parameters along the stress-strain curve are calculated, and the effects of different testing variables on these

parameters are discussed. Stress-strain curves for each coupon can be found in Appendix C.

Toughness tests were performed with Charpy V-notch specimens taken from the flanges, webs, and core regions. For each member, sixteen Charpy specimens were taken from the flanges (four from each flange) and eight from the core regions (four from each web-flange junction). Where the web thickness was adequate (>0.50 inches), six specimens were taken from the web. Figure 1.1.3 shows the locations of the Charpy specimens taken from each member. As can be seen, web Charpy specimens were taken from every section except C1 and N1. The exact locations of these specimens relative to the cross section are shown in Appendix B.

	Flange	Web	Core
C1	X		X
N1	X		X
N2	X	X	X
N3	X	X	X
N4	X	X	X
N5	X	X	X
N6	X	X	X
B1	X	X	X
B2	X	X	X
B3	X	X	X
B4	X	X	X
T1	X	X	X
T2	X	X	X
T3	X	X	X
T4	X	X	X
T5	X	X	X
T6	X	X	X

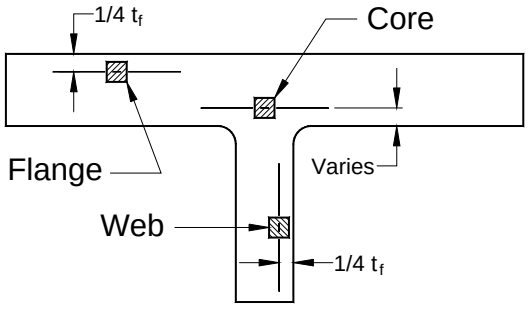

Charpy Specimen Layout

Figure 1.1.3 Locations of Charpy Specimens

Chapters 5 and 6 present the toughness testing procedure and document the results. The specimens were tested over a wide temperature range to capture the brittle-to-ductile transition region. Graphs of the Energy vs. Temperature relationship for the flange, web, and core regions of each member are shown in Appendix D. These graphs also show the exact location of each core region specimen within the web-flange junction.

Chapter 7 lists the chemical composition of each member. The relative amounts of a number of different elements were obtained from an independent testing laboratory. These results are compared with those given by the producers in their mill test reports. The effect of different elements on the toughness behavior is then discussed. Finally, Chapter 8 presents a summary of the results and suggests some areas of possible future research.

1.2 DEFINITIONS AND NOMENCLATURE

1.2.1 Tensile Behavior

All stress and strain values given in this report are engineering stress and strain. True stress is obtained by dividing the load by the cross-sectional area. The difference between engineering stress and true stress is that engineering stress always uses the cross-sectional area at zero load—it does not take into account the change in cross-sectional area due to longitudinal deformation. The equation for engineering stress is given by

$$\sigma = \frac{P}{A_0} \qquad \text{[Eq. 1.1],}$$

where σ is the calculated stress, P is the applied tension load, and A_0 is the original cross-sectional area before loading. Similarly, the calculated strain parameters (ε_{sh}, ε_u) refer to engineering strain, which is given by

$$\varepsilon = \frac{\Delta l}{l_0}, \qquad \text{[Eq. 1.2]}$$

where ε is the calculated strain, Δl is the change in length, and l_0 is the undeformed gage length. Figure 1.2.1 shows a typical tensile stress-strain curve with the labeling conventions used in this report. Brief definitions of each parameter are given in the table below it, followed by a short discussion of the strain-aging concept.

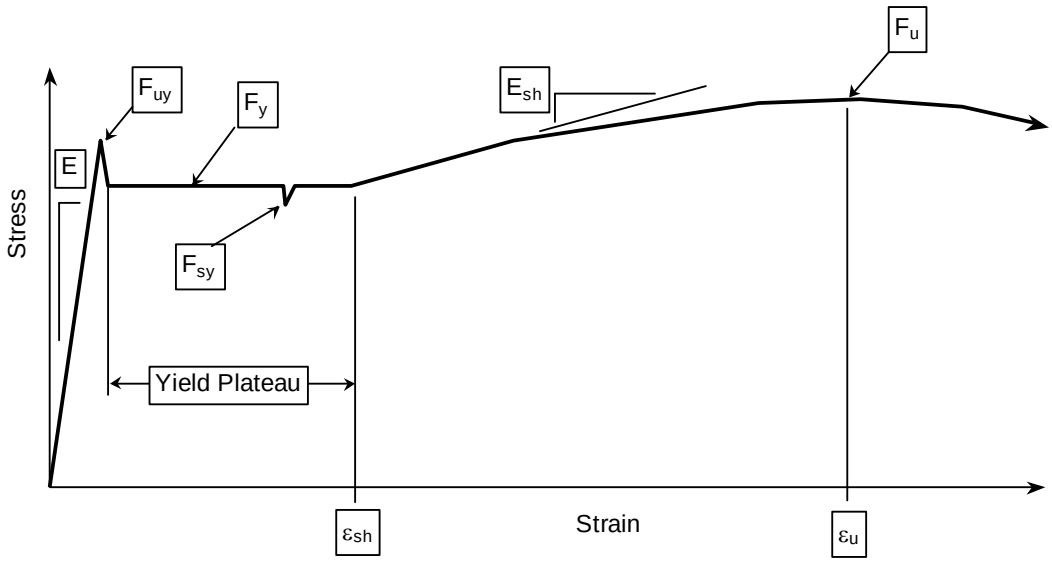

E	Young's modulus of elasticity
F_{uy}	Upper yield point
F_y	Yield strength (Obtained by 0.2% offset method)
F_{sy}	Static yield strength
ε_{sh}	Strain at strain-hardening
E_{sh}	Strain-hardening modulus
F_u	Ultimate strength
ε_u	Strain at ultimate strength

Figure 1.2.1 Typical Stress-Strain Curve for Uniaxial Tension Test

Strain aging occurs when structural steel is loaded into the strain-hardening region, then completely unloaded and allowed to age for several days [Barsom and Korvink, 1998.] It has the effect of increasing yield strength, increasing the tensile strength, and decreasing the ductility at fracture. Wide-flange shapes often experience high stresses and subsequent strain-aging during

production, often due to the roller-straightening process used by mills to reduce the camber or sweep of rolled shapes.

1.2.2 Toughness Behavior

Toughness is defined as "a measure of the ability of steel to resist fracture; i.e., to absorb energy [Salmon 1990]," and was measured in this project by results from Charpy V-notch impact tests. A Charpy V-notch specimen is a small rectangular simply-supported bar that has a V-notch at midlength. The bar is fractured by the impact from a swinging pendulum, and the amount of energy absorbed by the specimen is recorded. Strictly speaking, the Charpy V-notch test measures notch-toughness, "the resistance of a metal to the start and propagation of a crack at the base of a standard notch [Salmon]," but for the purposes of this report, its results will be referred to as "toughness values."

From results of the Charpy tests, steel can be classified as having "ductile" or "brittle" behavior. Ductile steel can absorb large amounts of energy before fracture, while brittle material fractures at low energy levels. Ductile material behavior is vital to structural connection and element design.

Steel toughness is known to increase with increasing temperature. Figure 1.2.2 shows the trend of a typical Energy vs. Temperature transition curve for a set of Charpy specimens.

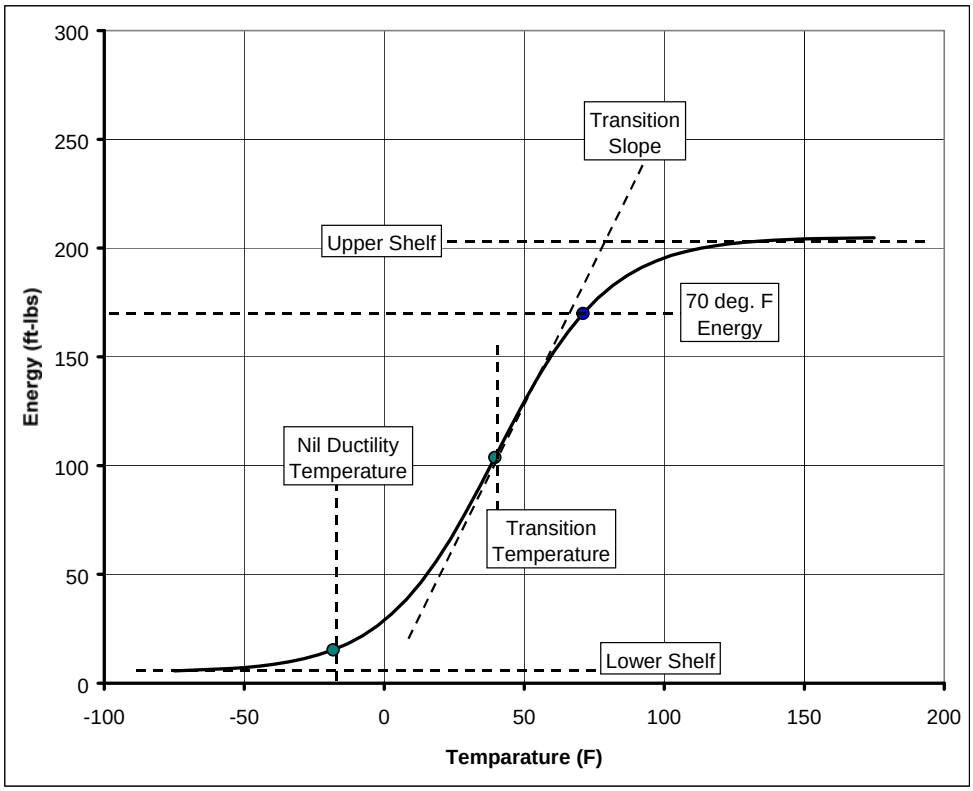

Figure 1.2.2 Typical Energy vs. Temperature Transition Curve

The Upper and Lower Shelves are approximate maximum and minimum energy levels reached by the material. The Upper Shelf parameter is a function of the geometry of the Charpy specimen as well as the toughness of the steel. Theoretically, the amount of energy absorbed would continue to rise with temperature if physical limits due to the size of the specimen were not present. The Lower Shelf is typically around 2 ft-lbs.

The 70°F energy is simply the recorded energy of a specimen tested at 70°F. AISC specifies a minimum 70°F energy of 15 ft-lbs [AISC A3.1c] for Group 4 and 5 rolled shapes used as tension members. The Nil Ductility

Temperature is defined as the temperature at which the Energy vs. Temperature curve crosses 15 ft-lbs for low strength steels. This parameter is important because it alerts the engineer of the highest temperature at which the material exhibits brittle behavior.

The Transition Temperature is defined as the point of highest slope along the Energy vs. Temperature transition curve. Like the Nil Ductility Temperature, this parameter characterizes the temperature at which the steel exhibits a certain toughness characteristic. The Transition Slope is the maximum slope of the curve (or the slope at the Transition Temperature.) Along with the Upper Shelf, Lower Shelf, and Transition Temperature, it is used as a parameter in the mathematical model of the Energy vs. Temperature transition curve used in this report.

Chapter 2: Dimensions and Geometric Properties

2.1 INTRODUCTION

Dimensions of flange thickness (t_f), web thickness (t_w), member depth (d), and flange width (b_f) were measured for each wide-flange shape. These data were first used to observe the dimensional variations throughout the member, as well as to check against ASTM and Japanese Industrial Standard geometric specifications. Next, section properties based on these measured dimensions were calculated for all members, and compared to nominal values. Finally, the effects of cross-sectional asymmetry on the flexural behavior of the members was discussed.

2.2 MEASUREMENT LOCATIONS AND TECHNIQUE

The member depth (d), flange width (b_f), flange thickness (t_f), and web thickness (t_w) were measured at two locations in each member. Figure 1.1.1 shows the approximate locations of the measurements. The dimensional notation in the figure will be used in the remainder of this chapter to describe the specific location of a measurement. For instance, the top-left flange thickness at Section A-A will be referred to as t_{f1}.

Dimensions for t_f and t_w were obtained with micrometers, accurate to 0.001 inches. The depth and flange width dimensions were obtained using a scale accurate to 1/32 of an inch. The surfaces of the specimens from Mill T showed substantial corrosion. To obtain accurate flange and web thickness dimensions, it was necessary to remove the mill scale with a small hand-held surface grinder. The members were lightly ground at the measurement locations until a smooth surface was present.

2.3 VARIATION OF MEASUREMENT DATA

The table in Appendix A gives a complete listing of all measurement data compiled. In the following sections, the variability of this data is analyzed and observations are made about the consistency of the dimensions throughout the member. Variability along the length of the member is discussed first, followed by a study of the measured variability within individual cross sections.

Conclusions drawn from these two analyses are used to create a model of a typical cross section that reflects the observed dimensional variability.

2.3.1 Variability along Rolling Direction

A comparison was made between cross-sectional measurements at two locations along each member, approximately 6 feet apart, in order to estimate the variability along its length (see Figure 1.1.1). First, the average change in corresponding measurements (t_{f1}-t_{f5}, t_{w1}-t_{w4}, etc.) was calculated. The equation used to calculate the average change of flange thickness is shown in Equation 2.1.

$$Ave.Ch_{tf} = \frac{\left|t_{f1} - t_{f5}\right| + \left|t_{f2} - t_{f6}\right| + \left|t_{f3} - t_{f7}\right| + \left|t_{f4} - t_{f8}\right|}{4} \qquad \text{[Eq. 2.1]}$$

For this calculation, the sign of the change was not considered—only the absolute values of the differences were used to calculate the average change. The relative change was calculated by dividing the average change by the mean value of the dimension. For instance, the relative change of t_f ($\%Ch_{tf}$) was obtained from Equation 2.2:

$$\%Ch_{tf} = \frac{Ave.Ch_{tf}}{(t_{f1} + t_{f2} + t_{f3} + t_{f4} + t_{f5} + t_{f6} + t_{f7} + t_{f8})/8} \qquad \text{[Eq. 2.2]}$$

In Table 2.3.1, relative change (%Ch) will be the parameter used to compare variability between Section A-A and B-B.

Table 2.3.1 Variability of Dimensions along Rolling Direction

			t_f	t_w	d	b_f
C1	**W24x62**	Ave. Ch.	0.002	0.001	0.05	0.02
		%Ch.	0.3%	0.2%	0.2%	0.2%
N1	**W24x62**	Ave. Ch.	0.004	0.000	0.03	0.03
		%Ch.	0.7%	0.1%	0.1%	0.4%
N2	**W30x211**	Ave. Ch.	0.012	0.014	0.06	0.03
		%Ch.	1.0%	1.7%	0.2%	0.2%
N3	**W36x300**	Ave. Ch.	0.023	0.006	0.03	0.03
		%Ch.	1.4%	0.6%	0.1%	0.2%
N4	**W14x211**	Ave. Ch.	0.018	0.006	0.00	0.03
		%Ch.	1.2%	0.6%	0.0%	0.2%
N5	**W36x150**	Ave. Ch.	0.008	0.006	0.09	0.05
		%Ch.	0.9%	0.9%	0.3%	0.4%
N6	**W14x311**	Ave. Ch.	0.014	0.002	0.00	0.03
		%Ch.	0.6%	0.2%	0.0%	0.2%
B1	**W14x211**	Ave. Ch.	0.007	0.004	0.00	0.00
		%Ch.	0.5%	0.4%	0.0%	0.0%
B2	**W14x311**	Ave. Ch.	0.019	0.030	0.00	0.06
		%Ch.	0.9%	2.1%	0.0%	0.4%
B3	**W36x300**	Ave. Ch.	0.018	0.012	0.02	0.05
		%Ch.	1.1%	1.2%	0.0%	0.3%
B4	**W36x150**	Ave. Ch.	0.009	0.004	0.03	0.03
		%Ch.	0.9%	0.6%	0.1%	0.3%
T1	**W24x162**	Ave. Ch.	0.012	0.004	0.03	0.06
		%Ch.	1.0%	0.6%	0.1%	0.5%
T2	**W30x211**	Ave. Ch.	0.003	0.014	0.03	0.09
		%Ch.	0.2%	1.7%	0.1%	0.6%
T3	**W36x300**	Ave. Ch.	0.005	0.003	0.06	0.03
		%Ch.	0.3%	0.3%	0.2%	0.2%
T4	**W14x211**	Ave. Ch.	0.015	0.006	0.06	0.00
		%Ch.	1.0%	0.6%	0.4%	0.0%
T5	**W36x150**	Ave. Ch.	0.006	0.006	0.22	0.13
		%Ch.	0.7%	1.0%	0.6%	1.0%
T6	**W14x311**	Ave. Ch.	0.015	0.011	0.03	0.00
		%Ch.	0.7%	0.8%	0.2%	0.0%
Average %Change:			**0.8%**	**0.8%**	**0.2%**	**0.3%**

The measured dimensions were very nearly constant along the length of the members. As can be seen, the changes were very low—the average change was less than 1% for all four dimensions.

Based on this data, it was concluded that the members were relatively uniform in the rolling direction. To reflect this, Sections A-A and B-B were combined into a single cross section by averaging the corresponding measurements. For example, t_{f1} was combined with t_{f5}, resulting in a new value for t_{f1}: $(t_{f1}+t_{f5})/2$. The number of dimensions was thereby reduced to eleven—four of flange thickness (t_f), three of web thickness (t_w), two of depth (d), and two of flange width (b_f).

2.3.2 Variability Within Cross sections

The relative change in dimension (%Ch) was again used to compare variations between different members. It was calculated by dividing the magnitude of the difference in measurements by the average value of the dimension. For example, the relative change in the depth was calculated from Equation 2.3:

$$\%Ch = \frac{|d_1 - d_2|}{(d_1 + d_2)/2} \qquad \text{[Eq. 2.3]}$$

Five sets of calculations were made—one each for d, b_f, and t_w, and two for t_f. Two sets of calculations were necessary for the flange width measurements because the relative change was obtained within individual flanges as well as between top and bottom flanges. The %Ch within the top flange was calculated using Equation 2.4:

$$\%Ch = \frac{\left|t_{f1} - t_{f2}\right|}{(t_{f1} + t_{f2})/2} \qquad \text{[Eq. 2.4]}$$

The %Ch between the left side of the top and bottom flanges was calculated using Equation 2.5:

$$\%Ch = \frac{\left|t_{f1} - t_{f3}\right|}{(t_{f1} + t_{f3})/2} \qquad \text{[Eq. 2.5]}$$

For the web thickness (t_w), the minimum of the three measurements was subtracted from the maximum, and then divided by the average, as shown in Equation 2.6:

$$\%Ch = \frac{Max(t_{w1}, t_{w2}, t_{w3}) - Min(t_{w1}, t_{w2}, t_{w3})}{(t_{w1} + t_{w2} + t_{w3})/3} \qquad \text{[Eq. 2.6]}$$

The results for each of the dimensions are shown in Tables 2.3.2-2.3.4. The maximum values of % Ch are shown in bold.

Table 2.3.2 Variation of t_f Within Same Flange

Flange Thickness (t_f)

Within Same Flange

	t_{f1}-t_{f2}	% Ch	Average	t_{f3}-t_{f4}	% Ch	Average
C1	0.006	1.0%	**1.0%**	0.008	1.3%	**1.3%**
N1	0.001	0.2%		0.014	2.6%	
N2	0.039	**3.2%**		0.059	4.6%	
N3	0.019	1.2%	**1.5%**	0.012	0.8%	**2.2%**
N4	0.027	1.8%		0.006	0.4%	
N5	0.024	2.6%		0.029	**3.3%**	
N6	0.007	0.3%		0.032	1.4%	
B1	0.023	1.5%		0.016	1.1%	
B2	0.060	2.8%	**1.4%**	0.010	0.4%	**0.7%**
B3	0.003	0.2%		0.010	0.6%	
B4	0.009	1.0%		0.006	0.6%	
T1	0.002	0.2%		0.047	3.9%	
T2	0.029	2.2%		0.001	0.1%	
T3	0.040	2.4%	**1.5%**	0.022	1.3%	**2.0%**
T4	0.023	1.5%		0.027	1.8%	
T5	0.011	1.1%		0.035	3.7%	
T6	0.032	1.4%		0.028	1.3%	

Average % Ch: 1.6%

Table 2.3.3 Variation of t_f Between Top and Bottom Flanges

Flange Thickness (t_f)

Between Top & Bottom Flanges on Same Side of Web

	t_{f1}-t_{f3}	% Ch	Average	t_{f2}-t_{f4}	% Ch	Average
C1	0.005	0.8%	**0.8%**	0.009	1.5%	**1.5%**
N1	0.010	1.8%		0.025	4.5%	
N2	0.106	**8.4%**		0.008	0.6%	
N3	0.017	1.1%	**2.4%**	0.013	0.9%	**2.9%**
N4	0.004	0.3%		0.024	1.6%	
N5	0.023	2.6%		0.075	**8.4%**	
N6	0.011	0.5%		0.036	1.6%	
B1	0.013	0.9%		0.006	0.4%	
B2	0.026	1.2%	**1.5%**	0.025	1.2%	**1.5%**
B3	0.039	2.4%		0.047	2.8%	
B4	0.014	1.4%		0.017	1.8%	
T1	0.020	1.6%		0.029	2.4%	
T2	0.011	0.8%		0.020	1.5%	
T3	0.014	0.8%	**2.1%**	0.004	0.2%	**2.0%**
T4	0.086	5.6%		0.035	2.3%	
T5	0.017	1.7%		0.029	3.1%	
T6	0.046	2.1%		0.050	2.3%	

Average % Ch: 2.1%

Table 2.3.4 Variation of t_w, d, and b_f

	Web Thickness (t_w)			Depth (d)			Flange Width (b_f)		
	max-min	% Ch	Average	Diff.	% Ch	Average	Diff.	% Ch	Average
C1	0.009	2.1%	**2.1%**	0.02	0.1%	**0.1%**	0.05	0.7%	**0.7%**
N1	0.004	0.8%		0.09	0.4%		0.09	**1.3%**	
N2	0.005	0.6%		0.13	0.4%		0.16	1.0%	
N3	0.012	1.2%	**0.6%**	0.16	0.4%	**0.5%**	0.03	0.2%	**0.6%**
N4	0.001	0.2%		0.13	0.8%		0.03	0.2%	
N5	0.005	0.8%		0.03	0.1%		0.05	0.4%	
N6	0.004	0.3%		0.13	0.7%		0.03	0.2%	
B1	0.025	2.5%		0.06	0.4%		0.00	0.0%	
B2	0.024	1.7%	**1.6%**	0.19	**1.1%**	**0.5%**	0.13	0.8%	**0.3%**
B3	0.007	0.7%		0.14	0.4%		0.05	0.3%	
B4	0.009	1.4%		0.03	0.1%		0.03	0.3%	
T1	0.016	2.3%		0.03	0.1%		0.06	0.5%	
T2	0.011	1.4%		0.09	0.3%		0.03	0.2%	
T3	0.034	**3.5%**	**1.7%**	0.38	1.0%	**0.4%**	0.03	0.2%	**0.3%**
T4	0.011	1.1%		0.06	0.4%		0.00	0.0%	
T5	0.004	0.7%		0.09	0.3%		0.06	0.5%	
T6	0.017	1.2%		0.03	0.2%		0.06	0.4%	
Average:		**1.3%**			**0.4%**			**0.4%**	

As can be seen, the flange thickness between opposite flanges showed the highest average value of %Ch, 2.1%, as well as the highest single value, 8.4%. Flange thickness variation within individual flanges was the next highest at 1.6%, followed by the web thickness variation, which averaged 1.3%. The depth and the flange width showed practically no variation within the cross section.

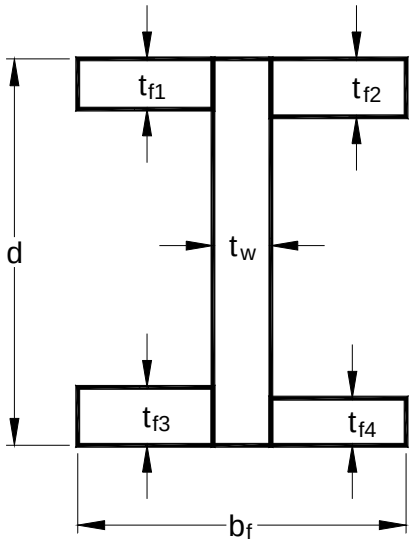

Figure 2.3.1 Model of Typical Cross section Reflecting Observed Variability in Flange Thickness

From these results, a model of a typical cross section was created that reflects the observed dimensional variability as shown in Figure 2.3.1. As can be seen, the model accounts for the high variability of the flange thickness measurements—both within a flange and between opposite flanges—and the relatively low variability of the depth, flange width, and web thickness measurements. The extremely low changes in depth and flange width observed in Table 2.3.4 indicate that they were practically uniform within a typical cross section, making it acceptable to average them into single dimensions of d and b_f. Although the average %Ch was slightly higher for t_w than for d and b_f,, it was considered uniform as well, and the individual web thickness measurements combined into a single average value for t_w.

Tablel 2.3.5 shows the data used to model the cross-sectional geometry of the members in this study. These dimensions will be used in the calculations in the next section, but they will not be used to check against the ASTM and Japanese Industrial Standard specifications. These checks were performed with actual measurements, not averaged values.

Table 2.3.5 Dimensions Used to Model Cross-sectional Geometry of Members

	Shape	t_{f1}	t_{f2}	t_{f3}	t_{f4}	t_w	d	b_f
C1	W24x62	0.602	0.596	0.597	0.605	0.420	23.68	6.98
N1	W24x62	0.561	0.562	0.551	0.537	0.419	23.73	7.11
N2	W30x211	1.205	1.244	1.311	1.252	0.825	30.81	15.23
N3	W36x300	1.589	1.570	1.572	1.584	0.992	36.67	16.80
N4	W14x211	1.499	1.473	1.503	1.497	0.940	15.63	15.92
N5	W36x150	0.910	0.933	0.887	0.858	0.651	35.98	12.20
N6	W14x311	2.215	2.208	2.204	2.172	1.366	17.00	16.20
B1	W14x211	1.528	1.505	1.515	1.499	0.972	15.72	15.63
B2	W14x311	2.203	2.143	2.178	2.168	1.451	17.09	16.09
B3	W36x300	1.656	1.659	1.695	1.705	0.950	36.80	16.51
B4	W36x150	0.941	0.951	0.928	0.934	0.638	35.77	11.86
T1	W24x162	1.209	1.211	1.229	1.182	0.703	25.17	13.13
T2	W30x211	1.297	1.327	1.308	1.307	0.810	31.02	15.30
T3	W36x300	1.673	1.634	1.659	1.637	0.958	36.78	16.92
T4	W14x211	1.578	1.555	1.492	1.520	0.981	15.84	15.81
T5	W36x150	0.956	0.967	0.972	0.937	0.616	35.77	12.03
T6	W14x311	2.198	2.167	2.245	2.216	1.416	17.17	16.22

Units: inches

2.4 COMPARISON OF MEASURED AND NOMINAL DIMENSIONS

In this section, the measured cross-sectional dimensions are compared to their nominal values, given in ASTM A6. Values for flange thickness, flange width, and depth were also checked against code-specified tolerances to see if the

members met ASTM or Japanese Industrial Standard (JIS) requirements. Code requirements were not checked for t_w because currently, neither ASTM nor JIS specifies required tolerances for this dimension in wide-flange shapes.

The flange thickness measurements are compared with the nominal values, given in ASTM A6, and the tolerances specified in JIS G3136. The Japanese specifications were originally written in metric units, but were converted to English units in Table 2.4.1.

Table 2.4.1 Allowable Flange Thickness Tolerance, per JIS G3136

Flange Thickness (t_f)	Over Theoretical	Under Theoretical
.24-.63	+0.067	-0.012
.63-1.57	+0.091	-0.028
1.57-3.94	+0.098	-0.059

All values in inches.

Table 2.4.2 lists for each member the nominal flange thickness ($t_{f\ nom}$), the upper and lower limits allowed by JIS G3136 (JIS_{max}, JIS_{min}), the maximum and minimum measured thickness ($t_{f\ max}$, $t_{f\ min}$), the average flange width dimension ($t_{f\ avg}$), and the relative error (%Err). The maximum and minimum flange thicknesses are the actual dimensions, not average dimensions. The relative error is calculated from Equation 2.7:

$$\%Err = \frac{(t_{favg} - t_{fnom})}{t_{fnom}} \qquad \text{[Eq. 2.7]}$$

Values shown in bold were outside of the JIS code-specified range.

Table 2.4.2 Comparison of Measured t_f Dimensions with JIS G3136 Code-specified Tolerances

		$t_{f\ nom}$	JIS_{max}	JIS_{min}	$t_{f\ max}$	$t_{f\ min}$	$t_{f\ avg}$	%Err
C1	W24x62	0.590	0.657	0.578	0.606	0.595	0.600	1.6%
N1	W24x62	0.590	0.657	0.578	**0.563**	**0.532**	**0.553**	-6.3%
N2	W30x211	1.315	1.406	1.287	1.320	**1.203**	**1.253**	-4.7%
N3	W36x300	1.680	1.778	1.621	**1.611**	**1.552**	**1.578**	-6.0%
N4	W14x211	1.560	1.651	1.532	**1.514**	**1.454**	**1.493**	-4.3%
N5	W36x150	0.940	1.031	0.912	0.935	**0.852**	**0.897**	-4.6%
N6	W14x311	2.260	2.358	2.201	2.217	**2.166**	**2.199**	-2.7%
B1	W14x211	1.560	1.651	1.532	**1.530**	**1.493**	**1.511**	-3.1%
B2	W14x311	2.260	2.358	2.201	2.206	**2.128**	**2.173**	-3.9%
B3	W36x300	1.680	1.778	1.621	1.711	1.643	1.679	-0.1%
B4	W36x150	0.940	1.031	0.912	0.958	0.926	0.938	-0.2%
T1	W24x162	1.220	1.311	1.192	1.231	**1.165**	1.208	-1.0%
T2	W30x211	1.315	1.406	1.287	1.329	1.296	1.309	-0.4%
T3	W36x300	1.680	1.778	1.621	1.674	1.630	1.651	-1.7%
T4	W14x211	1.560	1.651	1.532	1.579	**1.489**	1.536	-1.5%
T5	W36x150	0.940	1.031	0.912	0.975	0.932	0.958	1.9%
T6	W14x311	2.260	2.358	2.201	2.247	**2.160**	2.206	-2.4%

All values in inches.

The average flange thickness of all six members from Mill N and two column sections from Mill B were consistently below minimum JIS requirements. Mill T had isolated values of t_f below JIS_{min}, but the average values were all within the specified tolerances. Only two sections had average flange thickness dimensions that were greater than $t_{f\ nom}$ (C1 and T5), but neither measurement approached JIS_{max}. ASTM A6 requires shape producers to meet member depth and flange width constraints. The maximum allowable tolerances for each are listed in Table 2.4.3.

Table 2.4.3 Tolerances on Member Depth and Flange Width, per ASTM A6, Table 16

	Over Theoretical	Under Theoretical
Depth (in.)	1/8	1/8
Flange Width (in.)	1/4	3/16

All values in inches.

Table 2.4.4 lists the nominal dimensions (d_{nom}), the upper and lower limits allowed by ASTM ($ASTM_{max}$, $ASTM_{min}$), the maximum and minimum measured member depths (d_{max}, d_{min}), and the average member depth (d_{avg}).

Table 2.4.4 Comparison of Measured Member Depth Dimensions with ASTM A6 Code-specified Tolerances

		d_{nom}	$ASTM_{max}$	$ASTM_{min}$	d_{max}	d_{min}	d_{avg}	%Err
C1	W24x62	23.74	23.87	23.62	23.72	23.63	23.68	-0.3%
N1	W24x62	23.74	23.87	23.62	23.81	23.69	23.73	0.0%
N2	W30x211	30.94	31.07	30.82	30.94	**30.75**	**30.81**	-0.4%
N3	W36x300	36.74	36.87	36.62	36.75	**36.56**	36.67	-0.2%
N4	W14x211	15.72	15.85	15.60	15.69	**15.56**	15.63	-0.6%
N5	W36x150	35.85	35.98	35.73	**36.06**	35.88	35.98	0.4%
N6	W14x311	17.12	17.25	17.00	17.06	**16.94**	17.00	-0.7%
B1	W14x211	15.72	15.85	15.60	15.75	15.69	15.72	0.0%
B2	W14x311	17.12	17.25	17.00	17.19	17.00	17.09	-0.2%
B3	W36x300	36.74	36.87	36.62	**36.88**	36.72	36.80	0.2%
B4	W36x150	35.85	35.98	35.73	35.81	35.75	35.77	-0.2%
T1	W24x162	25.00	25.13	24.88	**25.19**	25.13	**25.17**	0.7%
T2	W30x211	30.94	31.07	30.82	31.06	30.94	31.02	0.2%
T3	W36x300	36.74	36.87	36.62	**37.00**	**36.56**	36.78	0.1%
T4	W14x211	15.72	15.85	15.60	**15.88**	15.75	15.84	0.8%
T5	W36x150	35.85	35.98	35.73	35.94	**35.63**	35.77	-0.2%
T6	W14x311	17.12	17.25	17.00	17.19	17.13	17.17	0.3%

All values in inches.

Ten members shown in bold had individual measurements fall outside of ASTM A6 specifications—five from Mill N, four from Mill T, and one from Mill B. Of these ten members, two showed average depths that fell outside of the specified tolerances. The W30x211 specimen from Mill N was only slightly outside the allowable range, but T1, the W24x162 specimen from Mill T, was well outside. Three other members, N5, N6 and T4, were just within allowable tolerances.

Four members from Mill N showed minimum depth measurements that were below $ASTM_{min}$. One member from Mill T (T3) showed one value above $ASTM_{max}$ and another below $ASTM_{min}$. In addition to failing the ASTM depth tolerances, the flanges of this section were out-of-square by 7/16”—more than the maximum of 5/16” allowed by ASTM A6, Table 16.

Nominal and measured web thickness values, as well as the relative errors, are tabulated in Table 2.4.5. Mill N showed poor dimensional control of the web thickness, with all six members recording average measurements ranging from 2.6% less to 6.5% greater than the nominal values. The highest relative error of 6.5% came from N2, a W30x211 section. Two other members, N3 and N5, had web thicknesses oversized by 5.0% and 4.1%, respectively. The other three members from Mill N showed undersized webs. Of these, member N4 had the greatest error, -4.0%. Dimensions from the other three mills were consistently closer to the nominal values, than those from Mill N. The only other member to have a noticeable relative error was specimen T2, for which %Err was 4.5%.

Table 2.4.5 Comparison of Nominal and Measured Web Thickness Values

		$t_{w\ nom}$	$t_{w\ max}$	$t_{w\ min}$	$t_{w\ avg}$	%Err
C1	W24x62	0.430	0.424	0.414	0.420	-2.3%
N1	W24x62	0.430	0.420	0.416	0.419	-2.6%
N2	W30x211	0.775	0.836	0.817	0.825	6.5%
N3	W36x300	0.945	1.003	0.983	0.992	5.0%
N4	W14x211	0.980	0.944	0.937	0.940	-4.0%
N5	W36x150	0.625	0.655	0.644	0.651	4.1%
N6	W14x311	1.410	1.369	1.362	1.366	-3.1%
B1	W14x211	0.980	0.987	0.959	0.972	-0.8%
B2	W14x311	1.410	1.475	1.423	1.451	2.9%
B3	W36x300	0.945	0.959	0.938	0.950	0.5%
B4	W36x150	0.625	0.645	0.632	0.638	2.1%
T1	W24x162	0.705	0.712	0.690	0.703	-0.2%
T2	W30x211	0.775	0.833	0.797	0.810	4.5%
T3	W36x300	0.945	0.975	0.940	0.958	1.4%
T4	W14x211	0.980	0.994	0.974	0.981	0.1%
T5	W36x150	0.625	0.625	0.613	0.616	-1.4%
T6	W14x311	1.410	1.436	1.405	1.416	0.4%

All values in inches.

Table 2.4.6 gives the following flange width measurements: nominal values ($b_{f\ nom}$); the range of permissible widths given by ASTM A6 ($ASTM_{max}$, $ASTM_{min}$); the maximum, minimum, and average measured flange widths ($b_{f\ max}$, $b_{f\ min}$, $b_{f\ avg}$); and the relative errors between the measured and nominal values.

Table 2.4.6 Comparison of Measured Flange Width Dimensions with ASTM A6 Code-specified Tolerances

		$b_{f\ nom}$	$ASTM_{max}$	$ASTM_{min}$	$b_{f\ max}$	$b_{f\ min}$	$b_{f\ avg}$	%Err
C1	W24x62	7.04	7.29	6.85	7.00	6.94	6.98	-0.9%
N1	W24x62	7.04	7.29	6.85	7.16	7.03	7.11	1.0%
N2	W30x211	15.11	15.36	14.92	15.31	15.13	15.23	0.9%
N3	W36x300	16.66	16.91	16.47	16.81	16.75	16.80	0.9%
N4	W14x211	15.80	16.05	15.61	15.94	15.88	15.92	0.8%
N5	W36x150	11.98	12.23	11.79	**12.25**	12.16	12.20	1.8%
N6	W14x311	16.23	16.48	16.04	16.25	16.19	16.20	-0.2%
B1	W14x211	15.80	16.05	15.61	15.63	15.63	15.63	-1.1%
B2	W14x311	16.23	16.48	16.04	16.19	**16.00**	16.09	-0.8%
B3	W36x300	16.66	16.91	16.47	16.56	16.47	16.51	-0.9%
B4	W36x150	11.98	12.23	11.79	11.88	11.81	11.86	-1.0%
T1	W24x162	12.96	13.21	12.77	13.19	13.06	13.13	1.3%
T2	W30x211	15.11	15.36	14.92	**15.38**	15.25	15.30	1.3%
T3	W36x300	16.66	16.91	16.47	**16.94**	16.88	**16.92**	1.6%
T4	W14x211	15.80	16.05	15.61	15.81	15.81	15.81	0.1%
T5	W36x150	11.98	12.23	11.79	12.13	11.94	12.03	0.5%
T6	W14x311	16.23	16.48	16.04	16.25	16.19	16.22	-0.1%

All values in inches.

Four members showed individual flange width values outside of the ASTM-specified range—two from Mill T, and one each from Mills N and B. Only one member, T3, showed an average flange width value outside of ASTM A6. The majority of the measurements failing A6 were above the maximum allowable values, while most failing the flange thickness and member depth specifications were below the minimum allowable values.

2.5 EFFECT OF DIMENSIONAL VARIATION ON CALCULATED GEOMETRIC PROPERTIES

The relationship between nominal section properties and the actual section properties obtained through direct measurements of the cross sections are reported. These properties are cross-sectional area (A), moment of inertia about the X and Y-axes (I_x, I_y), the section modulus about the X and Y-axes (S_x, S_y), and the plastic section modulus about the X and Y-axes (Z_x, Z_y). The calculated values are presented, and their effects on member behavior are discussed.

2.5.1 Approximate Nominal Properties (ANP)

The section properties of the measured members are compared with the nominal section properties given in the AISC Manual of Steel Construction to study the effects of dimensional variation on the structural behavior of a member. A direct comparison cannot be made, however, because the nominal properties take into account the fillets at the web-flange junctions which were not measured in this research. In order to compare the actual and nominal section properties, the effects of the fillets on the nominal section properties were removed by recalculating the nominal section properties using only the nominal values of t_f, t_w, d, and b_f—the radii at the web-flange junctions were ignored. The results of these calculations, hereafter referred to as the Approximate Nominal Properties or ANP, can be found in Table 2.5.1.

Table 2.5.1 Comparison of Approximate with Exact Nominal Section Properties for All Shapes in Project

		W24x62	W30x211	W36x300	W14x211	W36x150	W14x311	W24x162
A (in^2)	**Exact**	18.2	62.0	88.3	62.0	44.2	91.4	47.7
	Approx.	18.0	61.7	87.5	61.6	43.7	91.1	47.5
	%Err	-1.1%	-0.5%	-0.9%	-0.6%	-1.1%	-0.3%	-0.4%
I_x (in^4)	**Exact**	1550	10300	20300	2660	9040	4330	5170
	Approx.	1525	10187	20139	2644	8903	4316	5147
	%Err	-1.6%	-1.1%	-0.8%	-0.6%	-1.5%	-0.3%	-0.4%
S_x (in^3)	**Exact**	131	663	1110	338	504	506	414
	Approx.	128	659	1096	336	497	504	412
	%Err	-2.3%	-0.6%	-1.3%	-0.6%	-1.4%	-0.4%	-0.5%
Z_x (in^3)	**Exact**	153	749	1260	390	581	603	468
	Approx.	151	744	1244	388	573	601	466
	%Err	-1.3%	-0.7%	-1.3%	-0.5%	-1.4%	-0.3%	-0.4%
I_y (in^4)	**Exact**	34.5	757	1300	1030	270	1610	443
	Approx.	34.5	756	1296	1027	270	1613	443
	%Err	0.0%	-0.1%	-0.3%	-0.3%	0.0%	0.2%	0.0%
S_y (in^3)	**Exact**	9.80	100	156	130	45.1	199	68.4
	Approx.	9.79	100	156	130	45.0	199	68.4
	%Err	-0.1%	0.0%	0.0%	0.0%	-0.2%	0.0%	0.0%
Z_y (in^3)	**Exact**	15.7	154	241	198	70.9	304	105
	Approx.	15.7	154	240	198	70.7	304	105
	%Err	0.0%	0.0%	-0.4%	0.0%	-0.3%	0.0%	0.0%

For the cross-sectional area and the section properties about the X-axis, the Approximate Nominal Properties varied from the exact values by 0.3-2.3%. The difference was even smaller between Iy, Sy, and Zy (0.0-0.4%) since the fillets were nearer to the neutral axes. The agreement between the two properties shows that the ANP values give a very good estimation of the true section properties, and at the same time provide a more accurate basis of comparison for the measured cross-sectional properties.

2.5.2 Actual vs. Nominal Section Properties

Table 2.5.2 lists the calculated section properties of each member and compares them to their Approximate Nominal Properties.

Table 2.5.2 Comparison of Calculated Section Properties with Approximate Nominal Properties

		A (in^2)	I_x (in^4)	I_y (in^4)	S_x (in^3)	S_y (in^3)	Z_x (in^3)	Z_y (in^3)	Averages
C1	Value	17.8	1510	34.1	128	9.8	150.0	15.6	
W24x62	% of ANP	98.9%	99.0%	98.9%	99.5%	99.8%	99.4%	99.5%	**99.3%**
N1	Value	17.3	1460	33.3	124	9.4	145.0	15.0	
W24x62	% of ANP	**96.3%**	**95.8%**	96.6%	**96.4%**	95.8%	**96.1%**	95.5%	**96.1%**
N2	Value	61.5	9900	740	650	97.3	729.0	150.0	
W30x211	% of ANP	99.8%	97.2%	97.9%	98.8%	97.2%	98.0%	97.2%	**98.0%**
N3	Value	86.3	19400	1250	1060	149.0	1210.0	231.0	
W36x300	% of ANP	98.6%	96.3%	96.5%	96.7%	95.7%	97.2%	96.1%	**96.7%**
N4	Value	59.4	2540	1010	326	127.0	373.0	192.0	
W14x211	% of ANP	96.4%	96.1%	98.4%	96.9%	97.7%	96.2%	97.1%	**97.0%**
N5	Value	44.1	8900	273	501	44.8	574.0	70.3	
W36x150	% of ANP	100.9%	100.0%	101.2%	100.8%	99.4%	100.1%	99.4%	**100.3%**
N6	Value	88.5	4160	1560	491	193.0	582.0	295.0	
W14x311	% of ANP	97.1%	96.4%	96.7%	97.3%	97.1%	96.8%	97.1%	**96.9%**
B1	Value	59.6	2560	962	326	123.0	375.0	188.0	
W14x211	% of ANP	96.6%	96.8%	**93.7%**	96.9%	**94.7%**	96.7%	95.1%	**95.8%**
B2	Value	88.4	4170	1510	488	189.0	581.0	288.0	
W14x311	% of ANP	97.0%	96.6%	93.6%	96.8%	95.1%	96.7%	**94.8%**	**95.8%**
B3	Value	87.2	20100	1260	1100	153.0	1240.0	236.0	
W36x300	% of ANP	99.6%	99.8%	97.2%	100.3%	98.3%	99.7%	98.1%	**99.0%**
B4	Value	43.9	8820	262	495	44.2	571.0	69.4	
W36x150	% of ANP	100.3%	99.1%	97.0%	99.7%	98.0%	99.6%	98.2%	**98.8%**
T1	Value	47.7	5250	456	417	69.7	471.0	107.0	
W24x162	% of ANP	100.4%	102.0%	102.9%	101.3%	101.9%	101.2%	101.7%	**101.6%**
T2	Value	63.1	10400	782	671	103.0	758.0	158.0	
W30x211	% of ANP	**102.2%**	**102.1%**	**103.4%**	**101.8%**	102.8%	**101.9%**	102.4%	**102.4%**
T3	Value	87.9	20200	1340	1100	158.0	1250.0	244.0	
W36x300	% of ANP	100.5%	100.3%	103.4%	100.3%	101.5%	100.5%	101.5%	**101.1%**
T4	Value	61.1	2670	1010	340	128.0	387.0	195.0	
W14x211	% of ANP	99.1%	101.0%	98.4%	101.2%	98.5%	99.8%	98.6%	**99.5%**
T5	Value	43.9	8970	279	503	46.4	578.0	72.5	
W36x150	% of ANP	100.4%	100.8%	103.3%	101.2%	**103.0%**	100.8%	**102.6%**	**101.7%**
T6	Value	89.6	4280	1570	502	194.0	593.0	297.0	
W14x311	% of ANP	98.4%	99.2%	97.3%	99.5%	97.6%	98.7%	97.7%	**98.3%**
	Mean	**99.0%**	**98.7%**	**98.6%**	**99.1%**	**98.5%**	**98.8%**	**98.4%**	**98.7%**
	Min.	**96.3%**	**95.8%**	**93.6%**	**96.4%**	**94.7%**	**96.1%**	**94.8%**	**95.8%**
	Max.	**102.2%**	**102.1%**	**103.4%**	**101.8%**	**103.0%**	**101.9%**	**102.6%**	**102.4%**
	Std. Dev.	**1.8%**	**2.2%**	**3.2%**	**1.9%**	**2.6%**	**1.9%**	**2.5%**	**2.2%**

Overall, the calculated section properties are slightly lower than the Approximate Nominal Properties. The calculated section properties averaged 98.7% of the ANP, with a low of 93.7% and a high of 103.4% of the ANP. No one section property was significantly more sensitive to the dimensional variation than the others.

ASTM A6 paragraph 13.3.3 requires that the cross-sectional area of each shape be within 2.5% of the theoretical amounts. Table 2.5.2 shows that several members did not meet this requirement. Three members from Mill N (N1, N4, and N6) and two from Mill B (B1 and B2) had calculated areas that were less than 97.5% of the approximate nominal area, implying that they were too light. Table 2.5.3 compares the theoretical weights with the weights calculated from the Approximate Nominal Area. The density of steel was taken as 490 pounds/ft^3, as specified in ASTM A6 paragraph 13.1.

Table 2.5.3 Comparison of Theoretical vs. Calculated Weights

Shape		Nominal Weight	Calculated Weight	% Change
N1	W24x62	62	59	-4.8%
N4	W14x211	211	202	-4.2%
N6	W14x311	311	301	-3.2%
B1	W14x211	211	203	-3.9%
B2	W14x311	311	301	-3.2%

2.6 EFFECTS OF ASYMMETRY

The section properties calculated above assume bending about the axis perpendicular to the plane of loading—either the X- or Y-axis. This assumption

is valid for symmetric shapes in all cases, and for asymmetric shapes that are laterally restrained. For asymmetric beams that are not laterally restrained the neutral axis will be rotated some angle relative to the plane of loading, introducing biaxial bending. For each member in the study, an effective section modulus was calculated using measured dimensions and accounting for biaxial bending.

General flexural theory for symmetrical and unsymmetrical cross sections states that for a straight beam with a constant cross section, the stress at any point (x,y) on the cross section is given by Equation 2.8:

$$\sigma = \frac{M_x I_y - M_y I_{xy}}{I_x I_y - I_{xy}^2} y + \frac{M_y I_x - M_x I_{xy}}{I_x I_y - I_{xy}^2} x \qquad \text{[Eq. 2.8],}$$

where the X-and Y-axes are mutually perpendicular centroidal axes and the stress is proportional to strain [Salmon 1990]. The effects of asymmetry are given by I_{xy}, the product of inertia, which is defined as

$$I_{xy} = \int_A xy \cdot dA \qquad \text{[Eq. 2.9]}$$

For shapes that are symmetric about at least one principal axis, $I_{xy}=0$, and the neutral axis is perpendicular to the X- or Y-axis (assuming that the plane of loading is parallel to the X- or Y-axis). For nonsymmetrical shapes, $I_{xy}\neq 0$, and the neutral axis is not perpendicular to the X- or Y-axis. This concept is illustrated in Figure 2.6.1.

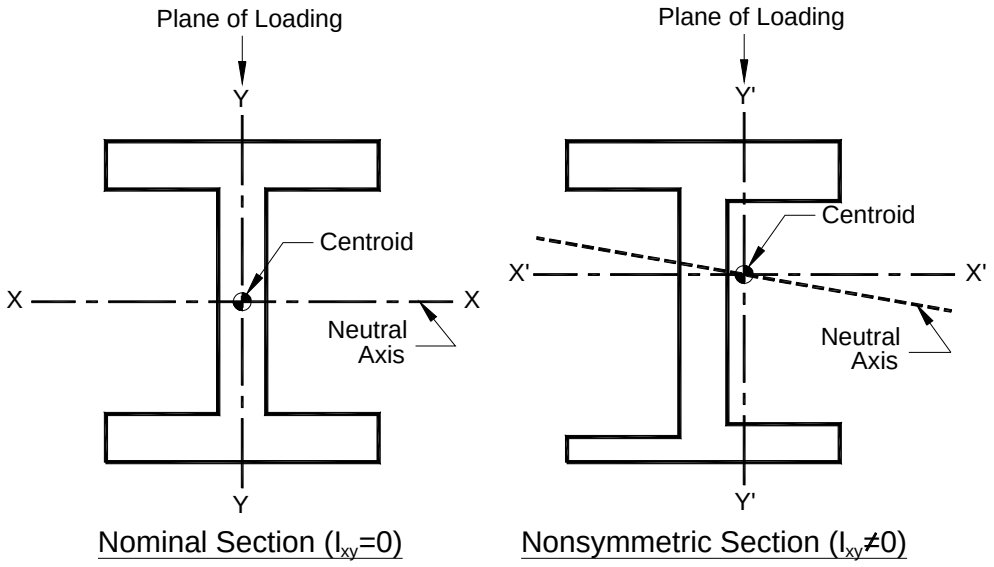

Figure 2.6.1 Affects of Asymmetry on Flexural Behavior

Table 2.6.1 lists calculated values of I_{xy}, and of Effective Section Moduli ($S_{x\ eff}$ and $S_{y\ eff}$.) The calculation procedures for $S_{x\ eff}$ and $S_{y\ eff}$ are described later. The product of inertia, I_{xy}, can be used as a way to compare the relative asymmetry of different members. For shapes that are perfectly symmetric about the X- or Y-axis, I_{xy}=0 and bending occurs in the same plane as the loading. As I_{xy} increases in magnitude (the sign is unimportant) the plane of bending rotates farther from the loading plane, and the member begins to exhibit biaxial bending. For highly asymmetric shapes, $|I_{xy}|$ is large and effects of biaxial bending become more pronounced.

Table 2.6.1 Effect of Asymmetry of Section on Calculated Section Modulus Values

	Shape	I_{xy}	$S_{x\ eff}$	% Lower than S_x	% of ANP	$S_{y\ eff}$	% Lower than S_y	% of ANP
C1	W24x62	-0.95	127	1.0%	98.5%	9.74	0.3%	99.5%
N1	W24x62	1.08	121	2.2%	94.3%	9.33	0.5%	95.3%
N2	W30x211	**40.0**	**618**	**4.9%**	**93.9%**	**96.3**	**1.1%**	**96.1%**
N3	W36x300	-18.0	1050	1.0%	95.8%	148	0.3%	95.4%
N4	W14x211	-4.02	323	1.0%	96.0%	126	0.6%	96.8%
N5	W36x150	**16.5**	**479**	**4.4%**	**96.4%**	44.5	0.6%	98.8%
N6	W14x311	5.08	486	0.9%	96.5%	192	0.5%	96.7%
B1	W14x211	-1.23	324	0.5%	96.4%	123	0.5%	94.5%
B2	W14x311	-10.3	485	0.6%	96.2%	187	0.9%	94.0%
B3	W36x300	-3.91	1080	1.6%	98.5%	153	0.2%	98.1%
B4	W36x150	1.02	491	0.9%	98.8%	44.1	0.2%	97.8%
T1	W24x162	12.0	411	1.6%	99.7%	**68.9**	**1.1%**	**100.8%**
T2	W30x211	12.6	664	1.0%	100.8%	102	0.6%	101.7%
T3	W36x300	-10.4	1100	0.2%	100.3%	157	0.7%	101.0%
T4	W14x211	-10.2	329	3.3%	97.9%	128	0.4%	98.2%
T5	W36x150	14.1	493	2.0%	99.2%	46.0	0.8%	102.2%
T6	W14x311	-0.77	495	1.2%	98.3%	193	0.6%	97.2%
		Averages:		**1.7%**	**97.5%**		**0.6%**	**97.9%**
		Min.		**0.2%**	**93.9%**		**0.2%**	**94.0%**
		Max.		**4.9%**	**100.8%**		**1.1%**	**102.2%**
		Std. Dev.		**1.3%**	**2.0%**		**0.3%**	**2.5%**

Units for I_{xy}=in.^{4}

Units for $S_{x\ eff}$, $S_{y\ eff}$=in.^{3}

The three most asymmetric members were produced by Mill N. The largest calculated I_{xy} value, 40.0 in^4, belonged to Member N2. This was followed by –18.0 in^4 for Member N3 and 16.5 in^4 for Member N5. The high calculated I_{xy} was expected in Member N2 because it showed the most variation in t_f between opposite flanges (see Table 2.3.3).

Using the general equation of flexure, the Effective Section Moduli S_{xeff} and S_{yeff} were calculated using the measured dimensions of each member. These values are given in Table 2.6.1, where

$$\sigma_{\max X} = \frac{M_x}{S_{xeff}} \qquad \text{[Eq. 2.10]}$$

gives the maximum stress when loaded in the strong-axis direction, and

$$\sigma_{\max Y} = \frac{M_y}{S_{yeff}} \qquad \text{[Eq. 2.11]}$$

gives the maximum stress when loaded in the weak-axis direction. The columns to the right of the tabulated values of $S_{x\ eff}$ and $S_{y\ eff}$ show the change in the calculated values due to biaxial bending. For instance, the Effective Section Modulus for strong-axis bending in Member N2 was 4.9% lower due to biaxial bending introduced by cross-sectional asymmetry. Member N5 showed the next greatest drop: 4.4%. It was expected that these members would be the most affected by biaxial bending because they had the highest values of I_{xy}, as was discussed previously.

The percentages given under the column heading "% of ANP" show the relative values of $S_{x\ eff}$ and $S_{y\ eff}$ compared to the approximate nominal properties of S_x and S_y. The calculated value of $S_{x\ eff}$ for Member N2 was 93.9% of its Approximate Nominal Property. This means that when loaded in the strong direction and free to deflect laterally, the moment at which first yield occurs in Member N2 will be 6.1% lower than in a section with nominal dimensions. The averages of $S_{x\ eff}$ and $S_{y\ eff}$ were about 98% of their respective Approximate Nominal Properties. Several members from Mill T still showed a calculated

flexural capacity higher than nominal. Members T2 and T3 had improved capacity for loading in both the strong-axis and the weak-axis directions. Members T1 and T5 showed improved capacity in the weak-axis direction only.

2.7 EFFECT OF ASTM AND JIS GEOMETRIC SPECIFICATIONS ON FLEXURAL BEHAVIOR

It was found in Section 2.4 that many of the rolled shapes in this study did not meet ASTM or JIS dimensional specifications resulting in flexural capacities that differed significantly from the theoretical values due to geometric variation. Table 2.7.1 presents the calculated section properties of four sets of members: all members, those that met JIS flange thickness specifications, those that met ASTM depth and flange width specifications, and those that met both sets of specifications.

Table 2.7.1 Effect of Geometric Variation on Flexural Behavior

		A (in^2)	I_x (in^4)	I_y (in^4)	$S_{x\ eff}$ (in^3)	$S_{y\ eff}$ (in^3)	Z_x (in^3)	Z_y (in^3)
All Specimens	**Average**	99.0%	98.7%	98.6%	97.5%	97.9%	98.7%	98.4%
	Min.	**96.3%**	**95.8%**	**93.7%**	**93.9%**	**94.0%**	**95.9%**	**94.8%**
	Max.	102.2%	102.0%	103.4%	100.8%	102.2%	101.9%	102.6%
	Std. Dev.	1.8%	2.1%	3.1%	2.0%	2.5%	1.9%	2.5%
	# of Spec.	17	17	17	17	17	17	17
Specimens Meeting JIS G3136	**Average**	100.0%	100.3%	100.2%	99.1%	99.6%	100.1%	100.0%
	Min.	**98.4%**	**99.1%**	**97.0%**	**97.9%**	**97.2%**	**98.7%**	**97.6%**
	Max.	102.2%	102.0%	103.4%	100.8%	102.2%	101.9%	102.6%
	Std. Dev.	1.1%	1.1%	2.9%	1.0%	1.9%	1.0%	2.0%
	# of Spec.	9	9	9	9	9	9	9
Specimens Meeting ASTM A6	**Average**	98.7%	98.5%	98.0%	97.4%	97.6%	98.5%	98.0%
	Min.	**96.3%**	**95.8%**	**93.7%**	**94.3%**	**94.0%**	**95.9%**	**94.8%**
	Max.	102.2%	102.0%	103.4%	100.8%	102.2%	101.9%	102.6%
	Std. Dev.	1.8%	2.1%	3.0%	1.7%	2.5%	1.9%	2.4%
	# of Spec.	14	14	14	14	14	14	14
Specimens Meeting Both Specs.	**Average**	99.8%	100.1%	99.4%	98.9%	99.3%	99.9%	99.6%
	Min.	**98.4%**	**99.1%**	**97.0%**	**97.9%**	**97.2%**	**98.7%**	**97.6%**
	Max.	102.2%	102.0%	103.4%	100.8%	102.2%	101.9%	102.6%
	Std. Dev.	1.3%	1.1%	2.8%	1.0%	2.0%	1.1%	2.0%
	# of Spec.	7	7	7	7	7	7	7

All values given are percentages of Approximate Nominal Properties

As expressed in the footnote, all percentages shown in the table above are percentages of the Approximate Nominal Properties. The calculated section properties and their % of ANP for all members are given in Tables 2.5.2 and 2.6.1. The shapes meeting JIS G3136, the Japanese Specification for rolled steel shapes for building structures, are given in Table 2.4.2. Sections were considered within the specification if their average flange thicknesses met the given tolerances. As can be seen in Table 2.4.2, sections T1, T4, and T6 had individual measurements that fell outside of the JIS G3136 requirements, but they were still

considered as passing because their average t_f was within the requirements. This same criterion was used in Tables 2.4.4 and 2.4.6 to determine which sections met the ASTM A6 geometric requirements for member depth and flange width. Nine sections had average flange thicknesses within JIS G3136 requirements and were therefore considered passing. Fourteen sections met ASTM A6 dimensional requirements, and seven sections met both JIS G3136 and ASTM A6.

As can be seen from examining the rows with the minimum values (shown in bold in Table 2.7.1) members that met JIS G3136 had section properties much closer to the Approximate Nominal Properties than those that met ASTM A6. The minimum calculated values for all data ranged from 93.7-96.3% of the ANP. Removing those members that did not meet ASTM A6 had no effect on the minimum calculated section properties—they still ranged from 93.7-96.3% of their ANP. If only those sections meeting JIS G3136 were considered though, the data ranged from 97.0-99.1% of the ANP—much closer to the theoretical section properties.

The section properties of rolled shapes used in the U.S. can be up to 6% lower than theoretical values, even for those sections meeting ASTM A6 geometric requirements. The flange thickness requirement in JIS G3136 significantly reduced this error. Those rolled shapes that met JIS G3136 had section properties a maximum of 3% lower than the theoretical properties.

2.8 CONCLUSIONS

The cross sections of all members were measured and the data were checked against current code-specified dimensions. Section properties were then calculated using these measurements, and compared to nominal values to estimate the differences in flexural behavior due to variation in member dimensions. From these studies, the following conclusions were drawn:

1. The cross-sectional dimensions were uniform along the length of the members.

2. The flange thickness measurements (t_f) were found to vary about 1.6% within the same flange and 2.1% between top and bottom flanges. The member depth (d), flange width (b_f), and web thickness (t_w) dimensions were fairly constant throughout individual cross sections.

3. The flange thickness dimensions of shapes from Mill N were consistently below the minimum values allowed by the Japanese Industrial Standard (JIS G3136)

4. One member from Mill T was found to be above the maximum depth allowed by ASTM A6, and one member from Mill N was found to be below the minimum. Only one member (T3) fell outside of the ASTM A6 flange width requirement.

5. Sectional properties such as area, section moduli, and moments of inertia calculated from measurement data were found to be about 1-2% below their respective nominal values.

6. The calculated weights of five sections—three from Mill N and two from Mill B—were more than 2.5% lighter than the nominal weights. These members fall outside of the allowable weight tolerance specified in ASTM 13.3.3.

7. Biaxial bending introduced by the asymmetry of the cross sections reduced the average flexural capacities of the members by 2-3% from their nominal values.

8. Tight control of flange thickness variation reduced the error between actual and theoretical flexural behavior. ASTM currently requires that members meet depth and flange width tolerances, but no flange thickness requirements are given. Those specimens that met ASTM A6 had calculated section properties up to 6% below their Approximate Nominal Properties. JIS-G3136, on the other hand, has a flange thickness requirement. Those that met the given tolerances of JIS-G3136 were a maximum of 3% lower than the theoretical values.

Chapter 3: Tensile Testing Procedure

3.1 INTRODUCTION

Tension tests were performed on coupons taken from the webs and flanges of all members. Most coupons were full thickness, 8-inch gage length specimens, referred to in this report as "strap" or "plate-type" coupons. The remaining specimens were machined down to standard 0.505-inch diameter specimens with 2-inch gage lengths and threaded ends. They will be referred to as ½-inch round coupons in this report. Of the 106 tensile tests performed in this study, 71 were performed with strap coupons and 35 with ½"-round coupons. The specified dimensions and allowable tolerances for both types of specimens are given in ASTM A370, Figures 3 and 4. Most coupons were tested in an MTS 220-kip hydraulic testing machine. A 200-kip load cell recorded load data, and an extensometer attached to the test specimens were used to obtain strain data. An Epsilon 8" gage length extensometer was used for all plate specimens, and a Tinius-Olsen 2" gage length extensometer for the ½-inch round specimens. A workstation connected to the MTS machine used a computer program called Telstar to run the test and to collect the load and strain data. The data acquisition system for the ½"-round specimens used a program developed in LabWindows to collect and graphically display load and strain output.

Tensile testing was initially performed on a 120-kip capacity, universal testing machine. After a number of tests were completed, a problem with its weighing system was discovered, which made much of the data unusable. After

specimens from each member were retested on the MTS 220-kip hydraulic machine, it was found that data from the original tests of two members—C1 and N1—matched the new results. It was concluded, then, that data from these two specimens were valid, and the original test results obtained using the 120-kip universal testing machine were reported. All other tensile test data were obtained from tests performed on the MTS 220-kip hydraulic machine.

3.2 SPECIMEN PREPARATION

3.2.1 Specimen Size

The size of a tension test specimen depended upon the thickness of the flange or web at the specimen location and the capacity of the testing machine. When possible, 8-inch gage length, plate-type, 1½-inch wide specimens were used, but when the specimen thickness reached a point at which the ultimate strength of the specimen approached the capacity of the testing machine, a smaller, ½-inch round specimen was used [ASTM A370]. The 200 kip capacity of the load cell and the upper bound of 80 ksi assumed for the ultimate strength of the material led to a maximum allowable thickness of 1.67 inches. Smaller, ½-inch round specimens were machined from the W14x311 members because their flange thickness of 2.26 inches would produce plate-type specimens that might have an ultimate load greater than the capacity of the machine. Though it would have been possible to take plate-type coupons from its web, ½-inch round specimens were taken from both the flange and the web of the W14x311 members

in order to prevent possible variations in test results due to different specimen size. The magnitude of this effect was explicitly considered in a test where a plate-type and a ½-inch round specimen were taken from adjacent locations along a member. The results of these two tests are compared in Section 4.3.

3.2.2 Specimen Location

Each specimen was oriented such that its longitudinal axis was parallel to the rolling direction of the member. Flange specimens were taken from the flat part of the flange, away from the web-flange connection. Web specimens were taken at least 2 inches from the flange-web junction. All ½-inch round specimens were centered as close as possible to a line ¼ of the thickness of the material from the surface. Approximate locations of each test specimen are shown in Figure 1.1.2, and the exact location of each test specimen can be found in Appendix B.

3.3 INSTRUMENT CALIBRATION

Before any tests were performed, the load cells from both testing machines, the 2" and 8" gage length extensometers, and the ram displacement output were all calibrated. The procedures for each are discussed in the sections to follow.

3.3.1 MTS Universal Testing Machine

The accuracy of the MTS 200-kip load cell used in the tension tests was verified from two different load cells and from a shunt calibration procedure. First, a 100-kip compression load cell was used to verify the accuracy of the MTS

over a range of 0-100 kips in compression. It was checked again, this time in tension, using a 20-kip tension load cell. These measurements showed agreements between the MTS and the tension load cell of better than 0.5%. Next, the shunt calibration procedure was performed. Using a shunt resistor and an internal voltmeter, the measured voltage was found to vary from the reference voltage by less than 0.01 V. All three methods showed that the load cell was operating adequately, so no adjustments were made.

The ram displacement calibration was checked using a 5-inch stroke dial gage. Under manual control, the ram was moved through a displacement of 4 inches in increments of 0.10 inches. The ram was stopped and values recorded from both the dial gage and the electronic readout. Data from the MTS agreed with the dial gage to within 0.001 inches, so no adjustment was deemed necessary.

3.3.2 Epsilon 8” Gage Length Extensometer

A complete calibration procedure, using a shunt calibration module, was performed for the extensometer. This verified that the extensometer was working properly and the signal conditioner settings were correct. Shunted voltages were then measured by the software using a shunt resistor in the workstation itself. These values were recorded and can be used to check the calibration in the future.

3.3.3 Tinius-Olsen 2” Gage Length Extensometer

The Tinius-Olsen 2” gage length extensometer, used to measure strain on the ½-inch round tensile coupons, was calibrated in two steps. First, an LVDT-

input signal conditioner was connected to transform the extensometer signal from AC to DC. The zero and span adjustments in the signal conditioner were manually adjusted until a 0.5" displacement on the extensometer corresponded to an output of roughly 10 V.

The relationship between specimen elongation and output voltage was determined using a milling machine, capable of measuring movements of 0.0005 inches, and reading the output voltages with a voltmeter. The extensometer was mounted on a broken specimen and displaced a total of 0.2000 inches, in increments of 0.0050 inches. Output signals from the extensometer were recorded with a voltmeter, and used to calculate a voltage-to-displacement calibration factor.

3.4 TESTING PROCEDURE

3.4.1 8"-Gage Length Plate Coupons

The coupons were placed in hydraulic grips located in the ram and the crosshead of the MTS. These grips were capable of inducing huge stresses during the gripping process, so care was taken to prevent any accidental loading. Using a software package included with the MTS workstation, a program was written which loaded the specimens at a constant crosshead rate of 0.05 inches/min in the elastic region, corresponding to roughly 50 ksi/min, depending on the size of the specimen. After the specimen reached its yield plateau, loading was suspended for three minutes. The load in the specimen at the end this time was used to

calculate the static yield stress (see Section 4.4). The loading rate of 0.05 in/min was maintained along the yield plateau between the three static readings. The crosshead rate was then increased to 0.4 inches/min after the coupon reached strain-hardening. The extensometer remained on the coupon, recording strain data, until after the coupon reached ultimate stress. After the extensometer was removed and the specimen taken to fracture, the pieces of the broken coupon were removed from the grips and the total elongation was measured.

Data from the load cell and the Epsilon 8”-gage length extensometer were used to recreate the stress-strain curves shown in Appendix C. In the elastic region and along the yield plateau, data were sampled in 0.40-kip load increments and 0.0002-in/in strain increments. After the specimen reached strain-hardening, data points were sampled once every second.

3.4.2 ½-Inch Round Specimens

For ½-inch round specimen tests, the same MTS 200-kip testing machine applied the loads but a 2-inch extensometer was used to measure displacements. Special grips were attached to the loading machine, and the threaded ends of the specimen were screwed into the grips.

Once the specimen was placed in the testing machine and the data acquisition system was activated, testing was conducted at 0.02 inches/min, corresponding to the specified loading rate of 50 ksi/minute in the elastic range. This loading rate was held through the yield plateau, between three static yields. Once strain-hardening was reached, the cross-head speed of the machine was

increased to 0.2 inches/min and the specimen was loaded to its ultimate strength. After the test was completed, the pieces of the specimen were placed back together and total elongation was measured.

Chapter 4: Analysis of Tensile Test Data

4.1 INTRODUCTION

Analysis of the tensile test data focused on three main areas. First, results from the tension tests were used to calculate the effect of coupon size and location on the stress-strain behavior of the steel. Next, the data were summarized and used to estimate typical parameters of stress-strain behavior. These parameters were upper yield point (F_{uy}), yield plateau stress (F_y, obtained using the 0.2% offset method), static yield strength (F_{sy}), strain at which strain-hardening begins (ε_{sh}), strain-hardening modulus (E_{sh}), ultimate strength (F_u), and strain at ultimate strength (ε_u). Finally, the test results were compared to mill test reports in an effort to better understand and interpret the yield strength and ultimate strength values reported by the mills.

As was stated earlier in Chapter 1, all calculated stress parameters (F_{uy}, F_y, F_{sy}, and F_u) refer to Engineering Stress, given by the equation

$$\sigma = \frac{P}{A_0}, \text{ where}$$

σ is the calculated stress, P is the applied tension load, and A_0 is the original cross-sectional area before loading. Similarly, the calculated strain parameters (ε_{sh}, ε_u) refer to Engineering Strain, which is given by

$$\varepsilon = \frac{\Delta l}{l_0}, \text{ where}$$

ε is the calculated strain, Δl is the change in length, and l_0 is the original gage length.

4.2 EFFECT OF COUPON LOCATION

The webs of rolled sections normally have higher yield strengths than the flanges, due to the high stresses exerted on them during the course of the milling process. Beedle and Tall [1959] report that in a typical wide-flange shape, the yield strength in the web is 4-7% higher than in the flange. The effect of the coupon location was studied to find overall trends, as well as trends of individual producers. The ratio of $F_{yflange}/F_{yweb}$ was calculated by averaging the yield strength results from the flanges and web of each section. For instance, $F_{yflange}/F_{yweb}$ for member C1 was obtained from the formula

$$\frac{F_{yflange}}{F_{yweb}} = \frac{(F_{yC1A} + F_{yC1B} + F_{yC1C} + F_{yC1D})/4}{(F_{yC1E} + F_{yC1F} + F_{yC1G})/3},$$

where F_{yC1A} is the yield strength of the top-left flange coupon, F_{yC1B} is the yield strength of the top-right coupon, etc. The approximate locations of each coupon are shown in Figure 1.1.2, and the yield strengths were obtained using the 0.2% offset method described fully in Section 4.4.2. The distribution of $F_{yflange}/F_{yweb}$ for the entire set of coupons is shown in Figure 4.2.1.

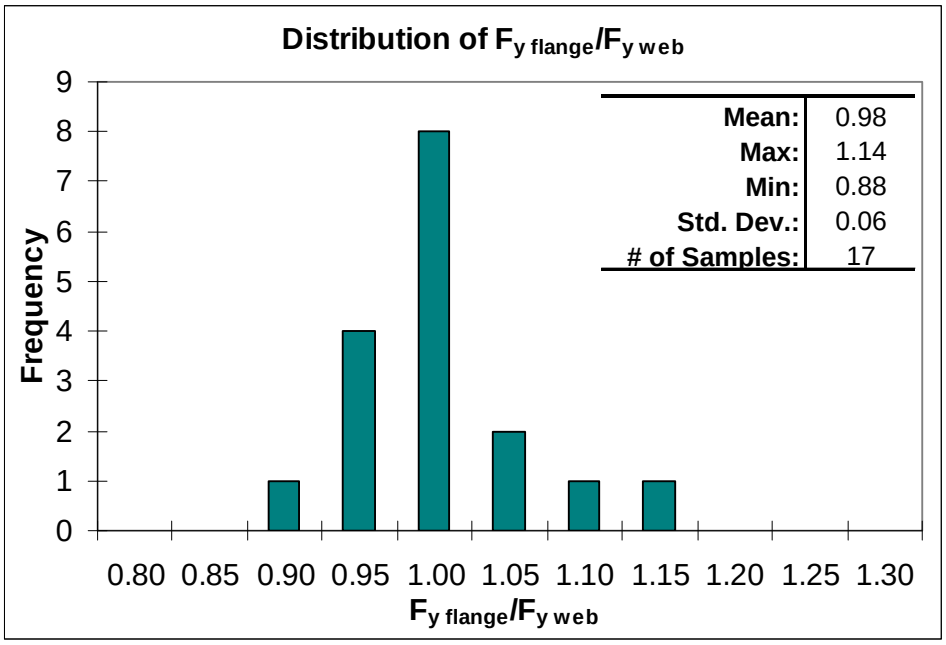

Figure 4.2.1 Distribution of $F_{yflange}/F_{yweb}$ for All Members

Overall, the ratio was about 98%—the flange strength was approximately the same as the web strength. As the data were grouped according to individual producers, slight differences emerged but the average $F_{yflange}/F_{yweb}$ ratio for each mill remained close to 1.00. Figure 4.2.2 compares the distributions for each of the four mills.

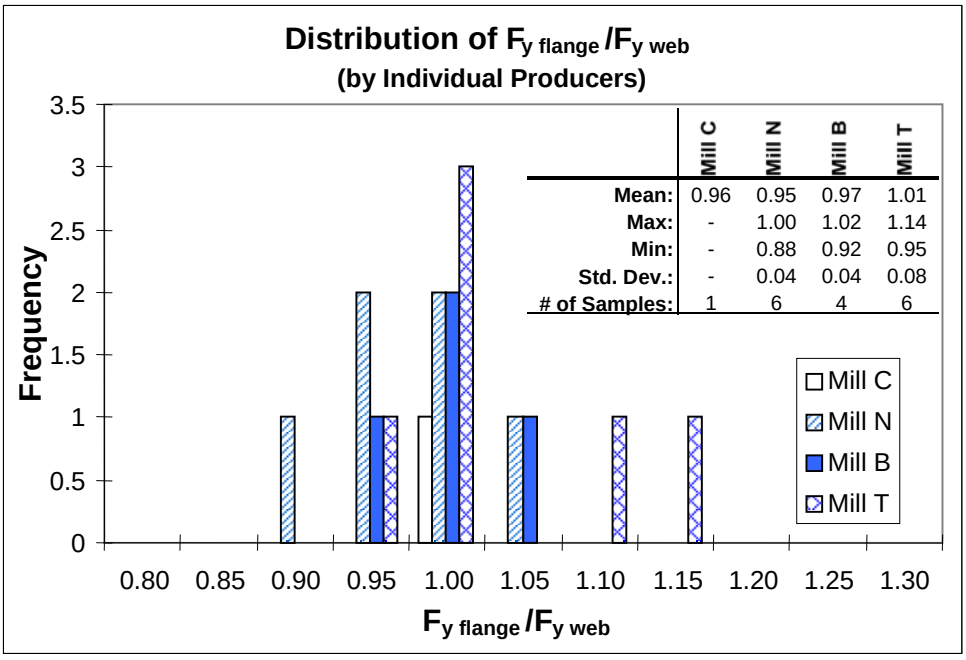

Figure 4.2.2 Distribution of $F_{yflange}/F_{yweb}$ Grouped by Individual Producers

Overall, $F_{yflange}$ varied considerably from F_{yweb}. The average flange yield strengths from Mills C, N, and B were 95-97% of the web yield strengths, but ranged from 88-102%. While $F_{yflange}/F_{yweb}$ for Mill T was closer to unity than the other three mills (101%), the standard deviation was twice that of Mills N and B, implying a much greater variability. The high standard deviations of the Mill T specimens are mainly due to two coupons with very high flange-to-web yield strength ratios: T1 ($F_{yflange}/F_{yweb}$=1.14) and T5 ($F_{yflange}/F_{yweb}$=1.09). Since the typical ratios of $F_{yflange}/F_{yweb}$ were less than unity and showed a high degree of variability overall, the yield strengths of the flange and web were considered fundamentally different. The remainder of the report distinguishes between stress-strain behavior of flange material and web material.

4.3 SENSITIVITY TO COUPON TYPE

A comparison was made between strap and ½"-round coupons, taken from the flanges of a Mill N W36x150 section, to see if stress-strain behavior was affected by coupon type. The stress-strain curves, shown in Figure 4.3.1, indicate that the strap coupon had lower yield and ultimate stress values and a slightly larger strain at strain-hardening than the ½"-round coupons.

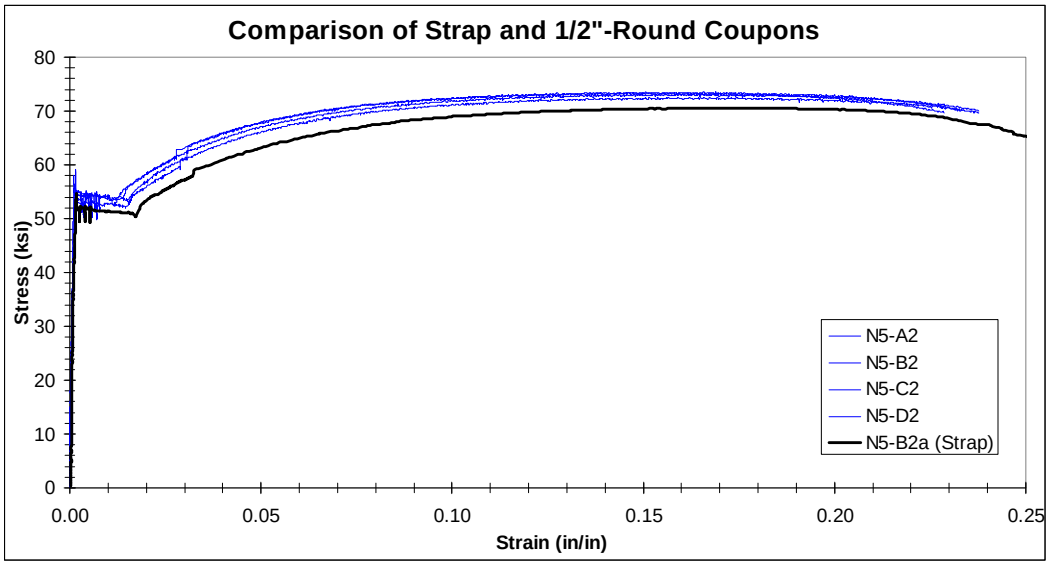

	f_y (ksi)		ε_{sh} (in/in)		f_u (ksi)	
	1/2" Round	Strap	1/2" Round	Strap	1/2" Round	Strap
Mean:	53.8	52.0	0.0119	0.0142	73.2	70.6
Maximum:	54.6	-	0.0138	-	73.6	-
Minimum:	53.0	-	0.0104	-	72.5	-
Std. Dev.	0.70	-	0.0017	-	0.49	-
# of Samples	4	1	4	1	4	1

Figure 4.3.1 Comparison of Strap and ½"-Round Coupons

As can be seen, the four ½"-round coupons, N5-A through N5-D, produced stress-strain curves that were very similar, showing that the flange material behaved almost uniformly throughout the section. The strap coupon

produced values of F_y and F_u slightly lower than the minimum values of the ½"-round, and a value of ε_{sh} higher than the maximum. It was assumed, therefore, that these differences were due to a variation in testing strain rate or coupon type, and not due to material variation. Figures 4.3.2-4.3.5 show the average strain rates along the yield plateau and around ultimate stress for Specimens N5-B2 (a ½"-round coupon) and N5-B2a (a strap coupon) taken from an adjacent location.

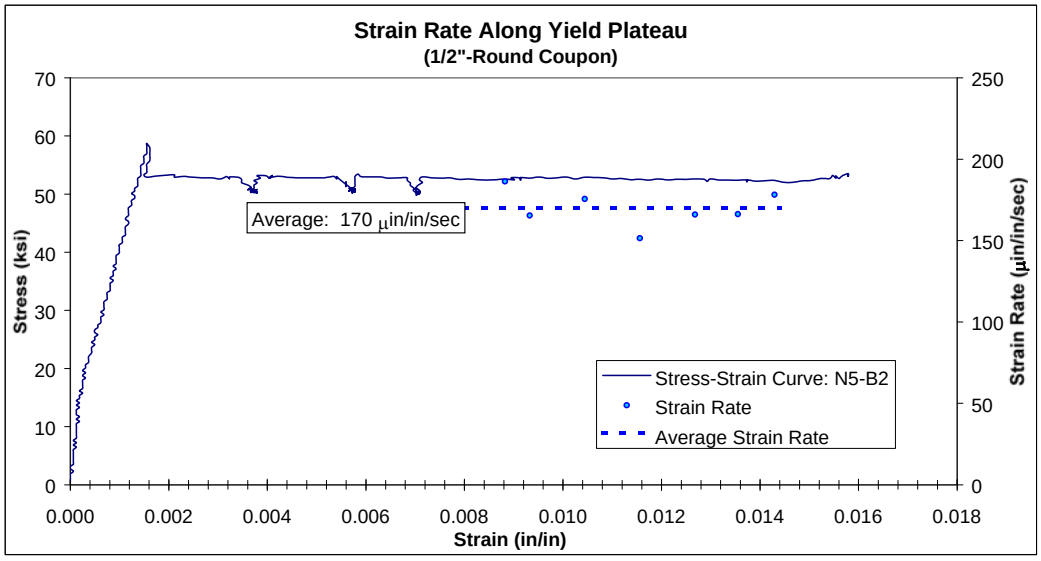

Figure 4.3.2 Strain Rate Along Yield Plateau for ½”-Round Coupon

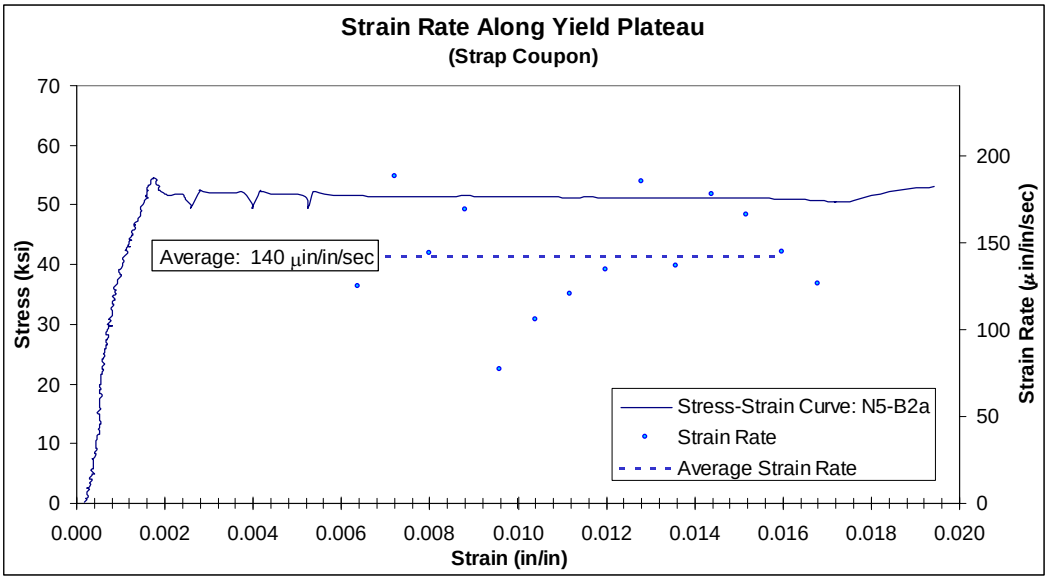

Figure 4.3.3 Strain Rate Along Yield Plateau for Strap Coupon

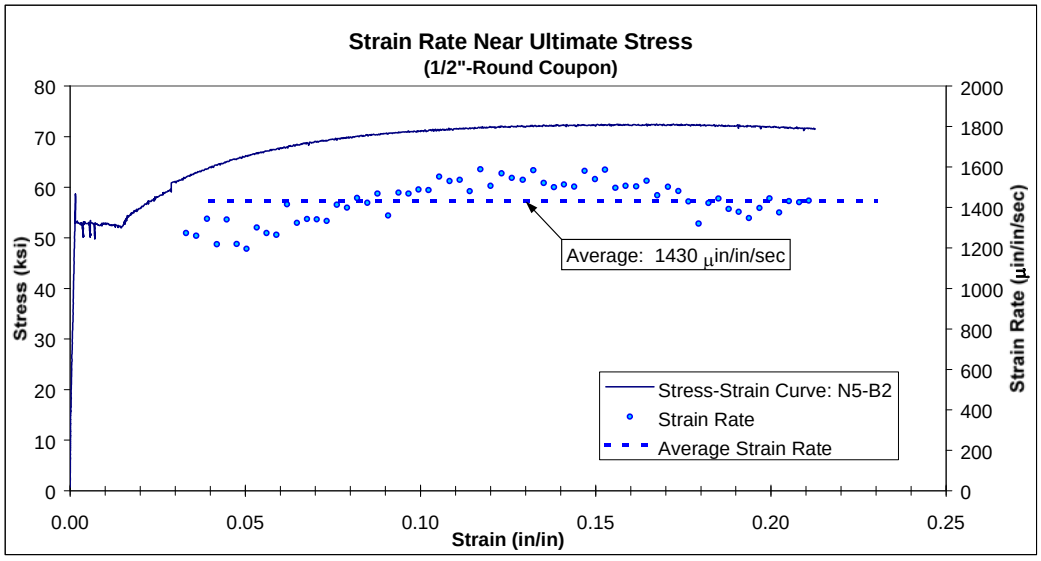

Figure 4.3.4 Strain Rate at Ultimate Stress for ½"-Round Coupon

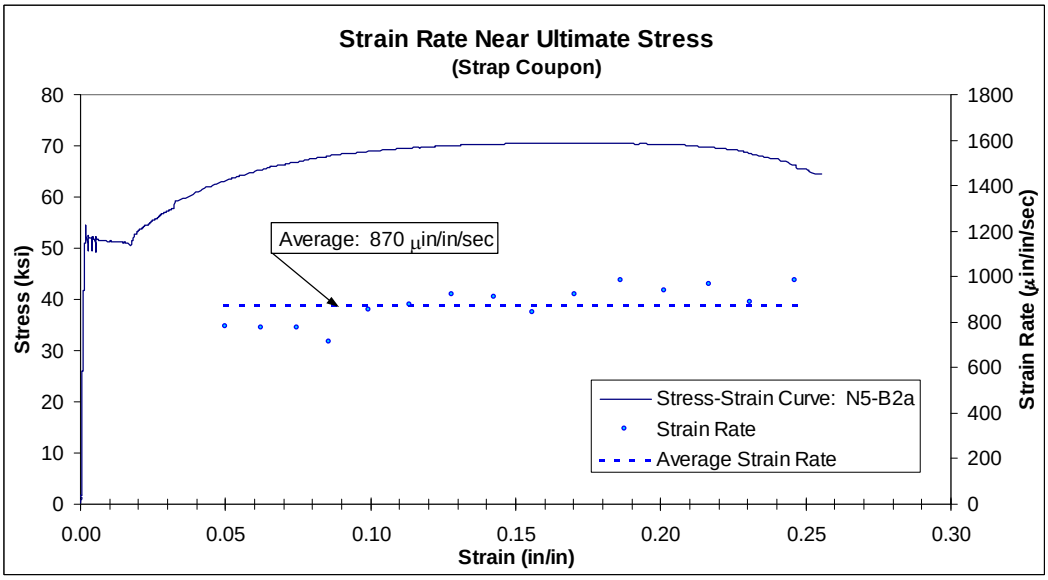

Figure 4.3.5 Strain Rate at Ultimate Stress for Strap Coupon

The individual strain rate points, shown on the graphs by the small circles, were calculated from the equation $\dot{\varepsilon} = \frac{\Delta\varepsilon}{\Delta t}$, where $\Delta\varepsilon$ is the change in strain and Δt is the time increment over which the change in strain occurs. These points were plotted in regions with fairly constant strain rates: the yield plateau past static yield tests, and the region around ultimate strength. The average strain rates were calculated by taking the mean of the strain rate points shown on the graphs.

Figures 4.3.2 and 4.3.3 show that the strain rates of both coupons were approximately the same along the yield plateau, but Figures 4.3.4 and 4.3.5 indicate that the strain rate of the ½"-round coupon was much higher (65%) than that of the strap coupon at ultimate strength. This increase in strain rate may account for the greater ultimate strength in the ½"-round coupon.

The differences in the stress-strain parameters of the ½"-round and strap coupons are shown in Table 4.3.1. Values of F_y, F_{sy}, F_u, ε_u, F_{uy}, ε_{sh}, and E_{sh} were tabulated for specimens N5-B2 and N5-B2a (the specimens taken from adjacent locations) and for the entire set of test data. The average strain rates are designated by $\Delta\varepsilon/\Delta t$.

Table 4.3.1 Stress-Strain Parameters of Strap vs. ½"-Round Coupons

Adjacent Locations

Coupon Type	F_{uy} (ksi)	F_y (ksi)	F_{sy} (ksi)	$\Delta\varepsilon/\Delta t$ (μin/in/sec)	ε_{sh} (in/in)	E_{sh} (ksi)	F_u (ksi)	ε_u (in/in)	$\Delta\varepsilon/\Delta t$ (μin/in/sec)
Strap	54.6	52.0	49.5	142	0.0142	387	70.6	0.158	870
1/2"-Round	58.7	53.0	50.1	170	0.0127	451	72.5	0.161	1430
% Change	7.5%	1.9%	1.3%	20%	-10.8%	16.6%	2.7%	2.2%	64.6%

All Data

Coupon Type	F_{uy} (ksi)	F_y (ksi)	F_{sy} (ksi)	ε_{sh} (in/in)	E_{sh} (ksi)	F_u (ksi)	ε_u (in/in)	Number of Specimens
Strap	57.1	55.6	53.3	0.0169	369	72.3	0.152	71
1/2"-Round	55.3	53.3	50.7	0.0113	447	72.0	0.145	35
% Change	-3.2%	-4.2%	-4.9%	-33.0%	21.0%	-0.5%	-4.4%	

In calculating the %Change, the strap coupon was the basis of comparison. For example, %Change in $F_y = (F_{yround}-F_{ystrap})/F_{ystrap}$. Also, the first set of strain rate measurements (fourth column from the left on the top chart) indicates the strain rates along the yield plateaus. The strain rates in the column on the far right reflect the increased loading rate used after the curves reached strain-hardening.

Based on data from the two coupons, coupon size did not affect F_y, F_{sy}, F_u, or ε_u, but might have influenced F_{uy}, ε_{sh}, and E_{sh}. The differences in F_y, F_{sy}, F_u, and ε_u were less than 3%, suggesting that all four factors were uninfluenced by the coupon type. As was stated earlier, the difference of 2.7% in the ultimate strength values could be due to the much higher strain rate in the ½"-round coupon. F_{uy} and E_{sh} were 7.5% and 16.6% higher and ε_{sh} was 10.8% lower in the ½"-round coupon than in the strap coupon, suggesting that these parameters might be influenced by coupon type. Data from the rest of the specimens show similar trends for E_{sh} and ε_{sh}, but the opposite trend for F_{uy}. Based on these tests then, it is concluded that the type of coupon used in the tensile tests affected the strain-

hardening modulus (E_{sh}) and the strain at strain-hardening (ε_{sh}). It may have also affected the upper yield point, but the test results were inconclusive.

4.4 SUMMARY OF STRESS-STRAIN BEHAVIOR

The following sections present the typical stress-strain behavior of flange material from ASTM A572 Grade 50 wide-flange sections. Mean values for the stress-strain parameters of F_{uy}, F_y, F_{sy}, ε_{sh}, E_{sh}, F_u, and ε_u were calculated from the 17 wide-flange members used in this study, and the results were compiled to create a typical flange stress-strain curve. The flanges were studied exclusively because the stress-strain behavior of the flange material influences the flexural behavior of a structural member much more than that of the web material.

4.4.1 Upper Yield Point (F_{uy})

The upper yield point phenomenon occurs often in ASTM A572 Gr. 50 and other low-strength structural steels. Designated in this report as F_{uy}, it is the peak stress immediately before the yield plateau and can be up to 10% greater than F_y. In most coupons exhibiting an upper yield point, the proportional limit coincides with F_{uy}. That is, the elastic region is relatively linear up to the point of yield. In the tests that do not show an upper yield point, the proportional limit occurs at some stress lower than F_y and the stress-strain curve shows a rounded transition from the elastic region to the yield plateau region. Examples of each kind of yield behavior are shown in Figure 4.4.1.

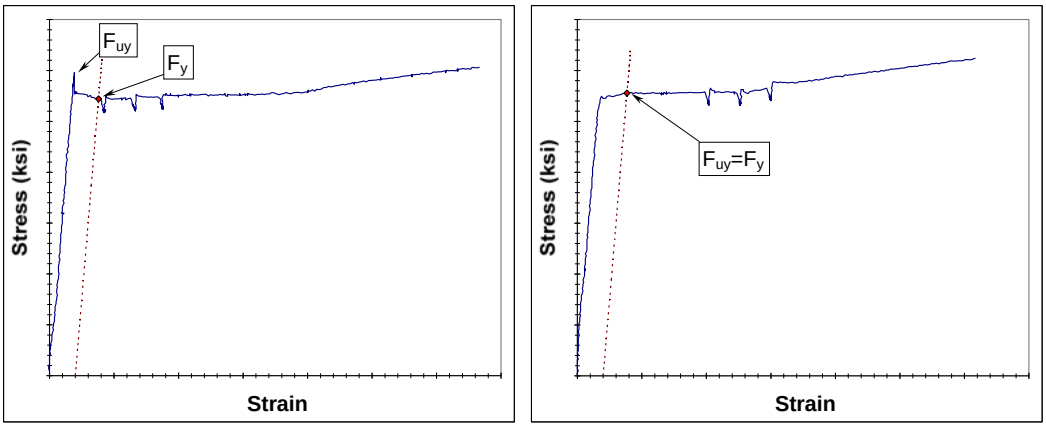

Figure 4.4.1 Examples of Upper Yield Point vs. Rounded Yield Transitions

These figures also illustrate the calculation method used to determine F_{uy}. In the tests where the stress-strain curve exhibited a peak at the end of the elastic range, F_{uy} was calculated as the maximum load divided by the undeformed cross-sectional area. In those cases where the stress-strain curve did not show a clear yield point but instead a rounded yield transition, F_{uy} was set to F_y, where F_y was calculated using the 0.2% offset method discussed in Section 4.4.2. Figure 4.4.1 shows examples of both types of behavior. Specimen T3-F on the left is a good example of a curve with an upper peak at the yield point. Specimen T3-A on the right shows a test in which there was no clear yield point, and F_{uy} was reported as equal to F_y.

A distribution of Upper Yield Point values obtained from the tension tests are shown in the histogram in Figure 4.4.2. The distribution is of results obtained from full-thickness strap coupons taken from the flanges of the rolled sections. Strap coupons were used exclusively because in Section 4.3 it was observed that

the Upper Yield Point values for a ½"-round and a strap coupon taken from the same location on a member were significantly different. Flange coupons are used because in Section 4.2 the web and flange yield strengths were found to differ significantly and because the flange material governs the flexural behavior of a rolled section. The F_{uy} values were plotted in relation to the nominal yield strength of ASTM A572 Gr. 50 steel (F_{yn}=50 ksi) in order to non-dimensionalize the graph.

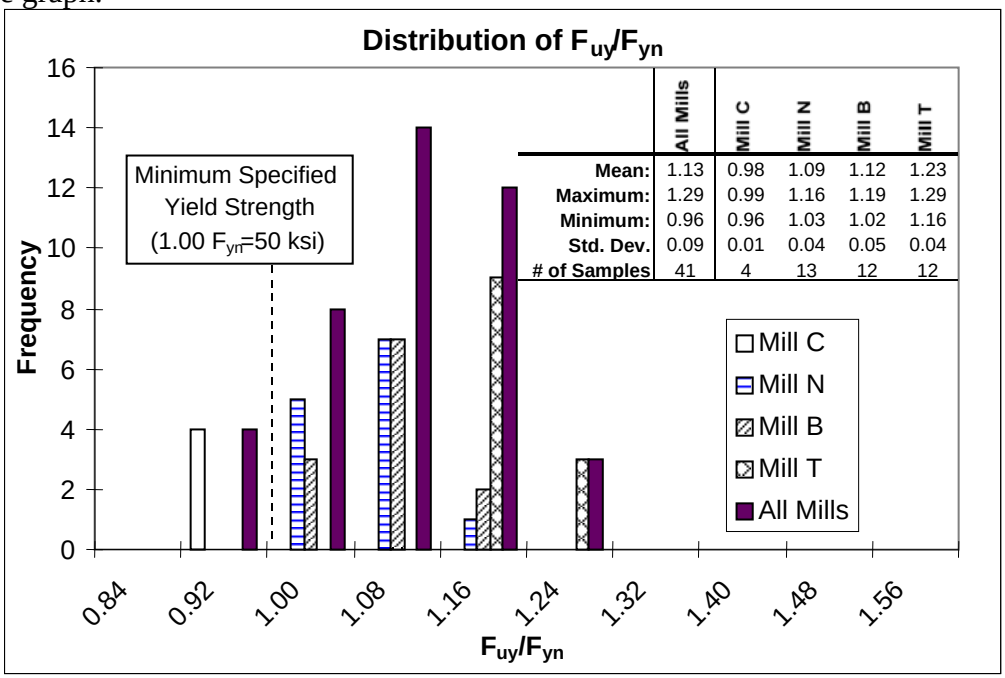

Figure 4.4.2 Distribution of F_{uy}/F_{yn}

The values of F_{uy}/F_{yn} ranged from 0.96-1.29, with an average of 1.13, corresponding to 56.5 ksi. Specimens from Mill C showed very low strength. As can be seen, all four specimens from Mill C fell below the minimum specified yield strength of 50 ksi, shown by the dashed line in the graph above. Mill T

showed the largest average value, 1.23, which corresponds to 61.5 ksi. Mills N, B, and T showed similar standard deviations. Mill C had the lowest standard deviation but no conclusions could be drawn about typical behavior because only one member was available to test.

The previous graph (Figure 4.4.2) was created from specimens that exhibited both Upper Yield Point behavior and rounded yield transition behavior. No distinction was made between the two types of behavior. In Figure 4.4.3, specimens that displayed upper yield point behavior were used to determine the typical magnitude of the stress peak, relative to the yield plateau. Only those members showing a clear Upper Yield Point were included; those with rounded elastic-to-yield transitions in which F_{uy} was set equal to F_y were not. The histogram in Figure 4.4.3 presents the distribution of F_{uy}/F_y for strap-type flange coupons that exhibit Upper Yield Point behavior similar to the example shown in Figure 4.4.1.

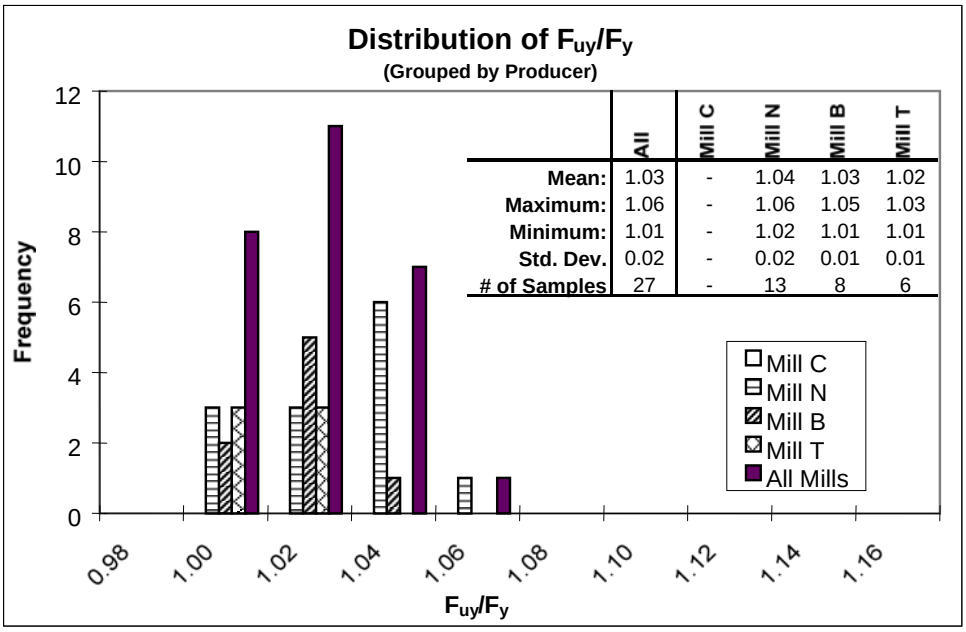

Figure 4.4.3 Distribution of F_{uy}/F_y for Specimens Exhibiting Upper Yield Point Behavior

Of the 41 strap-type coupons taken from flange material, 27 were found to exhibit Upper Yield Points. Of these 27 specimens, the most came from Mill N (13 of 13), followed by Mill B (8 of 12), Mill T (6 of 12) and Mill C (0 of 4). Ratios of F_{uy}/F_y for these specimens had a mean of 1.03, implying that for specimens that exhibit upper yield point behavior, the Upper Yield Point is around 3% larger than the plateau stress.

ASTM A370 permits steel producers to report F_{uy}, F_y, or any one of several other methods of estimating the plateau stress, as the yield strength of the steel. Since it is advantageous for the mills to use the highest possible value, in order to meet minimum strength requirements of ASTM A36 or A572, F_{uy} is generally reported. From an engineer's standpoint, however, the plateau stress,

F_y, is preferred. If it were possible to accurately and consistently convert from F_{uy} to F_y with a single conversion factor, the situation could be easily resolved, but problems arise when the relationship is examined.

The first problem is that there may or may not be an Upper Yield Point. In the tests performed for this project, an Upper Yield Point occurred in 27 out of 41 tests. The remaining 14 tests exhibited a rounded yield transition area in which F_{uy} was recorded as F_y. The second problem is the variability of the Upper Yield Point relative to the yield plateau stress. The magnitude of F_{uy} was shown to vary from 1-6% greater than F_y, with an average value of 3%. These problems associated with the high variability of F_{uy} suggest that it is a poor parameter to use in reporting the yield strength.

4.4.2 Yield Strength Plateau Stress (F_y)

The yield plateau stress is the parameter upon which most design specifications are based. To correctly model the behavior of any structural steel member or connection, an accurate estimation of F_y is necessary. Several methods exist for calculating the yield plateau stress: average plateau stress, stress at 0.5% strain, and 0.2% offset stress. The 0.2% offset method was chosen as the yield stress calculation method for this project but any other ASTM approved method would give comparable results.

The first step in calculating the yield plateau stress was to approximate the slope of the elastic portion of the stress-strain curve. Using linear regression, a best-fit line was drawn using the points on the elastic portion of the stress-strain

curve, up to the proportional limit. This was done only to eliminate some of the experimental errors and to obtain a more accurate value of F_y, not to measure Young's Modulus of Elasticity. This line was then offset by a strain of 0.002 to the right. The point where the stress-strain curve intersected the offset line was the 0.2% offset stress. This procedure is illustrated in Figure 4.4.4.

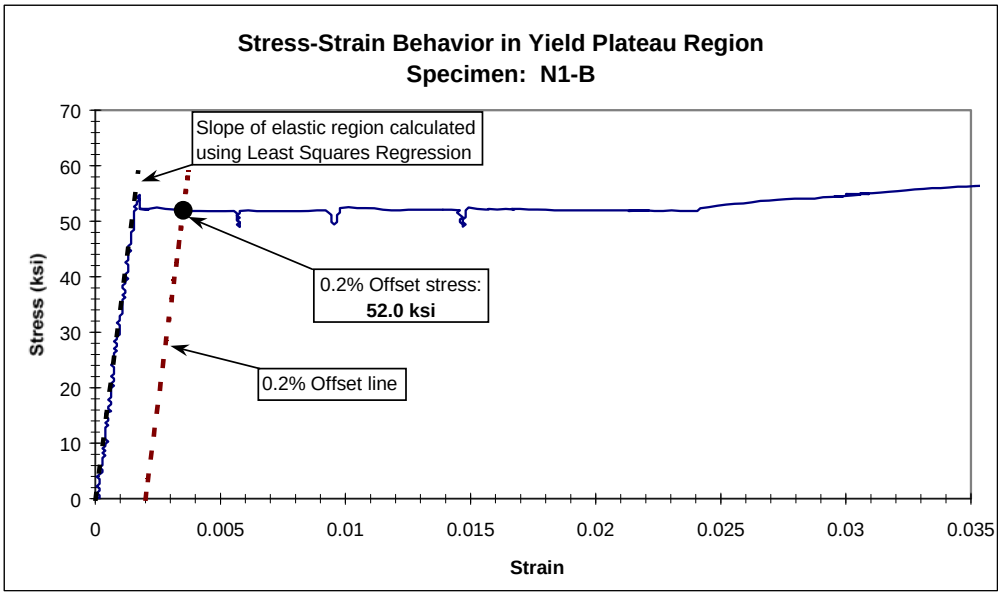

Figure 4.4.4 Method Used to Calculating 0.2% Offset Stress

The histogram in Figure 4.4.5 shows the distribution of the calculated values of F_y relative to the nominal yield strength (F_{yn}=50 ksi).

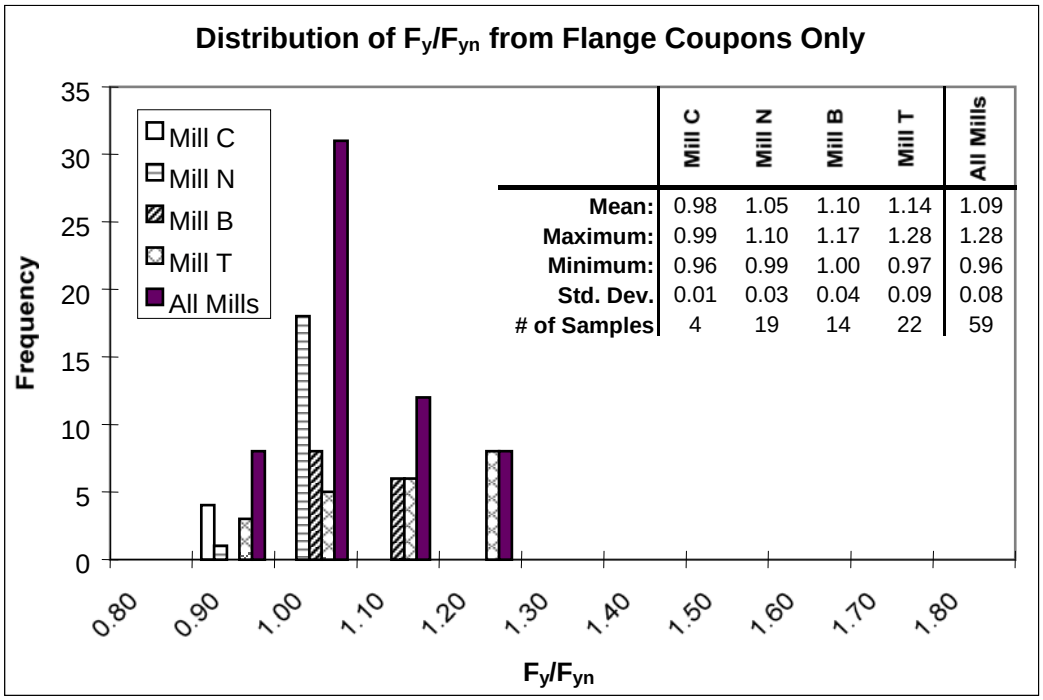

Figure 4.4.5 Distribution of F_y/F_{yn}

All four of the flange coupons from Mill C were found to have yield strengths below the nominal value. Of the remaining three mills, Mill T had the largest average yield strength and the greatest variation in test results. The standard deviation of 0.09 was more than twice the standard deviation of the next highest value, 0.04 from Mill B. One coupon from Mill N and three from Mill T had values of F_y below 50 ksi. The average yield strength of all mills combined was about 9% above the nominal strength, or 54.5 ksi.

4.4.3 Static Yield Stress (F_{sy})

The static yield stress is the stress level of a yielded specimen after being held for three minutes at a strain rate of zero. Static yield stress values were obtained during each tension test. When possible, three readings were taken from each specimen, but in some cases, the specimen reached its strain-hardening region before all three static readings were taken. Close examination of the stress-strain plots in Appendix C reveals that some static readings were performed after the coupons had reached strain hardening. In these cases, the readings were not used in this analysis of the test data. The static yield stress of a test specimen was calculated by taking the average of all usable static yield readings. Examples of usable and unusable readings are shown in Figure 4.4.6.

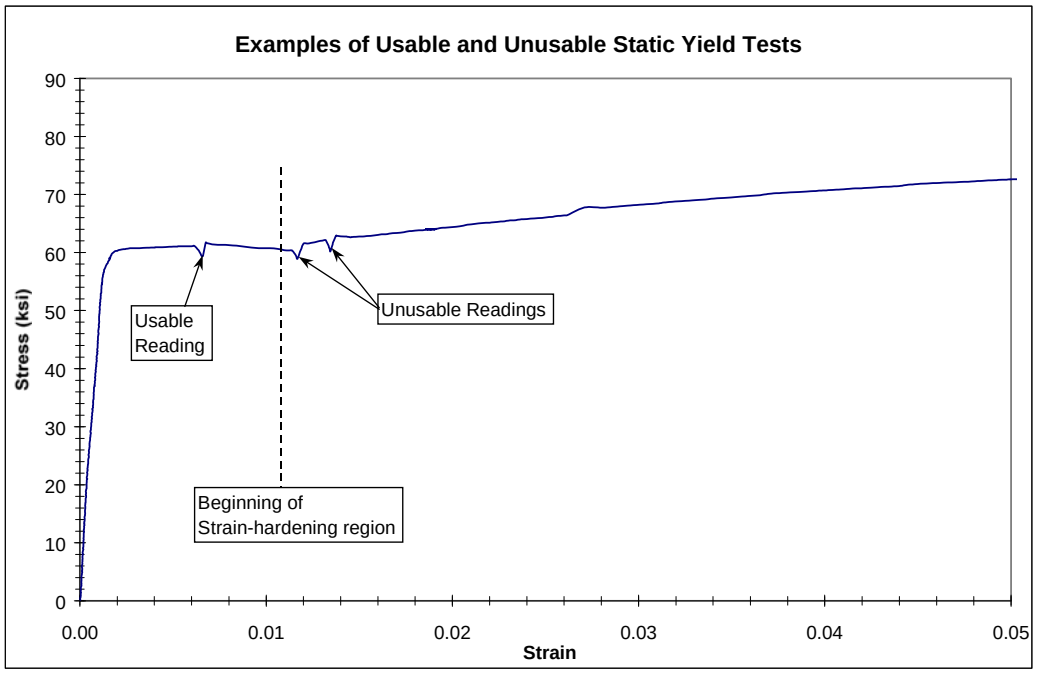

Figure 4.4.6 Examples of Usable and Unusable Static Yield Readings

Table 4.4.1 presents the static yield values of the specimens with three usable readings. Specimens with three readings only were used in this table so that the standard deviation of the individual F_{sy} readings could be used to compare the variability of the static yield within individual coupons. Comparing the standard deviation of two samples to that of three samples is an unfair comparison. The individual static yield values are shown under the headings of F_{sy1}, F_{sy2}, and F_{sy3}. The ratio of the average static yield reading to the yield strength of each coupon is given in the column labeled F_{sy}/F_y, and the column labeled S.D./F_y lists the standard deviation of the three individual readings divided by the yield strength. The maximum and minimum values of F_{sy}/F_y and S.D./F_y are shown in bold type. The small chart below the individual readings shows the average values of F_{ys}/F_y and S.D./F_y for the flange and web coupons.

Table 4.4.1 Individual Static Yield Readings and Variations

		F_{sy1}	F_{sy2}	F_{sy3}	F_{sy}/F_y	S.D./F_y
C1	**A**	45.4	45.6	45.7	0.948	0.00334
	C	45.7	45.9	45.8	0.935	0.00239
	D	46.6	46.3	46.5	0.941	0.00236
	E	48.4	48.5	48.6	0.942	0.00216
	F	49.7	49.5	49.8	0.946	0.00328
	G	47.5	47.8	47.8	0.958	0.00385
N1	**A**	48.9	48.7	49.0	0.951	0.00256
	B	48.9	49.4	49.0	0.946	0.00518
	C	49.7	49.7	49.2	0.956	0.00515
	D	48.7	49.1	49.0	0.940	0.00421
	E	50.6	50.3	50.2	**0.935**	0.00452
	F	52.4	52.3	52.4	0.945	0.00115
	G	51.5	51.9	51.1	0.943	0.00707
N2	**A**	52.8	53.0	53.1	0.967	0.00312
	E	54.0	53.9	53.8	0.955	0.00112
	F	55.5	55.4	55.3	0.957	0.00173
	G	53.6	53.9	53.8	0.962	0.00262
N3	**B**	49.0	49.2	49.7	0.963	0.00657
	D	48.3	48.5	48.6	0.959	0.00321
	F	53.8	52.8	53.1	0.968	**0.00983**
N4	**D**	49.1	48.6	48.9	0.961	0.00481
	F	49.4	49.3	49.2	0.955	0.00196
N5	**A**	51.1	51.5	51.3	0.959	0.00397
	B	50.2	50.2	49.8	0.945	0.00412
	C	51.8	51.7	51.6	0.948	0.00249
	D	51.3	51.6	51.8	0.952	0.00480
N5-2	**B**	49.5	49.5	49.4	0.951	0.00176
	F	56.4	56.4	56.0	0.955	0.00331
N6	**D**	49.2	48.9	48.4	0.946	0.00753
	F	47.6	47.7	47.1	0.942	0.00625
B1	**A**	54.1	54.2	54.3	0.976	0.00151
	B	55.5	55.8	56.0	0.971	0.00439
	C	56.0	56.1	56.1	0.977	0.00137
	E	55.8	56.2	56.0	0.972	0.00296
	F	55.8	55.5	55.4	0.966	0.00310
	G	56.9	56.6	56.8	0.963	0.00225
B2	**B**	51.7	51.6	51.7	0.955	0.00141
	D	50.6	50.7	50.8	0.955	0.00105
	E	51.1	51.1	51.1	0.948	**0.00047**
	F	50.2	50.0	49.6	0.951	0.00552
	G	50.2	50.4	50.4	0.954	0.00254
B3	**C**	50.2	50.3	49.8	0.956	0.00484
	D	49.0	49.2	49.5	0.980	0.00420
	E	49.2	49.2	49.0	0.951	0.00283
	F	51.8	51.8	51.4	0.950	0.00433
	G	49.0	48.7	48.8	0.945	0.00384
B4	**A**	53.1	52.7	53.3	0.962	0.00524
	B	52.0	51.7	51.9	0.944	0.00268
	C	53.4	52.8	52.8	0.950	0.00653
	D	52.3	51.7	52.0	0.960	0.00552
	E	55.0	54.4	54.1	0.953	0.00860
	F	60.8	59.9	59.9	0.951	0.00839
	G	56.4	56.4	56.3	0.954	0.00066
T1	**A**	59.3	58.9	59.0	0.971	0.00348
	B	55.2	54.7	54.6	0.962	0.00619
	C	57.1	57.4	57.2	0.954	0.00222
	D	56.7	56.4	56.4	0.974	0.00232
	G	47.0	46.8	46.6	0.951	0.00441
T2	**A**	46.1	45.9	45.7	0.944	0.00366
	B	47.4	48.0	47.6	0.957	0.00630
	C	45.5	45.6	45.4	0.942	0.00254
	E	45.3	45.4	45.4	0.958	0.00151
	F	50.2	49.5	49.8	0.943	0.00665
	G	46.6	46.0	45.8	0.940	0.00807
T3	**A**	53.2	53.1	54.1	0.963	0.00975
	B	53.2	53.6	53.9	0.950	0.00553
	C	49.8	49.9	50.2	0.958	0.00392
	D	51.7	51.7	51.9	0.956	0.00203
	F	51.7	52.0	52.4	0.956	0.00633
T4	**C**	60.0	60.2	60.5	**0.987**	0.00363
	D	60.2	60.0	60.1	0.971	0.00112
T5	**A**	57.3	57.1	57.4	0.944	0.00182
	B	61.7	62.0	61.9	0.969	0.00287
	C	57.9	58.0	58.0	0.956	0.00106
	D	60.2	60.4	60.3	0.974	0.00130
	E	52.2	51.9	51.9	0.958	0.00253
	F	57.6	57.7	57.8	0.967	0.00138
	G	54.9	54.8	54.8	0.964	0.00132

	$F_{sy\ ave}/F_y$	Std. Dev/F_y
Flange Only	0.957	0.0037
Web Only	0.953	0.0038
All Coupons	0.956	0.0038

Static yield readings showed very little variation within individual specimens. It was therefore concluded that one static yield reading anywhere along the yield plateau is more or less representative of the static yield strength of the material. Although data from the table show that the static yield strength was consistently around 4.6% lower than the yield strength, F_y, it should be noted that this parameter is sensitive to strain rate. If a different loading rate were used, the mean values for F_{sy}/F_y would vary accordingly.

The typical value of F_{sy}, shown in Figure 4.4.7, was obtained from flange coupons with at least one usable static yield reading. Both strap-type and ½"-round coupons were used in the calculations since the static yield strength was not found to be affected by the coupon type (Section 4.3). Figure 4.4.7 shows the distribution of F_{sy} relative to the nominal yield strength (F_{yn}=50 ksi) for the usable flange data.

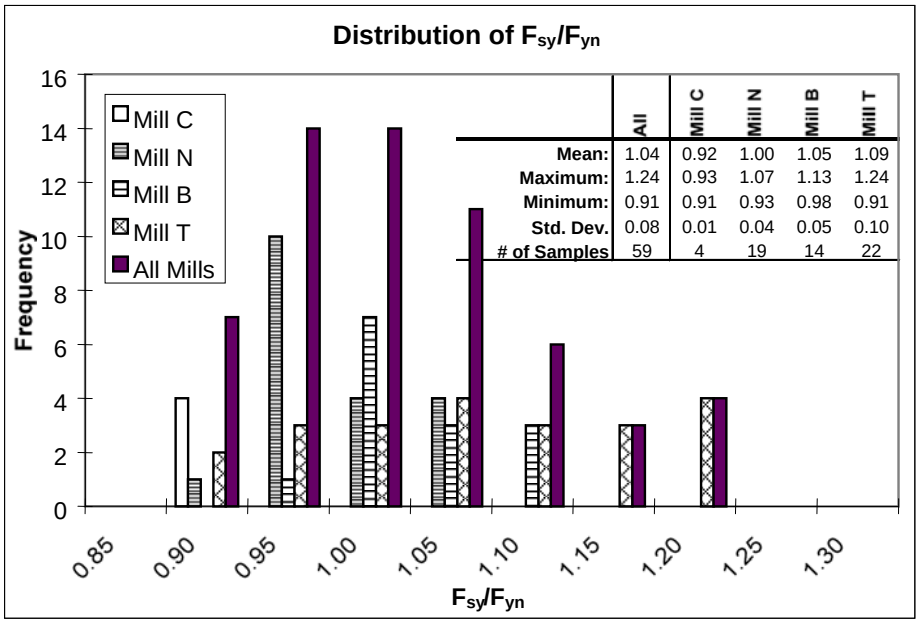

Figure 4.4.7 Distribution of Static Yield Data

The average static yield stress for all tests was $1.04 \cdot F_{yn}$, or 52.1 ksi, with a standard deviation of $0.08 \cdot F_{yn}$, or 4.1 ksi. Mill C showed the lowest strength, around $0.92 \cdot F_{yn}$, or 46.1 ksi—much lower than the nominal strength of 50 ksi. Mill T showed the greatest variation in static yield strength. Coupons from Mill T members exhibited both the highest (T5-B) and the lowest (T2-C) recorded values of F_{ys}. High variability was also observed from Mill T specimens in the Upper Yield Point (F_{uy}) and the yield strength (F_y) parameters.

4.4.4 Strain to Strain-Hardening (ε_{sh})

The strain at strain-hardening is an important indicator of a material's ductility, or its ability to redistribute loads. Ductile behavior is important in any

structure to accommodate any accidental overloads, but it is vital in seismic design. The current design philosophy assumes that in an earthquake, plastic hinges form in beams and undergo high levels of cyclic plastic rotation, both to accommodate displacements and to dissipate energy. Plastic design assumes that for a plastic hinge to form, the length of the yield plateau in the material needs to be around $10\varepsilon_y$ [Horne & Morris 1982.] This assumption was checked against measured values of ε_{sh} obtained in tensile tests, and observed trends were discussed.

Strain at strain-hardening can be defined as the point along the stress-strain curve at which the yield plateau ends and the strain-hardening region begins. Typical stress-strain curves do not exhibit a sharp transition at this point but rather a small dip immediately before strain-hardening, as is shown in Figure 4.4.8.

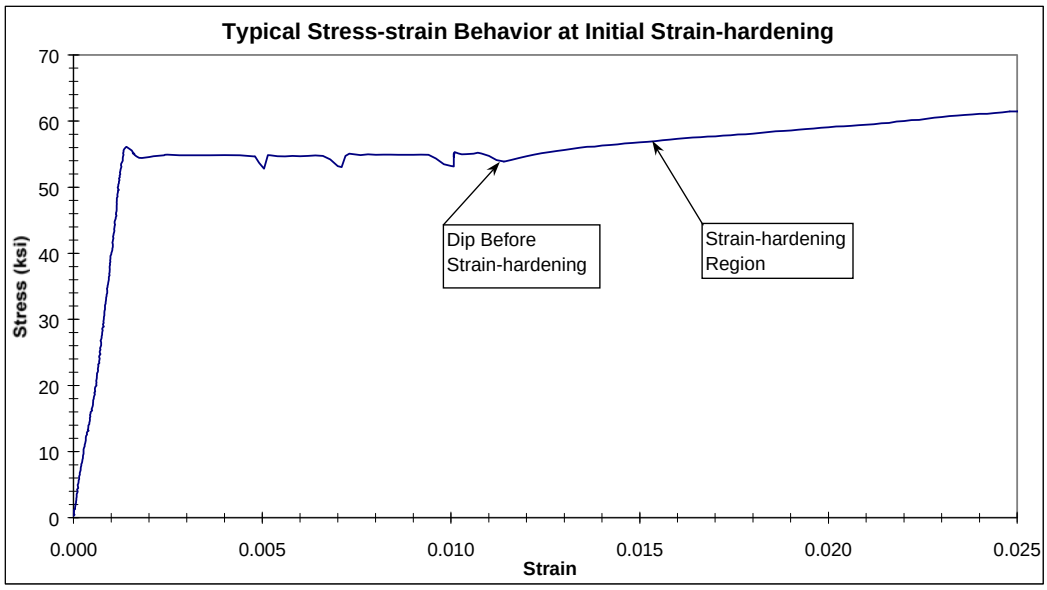

Figure 4.4.8 Typical Stress-strain Behavior at Point of Initial Strain-hardening

The exact location of the strain at strain-hardening was obtained using a method discussed in "Guide to Stability Design of Metal Structures" [1988]. The first step was to locate the dip before strain-hardening. Using this point as a reference, a line was drawn through two points along the stress-strain curve 0.003 in/in and 0.010 in/in to the right. The point where this line intersected the yield plateau was defined as ε_{sh}. Figure 4.4.9 illustrates the procedure used on the stress-strain curve of coupon N1-G.

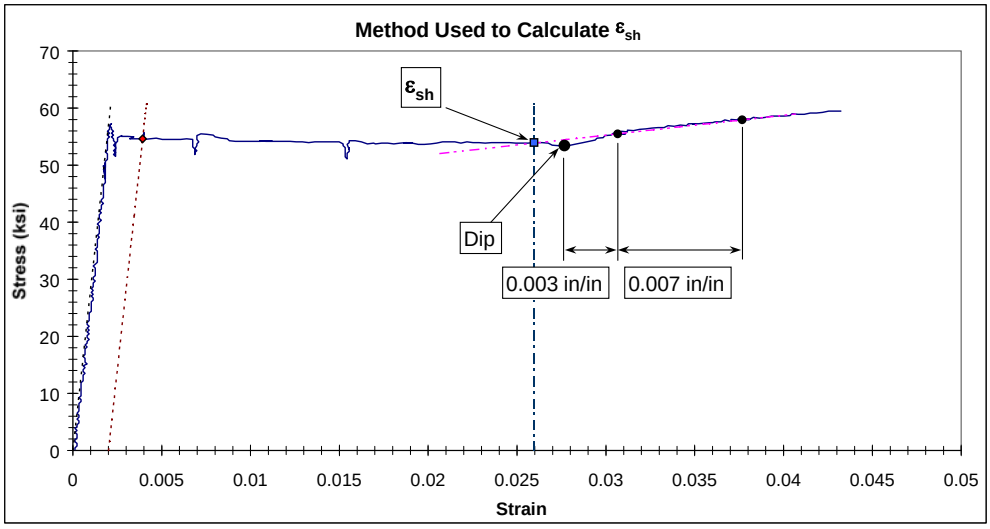

Figure 4.4.9 Method Used to Calculate ε_{sh}

The histogram shown in Figure 4.4.10 shows the distribution of ε_{sh} values obtained in the tension tests relative to the nominal yield strain, ε_{yn}. The nominal yield strain was obtained by dividing the nominal yield stress, 50 ksi, by Young's Modulus of Elasticity, 29000 ksi, resulting in ε_{yn}=0.001724. The values in the histogram were from full-thickness strap coupons taken from the flanges only. The reason for using strap coupons exclusively is that it was found in Section 4.3 that the coupon type may influence ε_{sh}.

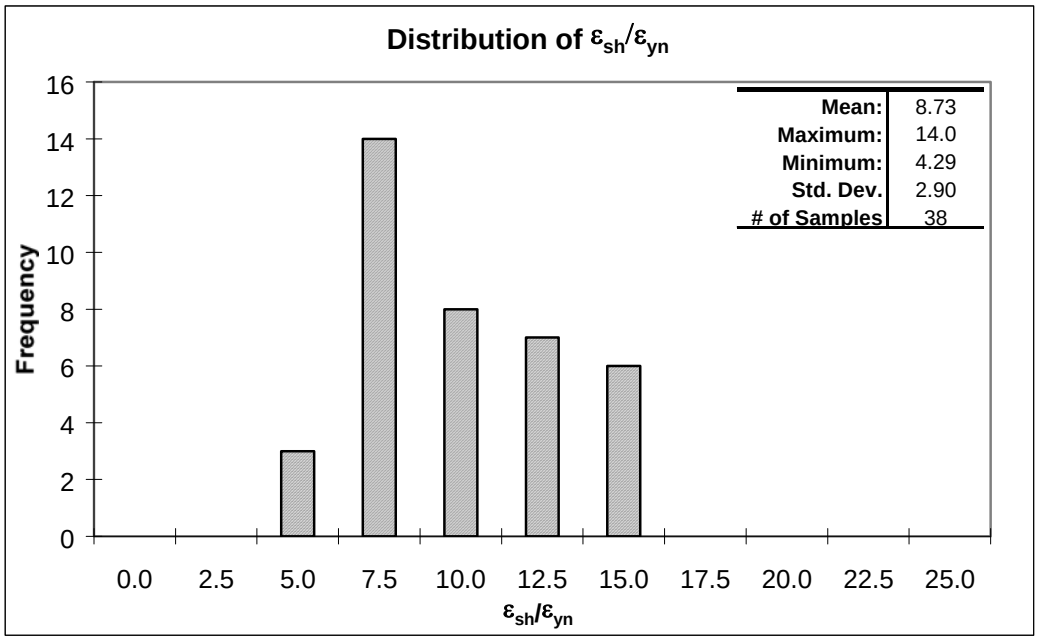

Figure 4.4.10 Distribution of $\varepsilon_{sh}/\varepsilon_{yn}$

As can be seen, the length of the yield plateau is well below the assumed value of $10\varepsilon_{yn}$ for many of the specimens. The mean value, 8.73, corresponds to a yield plateau length of

$$8.73\ \varepsilon_{yn}-1.00\varepsilon_{yn}=7.72\ \varepsilon_{yn}$$

The data show that overall, the members did not meet expected ductility requirements. Further analysis was performed to see if all four mills followed this trend, or if it was an isolated case. Table 4.4.2 summarizes the $\varepsilon_{sh}/\varepsilon_{yn}$ values for each of the producers.

Table 4.4.2 Summary of $\varepsilon_{sh}/\varepsilon_{yn}$ Grouped by Producer

	All	Mill C	Mill N	Mill B	Mill T
Mean:	8.73	9.54	8.09	8.68	9.25
Maximum:	14.0	10.2	12.9	12.5	14.0
Minimum:	4.29	8.89	4.29	5.34	4.87
Std. Dev.	2.90	0.58	3.29	3.04	2.95
# of Samples	38	4	13	10	11

Mill N showed the lowest mean and the highest standard deviation. The smallest recorded value of $\varepsilon_{sh}/\varepsilon_{yn}$ came from N2-B, a coupon from a W30x211 member from Mill N. Members from Mill C had the highest average values of strain-at-strain-hardening, but since only four samples were available, no conclusions can be drawn about overall behavior.

Next, the data were split up into two groups to see if ε_{sh} was affected by member size. Coupons taken from W14x211 or W14x311 members were considered "column" specimens, and the rest were considered "beam" specimens. A histogram showing the distributions of the column specimens and the beam specimens is shown in Figure 4.4.11.

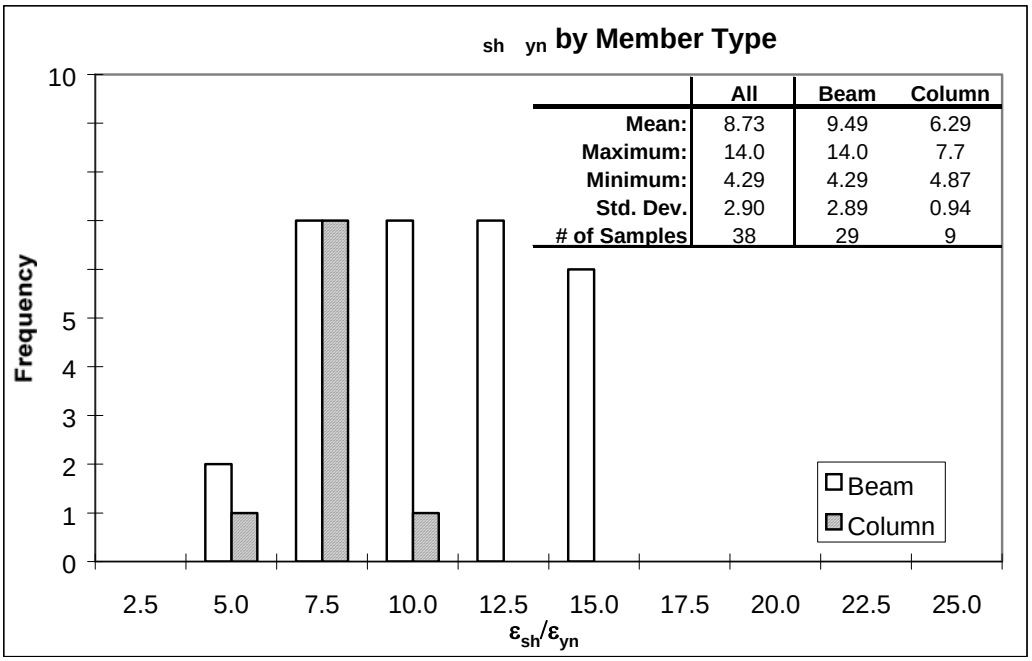

Figure 4.4.11 Distribution of $\varepsilon_{sh}/\varepsilon_{yn}$ (Grouped by Member Type)

The beam coupons showed significantly higher values of $\varepsilon_{sh}/\varepsilon_{yn}$ than did the column coupons. Average ε_{sh} values were $9.49\varepsilon_{yn}$ for beams and $6.29\varepsilon_{yn}$ for columns. Full-thickness strap coupons taken from the flanges were used in these calculations so that the effects of coupon type (strap vs. ½"-round) and location (flange vs. web) could be eliminated. It is therefore concluded that the differences shown in the figure above are due to material variation, and that the beam flange material was more ductile than the column flange material. However, even though the beam coupons showed longer yield plateaus than the column coupons, they were still well short of the yield plateau length of $10\varepsilon_y$ assumed for plastic design.

4.4.5 Strain-Hardening Modulus (E_{sh})

The strain-hardening modulus is an estimate of the initial slope of the stress-strain curve at strain-hardening. To accurately model any structural element that reaches a strain higher than ε_{sh} at any part of the cross section, the increase in stress due to E_{sh} must be taken into account.

The method used to calculate E_{sh} was similar to the one presented in Section 4.4.4, used to calculate the strain at which strain-hardening begins (ε_{sh}). In Figure 4.4.12, the strain-hardening modulus is set equal to the slope of the sloped dashed line.

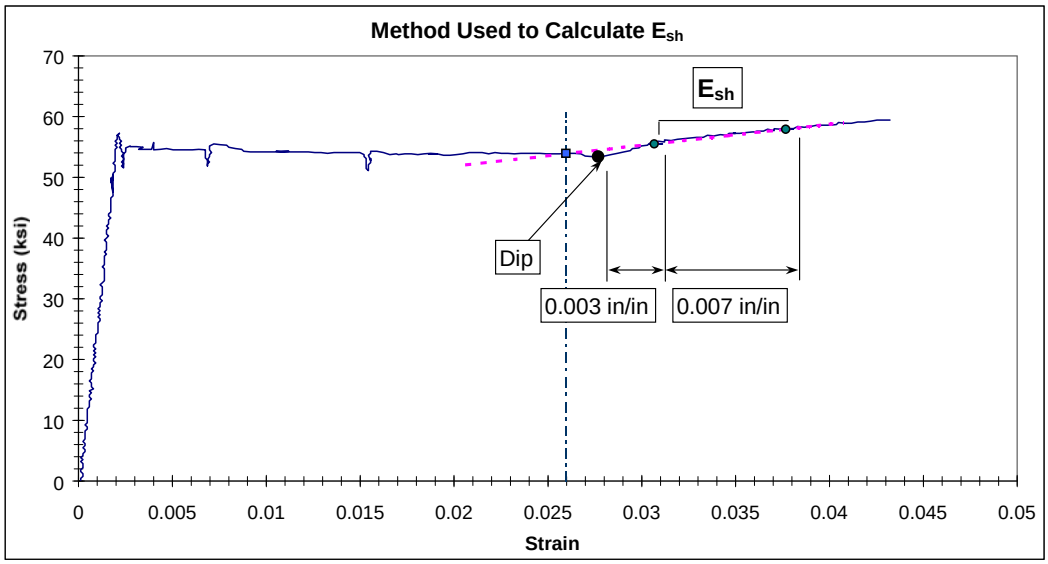

Figure 4.4.12 Method Used to Calculate Strain-hardening Modulus

The distribution of the calculated values of E_{sh}/E is shown in Figure 4.4.13. Full-thickness strap coupons taken from the flanges were used exclusively in this analysis because, as was discussed in Section 4.3, the coupon type may affect the strain-hardening modulus.

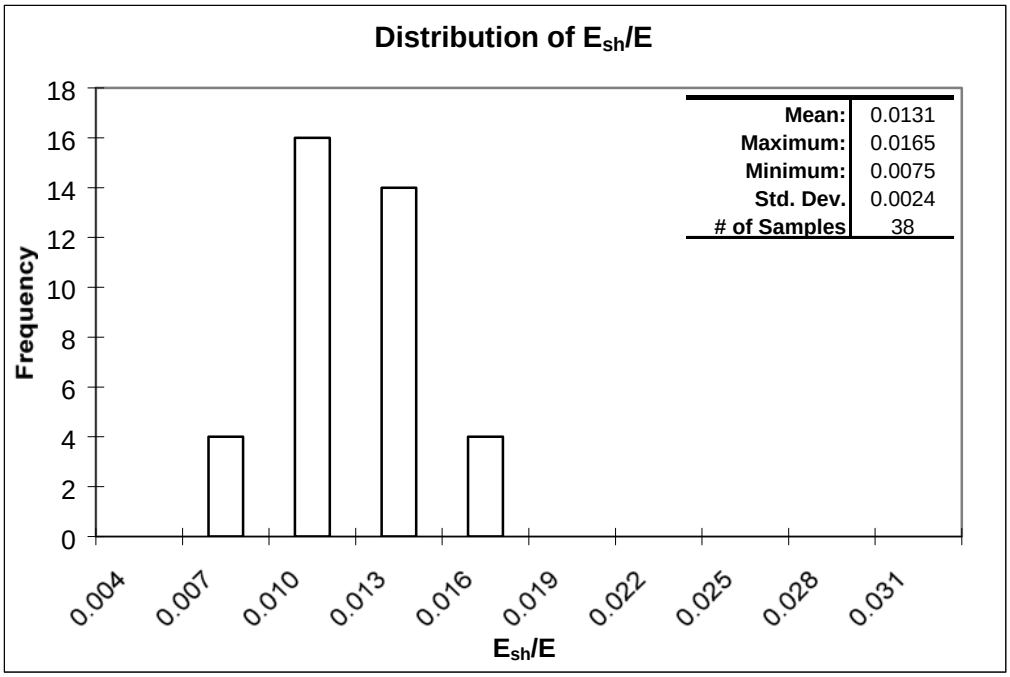

Figure 4.4.13 Distribution of E_{sh}/E

The mean value of E_{sh} was 0.0131·E, or 380 ksi, with a standard deviation of 0.0024·E, or 68 ksi. Compared to some other parameters, there was relatively little scatter in the distribution of E_{sh}.

4.4.6 Strain at Ultimate Stress (ε_u)

The strain at ultimate stress, ε_u, is the point along the strain axis at which the stress-strain curve reaches a maximum. This is not to be confused with the strain at fracture. After reaching its ultimate stress, the tensile coupon undergoes significant strains as it necks down, leading to fracture.

The measurement technique used to obtain ε_u, compared to those used in the other stress-strain parameters, was rather subjective. As a typical stress-strain curve approaches its ultimate stress, the slope of the curve decreases until it is almost flat, as can be seen in the stress-strain curves in Appendix C. This makes it difficult to determine the exact location of ε_u, since any point with a stress of F_u can be considered ε_u. The subjectivity involved in the estimation introduced some uncertainty into the readings, but for the purposes of this report, the measurements of ε_u were considered accurate to within ±0.01 in/in.

Figure 4.4.14 shows the distribution of $\varepsilon_u/\varepsilon_{yn}$ over the set of flange data, where ε_{yn} is the nominal strain at yield (50 ksi/29000 ksi). Both strap and ½"-round coupons were used in the analysis because coupon type was not found to affect ε_u (Section 4.3).

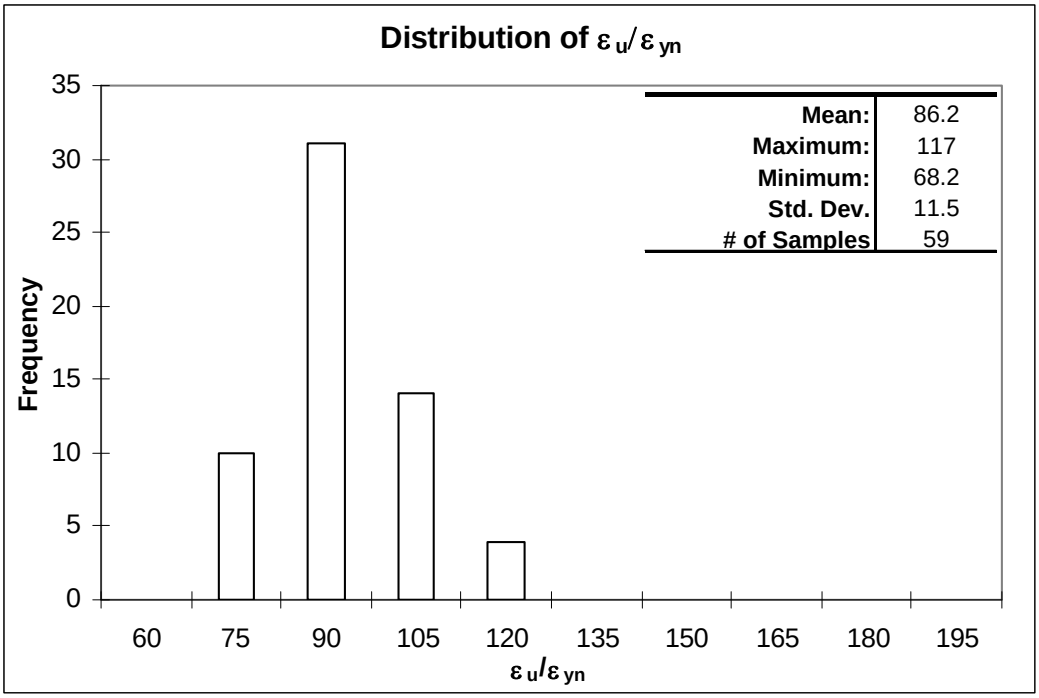

Figure 4.4.14 Distribution of $\varepsilon_u/\varepsilon_{yn}$

The average strain at ultimate stress, ε_u, was found to be $86.2 \cdot \varepsilon_{yn}$ with a standard deviation of $11.5 \cdot \varepsilon_{yn}$. The values ranged from $68.2 \cdot \varepsilon_{yn}$ (0.118 in/in) to $117 \cdot \varepsilon_{yn}$ (0.202 in/in). The range of values can be rounded to 0.11-0.21 in/in due to the uncertainty inherent in the measurement technique.

4.4.7 Ultimate Strength (F_u)

The ultimate strength is the largest stress a material can reach before it fractures. It is used explicitly in connection design to calculate the tensile strength of net sections and bearing capacity of bolted connections. The minimum allowable ultimate strength of ASTM A572 Gr. 50 is 65 ksi. The

histogram in Figure 4.4.15 shows the distribution of F_u/F_{yn} for flange coupons. The minimum specified strength of 65 ksi was plotted to show that all coupons exceeded the minimum allowable tensile strength.

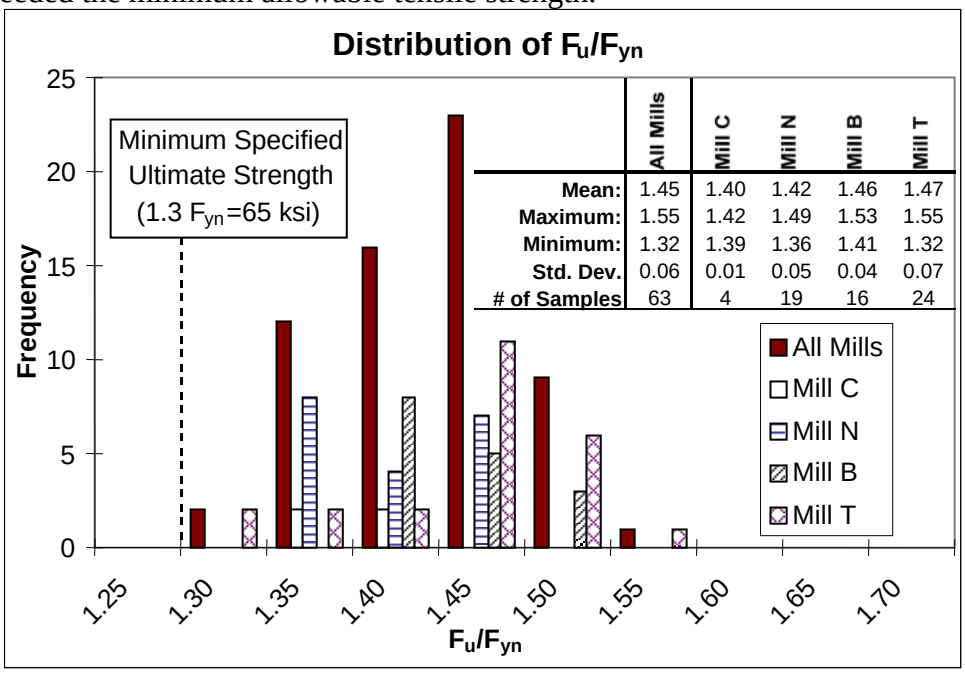

Figure 4.4.15 Distribution of F_u/F_{yn}

The average value of F_u/F_{yn} was 1.45, which corresponds to 72.3 ksi. As with the other strength parameters, Mill T showed the highest variability. Specimen T2-A had the lowest recorded ultimate strength—1.32·Fyn, or 66.1 ksi—but even it was above the minimum of 65 ksi.

The ratio of yield strength to ultimate strength, F_y/F_u, is a very important parameter of structural steel. Essentially, it describes the amount of post-yield load the material can handle before fracture. In an earthquake, structural engineers count on plastic hinges to absorb some of the seismic energy and to

dampen out the building motion. The lower the ratio of F_y/F_u, the more energy the hinge can absorb.

The new ASTM steel will specify a maximum F_y/F_u ratio of 0.85. As a basis of comparison, the nominal value for A36 steel is 36 ksi/58 ksi=0.62, and the nominal value for A572 Gr. 50 steel is 50 ksi/65 ksi=0.77. Figure 4.4.16 shows the measured values of F_y/F_u for the entire set of test specimens.

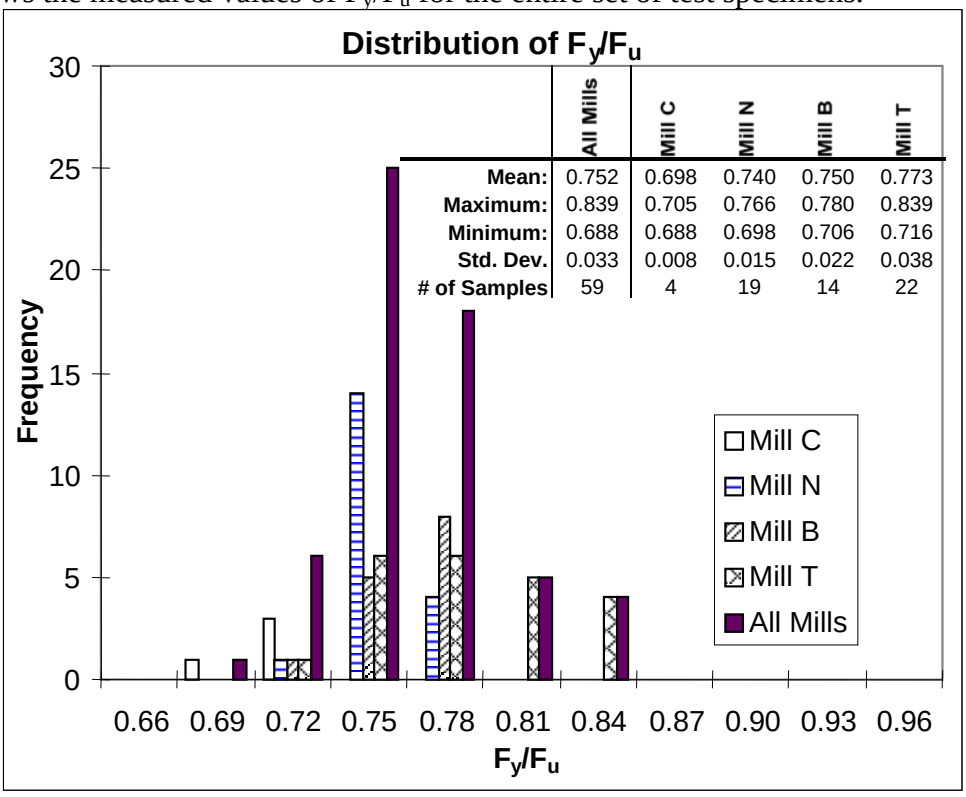

Figure 4.4.16 Distribution of F_y/F_u

The global mean is less than the nominal value of 0.77, indicating that overall the material exhibited adequate post-yield behavior. Mill T had the highest average value and Mill C the lowest. Mill T also had the highest

individual value, 0.839, but even it was below the maximum F_y/F_u ratio allowed in the specification for ASTM Gr. 50 steel with Special Provisions.

The results were then broken down even further to see the behavior of individual members. Table 4.4.3 lists the average F_y/F_u for each shape tested.

Table 4.4.3 Average F_y/F_u for Individual Members

Shape	Mill C	Mill N	Mill B	Mill T
W24x62	0.711	0.774		
W24x162				0.775
W30x211		0.753		0.743
W36x300		0.756	0.738	0.764
W14x211		0.741	0.766	0.795
W36x150		0.746	0.792	**0.823**
W14x311		0.717	0.732	0.735

All sections had F_y/F_u ratios below the new ASTM maximum of 0.85. The highest value came from the W36x150 section from Mill T (shown in bold) suggesting that this member would have a relatively small amount of post-yield load carrying capacity.

In conclusion, all test data show ultimate strength values above the ASTM required minimum of 65 ksi. Overall, the members showed adequate F_y/F_u ratios, implying good post-yield load capacity, but the W36x150 section from Mill T reported a value of 0.823—very near the upper limit of 0.85 specified in the new ASTM Gr. 50 with Special Requirements. A reason for the high value could be that the member was highly stressed during rolling and experienced some strain-aging.

4.5 TEST DATA VS. MILL TEST REPORTS

Steel mills are required to test coupons from each heat of steel, and report the results in what is called a mill test report. These tests verify that the steel meets the ASTM specified strength and ductility; they are not meant to be used in structural analysis or design. A paper by Beedle and Tall in 1959 states that the reported mill yield strength routinely overestimates the true flange static yield strength by 14-32%, due to three main factors: the upper yield point phenomenon (0-10%), strain rate effects (10-15%), and coupon location (4-7%). Figure 4.4.1, taken from their paper, illustrates the effects of these factors on the basic behavior of mill and laboratory tension tests.

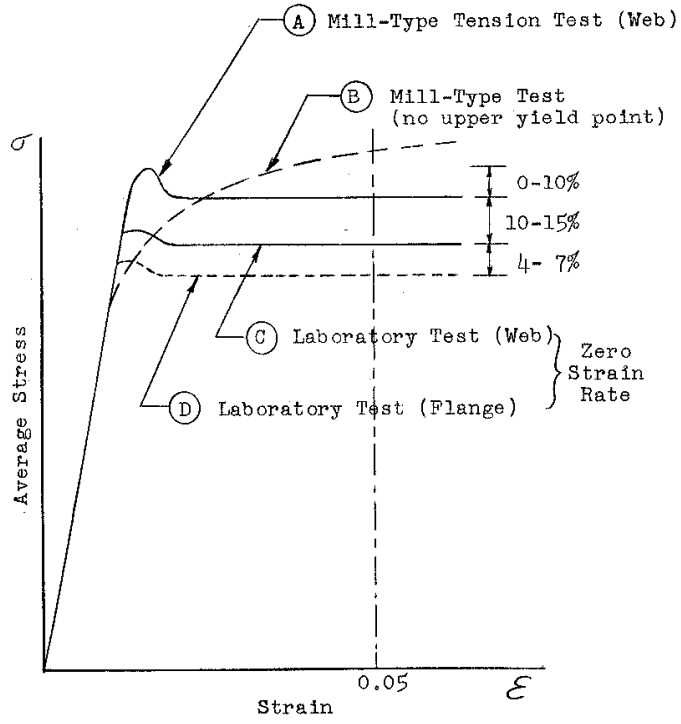

Figure 4.5.1 Influence of Different Variables on Laboratory vs. Mill Test Results

It should be noted that at the time Beedle and Tall were conducting this study, it was typical mill practice to take the tension specimens from the web of the rolled section. Today, mills are required to test coupons taken from the flange, thereby removing the estimated 4-7% flange vs. web effect shown above.

4.5.1 Estimating Stress-Strain Parameters from Mill Report Values

The relationships between the measured stress parameters and their reported mill test values were observed. Figure 4.5.1 shows the distribution of F_{uy}, F_y, and F_{sy}, relative to F_{ymill}, and F_u relative to F_{umill}. The histogram represents flange material only, since the flange properties have more influence on the flexural behavior of a wide-flange shape than do the web properties.

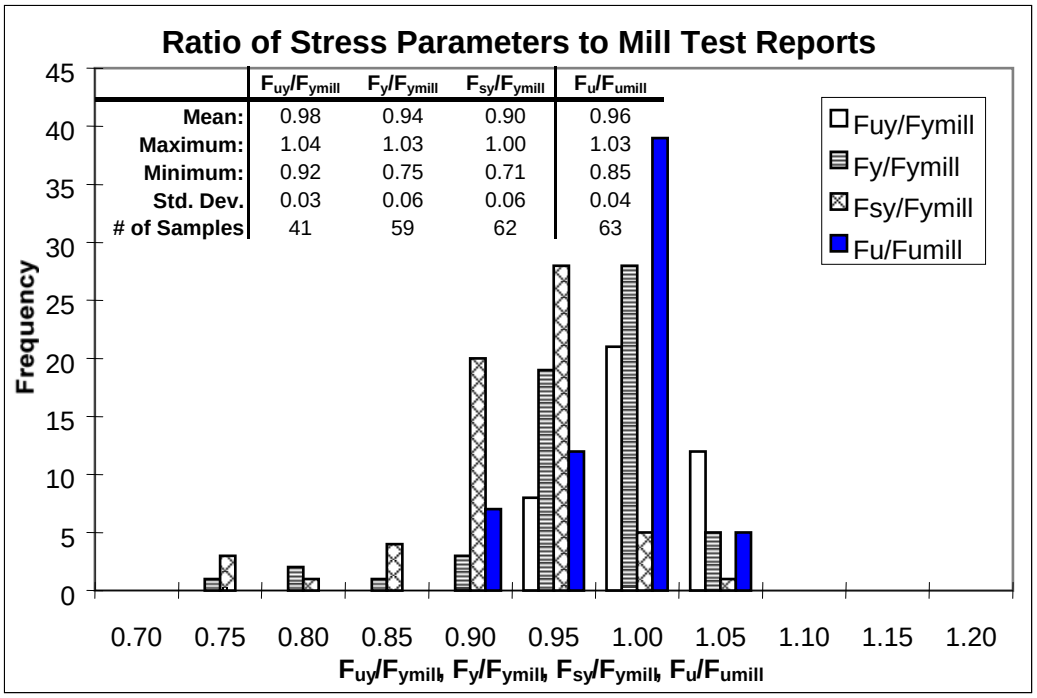

Figure 4.5.1 Distribution of Stress Parameters Relative to Mill Test Values

The average values of F_y/F_{ymill} and F_{sy}/F_{ymill} were 0.94 and 0.90, respectively, suggesting that good estimates of F_y and F_{sy} are around 95% and 90% of F_{ymill}. The observed value of F_u/F_{umill} was also about 95%.

Percent elongation is a measure of the ductility of a coupon at fracture. ASTM A572, Table 3 makes a distinction between the minimum allowable %Elongation of tensile specimens with 8-inch gage lengths (full-thickness strap coupons) and 2-inch gage lengths (½"-round coupons). Since all mill tests were performed with strap coupons, the reported total elongation values were compared to test values obtained from strap coupons. Figure 4.5.2 shows the distribution of $\%Elong_{meas}/\%Elong_{mill}$ for each mill separately and then for all mills combined. The variable $\%Elong_{meas}$ was the average value of %Elongation for all coupons in

a given section—flange coupons were averaged with web coupons. The mill test certificate value is given by $\%Elong_{mill}$. Where two values were given in the mill test certificates, $\%Elong_{mill}$ is the average of the two.

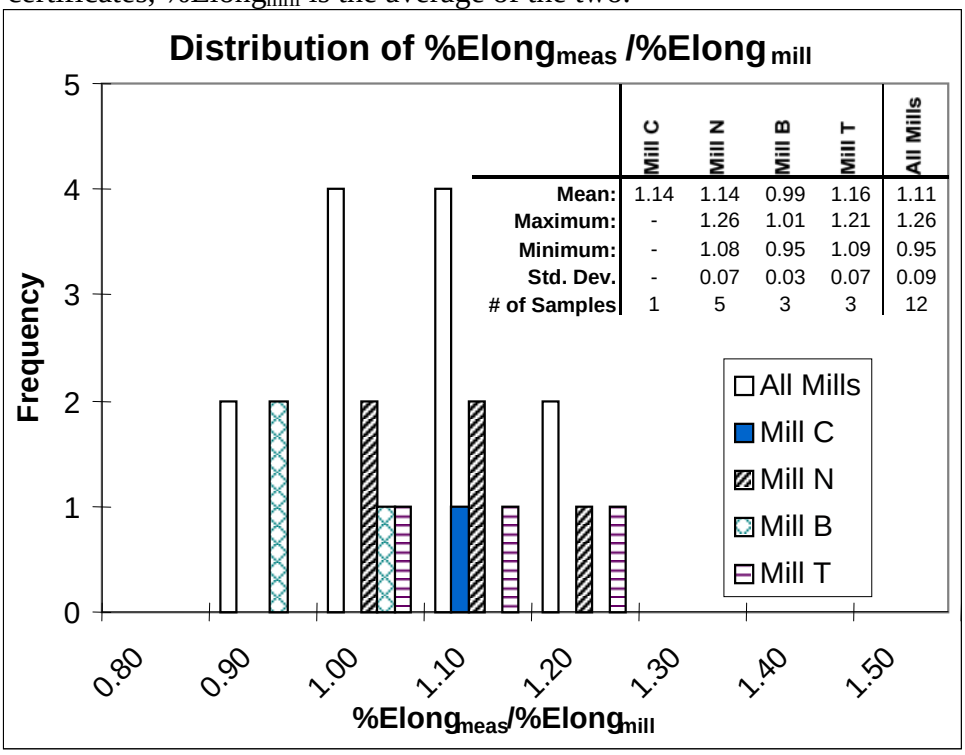

Figure 4.5.2 Distribution of $\%Elong_{meas}/\%Elong_{mill}$

Only two members—both from Mill B—had measured values of %Elongation below those in the mill test reports. All other measured values were well above the mill test values, probably due to the faster loading rates used by the mills in their tension tests.

4.5.2 Comparison of Individual Test Results with Mill Report Values

The three parameters given in the mill test reports—yield strength (F_{ymill}), ultimate strength (F_{umill}), and percent elongation ($\%Elong_{mill}$)—were compared with measured values of F_{uy}, F_y, F_{ys}, F_u, and %Elongation in Tables 4.5.1-4.5.4. Each table represents the entire set of data for an individual producer, and values in bold indicate unusually high differences between measured and mill test values.

Table 4.5.1 Tensile Test Data vs. Mill Report Values (Mill C)

			f_{uy} (ksi)	f_y (ksi)	f_{sy} (ksi)	f_u (ksi)	f_{uy}/f_{ymill}	f_y/f_{ymill}	f_{sy}/f_{ymill}	f_u/f_{umill}	% Elon.
Mill C	**C1 W24x62**	**Top Flange**	48.1	48.1	45.6	69.9	0.93	0.93	0.88	0.98	27.7%
			49.4	49.4	46.5	70.9	0.95	0.95	0.90	1.00	28.1%
		Bottom Flange	49.0	49.0	45.8	69.5	0.94	0.94	0.88	0.98	27.7%
			49.5	49.4	45.9	70.2	0.96	0.95	0.89	0.99	27.7%
		Web	53.3	51.5	48.5	71.5	1.03	0.99	0.94	1.00	26.2%
			56.8	52.5	49.6	70.2	1.10	1.01	0.96	0.99	26.6%
			51.2	49.8	47.7	69.7	0.99	0.96	0.92	0.98	26.2%
		Mill Tests	51.9			70.8					23.6%
			51.8			71.7					24.2%

Table 4.5.2 Tensile Test Data vs. Mill Report Values (Mill N)

				f_{uy} (ksi)	f_y (ksi)	f_{sy} (ksi)	f_u (ksi)	f_{uy}/f_{ymill}	f_y/f_{ymill}	f_{sy}/f_{ymill}	f_u/f_{umill}	% Elon.
Mill N	N1	W24x62	Top Flange	52.1	51.4	48.8	68.0	0.96	0.94	0.90	0.98	29.7%
				54.7	52.0	49.1	68.1	1.00	0.95	0.90	0.98	27.3%
			Bottom Flange	54.1	51.8	49.6	68.3	0.99	0.95	0.91	0.98	27.7%
				53.0	52.1	48.9	68.0	0.97	0.96	0.90	0.98	30.1%
			Web	54.0	53.9	50.4	68.6	0.99	0.99	0.92	0.99	27.8%
				57.4	55.4	52.4	69.3	1.05	1.02	0.96	1.00	28.1%
				57.3	54.6	51.5	69.1	1.05	1.00	0.95	0.99	29.3%
			Mill Tests	54.0			69.0					25.0%
				55.0			70.0					27.0%
	N2	W30x211	Top Flange	56.1	54.8	53.0	73.5	0.98	0.95	0.92	0.99	27.6%
				58.1	54.8	52.9	74.3	1.01	0.95	0.92	1.00	28.8%
			Bottom Flange	56.7	54.4	52.7	73.7	0.99	0.95	0.92	0.99	29.2%
				56.4	54.9	53.3	74.2	0.98	0.96	0.93	1.00	26.4%
			Web	57.6	56.4	53.9	73.3	1.00	0.98	0.94	0.98	26.2%
				59.5	57.9	55.4	74.0	1.0	1.01	0.96	0.99	26.6%
				57.7	55.9	53.8	73.4	1.00	0.97	0.93	0.99	25.9%
			Mill Tests	57.0			75.0					24.0%
				58.0			74.0					25.0%
	N3	W36x300	Top Flange	54.0	51.2	49.3	69.3	0.97	0.92	0.89	0.98	30.4%
			Bot. Flange	51.9	50.5	48.4	68.7	0.94	0.91	0.87	0.97	30.7%
			Web	57.0	55.0	53.2	69.4	1.03	0.99	0.96	0.98	28.1%
			Mill Tests	56.0			71.0					26.0%
				55.0			71.0					25.0%
	N4	W14x211	Top Flange	51.4	50.5	48.9	69.0	0.92	0.90	0.87	0.90	30.4%
			Bot. Flange	53.7	50.8	48.8	68.7	0.96	0.91	0.87	0.89	28.9%
			Web	54.5	51.6	49.3	68.6	0.97	0.92	0.88	0.89	27.5%
			Mill Tests	56.0			77.0					23.0%
				56.0			77.0					23.0%
	N5	W36x150	Top Flange	55.7	53.5	51.3	73.1	1.01	0.97	0.93	0.99	34.4%
				58.7	53.0	50.1	72.5	1.07	0.96	0.91	0.99	38.1%
			Bottom Flange	59.0	54.6	51.7	73.6	1.07	0.99	0.94	1.00	32.8%
				58.0	54.2	51.6	73.4	1.05	0.98	0.94	1.00	35.9%
			Mill Tests	54.0			72.0					24.0%
				56.0			75.0					25.0%
	N5-a	W36x150	Flange	54.6	52.0	49.5	70.6	0.99	0.95	0.90	0.96	27.1%
			Web	**61.4**	**58.9**	**56.3**	**73.9**	**1.12**	**1.07**	**1.02**	**1.00**	**25.6%**
			Mill Tests	54.0			72.0					24.0%
				56.0			75.0					25.0%
	N6	W14x311	Top Flange	52.0	49.4	46.3	70.8	0.95	0.91	0.85	0.96	35.5%
			Bot. Flange	56.3	51.7	48.9	70.5	1.03	0.95	0.90	0.95	35.5%
			Web	52.2	50.4	47.5	69.9	0.96	0.93	0.87	0.95	36.7%
			Mill Tests	55.0			75.0					22.0%
				54.0			73.0					23.0%

Table 4.5.3 Tensile Test Data vs. Mill Report Values (Mill B)

			f_{uy} (ksi)	f_y (ksi)	f_{sy} (ksi)	f_u (ksi)	f_{uy}/f_{ymill}	f_y/f_{ymill}	f_{sy}/f_{ymill}	f_u/f_{umill}	% Elon.
Mill B	**B1 W14x211**	**Top Flange**	55.7	55.5	54.2	74.0	0.97	0.97	0.95	0.97	29%
			57.4	57.4	55.8	75.2	1.00	1.00	0.97	0.99	29%
		Bottom Flange	58.6	57.4	56.1	76.5	1.02	1.00	0.98	1.00	29%
			59.3	58.7	56.7	76.7	1.04	1.02	0.99	1.01	29%
		Web	59.8	57.7	56.0	74.2	1.04	1.01	0.98	0.97	25%
			62.2	57.5	55.6	73.9	1.09	1.00	0.97	0.97	24%
			60.8	58.9	56.8	75.5	1.06	1.03	0.99	0.99	25%
		Mill Test	57.3			76.2					27%
	B2 W14x311	**Top Flange**	58.4	54.6	52.1	73.9	1.05	0.98	0.94	0.98	34%
			55.9	54.1	51.7	74.0	1.01	0.97	0.93	0.98	38%
		Bottom Flange	54.4	54.1	51.5	73.6	0.98	0.97	0.93	0.97	33%
			55.0	53.1	50.7	73.1	0.99	0.96	0.91	0.97	35%
		Web	54.6	53.9	51.1	73.1	0.98	0.97	0.92	0.97	38%
			52.6	52.5	49.9	72.1	0.95	0.94	0.90	0.95	34%
			55.5	52.7	50.3	72.7	1.00	0.95	0.91	0.96	38%
		Mill Test	55.6			75.5					24%
	B3 W36x300	**Top Flange**	52.0		49.5	72.0	0.94		0.89	0.98	32%
			52.7		49.7	71.9	0.95		0.90	0.98	30%
		Bottom Flange	54.2	52.4	50.1	71.3	0.98	0.95	0.91	0.97	32%
			51.2	50.2	49.2	71.1	0.93	0.91	0.89	0.97	32%
		Web	53.4	51.6	49.1	69.6	0.97	0.93	0.89	0.95	29%
			56.1	54.4	51.7	71.1	1.01	0.98	0.93	0.97	29%
			52.6	51.7	48.8	69.6	0.95	0.93	0.88	0.95	30%
		Mill Test	55.3			73.6					32%
	B4 W36x150	**Top Flange**	57.3	55.2	53.0	71.7	1.02	0.98	0.94	0.96	29%
			57.1	55.0	51.9	70.7	1.02	0.98	0.92	0.95	29%
		Bottom Flange	57.8	55.8	53.0	71.6	1.03	0.99	0.94	0.96	31%
			56.9	54.2	52.0	70.7	1.01	0.96	0.92	0.95	31%
		Web	60.6	57.2	54.5	71.5	1.08	1.02	0.97	0.96	27%
			65.5	**63.3**	**60.2**	**75.8**	**1.17**	**1.13**	**1.07**	**1.02**	**24%**
			60.3	59.1	56.4	72.5	1.07	1.05	1.00	0.97	26%
		Mill Test	56.2			74.6					28%

Table 4.5.4 Tensile Test Data vs. Mill Report Values (Mill T)

			f_{uy} (ksi)	f_y (ksi)	f_{sy} (ksi)	f_u (ksi)	f_{uy}/f_{ymill}	f_y/f_{ymill}	f_{sy}/f_{ymill}	f_u/f_{umill}	% Elon.
Mill T	T1 W24x162	Top Flange	62.1	60.8	59.0	76.6	1.00	0.98	0.95	0.96	25%
			58.2	57.0	54.8	73.7	0.94	0.92	0.89	0.93	28%
		Bottom Flange	60.3	60.0	57.2	74.9	0.97	0.97	0.92	0.94	29%
			58.7	58.0	56.5	74.8	0.95	0.94	0.91	0.94	27%
		Web	**52.9**	**50.3**	**47.7**	**67.7**	**0.85**	**0.81**	**0.77**	**0.85**	**29%**
			55.3	**55.3**	**52.5**	**69.1**	**0.89**	**0.89**	**0.85**	**0.87**	**27%**
			51.5	**49.2**	**46.8**	**66.6**	**0.83**	**0.80**	**0.76**	**0.84**	**27%**
		Mill Test	61.9			79.6					23%
	T2 W30x211	Top Flange	**53.0**	**48.6**	**45.9**	**66.1**	**0.82**	**0.75**	**0.71**	**0.85**	**44%**
			52.0	**49.8**	**47.6**	**67.7**	**0.81**	**0.77**	**0.74**	**0.87**	**42%**
		Bottom Flange	**51.6**	**48.3**	**45.5**	**66.1**	**0.80**	**0.75**	**0.71**	**0.85**	**41%**
						67.6				**0.87**	**41%**
		Web	**48.4**	**47.4**	**45.4**	**64.9**	**0.75**	**0.73**	**0.70**	**0.84**	**41%**
			57.9	**52.8**	**49.8**	**67.4**	**0.90**	**0.82**	**0.77**	**0.87**	**43%**
			51.4	**49.1**	**46.1**	**66.1**	**0.80**	**0.76**	**0.72**	**0.85**	**42%**
		Mill Test	64.5			77.4					24%
	T3 W36x300	Top Flange	55.5	55.5	53.5	73.2	0.93	0.93	0.90	0.94	36%
			58.5	56.3	53.5	72.8	0.98	0.94	0.90	0.94	25%
		Bottom Flange	**52.2**	**52.2**	**50.0**	**70.9**	**0.87**	**0.87**	**0.84**	**0.91**	**36%**
			55.5	54.1	51.7	71.5	0.93	0.91	0.87	0.92	33%
		Web	60.2	59.7	57.4	76.7	1.01	1.00	0.96	0.99	39%
			59.5	54.4	52.0	70.5	1.00	0.91	0.87	0.91	36%
			57.5	57.5	55.4	74.8	0.96	0.96	0.93	0.96	34%
		Mill Test	59.7			77.6					27%
	T4 W14x211	Top Flange	60.8	60.8	59.5	77.0	0.96	0.96	0.94	0.97	28%
			61.0		59.2	76.5	0.96		0.93	0.97	28%
		Bottom Flange	61.0	61.0	60.2	77.6	0.96	0.96	0.95	0.98	27%
			61.9	61.9	60.1	77.4	0.97	0.97	0.95	0.98	29%
		Web	65.7	64.8	63.0	81.1	1.03	1.02	0.99	1.02	25%
			64.2	63.9	62.3	80.5	1.01	1.01	0.98	1.01	25%
			65.7	65.7	63.8	81.6	1.03	1.03	1.01	1.03	22%
		Mill Test	63.5			79.3					22%
	T5 W36x150	Top Flange	61.7	60.7	57.3	72.6	1.00	0.98	0.93	0.98	27%
			64.3	63.8	61.9	76.1	1.04	1.03	1.00	1.03	25%
		Bottom Flange	61.4	60.6	58.0	73.3	0.99	0.98	0.94	0.99	26%
			64.0	61.9	60.3	74.9	1.04	1.00	0.98	1.02	26%
		Web	57.2	54.3	52.0	67.7	0.92	0.88	0.84	0.92	26%
			61.7	59.6	57.7	73.1	1.00	0.97	0.93	0.99	24%
			60.2	56.8	54.8	70.0	0.97	0.92	0.89	0.95	26%
		Mill Test	61.8			73.7					24%
	T6 W14x311	Top Flange	**56.5**	**54.9**	**52.4**	**74.7**	**0.90**	**0.87**	**0.83**	**0.92**	**36%**
			54.1	**54.1**	**51.6**	**74.1**	**0.86**	**0.86**	**0.82**	**0.91**	**37%**
		Bottom Flange	**57.5**	**57.2**	**54.1**	**76.2**	**0.91**	**0.91**	**0.86**	**0.93**	**36%**
			52.3	**52.3**	**49.5**	**73.0**	**0.83**	**0.83**	**0.79**	**0.90**	**34%**
		Web				**78.2**				**0.96**	**28%**
			56.5	**56.5**	**53.8**	**76.3**	**0.90**	**0.90**	**0.85**	**0.94**	**27%**
			55.4	**55.4**	**52.5**	**75.2**	**0.88**	**0.88**	**0.83**	**0.92**	**33%**
		Mill Test	62.9			81.5					20%

Mill test results from Mill T showed the most discrepancy between measured and reported values. The measured values of F_{uy} for members T1, T2 and T6 were, on average, 14%, 19% and 12% lower than the reported yield strength in the mill certificates. The elevated values of F_{ymill} and F_{umill} along with the low values of $\%Elong_{mill}$ suggest that the material tested at the mill might have undergone some strain aging.

4.5.3 Agreement of Individual Mills with Mill Test Reports

The relationship between F_y and F_{ymill} was explored in more detail to see if it varied significantly between producers. Figure 4.5.3 shows the distribution of $F_{y\ ave}/F_{ymill}$ for each mill, where $F_{y\ ave}$ is the average yield stress of all flange coupons taken from a particular section.

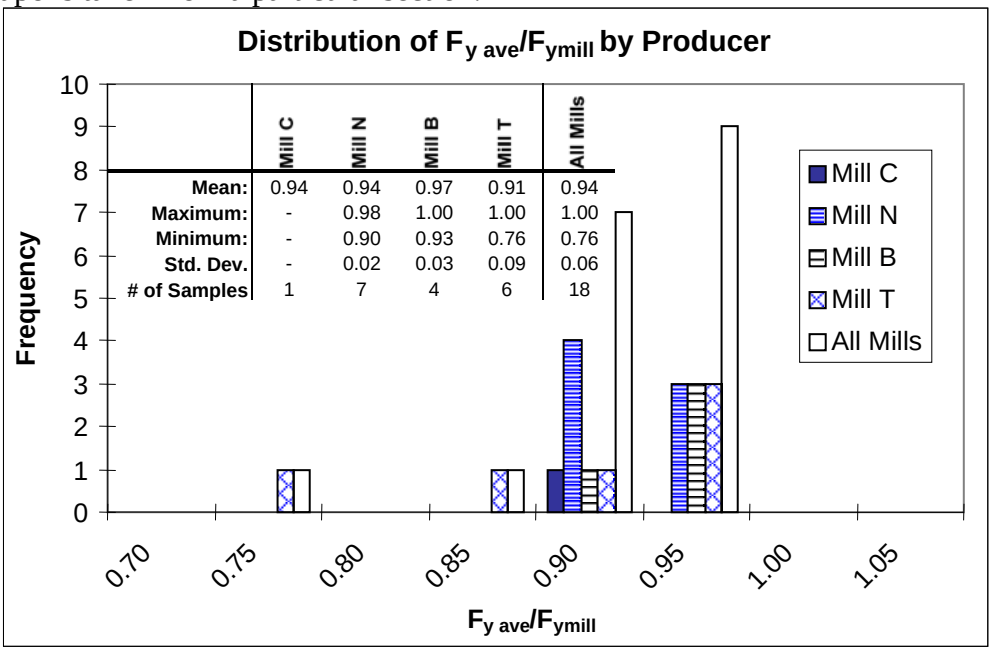

Figure 4.5.3 Distributions of $F_{y\ ave}/F_{ymill}$ Grouped by Producer

As is shown, Mill T had the lowest mean value (0.91) and Mill B the highest (0.97). The standard deviations of Mill N (0.02), and Mill B (0.03) were roughly equal, but the standard deviation of Mill T (0.09) was three times that of the next highest value. The low average of Mill T material suggests that extremely high strain rates might be used in the mill tension tests.

Based on these values, then, a reasonable approximation of the design yield stress is 95% of the mill test yield values. Care should be taken in interpreting mill reports from Mill T, as they may overestimate the actual yield stress by up to 10%. More samples from Mill C are necessary before any conclusions can be drawn regarding the accuracy of their mill test reports.

4.6 CONCLUSIONS

Tension tests were performed on coupons from the webs and flanges of all 17 rolled shapes. Analysis of the tensile test data focused on three main areas: the effects of coupon size and location on the stress-strain behavior; estimation of typical parameters of stress-strain behavior; and the relationship between measured values and values given in mill test reports. Conclusions drawn from the different areas of analysis are given below.

1. A significant difference was found between the yield strengths of coupons taken from the flanges and coupons taken from the webs. On average, $F_{yflange}$ was about 95% of F_{yweb} for Mills C, N, and B, but varied from 95-114% for Mill T. The flange and web material were considered fundamentally different, and were treated separately for the remainder of the report.

2. The type of coupon used in the tension test may influence the reported stress-strain parameters. Tension tests performed on a ½"-round coupon and a full-thickness strap coupon taken from the same member at adjacent locations suggest that E_{sh} is higher and ε_{sh} is lower in ½"-round coupons than in strap coupons. F_{uy} may also be higher in ½"-round coupons but more research is necessary to confirm this trend.

3. The tension stress-strain curve, shown in Figure 4.6.1, is an estimate of the behavior of flange material in typical rolled shapes. It was constructed using average values of the stress-strain parameters presented in Section 4.4. The table below the curve includes summary statistics for the data used to calculate the parameters.

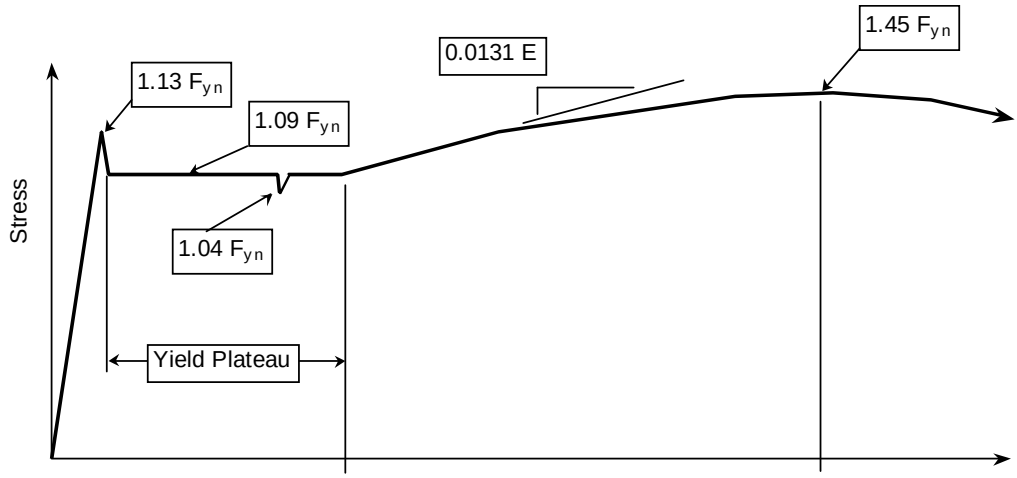

	F_{uy}/F_{yn}	F_y/F_{yn}	F_{sy}/F_{yn}	$\varepsilon_{sh}/\varepsilon_{yn}$	E_{sh}/E	$\varepsilon_u/\varepsilon_{yn}$	F_u/F_{yn}
Mean:	1.13	1.09	1.04	8.73	0.0131	86.2	1.45
Maximum:	1.29	1.28	1.24	14.0	0.0165	117	1.55
Minimum:	0.96	0.96	0.91	4.29	0.0075	68.2	1.32
Std. Dev.:	0.09	0.08	0.08	2.90	0.0024	11.5	0.06
# of Specimens:	41	59	59	38	38	59	63

Figure 4.6.1 Typical Tension Stress-Strain Curve of Flange Material of Rolled Shapes (F_{yn}=50 ksi, E=29000 ksi)

4. The measured yield strengths of coupons from Mills C, N, and B were approximately 95% of the reported mill test values. The measured yield strengths in the set of data from Mill T varied from 76-99% of the reported mill certificate values, with an average of 91%.

Chapter 5: Impact Testing Procedure

5.1 INTRODUCTION

The toughness characteristics of the rolled shapes in this study were obtained from the Charpy V-notch Impact Test procedure described in ASTM E23. Thirty Charpy V-Notch specimens were machined from 15 of the 17 rolled shapes—6 from the web, 8 each from the top and bottom flanges, and 4 each from the top and bottom core regions. In the remaining two members, the W24x62 sections, Charpy specimens were taken from the flanges and the core regions only, because of the extremely thin webs of the W24x62 sections. Impact tests were conducted over a wide enough temperature range to define upper and lower energy shelves (see Section 1.2.2 for definitions relating to toughness behavior.) The impact energy was plotted against test temperature, and the data used to estimate transition curves for each rolled shape. The toughness characteristics were found to vary with Charpy location within the cross section so separate transition curves were plotted for flange, web, and core specimens. This chapter presents the procedures followed for instrument calibration, Charpy specimen preparation, and the actual impact tests.

5.2 INSTRUMENT CALIBRATION

A Tinius-Olson pendulum-type testing machine was used for all impact testing. It was examined at the beginning of the testing program and found to comply with ASTM E23 Sections 5 and 6. ASTM E23 Section 6.2.6.2 outlines

the windage and friction loss test procedures. Friction loss per pendulum swing was checked at the beginning and end of the testing program and was found to be within the specified maximum of 0.4% of the scale range capacity. A windage test was performed every day of testing and was zero in all cases. The accuracy of the testing machine was verified by N.I.S.T. from the recorded fracture energies of Low-Energy and High-Energy Standard Calibration Charpy specimens.

A thermocouple connected to a digital readout was used to measure the temperature of the liquid bath used to heat or cool the Charpy specimens. The accuracy of the device was checked at the beginning of the testing program (October 1997) and at its completion (June 1998) with a certified thermometer accurate to ±1°F.

5.3 SPECIMEN SIZE

Standard Type A Charpy specimens were used in all impact tests. The required dimensions and permissible tolerances are given in ASTM E 23, Figure 6, and are shown in Figure 5.2.1.

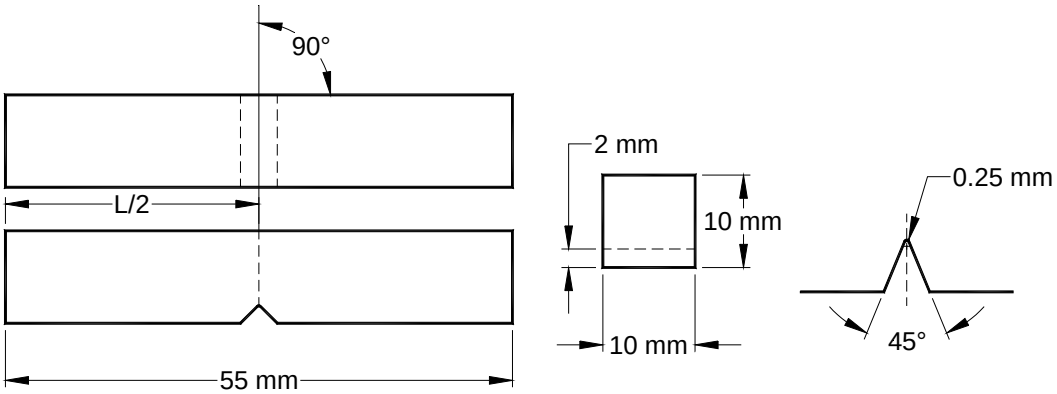

Type A Charpy (Simple Beam) Impact Specimen

Figure 5.3.1 Dimensions of Charpy V-notch Impact Specimens

These dimensions were verified on randomly selected specimens to insure that the ASTM guidelines were met. The accuracy of the notch was checked using an optical comparitor, a device used to measure the dimensions of small objects to a high precision by shining a light behind the object and measuring the shadow. Samples were taken at random from test batches throughout the duration of the project and the notch dimensions were measured and found to be within required tolerances at all times.

5.4 SPECIMEN LOCATIONS

Charpy specimens were taken from the flange and web-flange junction (core) regions of all members and from the web in all members with a web thickness greater than 0.5 inches. The precise locations for each member are

given in Appendix B. The centers of flange Charpy specimens were located as close as possible to one-fourth the flange thickness from the outside flange faces. For web Charpy specimens, the centers were as close as possible to one-fourth the web thickness from either external face. AISC A3.1c requires that the center of core specimens be located ¼ of the flange thickness from the inside face of the flange, as is shown in Figure 5.4.1.

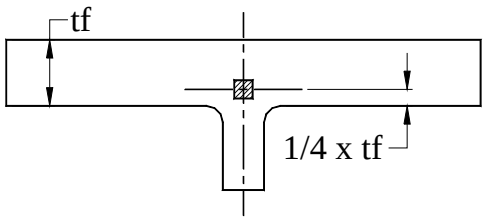

Figure 5.4.1 AISC Specified Location of Core Specimens

For this project, a number of core specimens were extracted from farther down in the flange-web junction than the specified location. The exact locations of the specimens within their cross sections are shown in Appendix B and Appendix D.

5.5 SPECIMEN PREPARATION

Charpy specimens undergo a large amount of preparation before testing. Using a hand-held acetylene cutting torch, each group of specimens was cut from its respective member. High temperatures from the cutting torch change the crystalline structure of adjacent steel so it was imperative that the flame cut was at least 2 inches from the nearest Charpy specimen. A grinding machine was used

to achieve the required cross-sectional dimensions and finish requirements for standard-sized specimens discussed in ASTM E23. A device called a mini-broach was used to notch the test specimens and the dimensions of the notch were checked using the optical comparitor.

5.6 TESTING PROCEDURE

The goal of the impact testing procedure was to test specimens over a broad enough range of temperatures to define upper and lower shelves, while including enough specimens in the transition region so that a reasonable estimation of the transition curve could be drawn. Figure 5.6.1 is an example of a complete Energy vs. Temperature curve. Impact test results for the Charpy Specimens taken from the flanges of member C1 were used to create the curve.

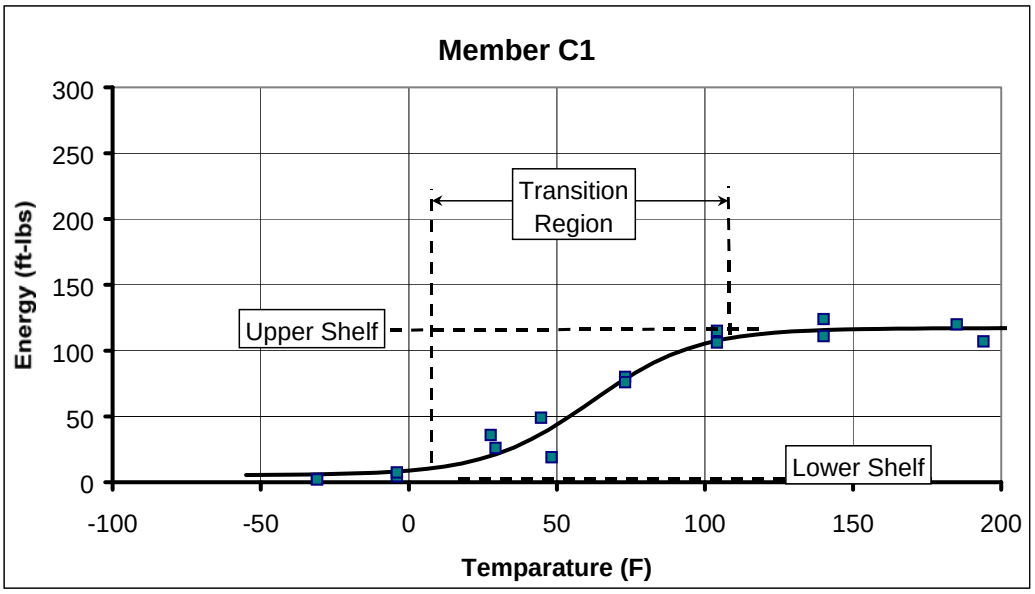

Figure 5.6.1 Impact Test Results from Flange Material of Member C1

A liquid bath with an electric motor powered agitator and a digitally monitored thermocouple were used to bring each test specimen to its desired temperature. Before a specimen was tested, it was placed in the bath and immersed a minimum of five minutes to equilibrate with the surrounding liquid. If the desired temperature was below room temperature, methanol was used in the bath because its low freezing point allowed specimens to be tested down to a temperature of –60°C. For temperatures above room temperature, water was used in the bath because it has a higher boiling point than methanol. Self-centering tongs, a tool designed explicitly for performing Charpy impact tests, were used to take the specimens from the bath to the testing machine. The ends of the tongs were also brought to the bath temperature over a period of at least five minutes. After the test specimen had been in the bath for the required time, the tongs were used to remove the specimen from the bath and place it in the testing machine. Immediately, the pendulum was released and the energy required to break the specimen was recorded. The total elapsed time from when the specimen was removed from the bath to when it was tested could be no greater than five seconds, per ASTM E23, Paragraph 12.2. A tabulated summary of the impact test results can be found in Appendix D.

Chapter 6: Analysis of Impact Testing Data

6.1 INTRODUCTION

Results from the Charpy V-notch impact tests were first checked against the minimum allowable toughness specified in AISC. The data were then used to estimate typical toughness trends in the members. Separate transition curves were calculated for the flange, web, and core regions of each member, and the observed behavior of each region was discussed. Definitions of useful terms related to impact testing are given in Section 1.2.2.

6.2 COMPARISON OF RESULTS WITH AISC SPECIFICATIONS

AISC A3.1c specifies a minimum core toughness of 15 ft-lbs. at 70°F for Group 4 and 5 rolled shapes used as tension members. This requirement was satisfied in the flange, web, and core regions of all sections in the program. Specimens from all four mills showed very good toughness throughout the cross section, with no single Charpy V-notch specimen even approaching this limit. The lowest room temperature toughness came from the flanges of the W36x300 section from Mill N, which had 70°F energies of 61, 65, and 25 ft-lbs., for an average of 50 ft-lbs. The 25 foot-pound reading was the lowest single room-temperature measurement in the entire testing program, and even it was above the minimum energy requirement.

The core region of Group 4 and 5 shapes, thought to be a low-toughness spot, showed toughness levels comparable to other size members. Mill B sections

showed exceptional toughness far above the AISC requirement. It is recommended that more research be done on the toughness of Mill C steel. Compared with the other mills, the W24x62 section from Mill C showed low toughness, but since only one specimen from their mill was available, it was impossible to draw conclusions about their consistency.

6.3 CALCULATING TRANSITION CURVES

The impact energy transition curve was estimated using a hyperbolic tangent model developed by Chun in 1972. Four parameters are required to plot the curve at the correct size and position. These parameters have been labeled β_1, β_2, β_3, and β_4 and their relationships to the transition curve are shown in Figure 6.3.1.

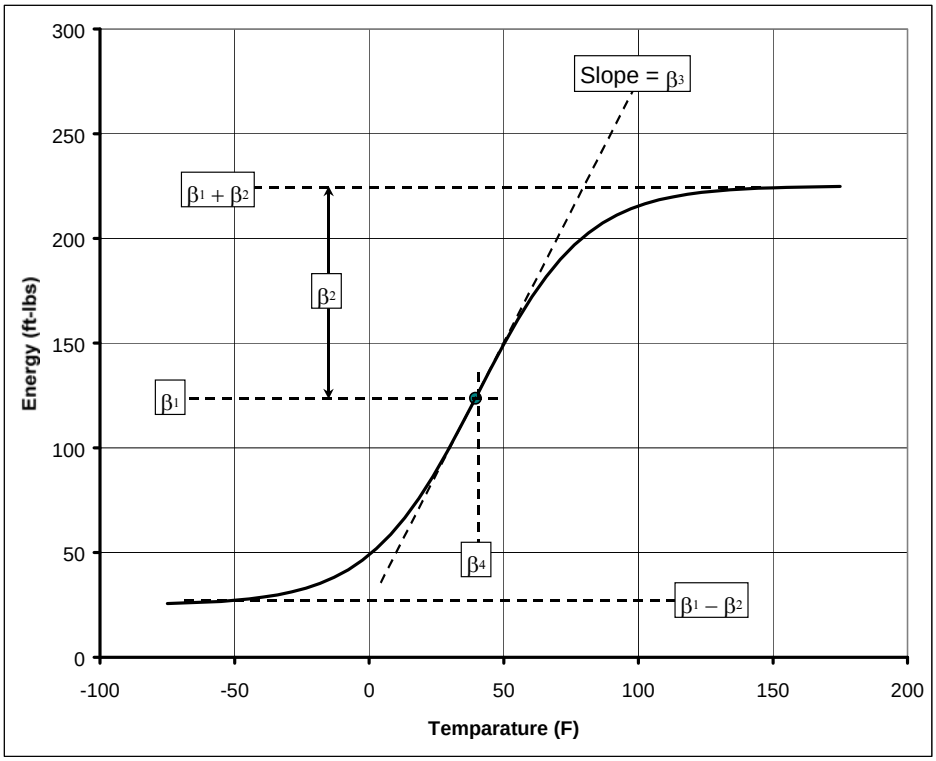

Figure 6.3.1 Parameters Required for Transition Curve Model

The β_1 parameter gives the mean value of the curve and β_2 gives the distance of the asymptotes above and below the mean, corresponding to the Upper and Lower Shelves. The β_3 parameter is a measure of the slope of the curve at the transition temperature, and β_4, the Transition Temperature, positions the function along the temperature axis.

These parameters were calculated on a spreadsheet program using a least-squares approach. It was necessary to set constraints on the range of the β values to insure reasonable results. For instance, the least squares calculations often gave lower shelves less than 0 ft-lbs or slopes in the transition region approaching

infinity. A lower bound of zero was set for the lower shelf value (β_1-β_2) and a maximum value of 0.25 was set for β_3. In many tests the scatter was so great that the computer algorithm gravitated toward unreasonable solutions. In these cases, the parameters were estimated based on testing experience.

Plotting all test results from each member on the same graph resulted in excessive scatter. Figure 6.3.2 illustrates the difficulty in inferring any kind of behavioral trend when specimens from the flange, web, and core are plotted together.

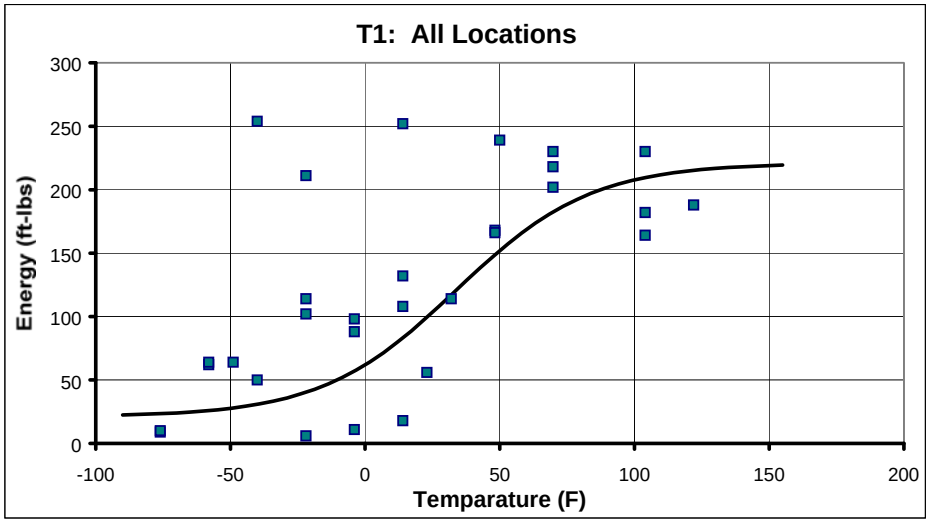

Figure 6.3.2 Member T1-W24x162 Charpy V-notch Test Results: All Locations

Individual trends seemed to emerge, however, when the tests were separated by locations. The graphs in Figure 6.3.3 are from the same wide-flange section as above, T1, but each location shows markedly different toughness behavior.

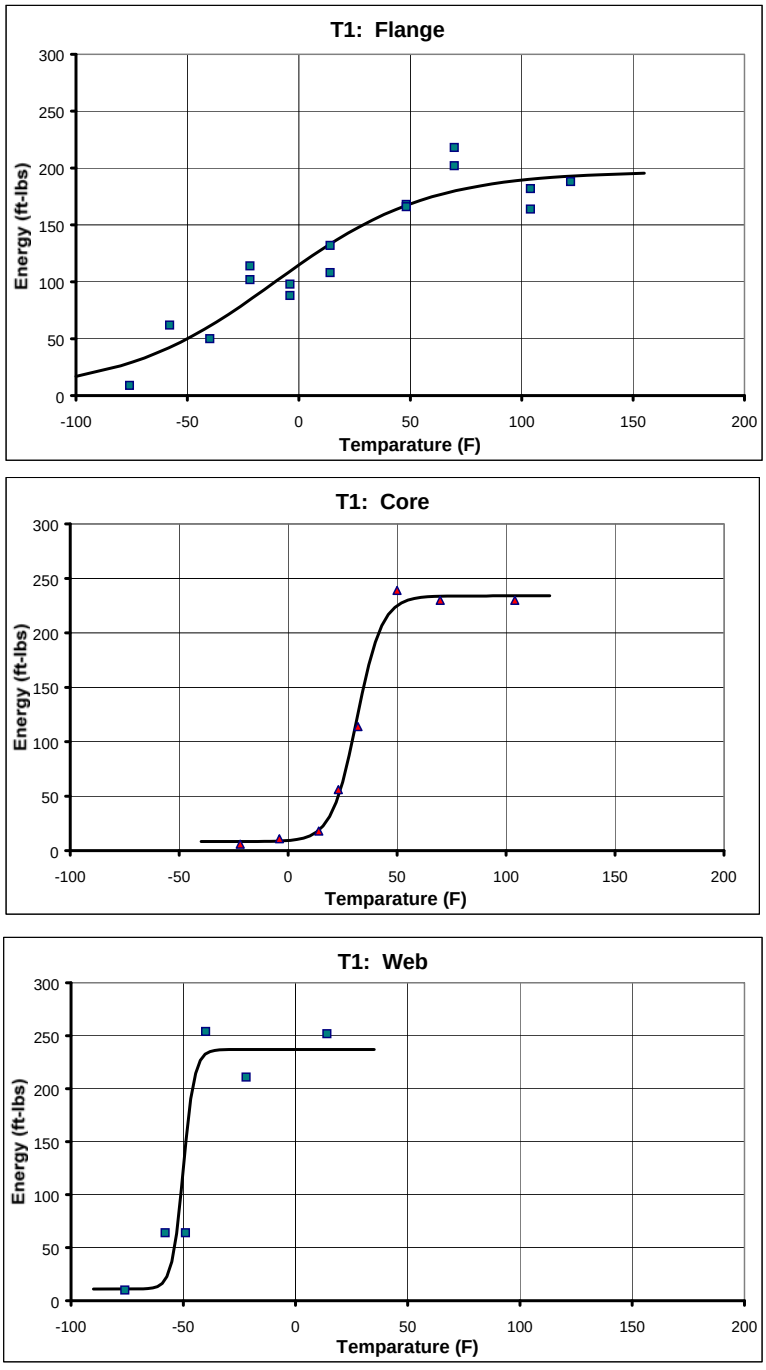

Figure 6.3.3 Member T1-W24x162 Charpy V-notch Test Results: Flange, Web, and Core

The flange region shows very good toughness at room temperature and a gradual transition to brittle behavior. The Nil Ductility Temperature (the temperature at 15 ft-lbs.) was very low—less than -75°F. The Transition Temperature was also relatively low, which means the material should exhibit ductile behavior at low temperatures.

The core material exhibited a higher Upper Shelf, corresponding to better toughness behavior at high temperatures, and the steep Transition Slope suggests a very sudden ductile-to-brittle transition. The Nil Ductility Temperature is also much higher in the core than in the flange region, indicating that material in the core region will begin to exhibit brittle behavior at higher temperatures than material in the flange.

The web material in the bottom graph shows the best toughness behavior of the three regions. The high Upper Shelf and low Transition Temperature show that the material is capable of absorbing high amounts of energy at very low temperatures.

6.4 TEST RESULTS

6.4.1 Toughness Parameters

The hyperbolic tangent model of the Energy vs. Temperature transition curve used in this report requires four parameters, β_1, β_2, β_3, and β_4. This section shows the distribution of each of these parameters over the entire set of members tested, and discusses any observed trends.

6.4.1.1 Upper Shelf ($\beta_1+\beta_2$)

The calculated values for the Upper-Shelf are shown in the Figure 6.4.1.

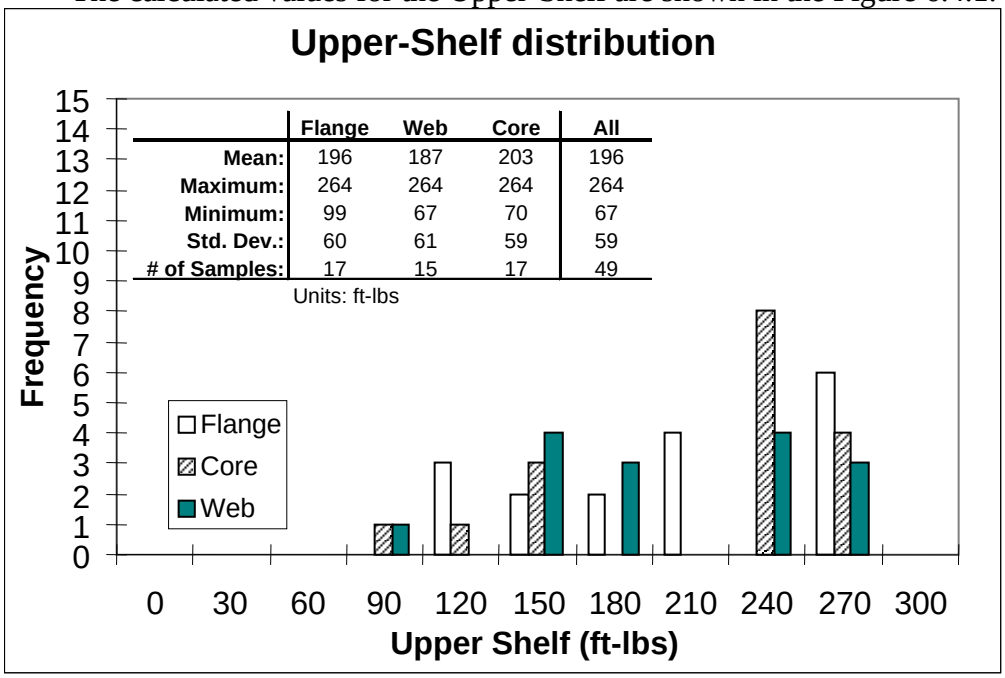

Figure 6.4.1 Distribution of Upper-Shelf values

The average upper-shelf value was around 200 ft-lbs, at all three locations. The core region showed the highest mean upper-shelf value, but it was only slightly higher than the flange and core regions. The distribution of the core region shows a definite peak between 210 and 240 ft-lbs.

6.4.1.2 Transition Slope (β_3)

The transition slope parameter is a measure of the abruptness of the transition between ductile and brittle behavior. Curves with high values of β_3 have very steep slopes, which means that for temperatures around the Transition Temperature, a small drop in temperature can result in a very large drop in

toughness. Members with gradual ductile-to-brittle transitions show much lower values of β_3. As a way to compare, Figure 6.4.2 shows examples of different transition slopes, and their effect on the Energy vs. Temperature curve.

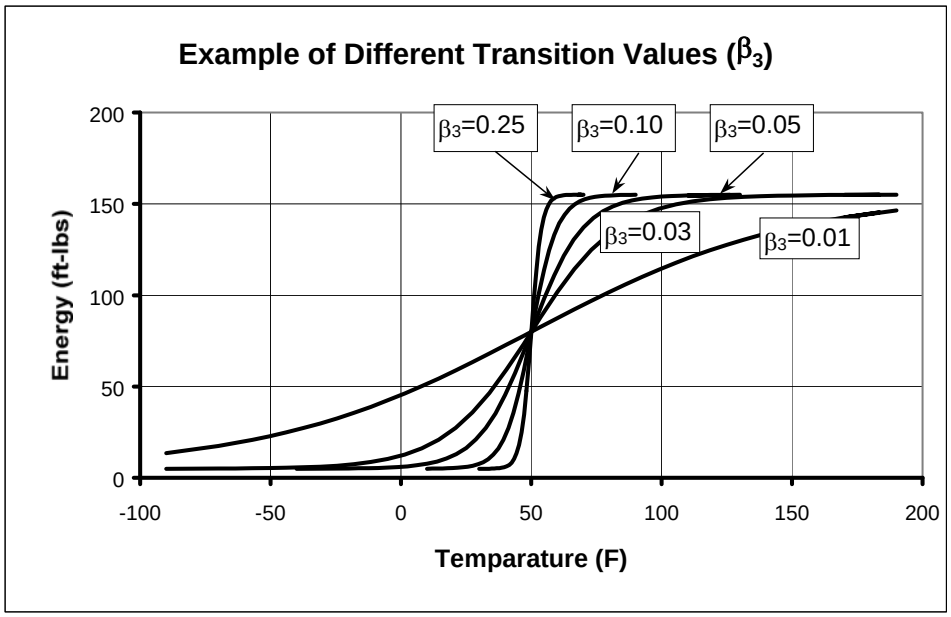

Figure 6.4.2 Effect of Transition Slopes on Energy vs. Temperature Curve

Depending on its Transition Temperature, a steep Transition Slope can denote either ductile or brittle behavior. The curves in Figure 6.4.3 illustrate this concept by comparing the behavior of two steep curves with a gradual one.

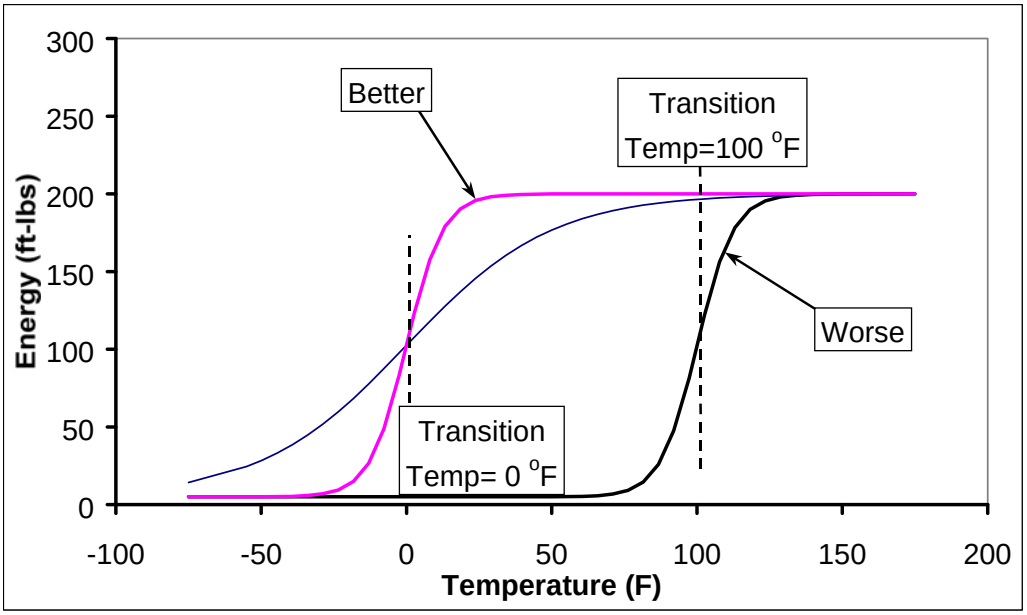

Figure 6.4.3 Desirable Toughness Behavior of Steep Transition Curves

All three curves have the same Upper and Lower Shelves, but different Transition Slopes and Transition Temperatures. The steep curve to the right is less desirable than the gradual curve because it exhibits brittle behavior at relatively high temperatures, as is shown by its high Transition Temperature. The steep curve on the left, however, may be more ductile than the gradual curve, depending on the expected service temperature of the steel. If the steel is expected to stay above 0°F, then the steep curve is advantageous because it offers more energy absorption in the range of 0°-100°F. If the material were used at very low temperatures, though, the gradual curve would be more desirable because it maintains relatively high levels of ductility down to less than -50°F.

The histogram in Figure 6.4.4 shows the distribution of the calculated β_3 values.

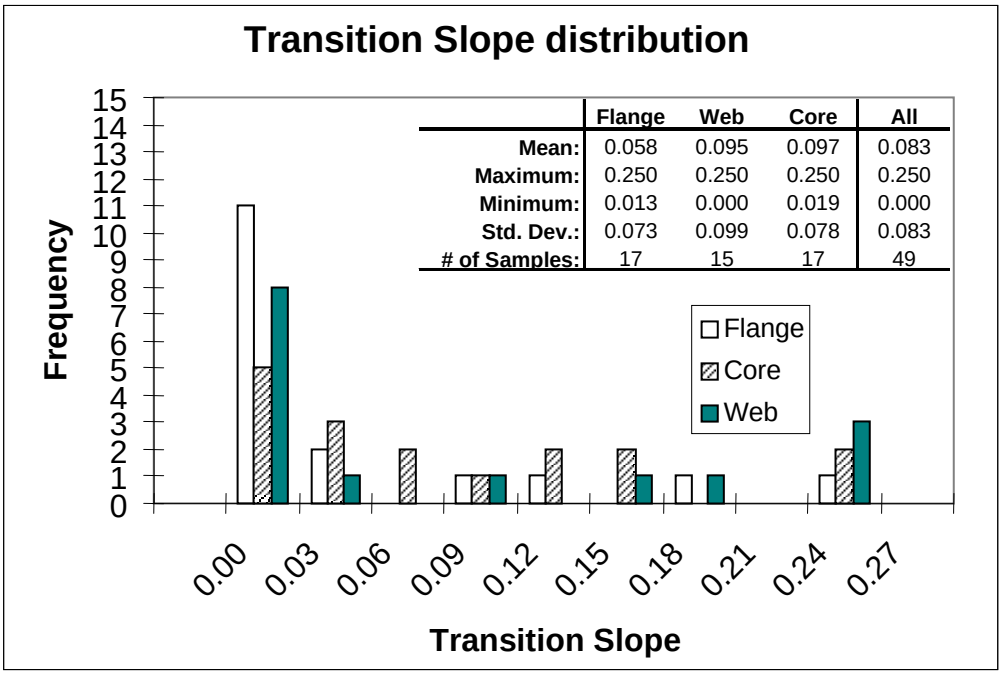

Figure 6.4.4 Distribution of Transition Slope Parameter (β_3)

As can be seen, 19 of 32 tests from the flange and web regions showed Transition Slopes less than 0.03, compared to only 5 of 17 from the core region. The core region also had the highest mean β_3 value. These two observations suggest that the core region may exhibit a more sudden ductile-to-brittle transition than the flange and web regions.

6.4.1.3 Nil Ductility Temperature

The test results showed that the Nil Ductility Temperature was very much dependent on the specimen location, as can be seen in Figure 6.4.5.

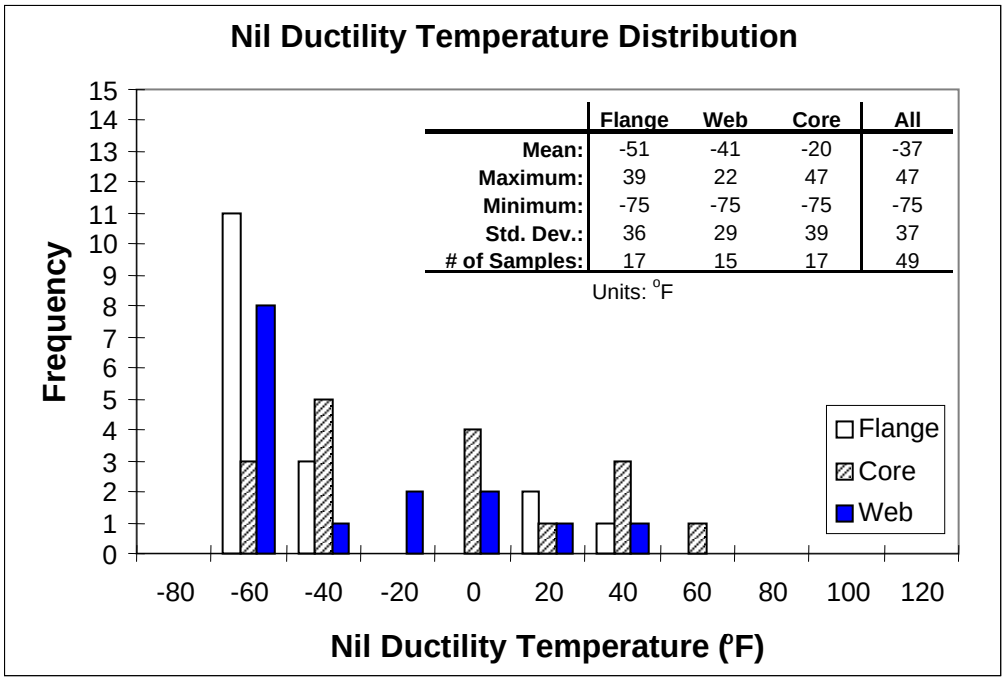

Figure 6.4.5 Distribution of Nil Ductility Temperatures

The distributions of the flange and web regions show a definite skew to the left. This is because the energy at 15 ft-lbs. could only be estimated in many cases because it was not possible to bring the methanol bath to a low enough temperature to achieve brittle behavior. In these cases, the Nil Ductility Temperature was given as the minimum temperature attained in that set of Charpy specimens. For instance, the transition curve of the flange specimens from Member B1 (see Appendix D) does not reflect a 15 ft-lbs temperature because the lowest recorded specimen energy was 39 ft-lbs. at -76°F. Experience shows that the ductility continues to decrease with temperature until a lower shelf of around 2 ft-lbs. is reached. Since it was impossible to attain a temperature that low with

the available equipment, the Nil-Ductility Temperature is reported as -76°F.

The core region showed the highest average Nil Ductility temperature, and the flange the lowest. This trend was consistent with results from individual members. In 10 of 17 members, the core Nil Ductility Temperature was higher than in both the flanges and webs.

Data suggest that the core regions of members have higher Upper Shelves (Section 6.4.1.1), more abrupt transitions (Section 6.4.1.2), and higher Nil Ductility Temperatures, relative to the flange and web regions. The combination of these factors is potentially dangerous; the high Upper Shelf at room temperature implies excellent toughness behavior, but the high Nil Ductility Temperature and Transition Slope could lead to extremely brittle behavior for relatively small decreases in temperature.

6.4.2 Core Toughness

Variations in core region toughness properties with respect to member type (column vs. beam) and producer were studied. Analysis showed that member type had no discernable effect on any of the toughness parameters, as can be seen in the graphs shown in Figure 6.4.6-6.4.8.

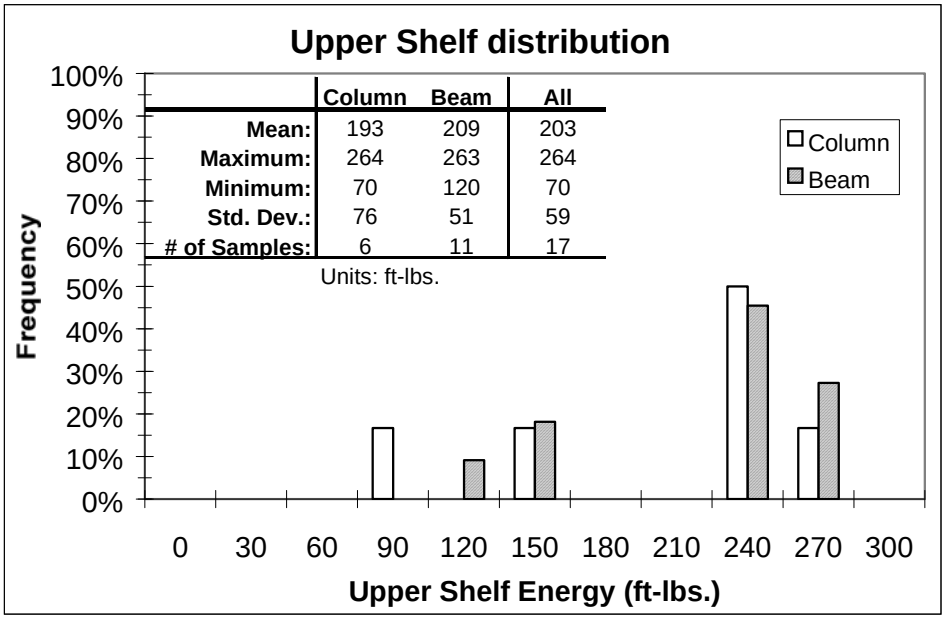

Figure 6.4.6 Effect of Member Type on Upper Shelf Value

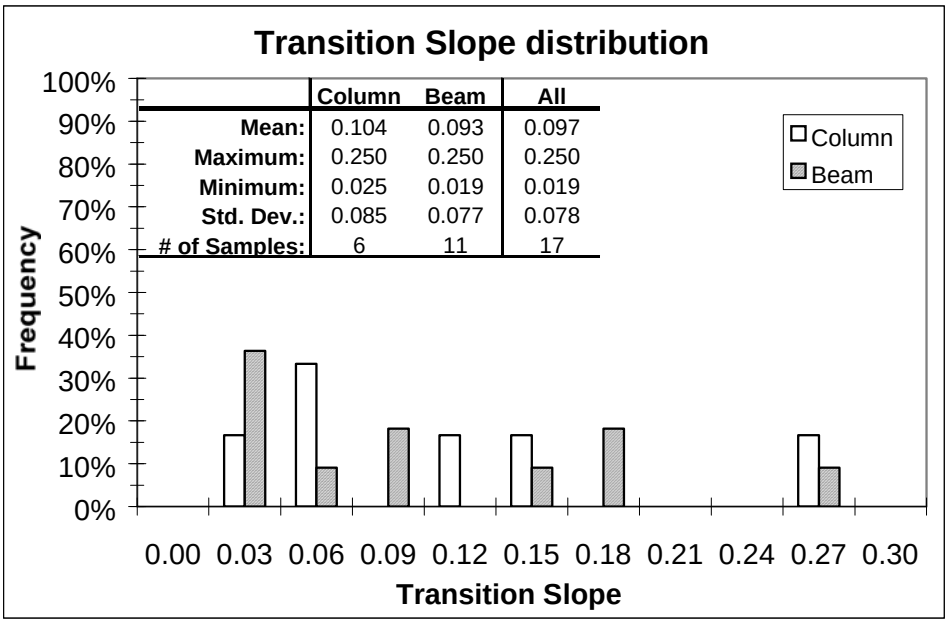

Figure 6.4.7 Effect of Member Type on Transition Slope

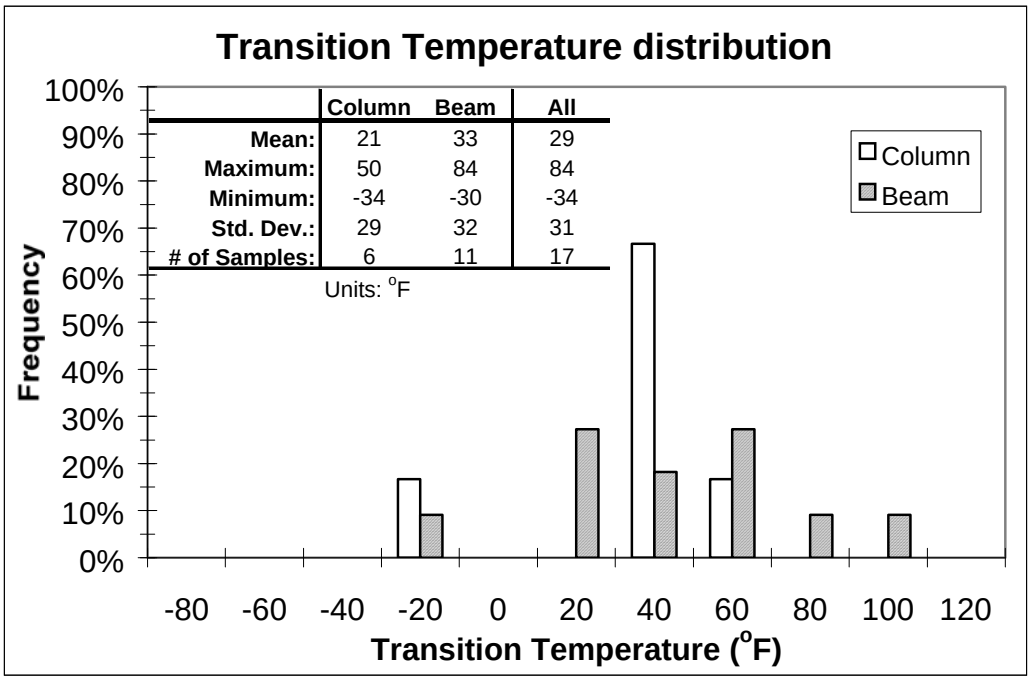

Figure 6.4.8 Effect of Member Type on Transition Temperature

In the charts above, the frequency was calculated by dividing the number of values within each bin by the total number of beam or column members. In Figure 6.4.8 above, one column curve had a Transition Temperature between –40 and –20 °F. The relative frequency was therefore 1÷6=17%.

As can be seen, data from both the beam and column groups in all three graphs follow roughly the same trends. It was therefore concluded that the toughness behavior of the core material did not vary significantly with the type of member.

6.4.3 Variation among Producers

The four Mill B specimens showed exceptional toughness. Table 6.4.1 shows that of the four producers, theirs had the highest Upper Shelf, the lowest Nil Ductility Temperature, and the lowest Transition Temperature.

Table 6.4.1 Average Toughness Values of Each Producer

	Mill C	Mill N	Mill B	Mill T
Upper Shelf (ft-lbs.)	130	184	**242**	184
Transition Slope (ft-lbs./^{o}F)	0.02	0.04	0.15	0.09
Nil Ductility Temp. (^{o}F)	3	-20	**-62**	-41
Transition Temp. (^{o}F)	57	36	**-32**	-7

One reason for this excellent behavior may be the low sulfur content of British Steel sections. This factor is explored in detail in Section 7.1.2.

6.4 CONCLUSIONS

From the analysis of the impact testing results, the following conclusions were drawn about the toughness behavior of the rolled sections in this project:

1. At room temperature, data show that the core regions showed toughness equal to or greater than the flange and web regions. However, as the temperature was lowered, the core region showed a relatively abrupt transition from ductile to brittle behavior, and it did so at a higher temperature than the flange and web regions. These observations back up reports of brittle behavior in the core region and suggest that during periods of low temperatures, the core region will be the first part of the cross section to exhibit brittle behavior.

2. The column core toughness was not found to differ significantly from the beam core toughness.

3. The members produced by Mill B showed exceptional toughness. Section 7.1.2 explores the correlation between low sulfur and copper content and high toughness.

4. The average Nil Ductility Temperature was -37°F, indicating very good toughness at low temperatures.

5. All members exhibited very high Upper Shelf values. The average Upper Shelf was 196 ft-lbs., indicating excellent overall toughness behavior.

Chapter 7: Chemical Analysis

7.1 INTRODUCTION

Mass spectrometer tests were performed by an independent laboratory to determine the chemical composition of each test section. The analysis included elements listed in ASTM A6 Table B, as well as several others from the new ASTM Gr. 50 specification for structural shapes. Small samples, approximately ½"x½"x¼", were taken from broken Charpy specimens and used to perform the chemical analysis. Only one sample was taken for each specimen, under the assumption that the steel was relatively homogeneous throughout the cross section.

7.2 LABORATORY VS. MILL REPORTS

The chemical compositions obtained from the independent testing laboratory were compared to those in the mill test reports, and were found to match very well. The following two pages show the results of the independent laboratory tests compared with the mill tests. Also shown are the ASTM A6 minimum standard and the proposed requirements for the new ASTM Grade 50 with Special Provisions. Measurements that fell outside the specified ranges are shown in bold.

Table 7.2.1 Comparison of Chemical Analyses from Laboratory and Mills

		% Carbon	% Manganese	% Phosphorus	% Sulfur	% Silicon	% Nickel	% Chromium	% Molybdenum	% Copper	% Aluminum
ASTM A6	**min.**		0.5								
	max.	0.23	1.35	0.04	0.05	0.4					
New ASTM	**min.**		0.5			0.1					0.015
Spec.	**max.**	0.23	1.5	0.035	0.045	0.4	0.45	0.35	0.15	0.6	
W24x62 (C1)	**lab.**	0.12	1.04	0.015	0.044	0.22	0.08	0.08	<0.01	0.23	<0.005
	mill	0.11	0.99	0.013	0.037	0.21	0.09	0.07	0.020	0.25	
W24x62 (N1)	**lab.**	0.07	1.18	0.015	**0.046**	0.13	0.11	0.08	<0.01	0.32	<0.005
	mill	0.07	1.19	0.01	0.04	0.14	0.12	0.07	0.03	0.33	
W30x211 (N2)	**lab.**	0.09	1.32	0.020	0.025	0.33	0.11	0.10	0.01	0.34	<0.005
	mill	0.09	1.28	0.00	0.01	0.32	0.10	0.08	0.02	0.36	
W36x300 (N3)	**lab.**	0.07	1.35	0.017	0.035	0.27	0.13	0.06	0.01	0.34	<0.005
	mill	0.06	1.33	0.01	0.02	0.26	0.13	0.05	0.03	0.34	
W14x211 (N4)	**lab.**	0.08	1.27	0.020	0.027	0.24	0.11	0.11	0.01	0.35	<0.005
	mill	0.06	**1.36**	0.02	0.02	0.24	0.12	0.09	0.03	0.38	
W36x150 (N5)	**lab.**	0.10	1.20	0.016	0.029	0.22	0.17	0.12	0.03	0.27	<0.005
	mill	0.08	1.21	0.02	0.02	0.23	0.18	0.09	0.04	0.30	
W14x311 (N6)	**lab.**	0.08	1.28	0.012	0.024	0.23	0.13	0.09	0.01	0.32	<0.005
	mill	0.07	1.32	0.01	0.01	0.23	0.14	0.08	0.03	0.33	
W14x211 (B1)	**lab.**	0.06	1.35	0.018	0.005	0.29	0.21	0.03	<0.01	0.30	**0.029**
	mill	0.08	**1.45**	0.017	0.003	0.308	0.233	0.025	0.003	0.329	
W14x311 (B2)	**lab.**	0.07	1.28	0.017	0.005	0.25	0.21	0.03	<0.01	0.31	**0.022**
	mill	0.08	**1.45**	0.017	0.003	0.308	0.233	0.025	0.003	0.329	
W36x300 (B3)	**lab.**	0.11	1.25	0.017	<0.005	0.24	0.01	0.03	<0.01	0.02	**0.020**
	mill	0.13	**1.39**	0.018	0.003	0.303	0.018	0.026	0.003	0.021	
W36x150 (B4)	**lab.**	0.11	1.31	0.016	0.008	0.27	0.02	0.03	<0.01	0.02	**0.029**
	mill	0.12	**1.40**	0.013	0.003	0.296	0.020	0.025	0.003	0.015	
W24x162 (T1)	**lab.**	0.09	0.97	0.025	0.029	0.18	0.10	0.18	<0.01	0.24	<0.005
	mill	0.09	1.07	0.027	0.016	0.20	0.12	0.19	0.032	0.26	
W30x211 (T2)	**lab.**	0.08	0.95	0.016	0.038	0.17	0.13	0.11	<0.01	0.16	<0.005
	mill	0.08	1.10	0.019	0.021	0.21	0.14	0.12	0.030	0.19	
W36x300 (T3)	**lab.**	0.07	0.95	0.019	0.037	0.18	0.13	0.14	<0.01	0.21	<0.005
	mill	0.08	1.02	0.020	0.025	0.19	0.14	0.14	0.032	0.24	
W14x211 (T4)	**lab.**	0.08	1.01	0.014	0.036	0.22	0.16	0.13	0.03	0.21	<0.005
	mill	0.08	1.08	0.015	0.024	0.21	0.17	0.12	0.053	0.23	
W36x150 (T5)	**lab.**	0.08	0.95	0.019	0.041	0.18	0.13	0.22	<0.01	0.17	<0.005
	mill	0.07	1.05	0.024	0.018	0.20	0.13	0.25	0.031	0.17	
W14x311 (T6)	**lab.**	0.08	0.93	0.022	0.034	0.19	0.13	0.17	<0.01	0.26	<0.005
	mill	0.09	1.06	0.026	0.027	0.23	0.14	0.17	0.037	0.29	

Table 7.2.1 (cont.) Comparison of Chemical Analyses from Laboratory and Mills

		% Vanadium	% Titanium	% Boron	% Niobium	% Lead	% Tin	% Nitrogen	Pcm	% Carbon Equivalent
ASTM A572	**min.**	0.01								
	max.	0.15						0.015		
New ASTM Spec.	**min.**									
	max.	0.05			0.05		0.02			0.45
W24x62 (C1)	**lab.**	<0.005	<0.005	<0.0005	0.013	<0.005	0.009	I.S.	0.00	0.37
	mill	0.002			0.010		0.011		0.19	0.35
W24x62 (N1)	**lab.**	<0.005	<0.005	<0.0005	0.012	<0.005	0.013	0.0074		0.34
	mill	0.00		0.0005			0.01		0.16	0.34
W30x211 (N2)	**lab.**	<0.005	<0.005	<0.0005	0.010	<0.005	0.018	I.S.		0.42
	mill	0.04		0.0005			0.02		0.20	0.42
W36x300 (N3)	**lab.**	<0.005	<0.005	<0.0005	0.005	<0.005	0.012	I.S.		0.39
	mill	0.05		0.0005			0.01		0.17	0.38
W14x211 (N4)	**lab.**	0.031	<0.005	<0.0005	<0.005	<0.005	0.012	0.0089		0.39
	mill	0.04		0.0005			0.01		0.17	0.39
W36x150 (N5)	**lab.**	0.029	<0.005	<0.0005	<0.005	<0.005	0.009	0.0087		0.40
	mill	0.03		0.0005			0.01		0.18	0.38
W14x311 (N6)	**lab.**	0.049	<0.005	<0.0005	0.006	<0.005	0.010	0.0100		0.39
	mill	0.05		0.0005			0.01		0.18	0.39
W14x211 (B1)	**lab.**	**0.120**	<0.005	<0.0005	<0.005	<0.005	<0.005	0.0077		0.40
	mill	**0.124**		0.000	0.004				0.20	0.44
W14x311 (B2)	**lab.**	**0.11**	<0.005	<0.0005	<0.005	<0.005	<0.005	0.0064		0.39
	mill	**0.124**		0.000	0.004				0.20	0.44
W36x300 (B3)	**lab.**	<0.005	<0.005	<0.0005	0.025	<0.005	<0.005	0.0050		0.37
	mill	0.003		0.000	0.037				0.21	0.43
W36x150 (B4)	**lab.**	<0.005	<0.005	<0.0005	0.030	<0.005	<0.005	0.0050		0.39
	mill	0.003		0.000	0.037				0.20	0.42
W24x162 (T1)	**lab.**	<0.005	<0.005	<0.0005	<0.005	<0.005	0.006	0.0087		0.34
	mill	0.001		0.000	0.007		0.013		0.18	0.37
W30x211 (T2)	**lab.**	<0.005	<0.005	<0.0005	<0.005	<0.005	0.006	0.0051		0.31
	mill	0.001		0.000	0.007		0.014		0.16	0.35
W36x300 (T3)	**lab.**	<0.005	<0.005	<0.0005	<0.005	<0.005	0.008	0.0090		0.31
	mill	0.001		0.000	0.007		0.014		0.16	0.34
W14x211 (T4)	**lab.**	<0.005	<0.005	<0.0005	0.008	<0.005	0.008	0.0100		0.34
	mill	0.001		0.000	0.006		0.013		0.16	0.36
W36x150 (T5)	**lab.**	<0.005	<0.005	<0.0005	<0.005	<0.005	0.006	0.0074		0.34
	mill	0.001		0.000	0.006		0.012		0.15	0.36
W14x311 (T6)	**lab.**	<0.005	<0.005	<0.0005	<0.005	<0.005	0.007	0.0101		0.33
	mill	0.001		0.000	0.006		0.016		0.18	0.38

One Mill N member and all four members from Mill B showed manganese levels above the maximum ASTM A572 requirement, but none exceeded the new ASTM Gr. 50 with Special Provisions requirement. Interestingly, in all cases of high manganese, the mill reports showed the violation but the laboratory results were within allowable limits.

In addition to high manganese, all four Mill B members reported excessive amounts of aluminum. One reason for this may be that of the four mills in this study, Mill B is the only one still using raw iron ore in their production process. The other mills, possibly because of their exclusive use of recycled materials, show tighter controls on these elements.

High amounts of vanadium were reported in the two Mill B column sections. Both members reported values above the maximum allowed by the new ASTM Grade 50 Specification. Results from three Mill N sections (W14x211, W14x311 and W36x150) are noteworthy because they are the only other sections with significant amounts of vanadium.

7.3 EFFECT OF CHEMISTRY ON TENSILE AND TOUGHNESS PROPERTIES

As was mentioned earlier in Chapter 6, Charpy specimens from Mill B exhibited outstanding toughness—consistently better than those from any of the other mills. One reason for this could be the low amount of sulfur in these steels. A correlation was found between toughness behavior and the amount of sulfur in the steel, as is shown in Figure 7.3.1.

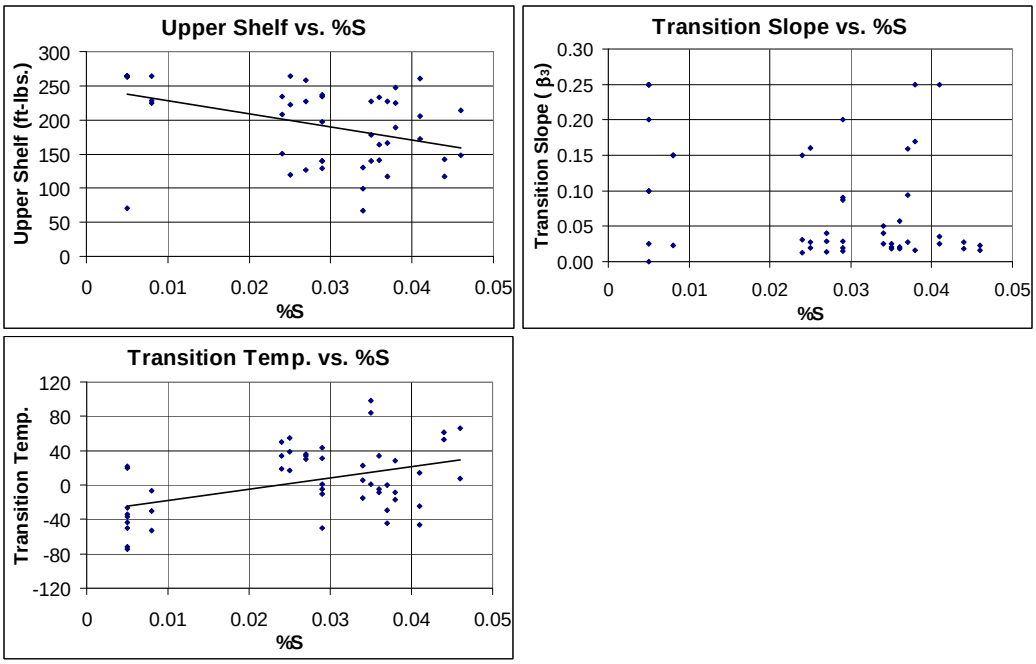

Figure 7.3.1 Effect of Sulfur on Toughness Parameters

These graphs show that as the amount of sulfur or copper increased, the upper shelf decreased and the transition temperature increased (the trend lines in the graphs were calculated using least-squares regression.). No relationship was observed between these elements and the transition slope, β_3.

Carbon, equivalent carbon, and manganese were also plotted against the toughness parameters but no relationship was observed between any of these three elements and toughness behavior. This was unexpected, since it is known that the presence of carbon increases the strength and decreases the ductility of steel. This trend was not observed in the test data, possibly because the amount of carbon was extremely small in all samples. The amount of carbon ranged from 0.06% to

0.12% over the set of specimens in the study and this range might have been too small to influence the toughness behavior significantly.

No relationship was observed between chemistry and tensile behavior. Sulfur, copper, carbon, equivalent carbon, and manganese were each plotted against F_{sy}, F_{uy}, and F_u, but no significant correlation was observed.

Chapter 8: Conclusions and Suggested Areas of Research

8.1 CROSS-SECTIONAL GEOMETRY

From the data in this project, the measured flange thickness dimensions tended to be smaller than the theoretical values and varied significantly within the cross section. A large reason for this is that currently, ASTM A6 does not specify any flange width tolerances for rolled shapes. A specification similar to JIS-G3136 allowing tighter control of the flange thickness dimension would result in member flexural behavior much closer to the theoretical behavior used in engineering design and analysis. It was found that the members that did not meet the flange thickness requirements given in JIS-G3136 had calculated section properties as much as 6% lower than theoretical. Of those that did meet the JIS-G3136 flange thickness specification, the maximum error between measured and theoretical section properties dropped to 3%.

From the measured values of member depth (d), flange width (b_f), flange thickness (t_f), and web thickness (t_w), the cross-sectional areas of the sections were calculated. Of the seventeen total specimens, five were shown to be below the minimum value allowed in ASTM A6, paragraph 13. Since the fillets were not measured as part of this project, they were assumed to be equal to the theoretical values. A spokesman from Mill N claimed that their practice of using over-sized fillet welds allows them to produce sections with smaller values of d, b_f, t_f, or t_w and still meet the specified weight/ft. requirements. A flange thickness

specification would eliminate this practice by forcing flanges to meet certain required minimum dimensions.

8.2 TENSILE PROPERTIES

Tension test results from the seventeen wide-flange members used in this project were compiled to create a typical tension stress-strain curve, shown in Figure 8.2.1. The flange yield strength was found to be about 95% of the web yield strength (one producer had widely varying results which increased the overall average), so the flange material was treated separately from the web material. The curve was specifically created to model flange material since the flanges play a greater role in the structural behavior of a rolled shape than the web does.

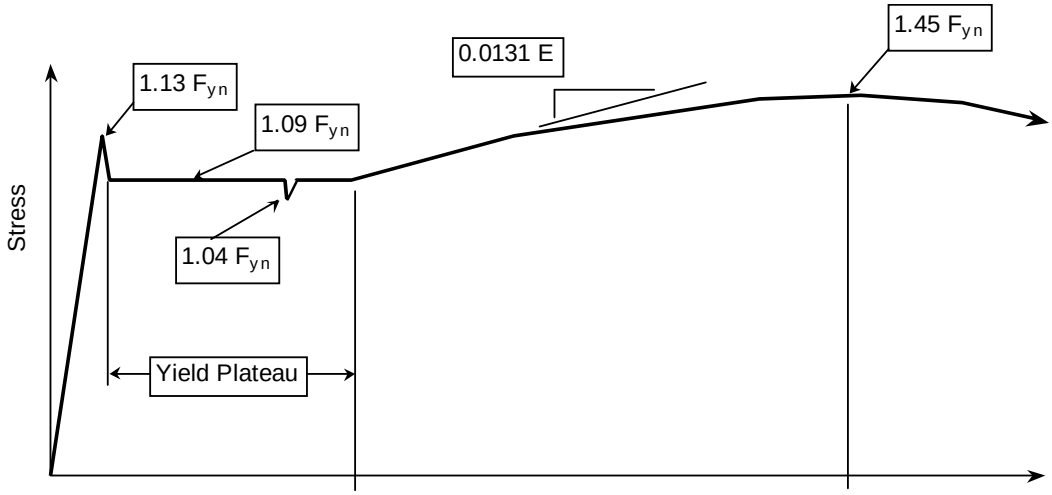

	F_{uy}/F_{yn}	F_y/F_{yn}	F_{sy}/F_{yn}	$\varepsilon_{sh}/\varepsilon_{yn}$	E_{sh}/E	$\varepsilon_u/\varepsilon_{yn}$	F_u/F_{yn}
Mean:	1.13	1.09	1.04	8.73	0.0131	86.2	1.45
Maximum:	1.29	1.28	1.24	14.0	0.0165	117	1.55
Minimum:	0.96	0.96	0.91	4.29	0.0075	68.2	1.32
Std. Dev.:	0.09	0.08	0.08	2.90	0.0024	11.5	0.06
# of Specimens:	41	59	59	38	38	59	63

Figure 8.2.1 Typical Tension Stress-strain Curve for Flange Material

The effect of coupon type on stress-strain parameters is another possible area of research. In this project only one test was performed comparing specimens of different type (strap vs. ½"-round) from adjacent locations on a cross section. Similar tests need to be performed to determine if the observed differences were indeed due to coupon type or to material variation.

Relationships between the measured stress-strain parameters and mill test report values were calculated. The measured Upper Yield Point stress (F_{uy}) was on average about 98% of the yield strength reported by the mills (F_{ymill}). The yield strength (F_y) and the static yield strength (F_{sy}) averaged 95% and 90%, respectively, of F_{ymill}. The ultimate strength (F_u) averaged about 96% of F_{umill}.

The mill test reports from Mill T should be interpreted with caution. On average they were found to overestimate the true yield strength by 9%, and in some cases as much as 24%.

8.3 TOUGHNESS BEHAVIOR

AISC A3.1c specifies a minimum core toughness of 15 ft-lbs. at 70°F for Group 4 and 5 rolled shapes used as tension members. This requirement was satisfied in the flange, web, and core regions of all sections in the program. Overall, the average Upper Shelf value was 196 ft-lbs. and the average nil ductility temperature was around -37°F.

At room temperature, data show that the core region of a typical section showed toughness equal to or greater than its flange and web regions. However, as the temperature was lowered, the core region showed a relatively abrupt transition from ductile to brittle behavior, and it did so at a higher temperature than the flange and web regions. These observations back up reports of brittle behavior in the core region and suggest that during periods of low temperatures, the core region will be the first part of the cross section to exhibit brittle behavior.

Specimens from all four mills showed very good toughness throughout their cross sections. The column core toughness was not found to differ significantly from the beam core toughness. Also, the core regions of Group 4 and 5 shapes, thought to be low-toughness spots, showed toughness levels comparable to other size members.

Appendix A: Measurements of Cross-sectional Dimensions

Flange Thickness

	t_{f1}	t_{f2}	t_{f3}	t_{f4}	t_{f5}	t_{f6}	t_{f7}	t_{f8}
C1	0.602	0.596	0.596	0.603	0.601	0.595	0.597	0.606
N1	0.56	0.563	0.55	0.542	0.562	0.561	0.552	0.532
N2	1.203	1.253	1.32	1.248	1.207	1.235	1.301	1.255
N3	1.566	1.552	1.575	1.585	1.611	1.588	1.568	1.582
N4	1.504	1.491	1.492	1.495	1.494	1.454	1.514	1.498
N5	0.912	0.931	0.881	0.852	0.907	0.935	0.892	0.864
N6	2.216	2.217	2.215	2.178	2.213	2.198	2.192	2.166
B1	1.525	1.508	1.518	1.504	1.53	1.502	1.511	1.493
B2	2.206	2.128	2.198	2.168	2.2	2.158	2.157	2.168
B3	1.643	1.646	1.69	1.699	1.668	1.671	1.7	1.711
B4	0.944	0.958	0.929	0.939	0.938	0.943	0.926	0.928
T1	1.212	1.21	1.227	1.165	1.206	1.212	1.231	1.199
T2	1.298	1.329	1.306	1.307	1.296	1.324	1.309	1.306
T3	1.672	1.63	1.662	1.639	1.674	1.637	1.656	1.635
T4	1.577	1.575	1.489	1.514	1.579	1.534	1.495	1.525
T5	0.955	0.962	0.969	0.942	0.956	0.971	0.975	0.932
T6	2.184	2.16	2.242	2.223	2.212	2.173	2.247	2.209

Units: inches

Figure A1 Measured Values of Flange Thickness

Web Thickness

	t_{w1}	t_{w2}	t_{w3}	t_{w4}	t_{w5}	t_{w6}
C1	0.423	0.414	0.423	0.424	0.415	0.422
N1	0.420	0.417	0.420	0.420	0.416	0.420
N2	0.836	0.829	0.832	0.820	0.817	0.817
N3	0.991	0.989	1.003	0.983	0.991	0.995
N4	0.944	0.937	0.937	0.938	0.942	0.944
N5	0.644	0.650	0.649	0.651	0.655	0.655
N6	1.365	1.369	1.367	1.362	1.366	1.366
B1	0.975	0.987	0.959	0.970	0.982	0.961
B2	1.451	1.472	1.475	1.423	1.450	1.435
B3	0.951	0.942	0.938	0.954	0.959	0.953
B4	0.632	0.638	0.642	0.637	0.635	0.645
T1	0.712	0.708	0.690	0.706	0.708	0.696
T2	0.808	0.797	0.803	0.813	0.833	0.804
T3	0.975	0.962	0.941	0.974	0.956	0.940
T4	0.984	0.977	0.974	0.983	0.994	0.975
T5	0.617	0.625	0.613	0.613	0.613	0.616
T6	1.436	1.421	1.406	1.409	1.417	1.405

Units: inches

Figure A2 Measurement of Web Thickness Data

	Depth				Flange Width			
	d_1	d_2	d_3	d_4	b_{f1}	b_{f2}	b_{f3}	b_{f4}
C1	23.63	23.69	23.72	23.69	6.97	7.00	6.94	7.00
N1	23.81	23.69	23.75	23.69	7.03	7.16	7.09	7.16
N2	30.81	30.75	30.94	30.75	15.31	15.19	15.31	15.13
N3	36.56	36.75	36.63	36.75	16.75	16.81	16.81	16.81
N4	15.69	15.56	15.69	15.56	15.88	15.94	15.94	15.94
N5	36.06	36.00	35.88	36.00	12.16	12.25	12.19	12.19
N6	17.06	16.94	17.06	16.94	16.19	16.19	16.25	16.19
B1	15.69	15.75	15.69	15.75	15.63	15.63	15.63	15.63
B2	17.19	17.00	17.19	17.00	16.06	16.19	16.00	16.13
B3	36.88	36.72	36.88	36.75	16.50	16.56	16.47	16.50
B4	35.75	35.81	35.75	35.75	11.88	11.81	11.88	11.88
T1	25.19	25.19	25.19	25.13	13.13	13.13	13.06	13.19
T2	30.94	31.06	31.00	31.06	15.25	15.25	15.38	15.31
T3	36.94	36.63	37.00	36.56	16.88	16.94	16.94	16.94
T4	15.88	15.75	15.88	15.88	15.81	15.81	15.81	15.81
T5	35.94	35.81	35.69	35.63	11.94	12.00	12.06	12.13
T6	17.13	17.19	17.19	17.19	16.19	16.25	16.19	16.25

Units: inches

Figure A3 Measurement of Member Depth and Flange Width Data

Appendix B: Locations of Test Specimens Within the Cross sections

SPECIMEN: C1
SHAPE: W24x62

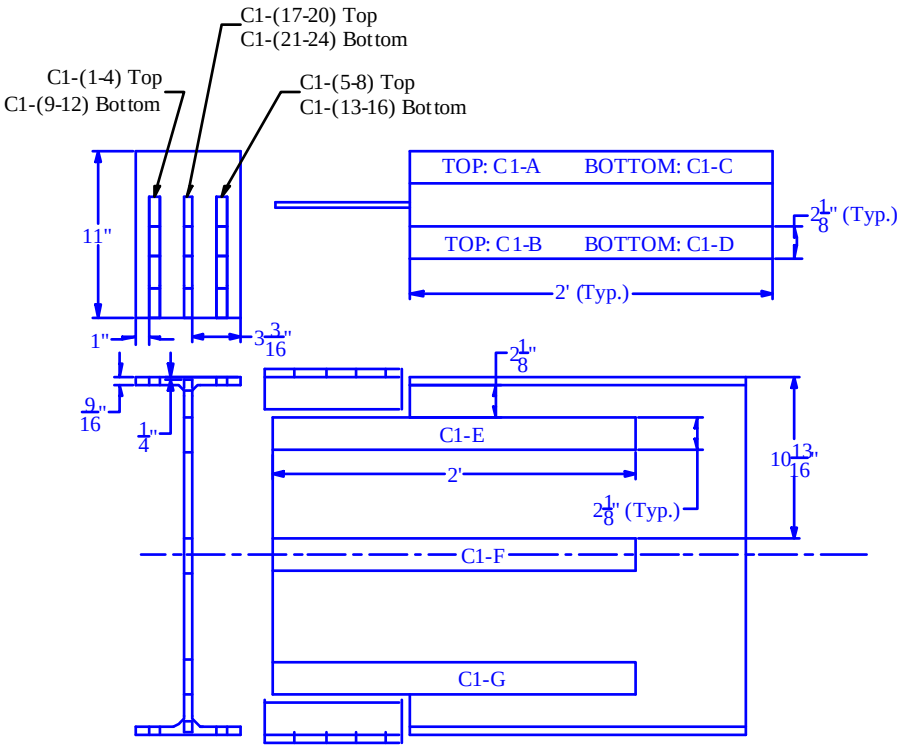

Initial Tensile Coupon Dimensions
(before machined to final dimensions)

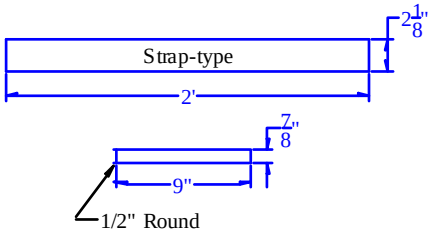

Initial Charpy Specimen Dimensions
(before machined to final dimensions)

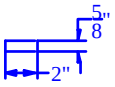

Figure B1.1 Member C1

SPECIMEN: N1
SHAPE: W24x62

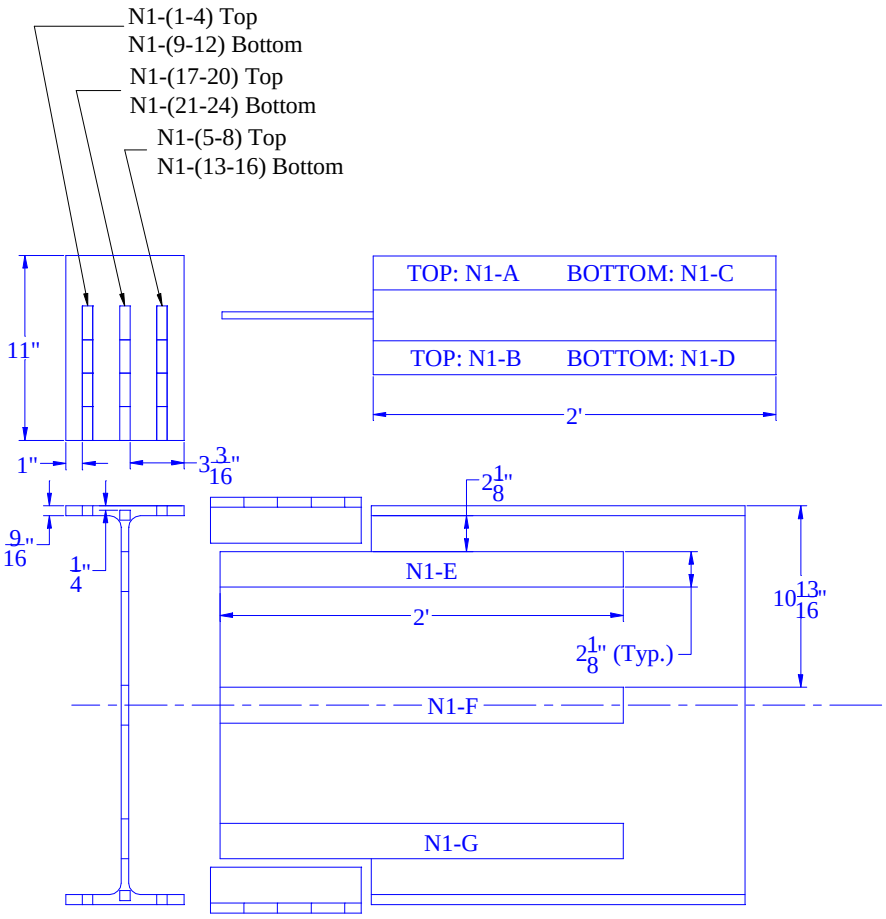

Figure B2.1 Member N1

SPECIMEN: N2
SHAPE: W30x211

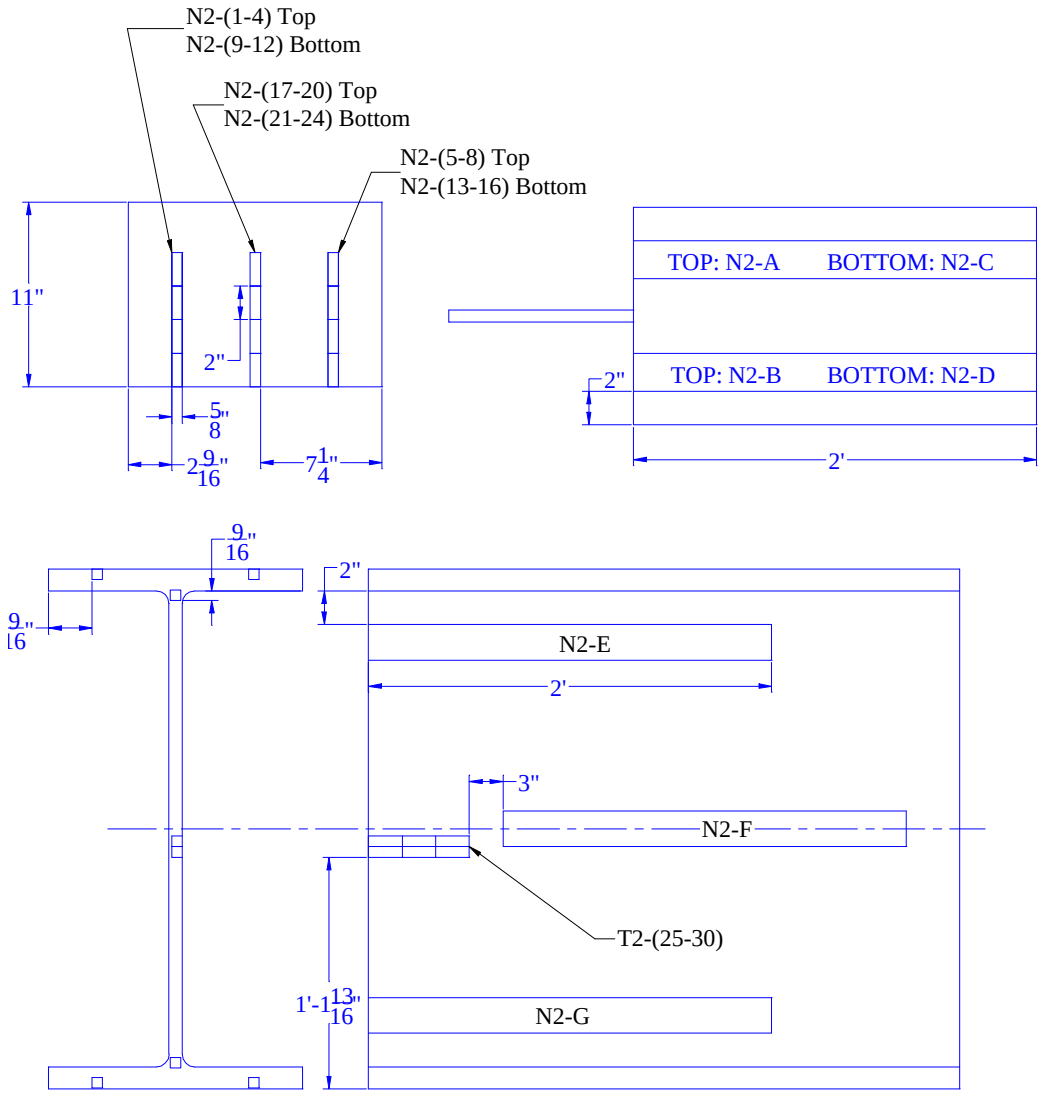

Figure B2.2 Member N2

SPECIMEN: N3
SHAPE: W36x300

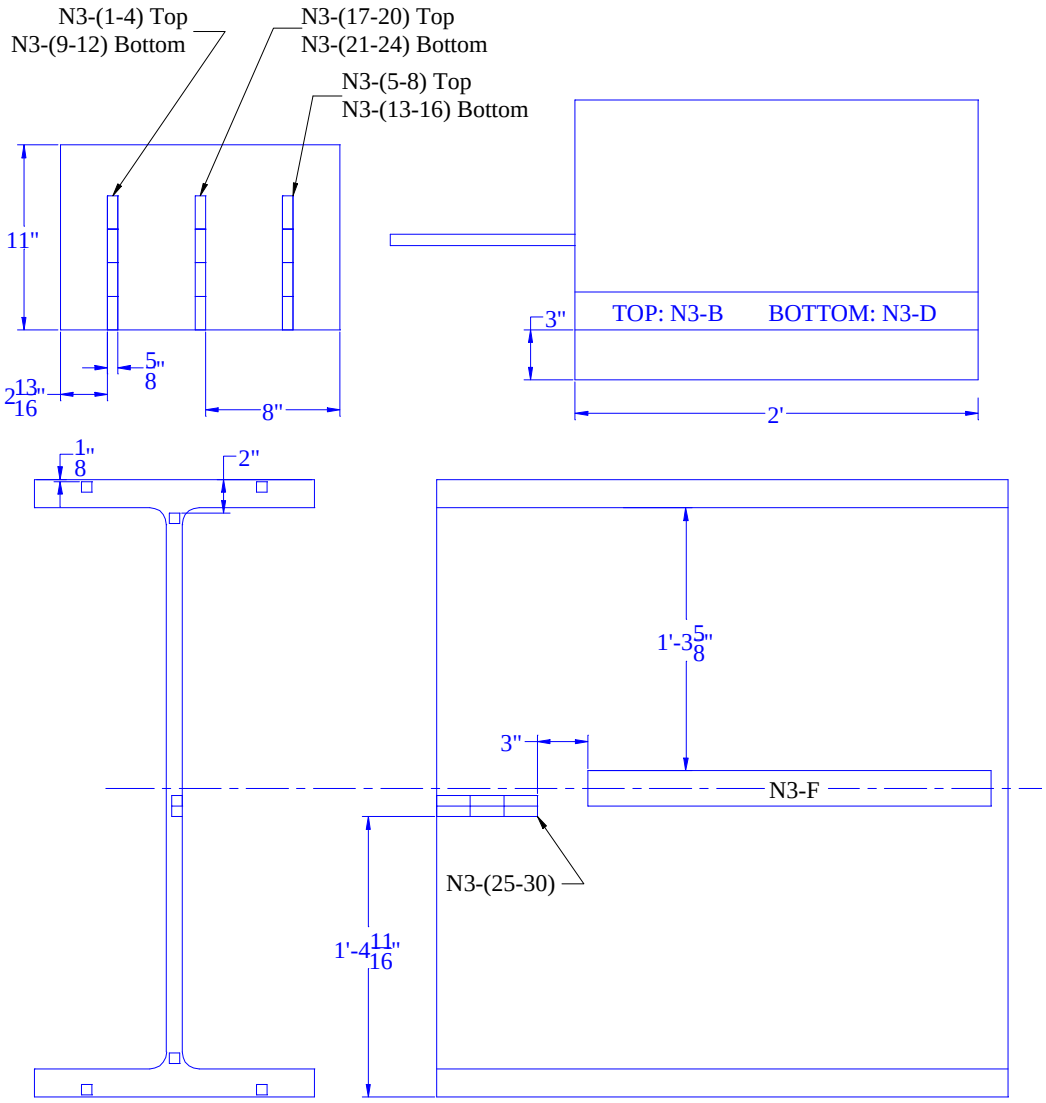

Figure B2.3 Member N3

SPECIMEN: N4
SHAPE: W14x211

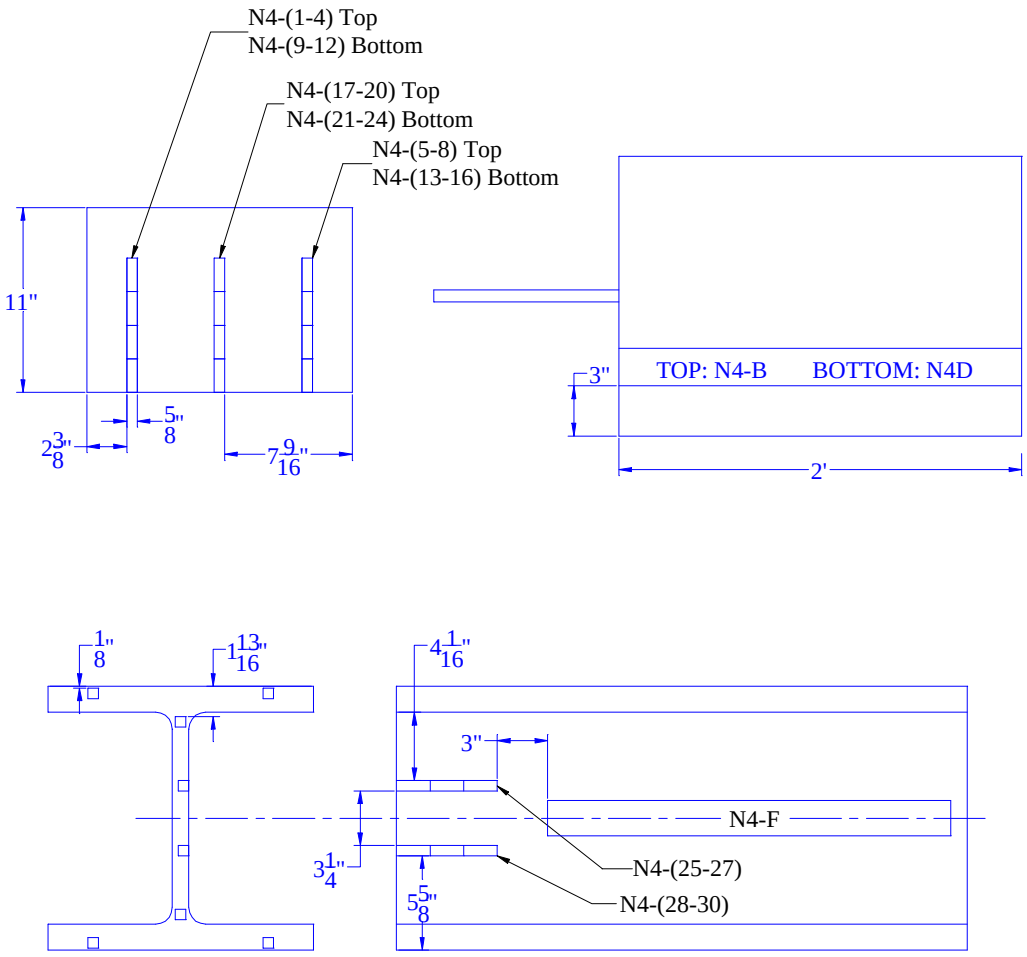

Figure B2.4 Member N4

SPECIMEN: N5
SHAPE: W36x150

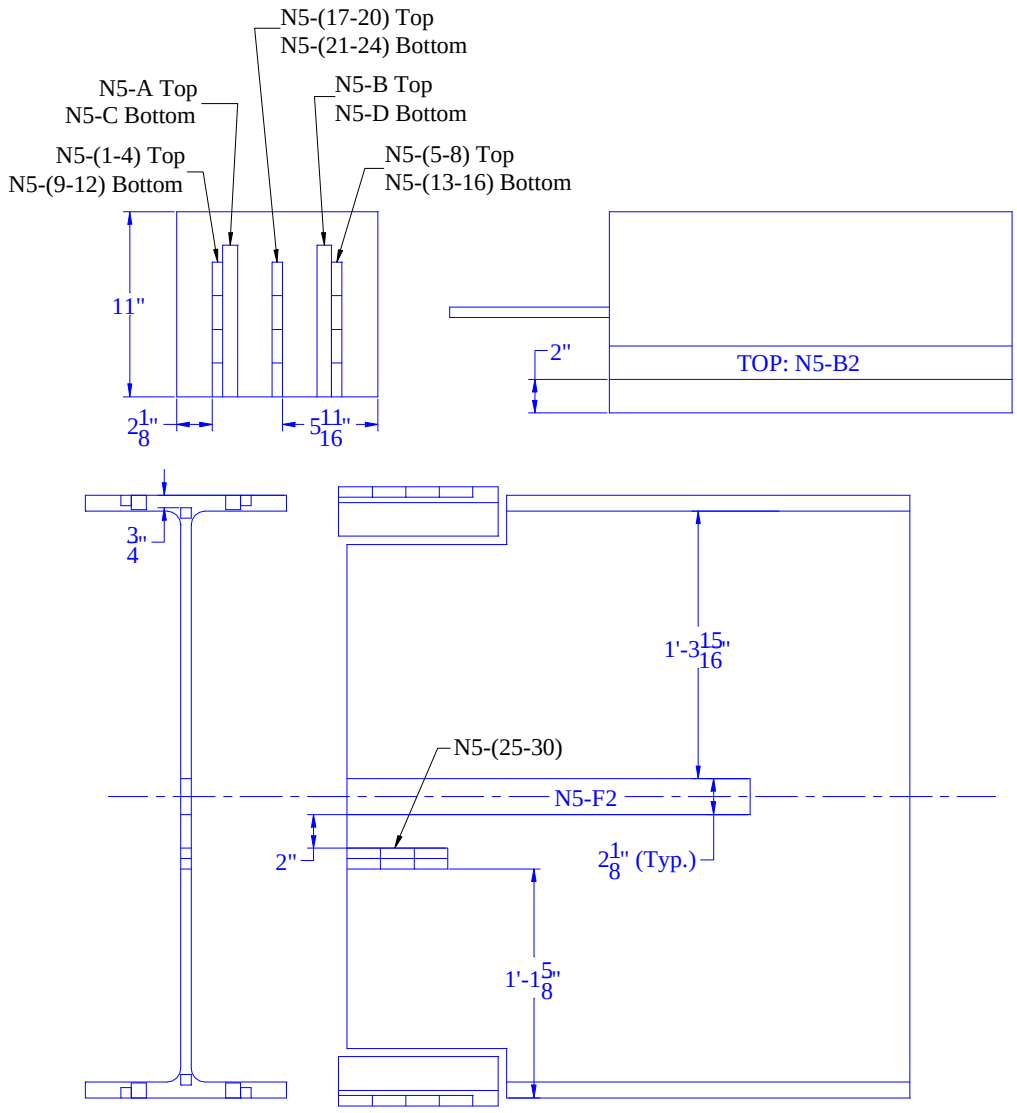

Figure B2.5 Member N5

SPECIMEN: N6
SHAPE: W14x311

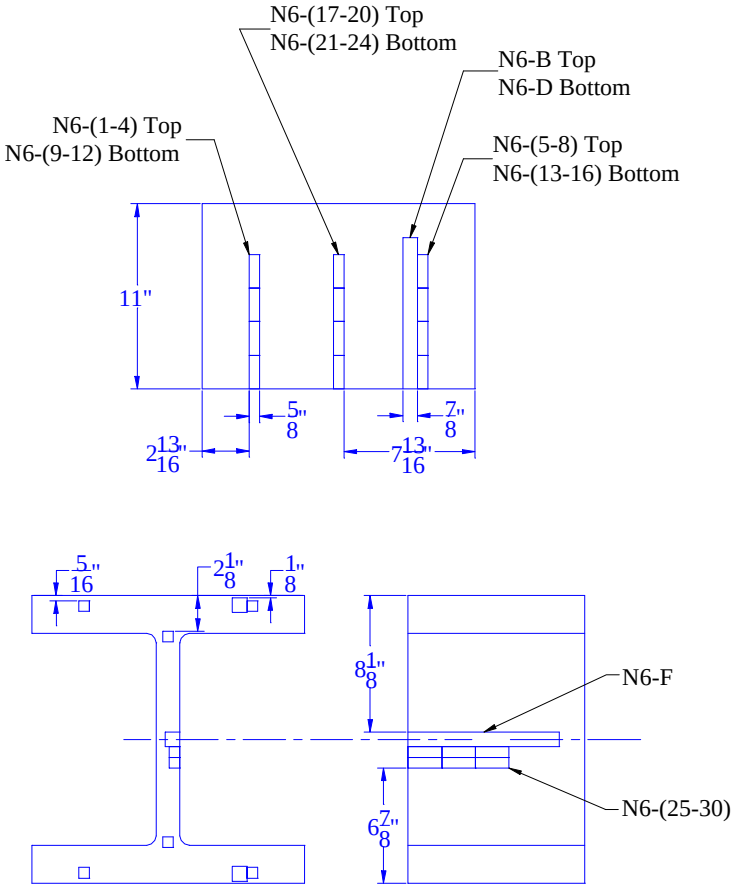

Figure B2.6 Member N6

SPECIMEN: B1
SHAPE: W14x211

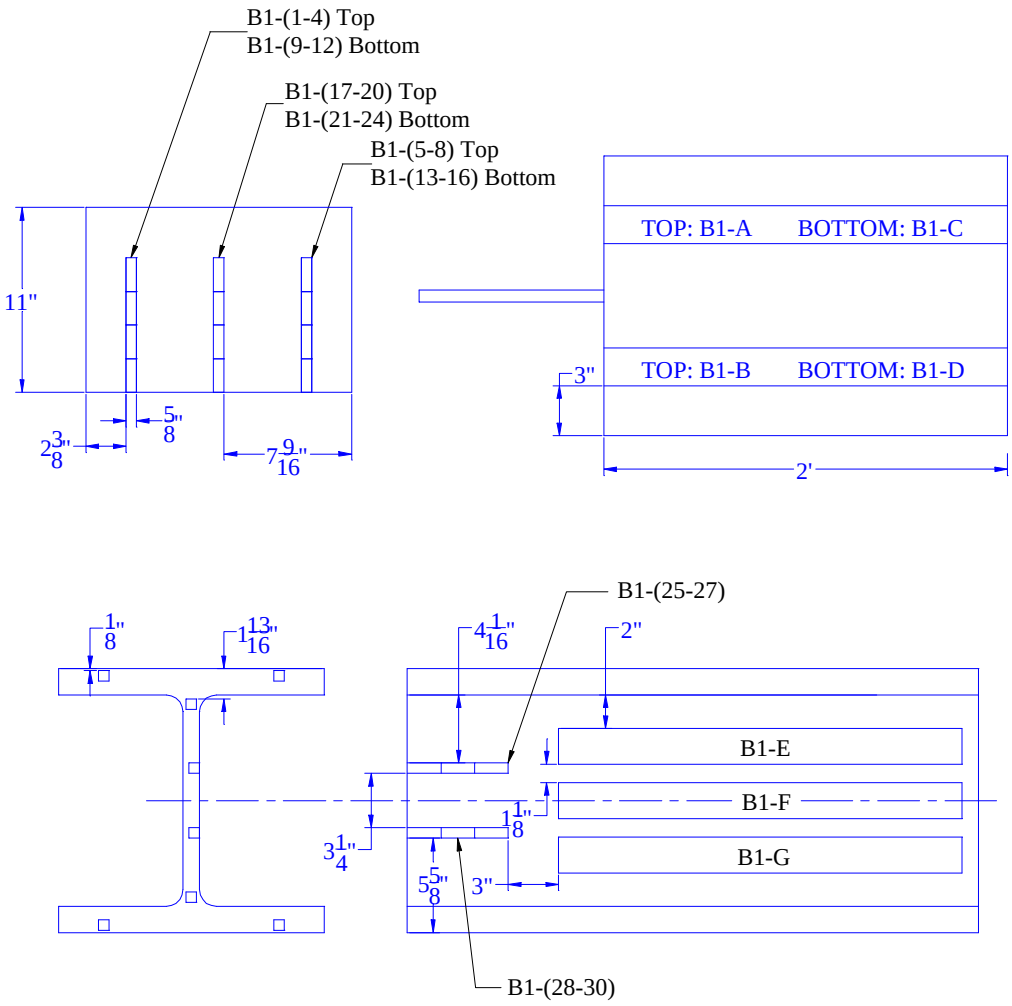

Figure B3.1 Member B1

SPECIMEN: B2
SHAPE: W14x311

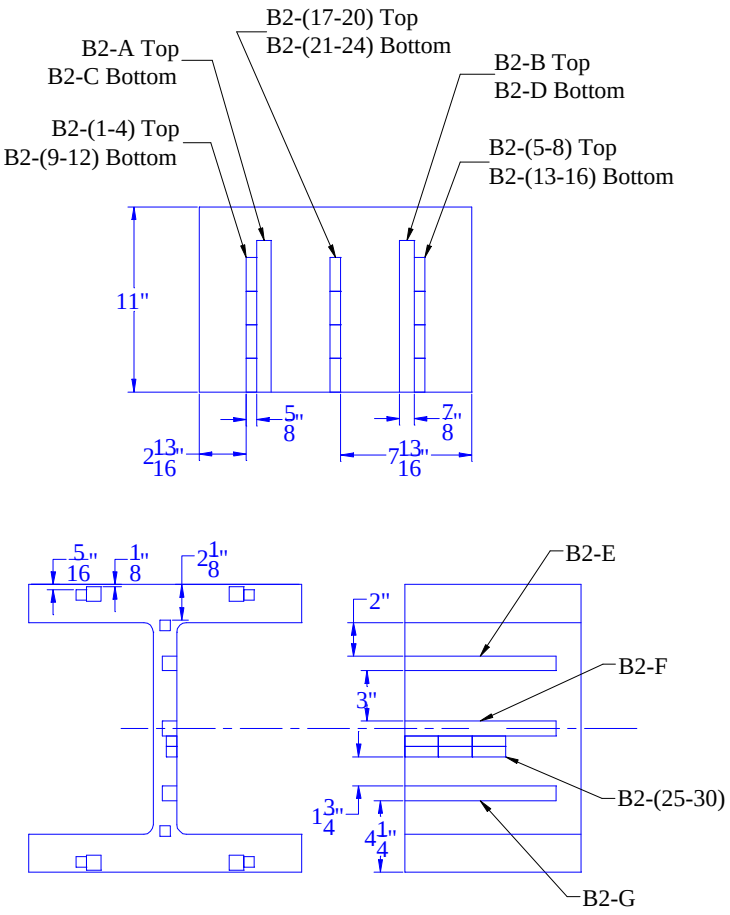

Figure B3.2 Member B2

SPECIMEN: B3
SHAPE: W36x300

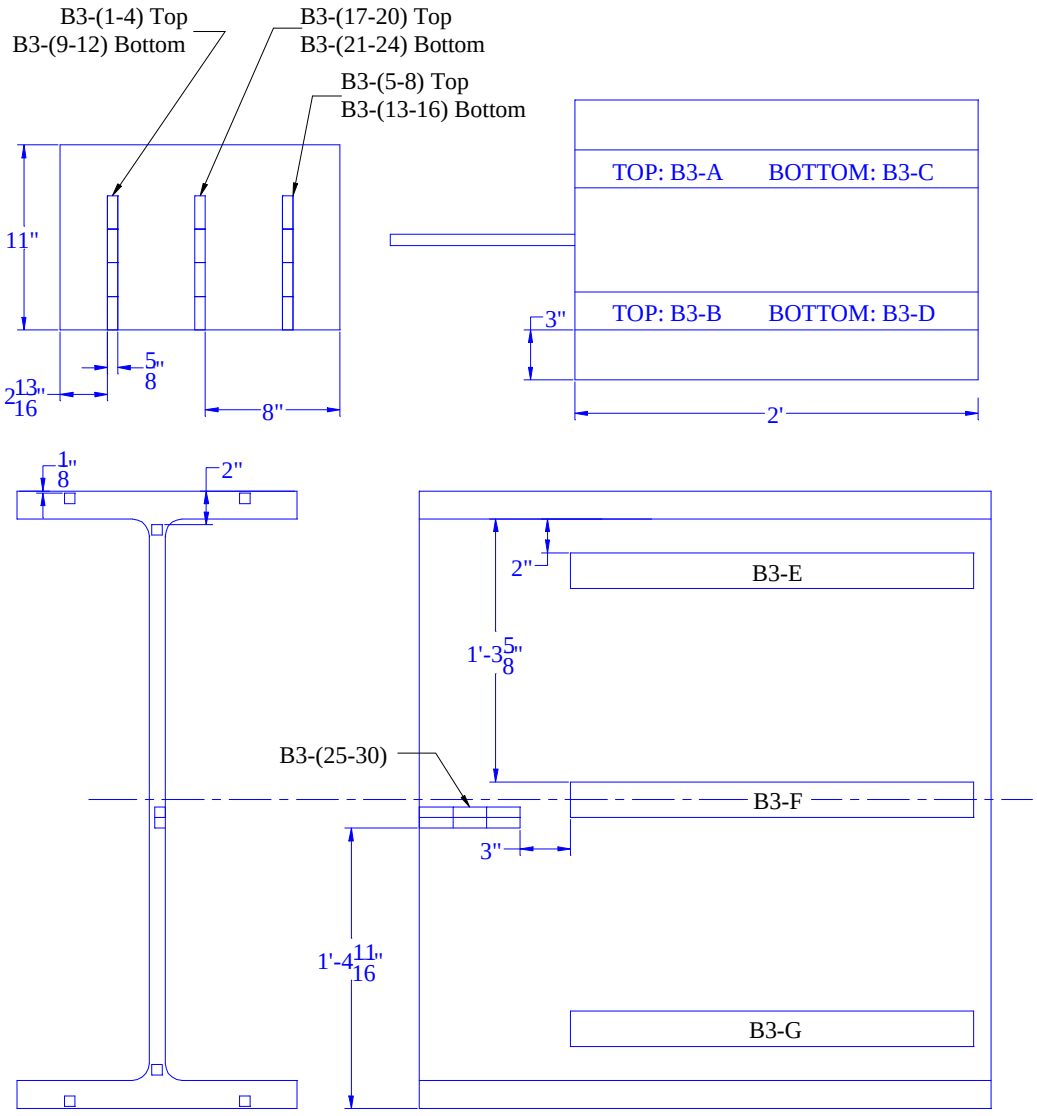

Figure B3.3 Member B3

SPECIMEN: B4
SHAPE: W36x150

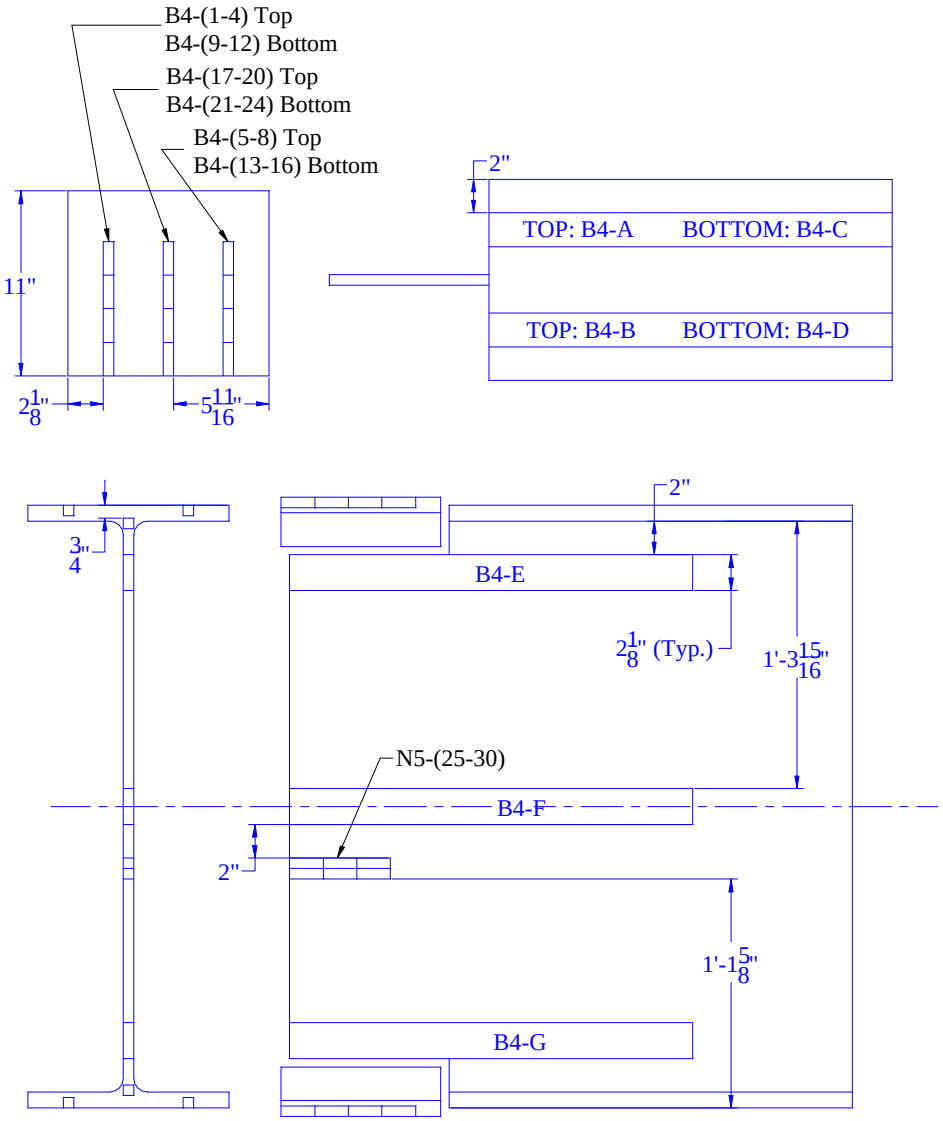

Figure B3.4 Member B4

SPECIMEN: T1
SHAPE: W24x162

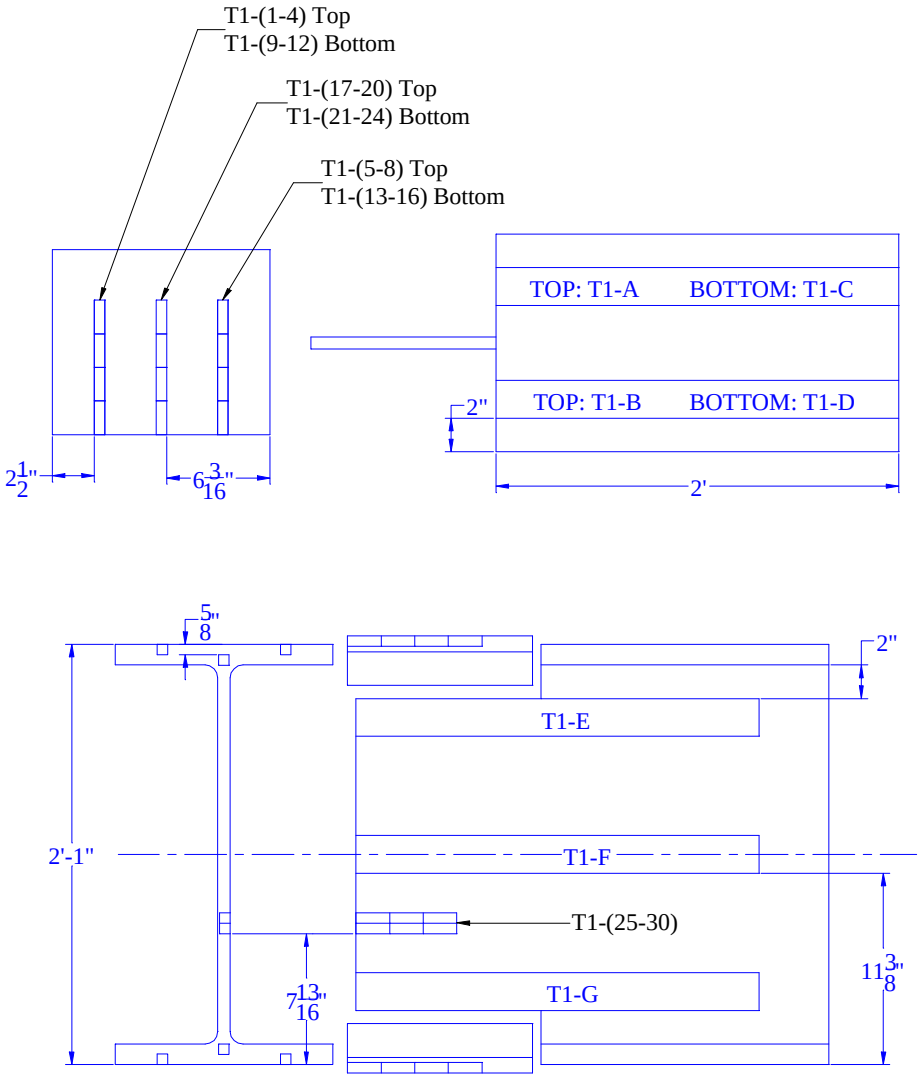

Figure B4.1 Member T1

SPECIMEN: T2
SHAPE: W30x211

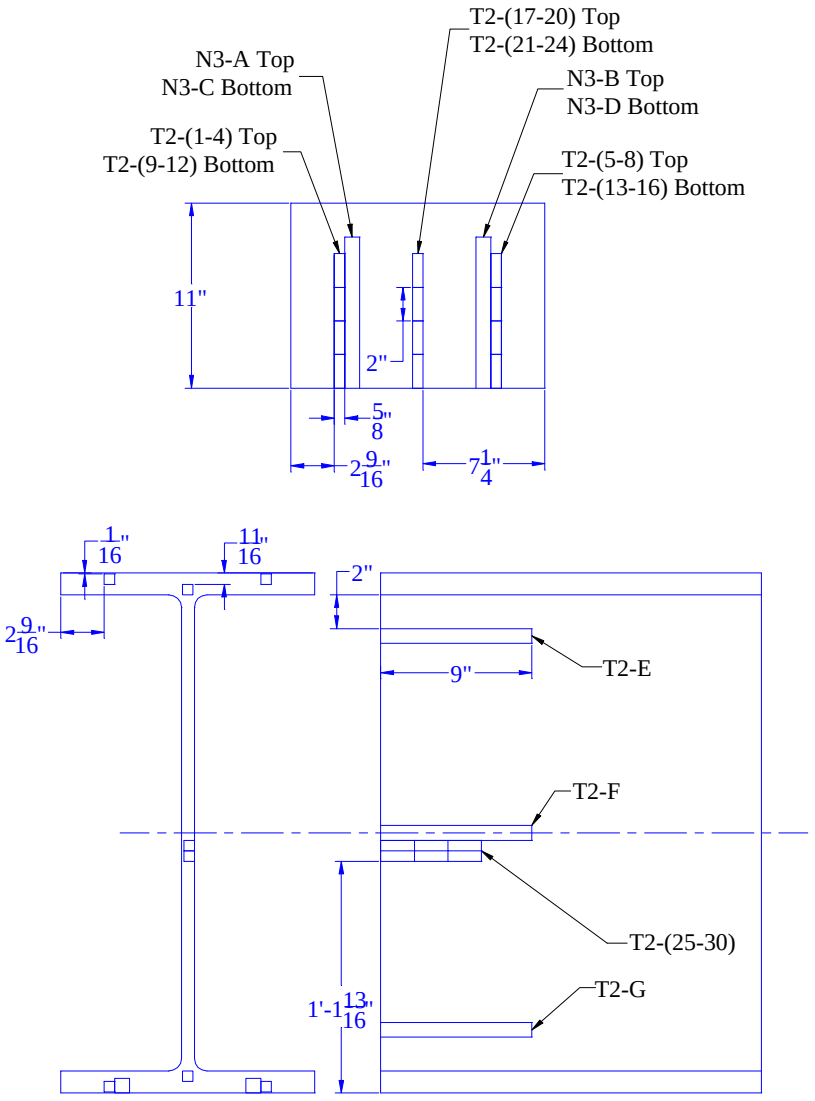

Figure B4.2 Member T2

SPECIMEN: T3
SHAPE: W36x300

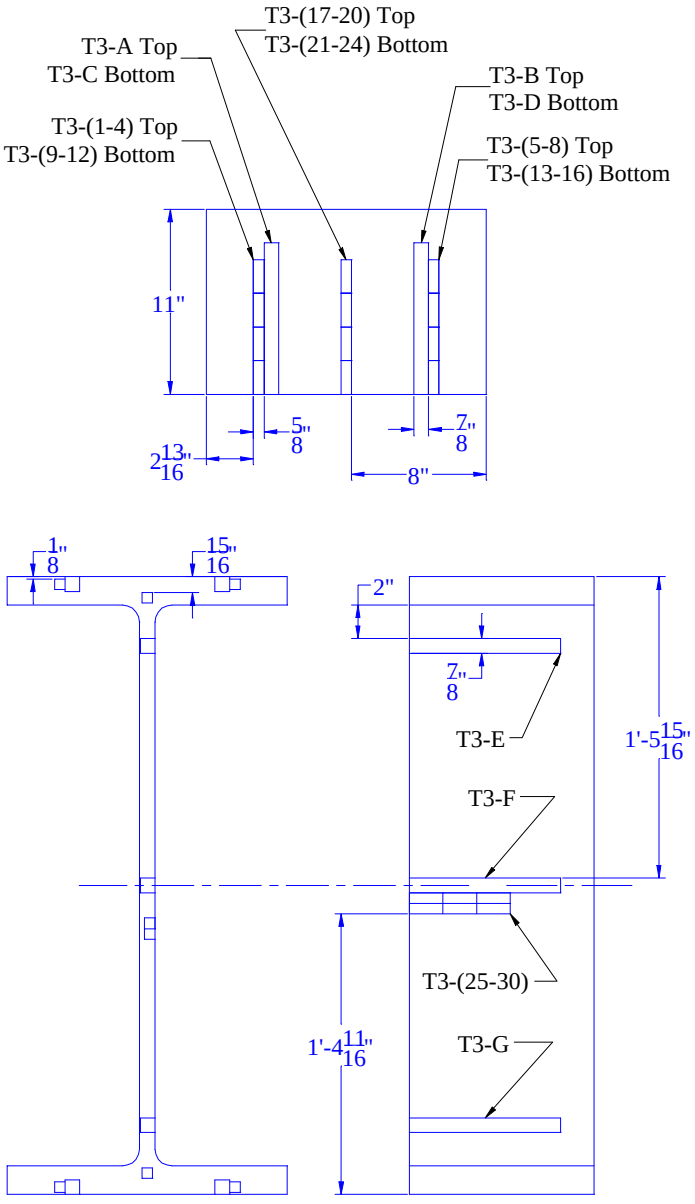

Figure B4.3 Member T3

SPECIMEN: T4
SHAPE: W14x211

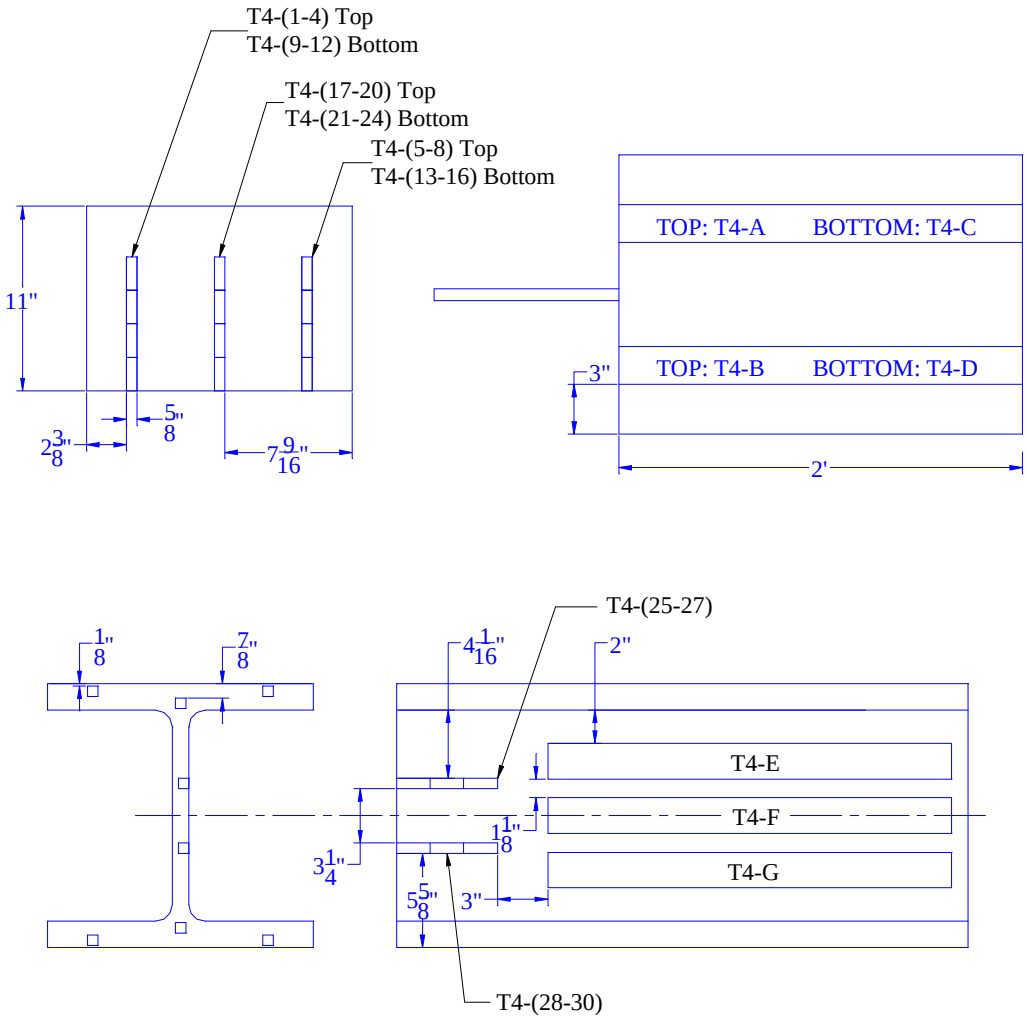

Figure B4.4 Member T4

SPECIMEN: T5
SHAPE: W36x150

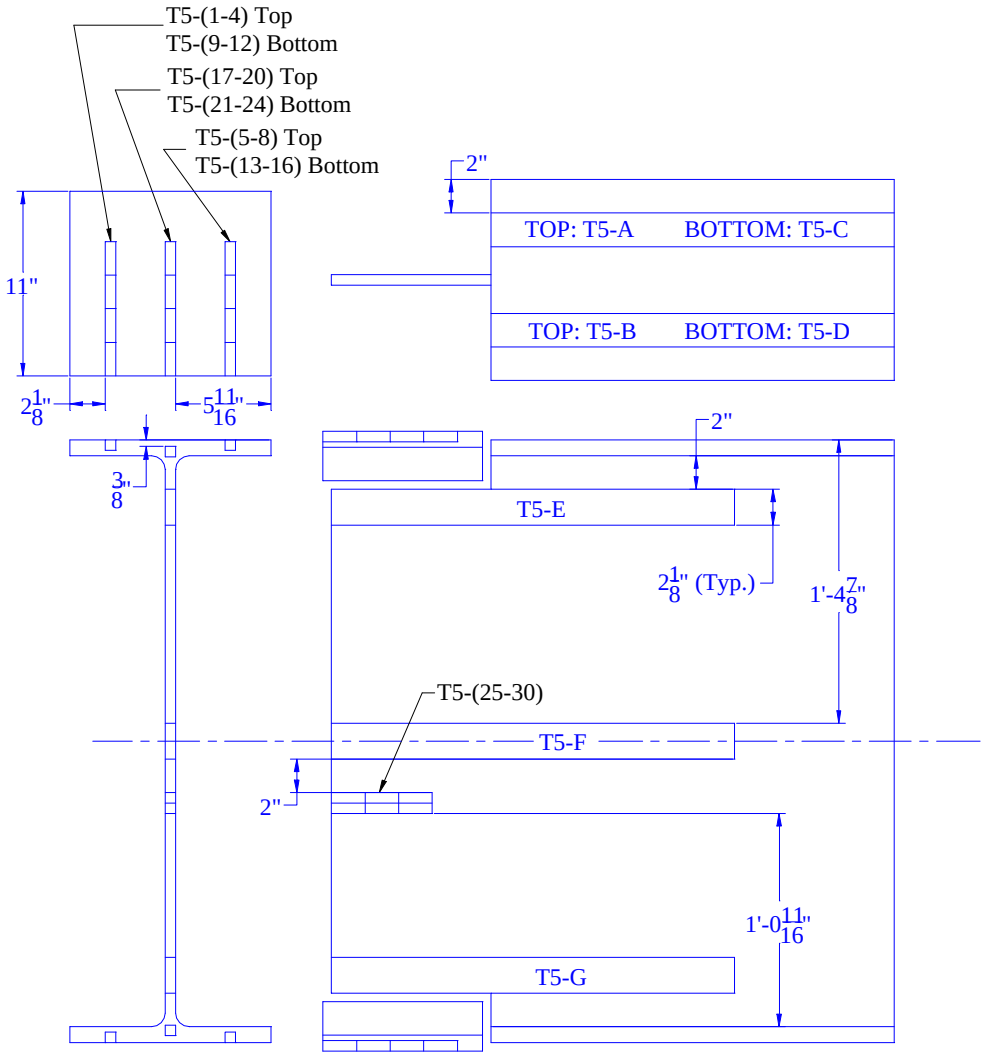

Figure B4.5 Member T5

SPECIMEN: T6
SHAPE: W14x311

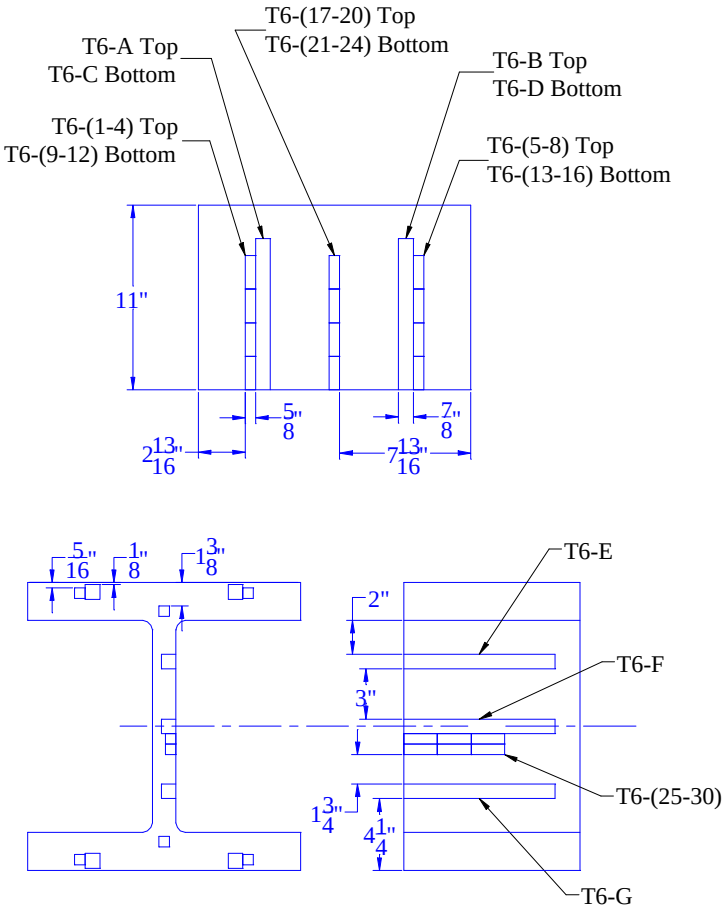

Figure B4.6 Member T6

Appendix C: Tensile Test Results

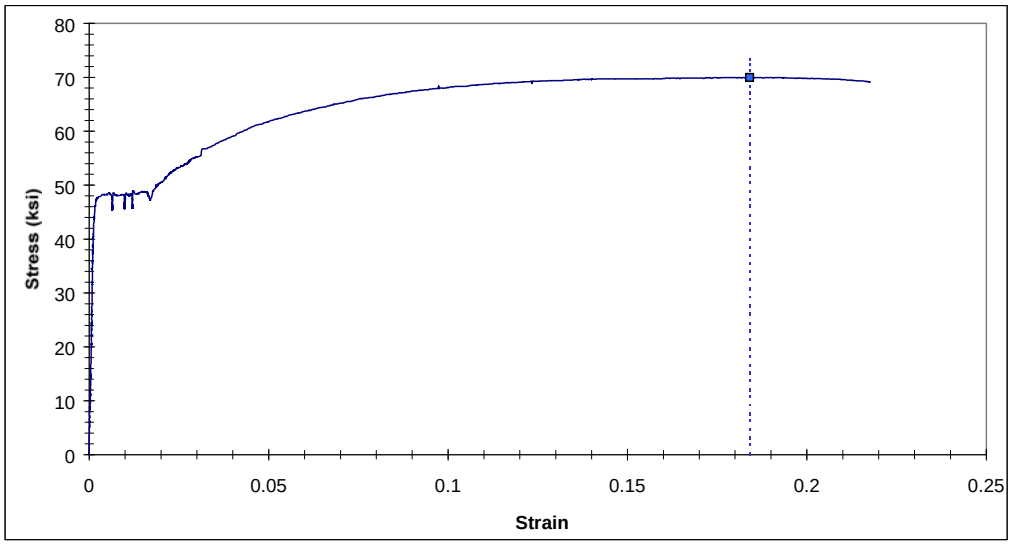

Figure C1.1.1 Complete Stress-strain Curve for Specimen C1-A

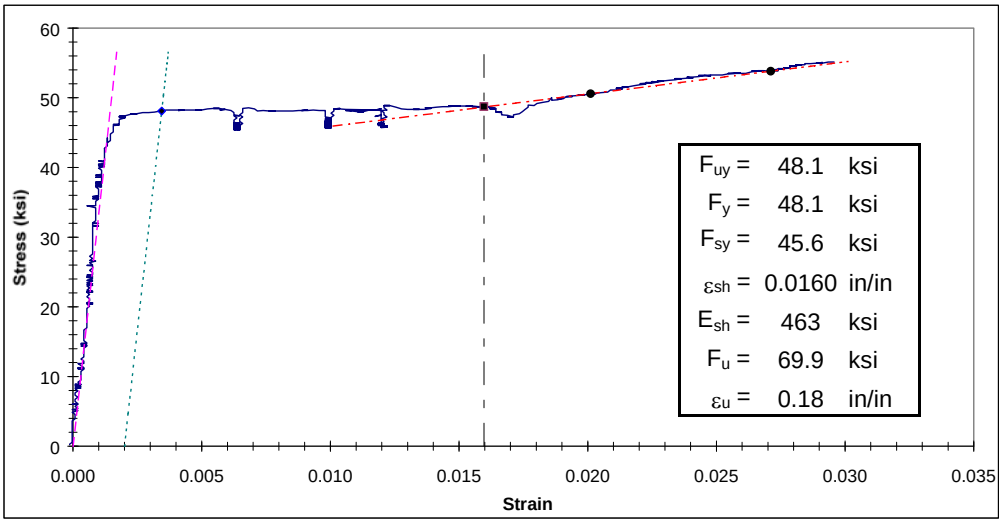

Figure C1.1.2 Yield Plateau and Tensile Test Results for Specimen C1-A

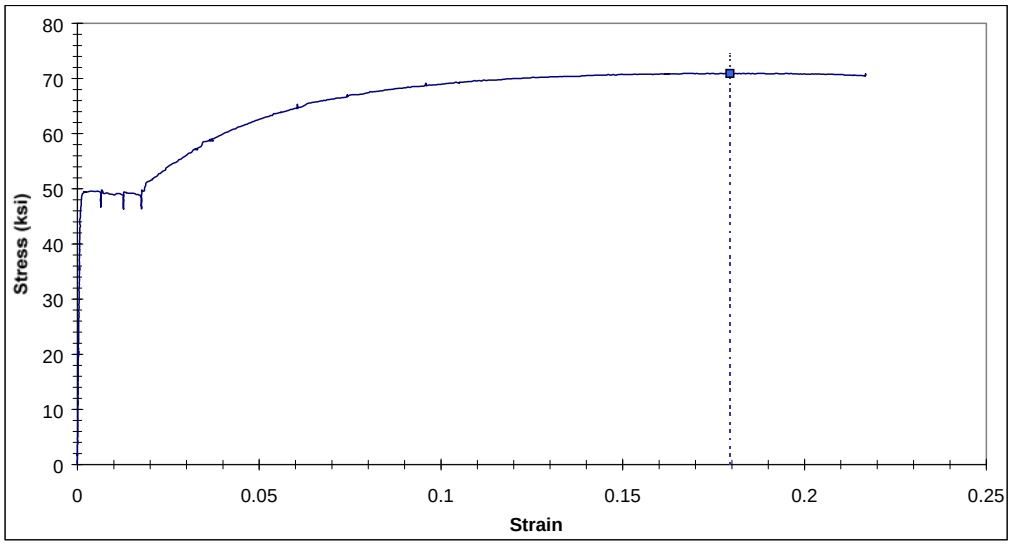

Figure C1.1.3 Complete Stress-strain Curve for Specimen C1-B

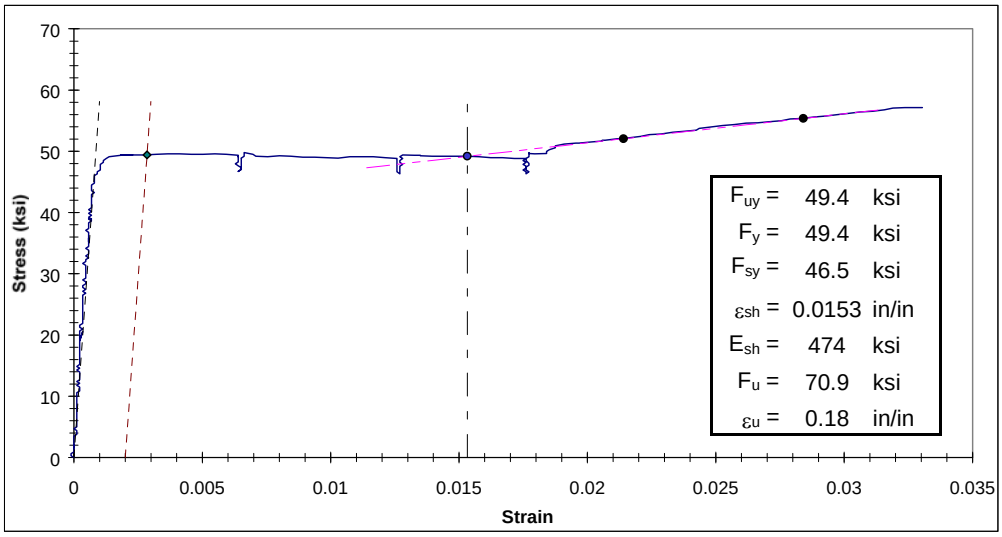

Figure C1.1.4 Yield Plateau and Tensile Test Results for Specimen C1-B

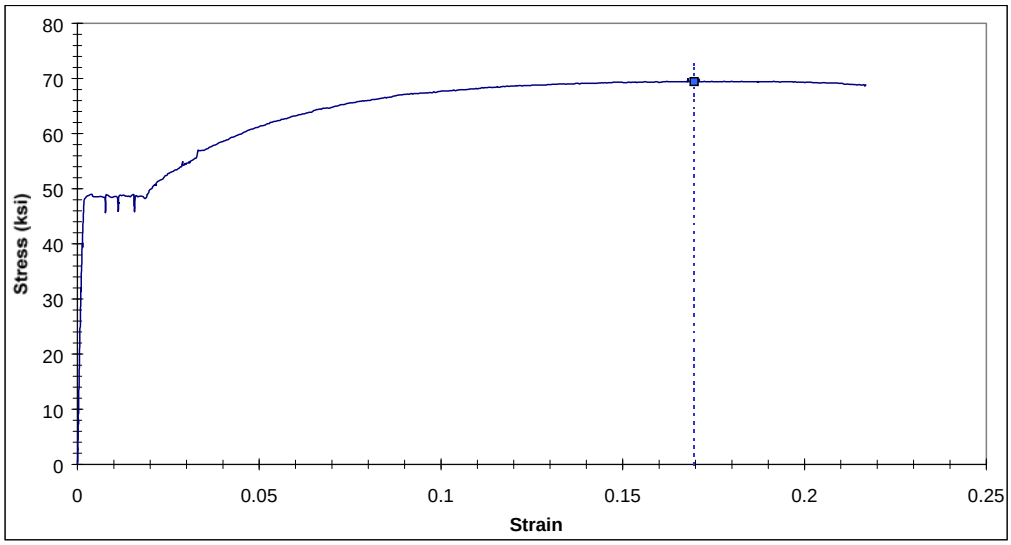

Figure C1.1.5 Complete Stress-strain Curve for Specimen C1-C

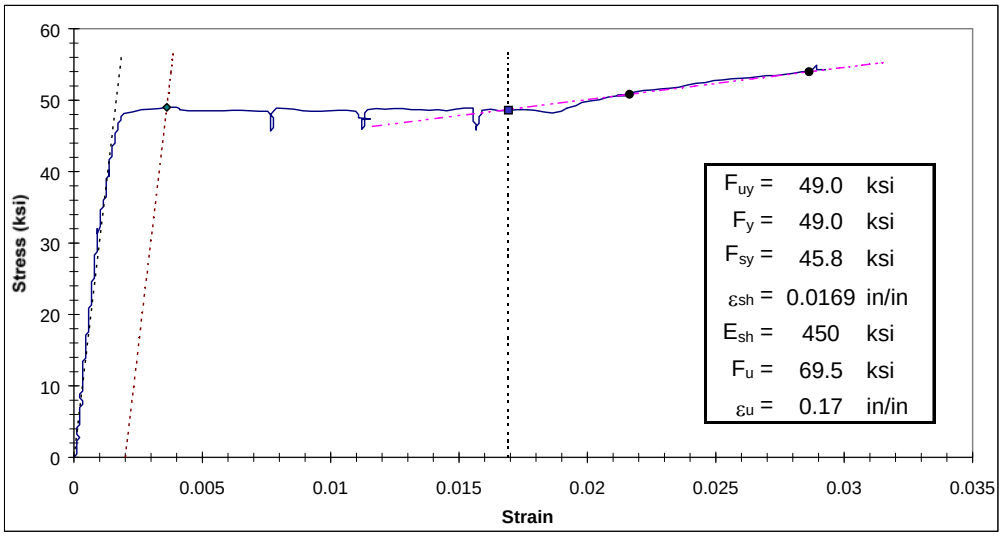

Figure C1.1.6 Yield Plateau and Tensile Test Results for Specimen C1-C

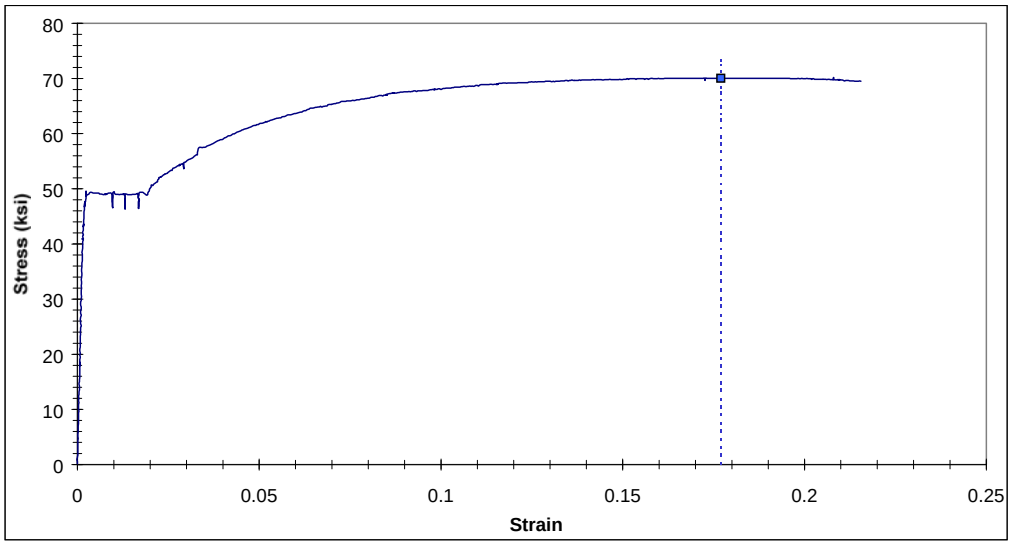

Figure C1.1.7 Complete Stress-strain Curve for Specimen C1-D

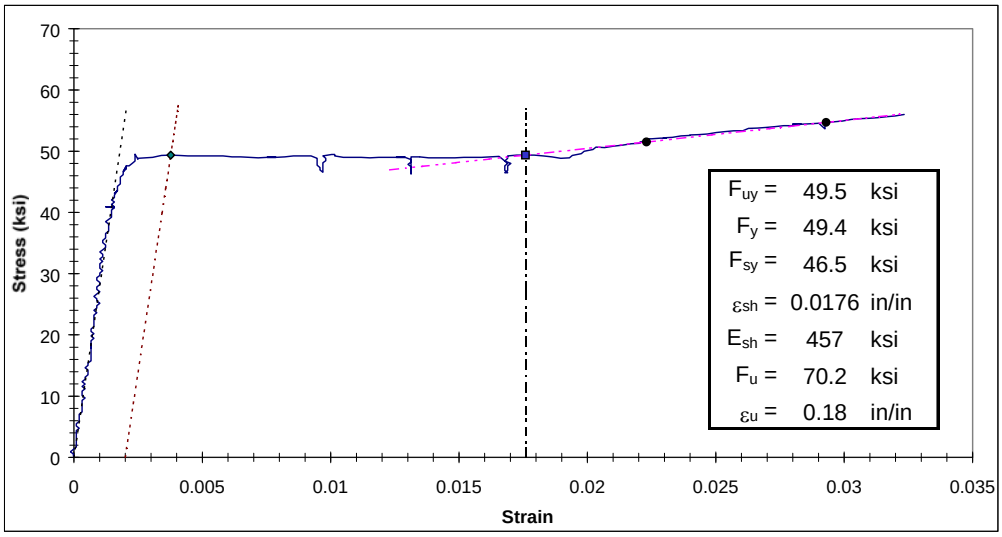

Figure C1.1.8 Yield Plateau and Tensile Test Results for Specimen C1-D

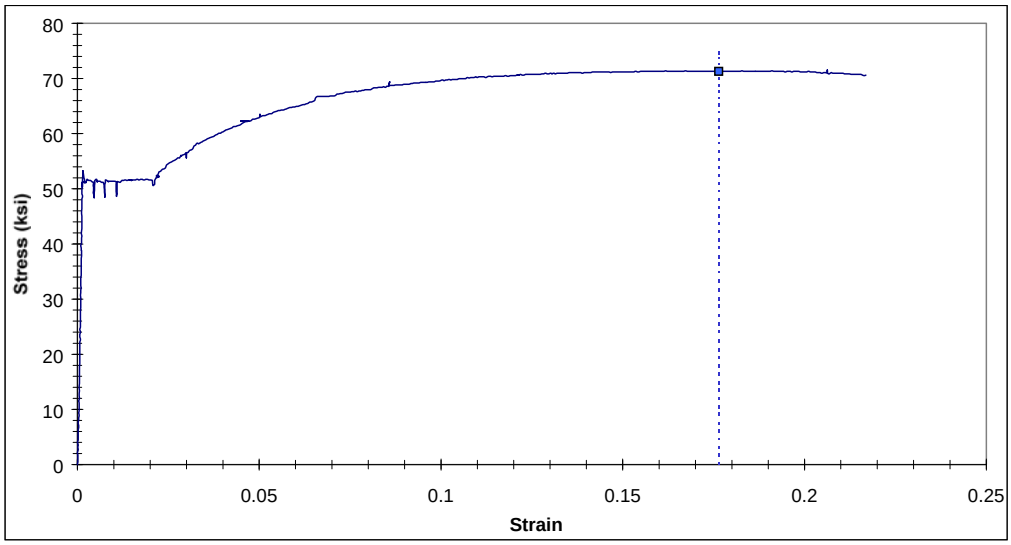

Figure C1.1.9 Complete Stress-strain Curve for Specimen C1-E

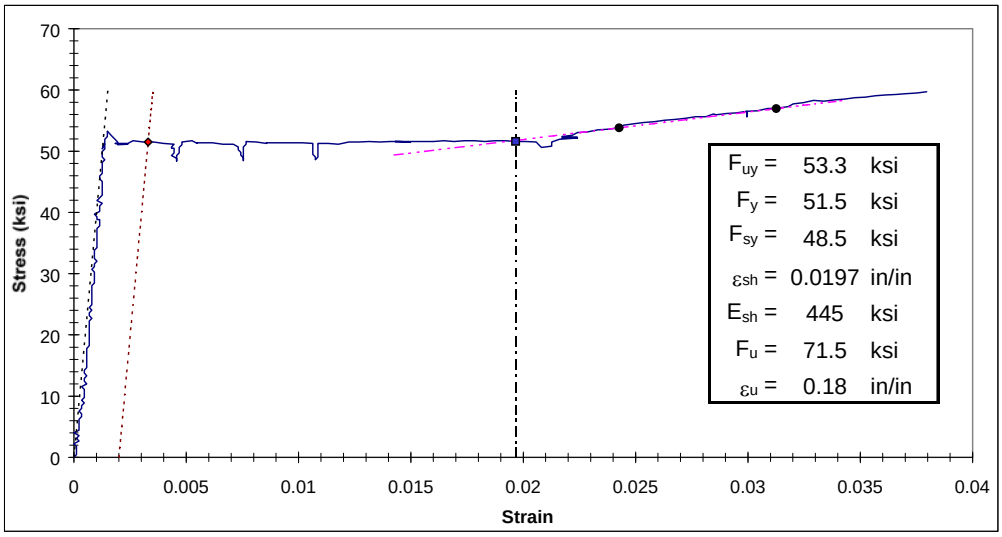

Figure C1.1.10 Yield Plateau and Tensile Test Results for Specimen C1-E

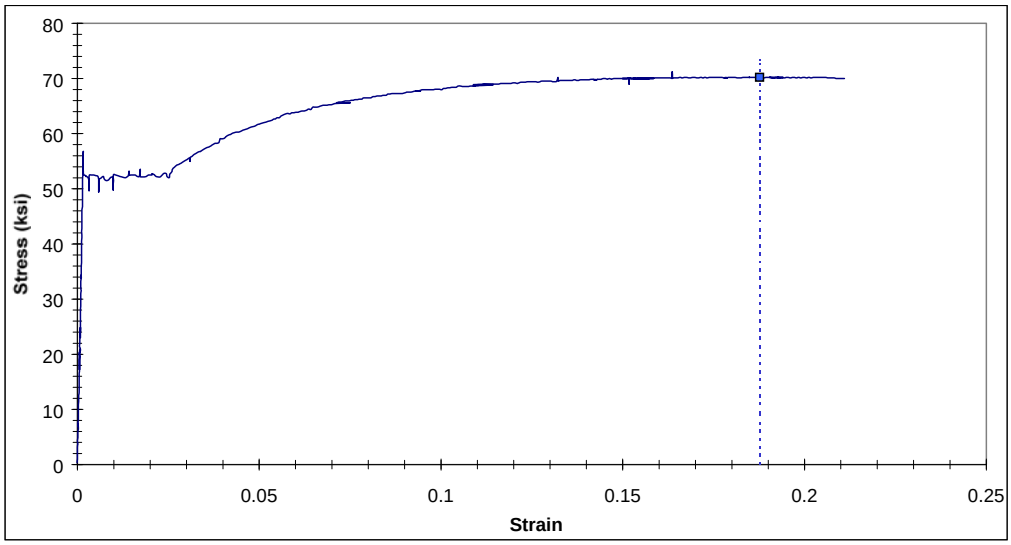

Figure C1.1.11 Complete Stress-strain Curve for Specimen C1-F

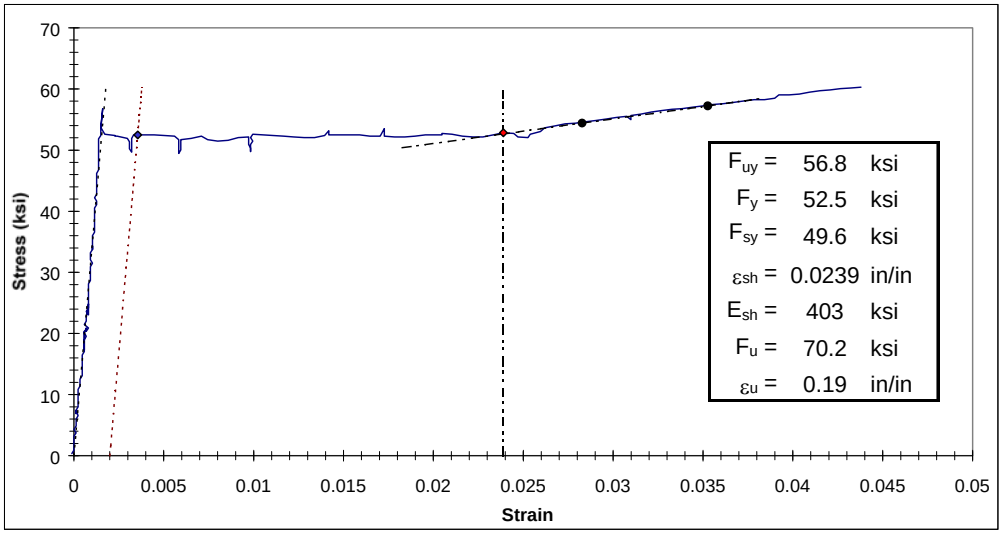

Figure C1.1.12 Yield Plateau and Tensile Test Results for Specimen C1-F

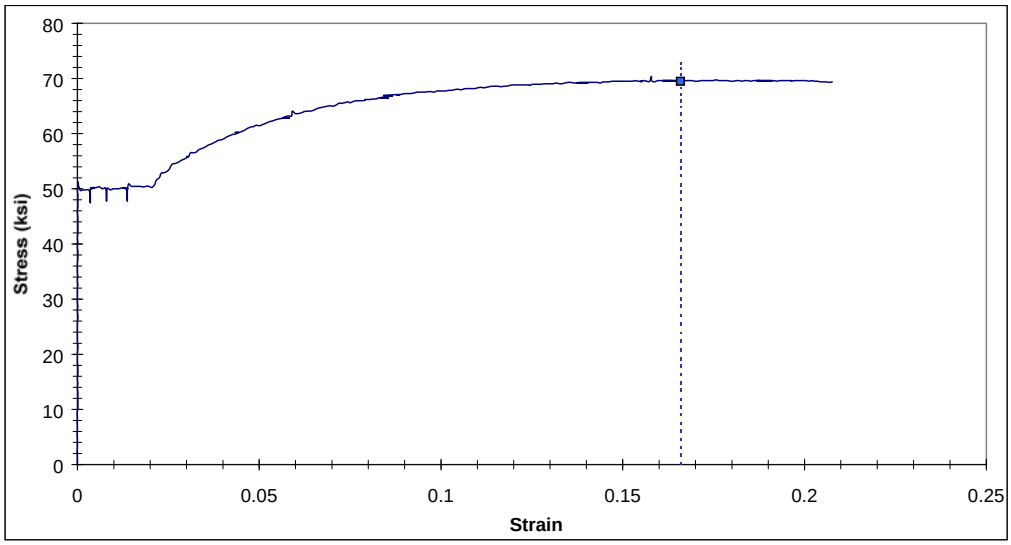

Figure C1.1.13 Complete Stress-strain Curve for Specimen C1-G

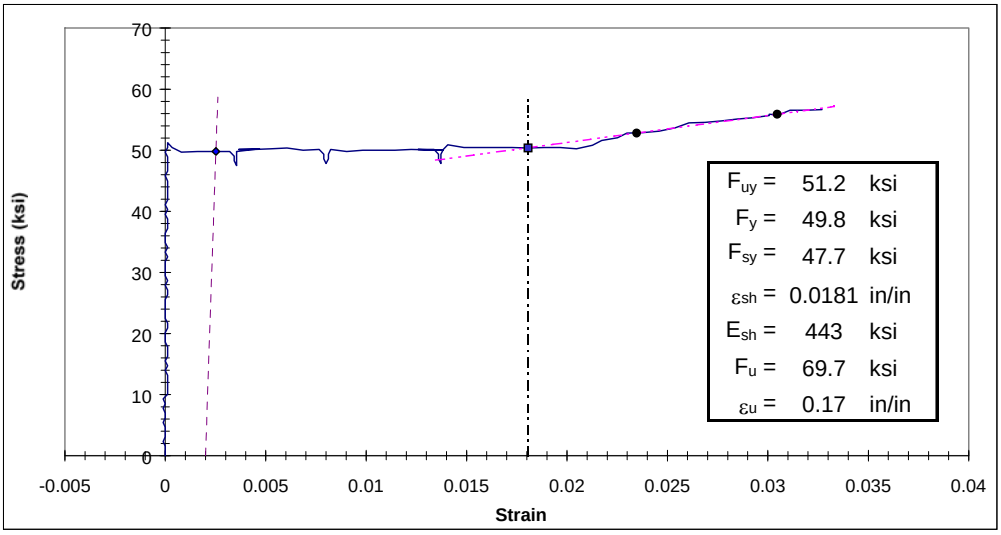

Figure C1.1.14 Yield Plateau and Tensile Test Results for Specimen C1-G

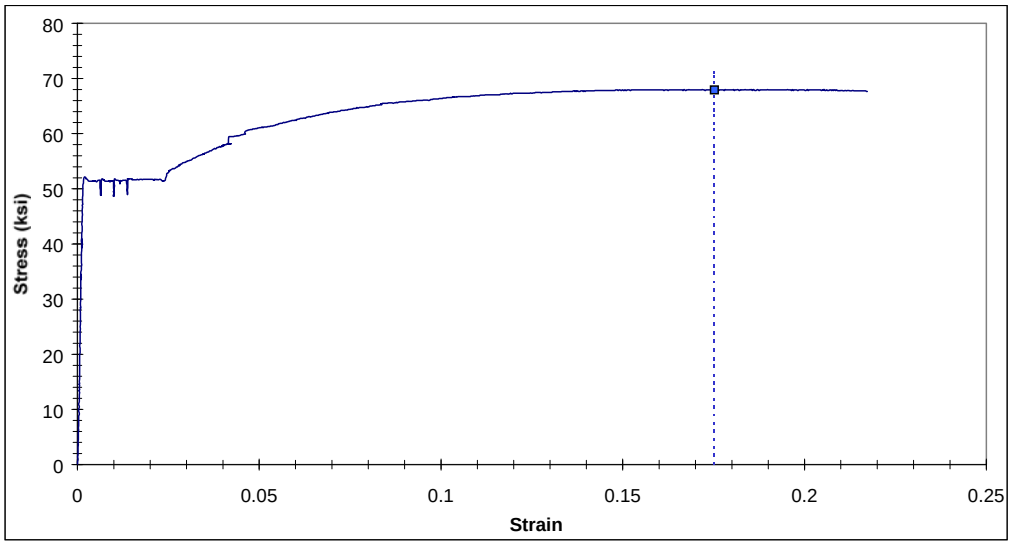

Figure C2.1.1 Complete Stress-strain Curve for Specimen N1-A

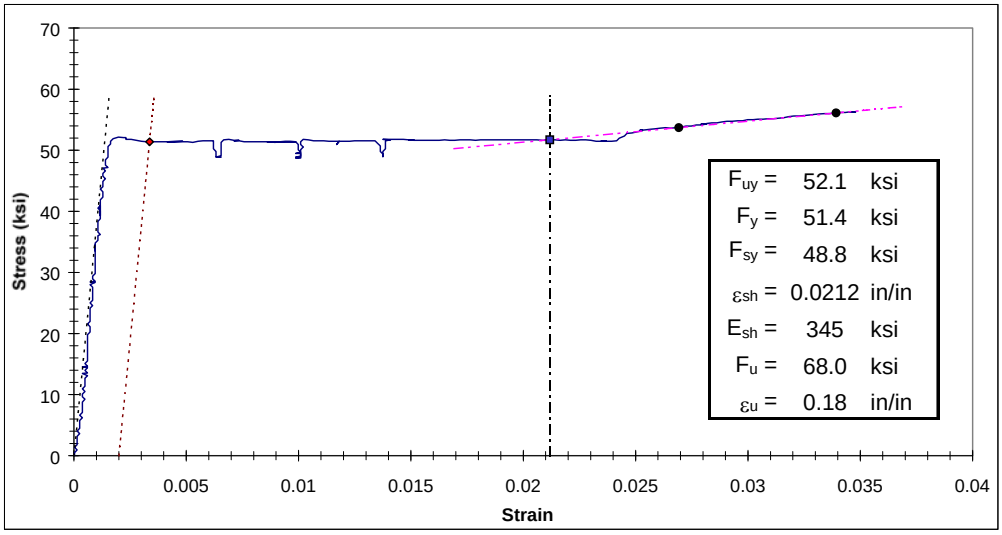

Figure C2.1.2 Yield Plateau and Tensile Test Results for Specimen N1-A

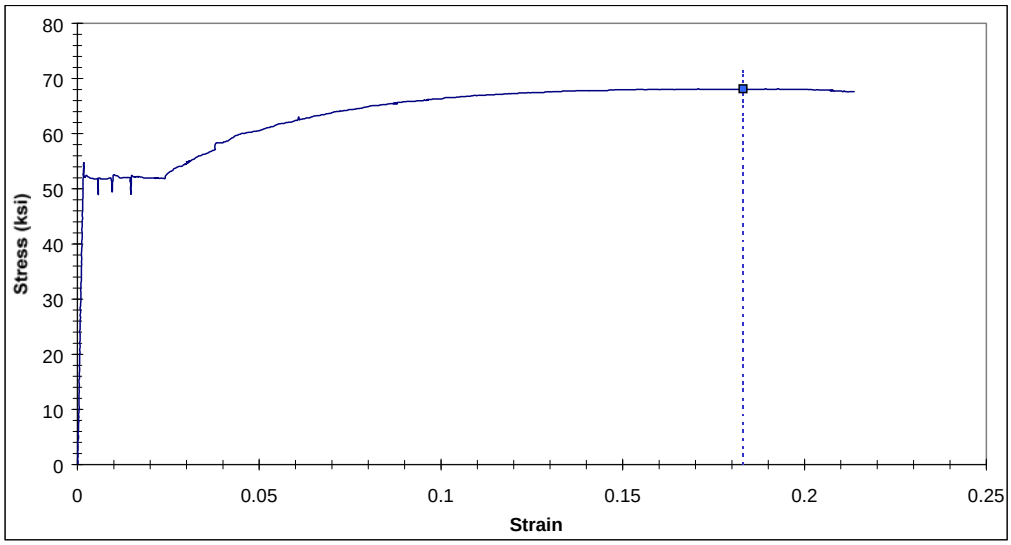

Figure C2.1.3 Complete Stress-strain Curve for Specimen N1-B

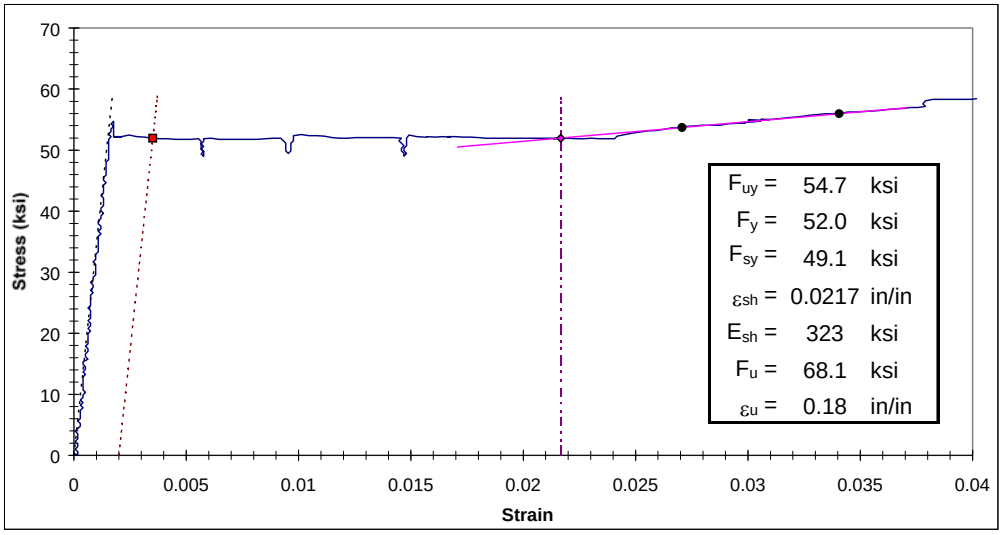

Figure C2.1.4 Yield Plateau and Tensile Test Results for Specimen N1-B

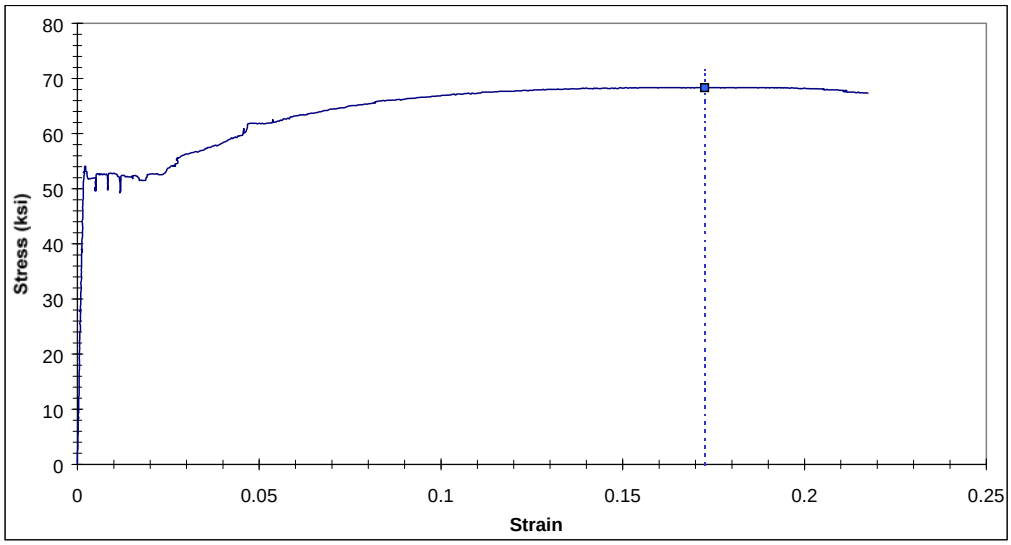

Figure C2.1.5 Complete Stress-strain Curve for Specimen N1-C

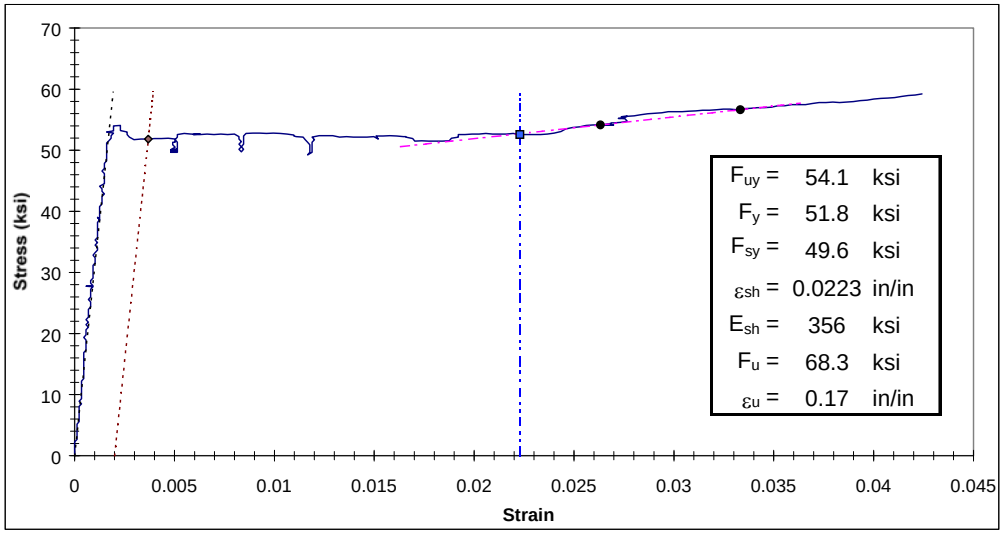

Figure C2.1.6 Yield Plateau and Tensile Test Results for Specimen N1-C

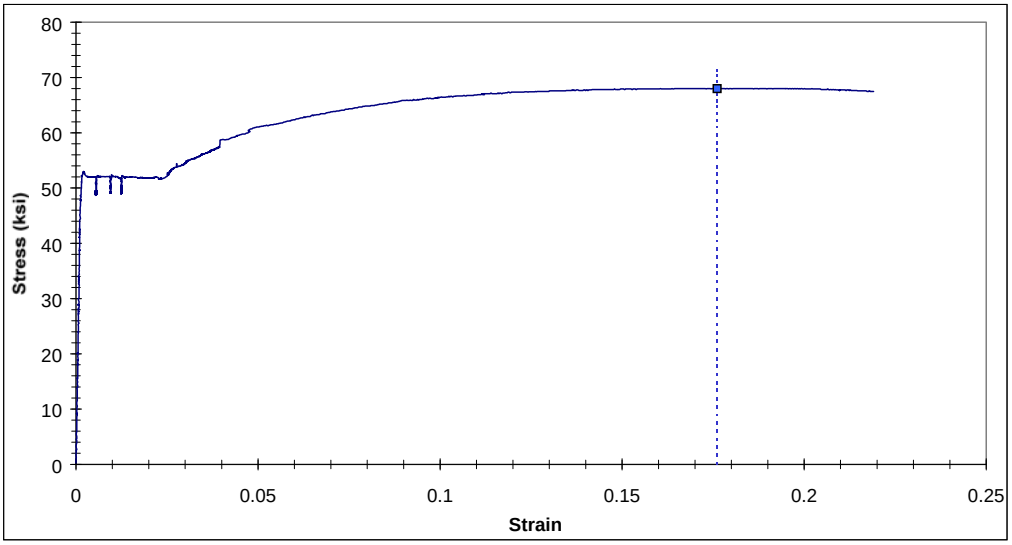

Figure C2.1.7 Complete Stress-strain Curve for Specimen N1-D

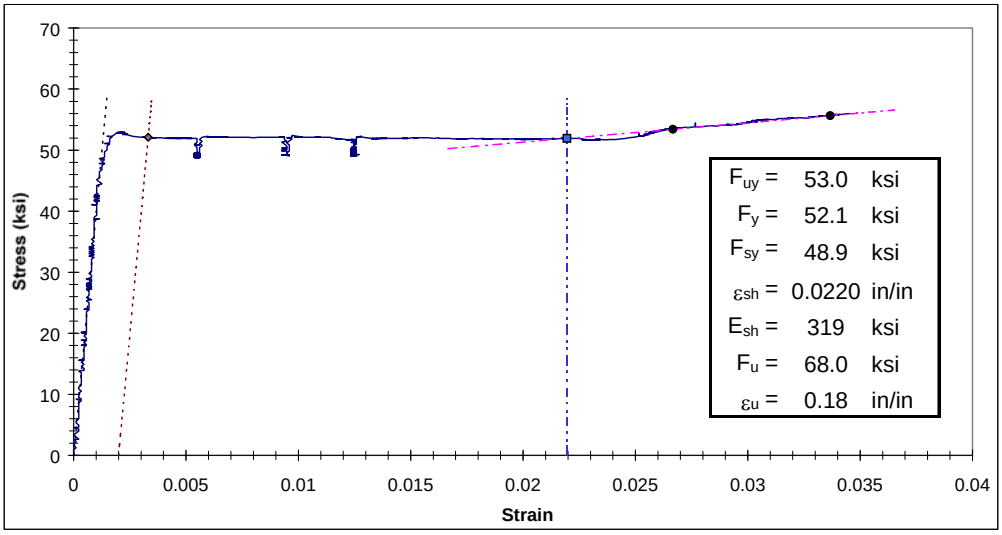

Figure C2.1.8 Yield Plateau and Tensile Test Results for Specimen N1-D

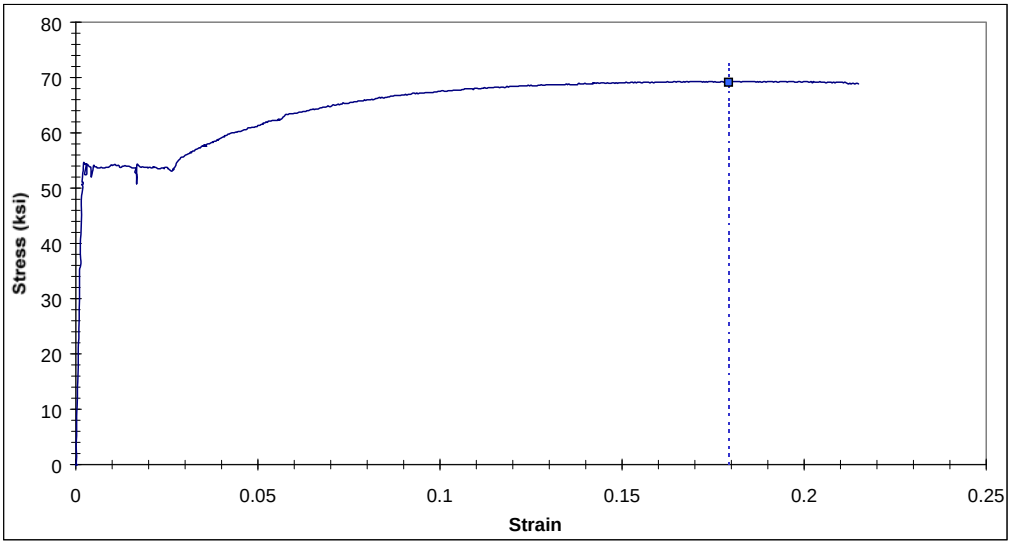

Figure C2.1.9 Complete Stress-strain Curve for Specimen N1-E

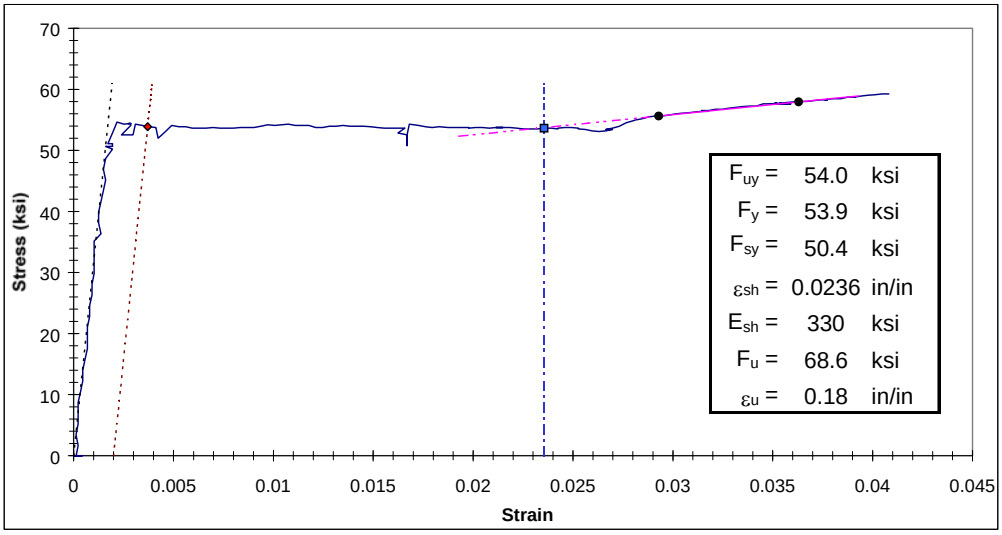

Figure C2.1.10 Yield Plateau and Tensile Test Results for Specimen N1-E

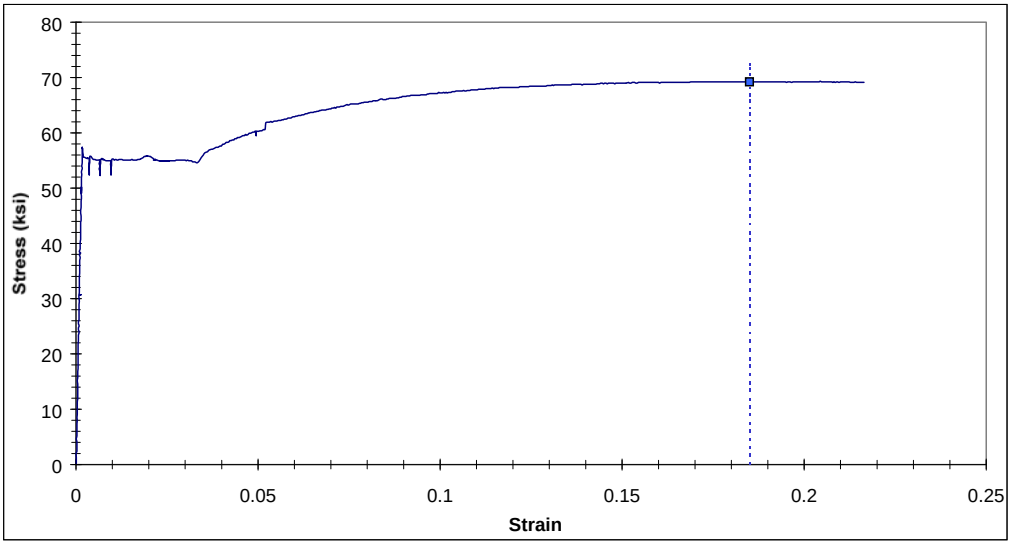

Figure C2.1.11 Complete Stress-strain Curve for Specimen N1-F

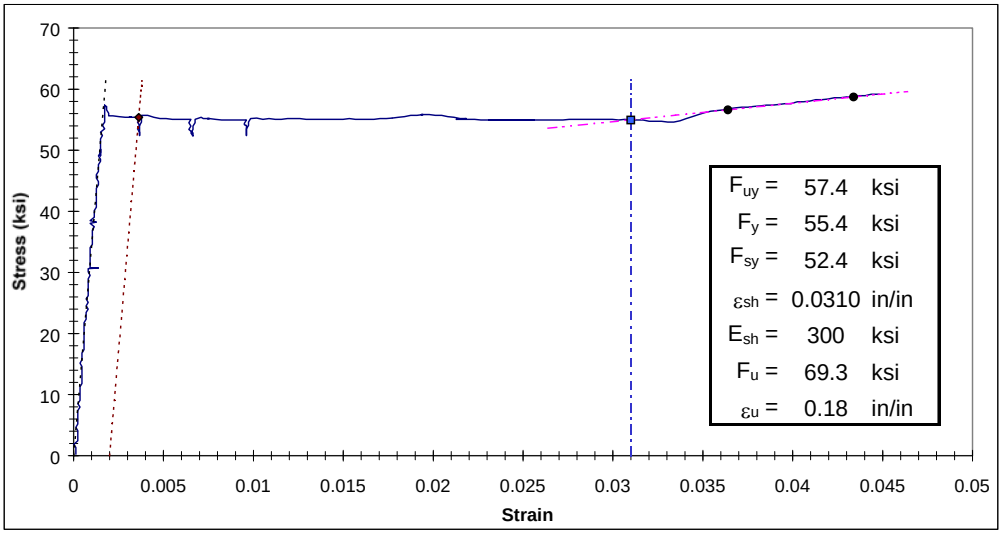

Figure C2.1.12 Yield Plateau and Tensile Test Results for Specimen N1-F

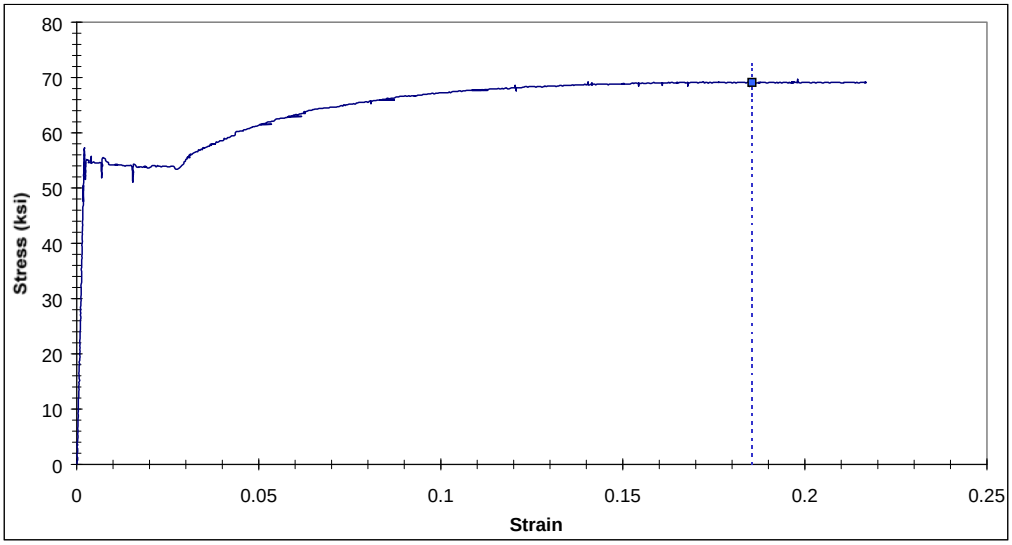

Figure C2.1.13 Complete Stress-strain Curve for Specimen N1-G

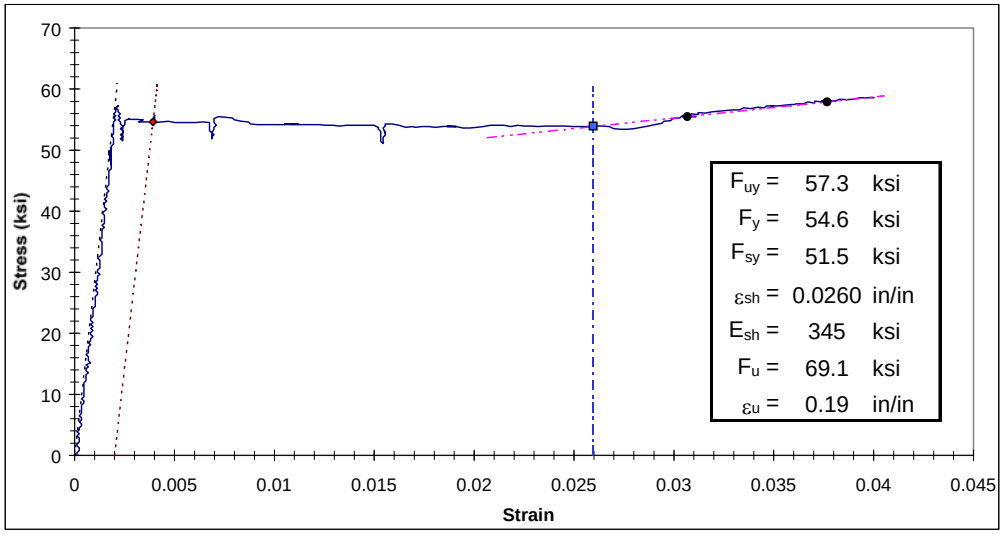

Figure C2.1.14 Yield Plateau and Tensile Test Results for Specimen N1-G

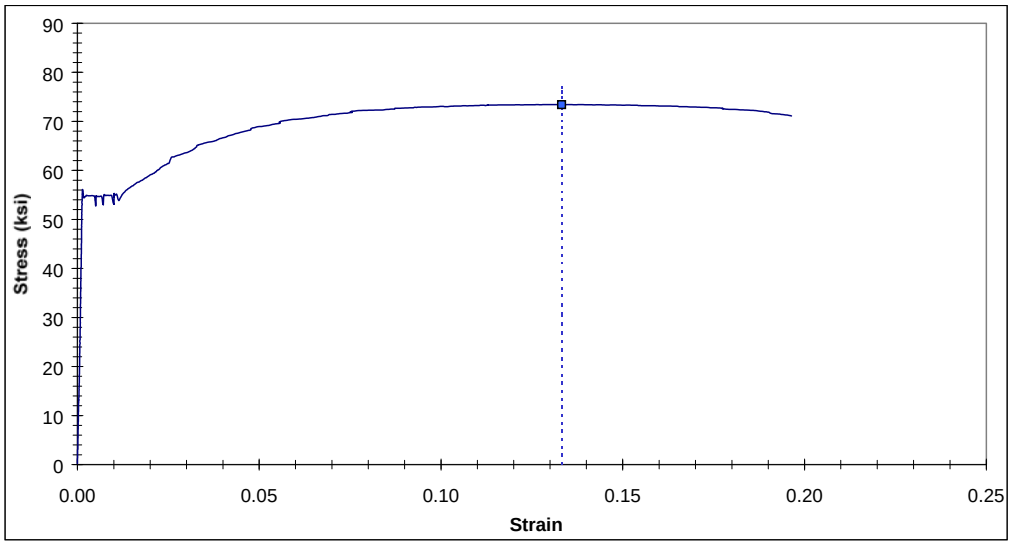

Figure C2.2.1 Complete Stress-strain Curve for Specimen N2-A

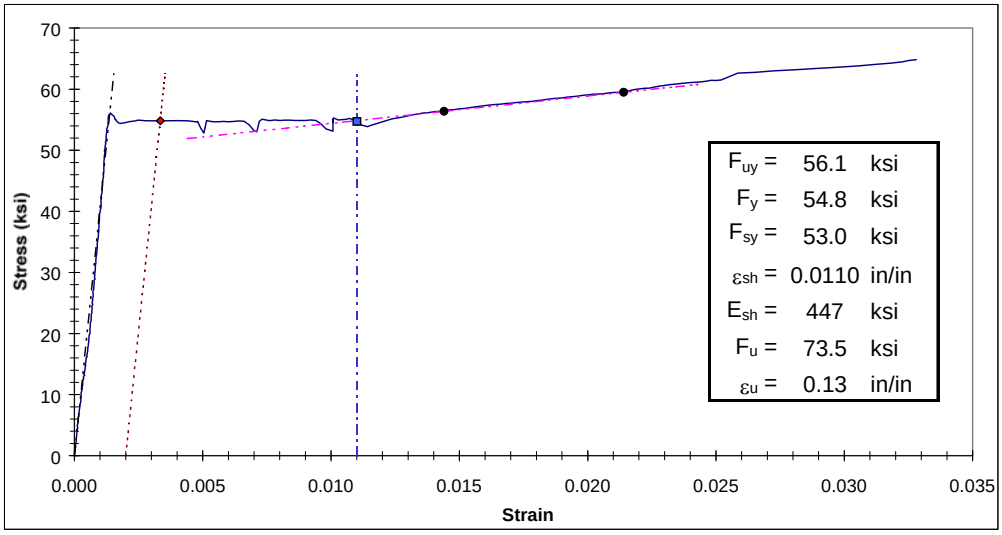

Figure C2.2.2 Yield Plateau and Tensile Test Results for Specimen N2-A

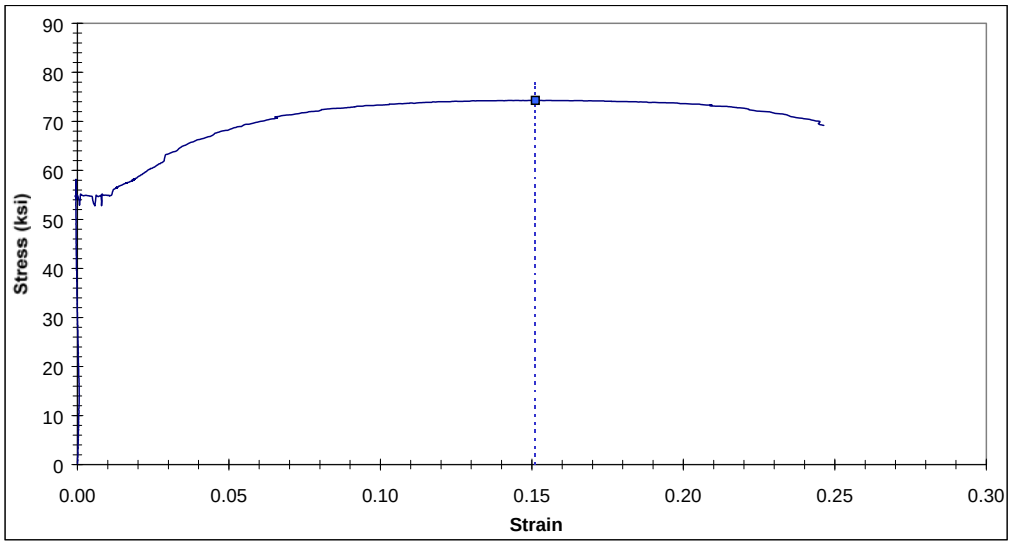

Figure C2.2.3 Complete Stress-strain Curve for Specimen N2-B

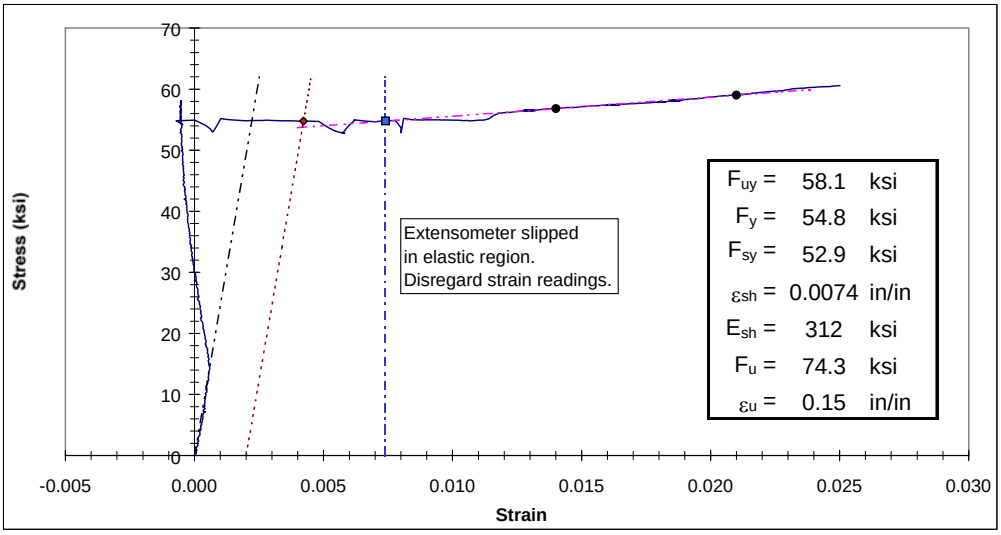

Figure C2.2.4 Yield Plateau and Tensile Test Results for Specimen N2-B

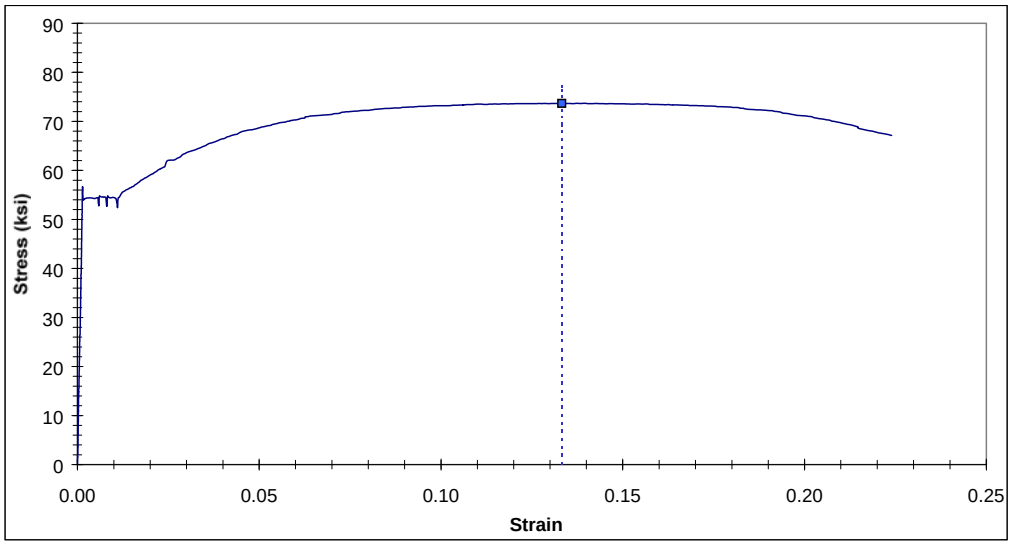

Figure C2.2.5 Complete Stress-strain Curve for Specimen N2-C

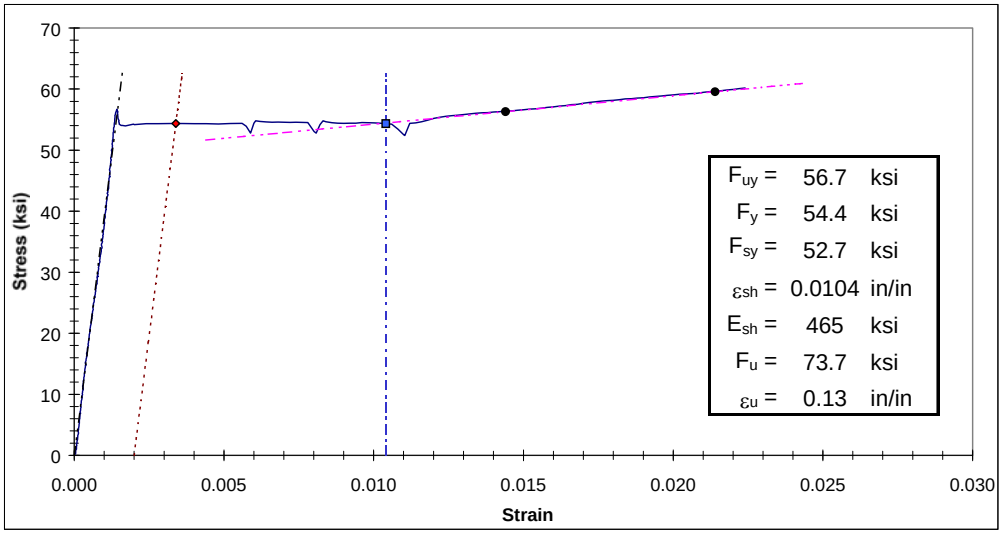

Figure C2.2.6 Yield Plateau and Tensile Test Results for Specimen N2-C

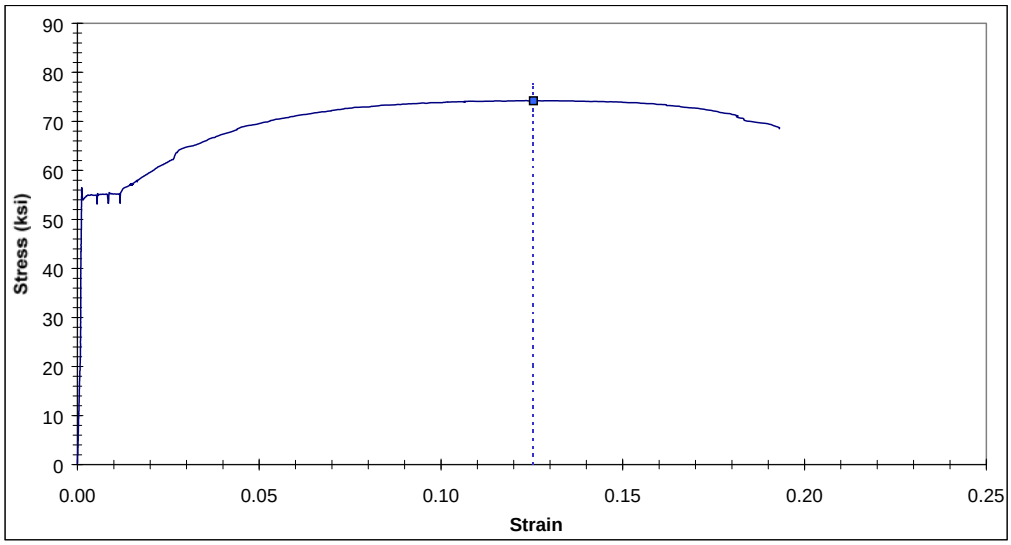

Figure C2.2.7 Complete Stress-strain Curve for Specimen N2-D

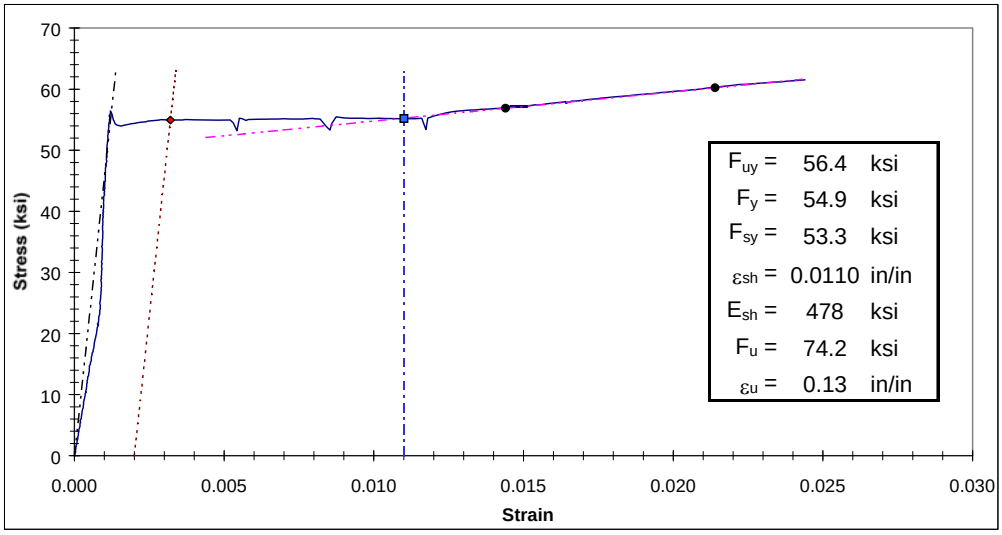

Figure C2.2.8 Yield Plateau and Tensile Test Results for Specimen N2-D

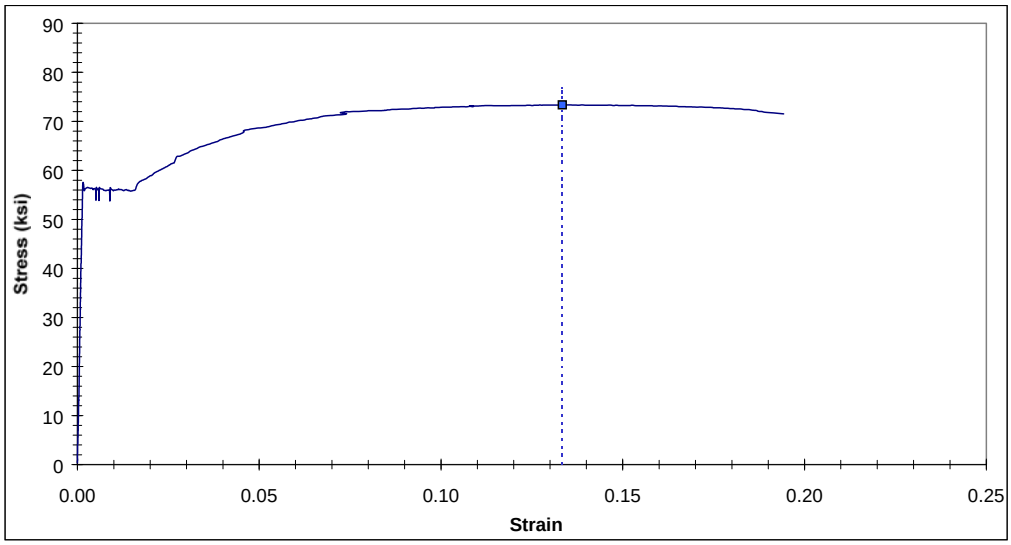

Figure C2.2.9 Complete Stress-strain Curve for Specimen N2-E

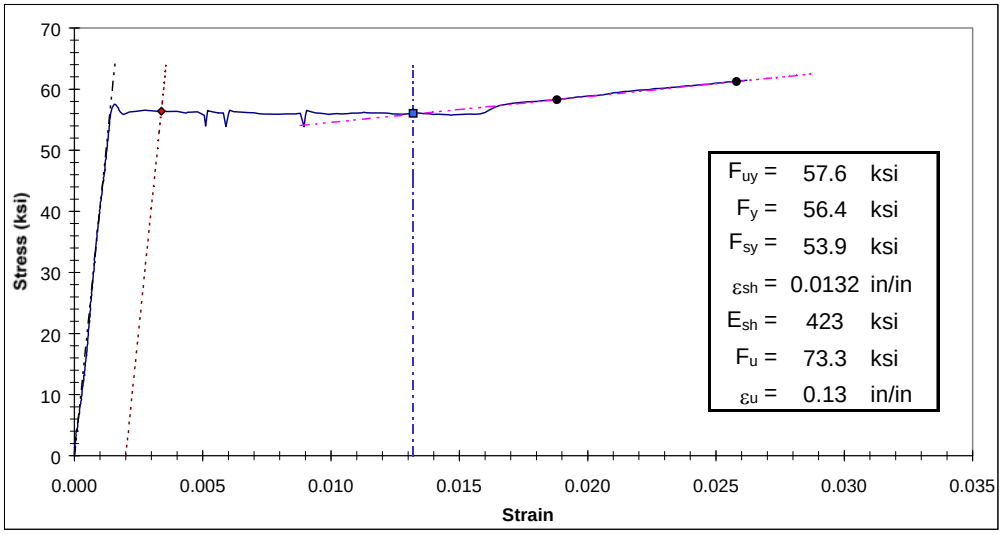

Figure C2.2.10 Yield Plateau and Tensile Test Results for Specimen N2-E

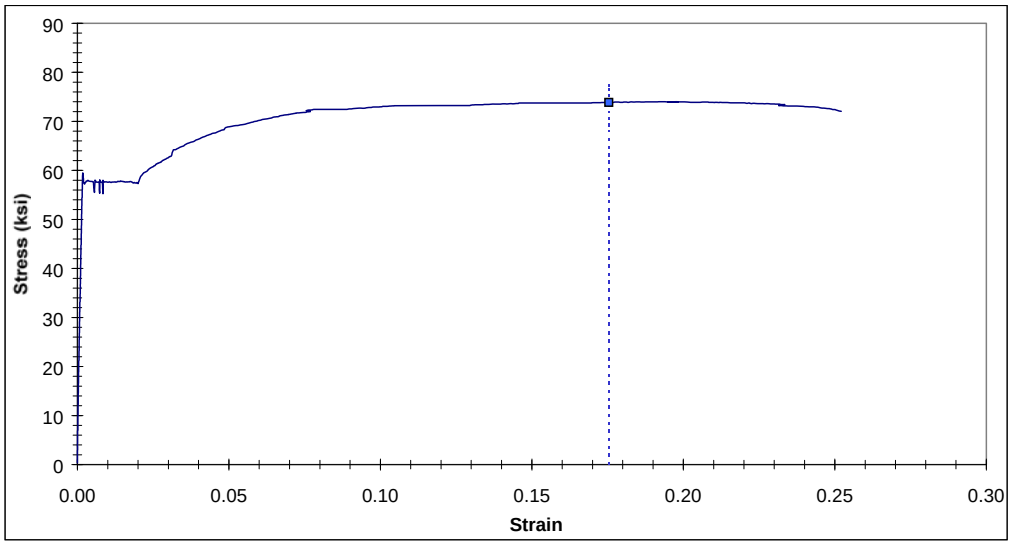

Figure C2.2.11 Complete Stress-strain Curve for Specimen N2-F

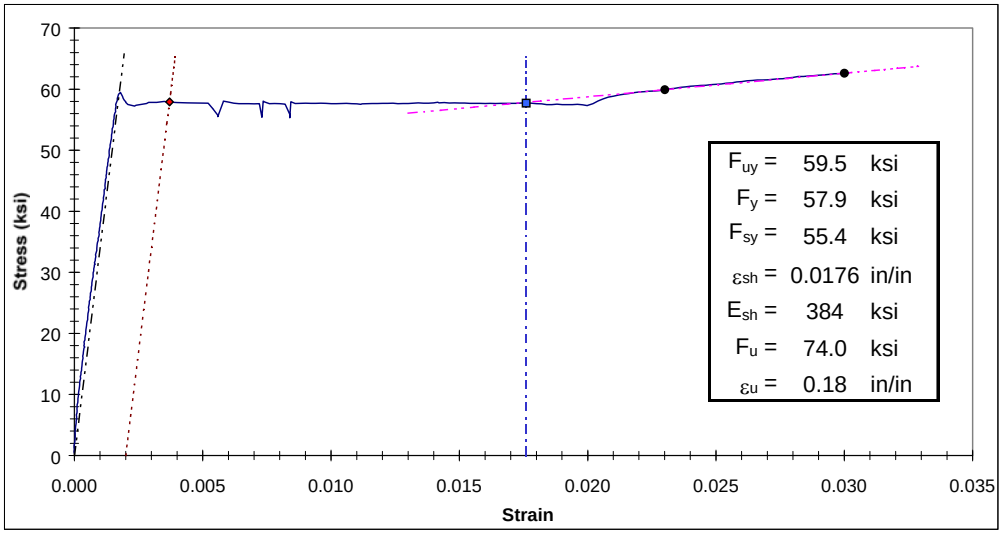

Figure C2.2.12 Yield Plateau and Tensile Test Results for Specimen N2-F

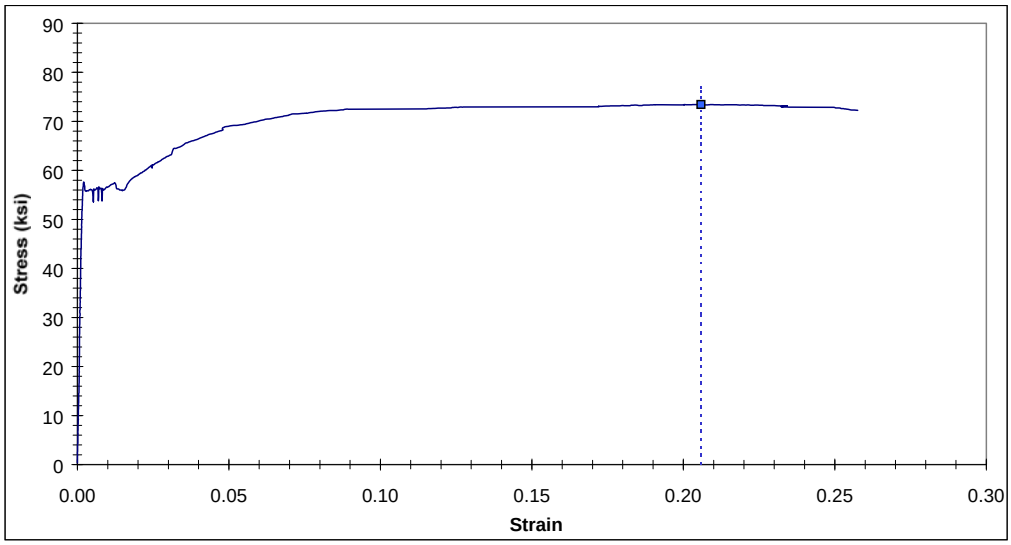

Figure C2.2.13 Complete Stress-strain Curve for Specimen N2-G

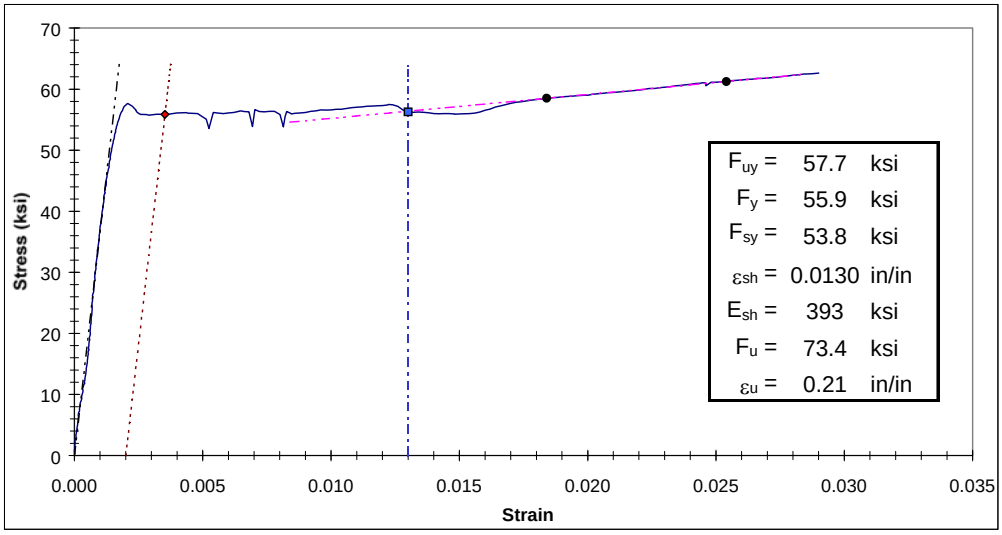

Figure C2.2.14 Yield Plateau and Tensile Test Results for Specimen N2-G

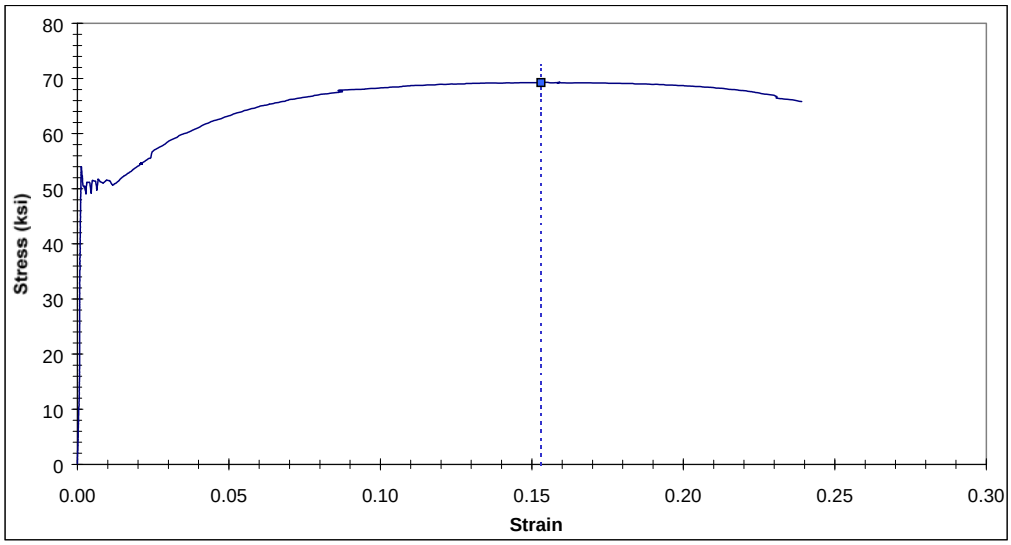

Figure C2.3.1 Complete Stress-strain Curve for Specimen N3-B

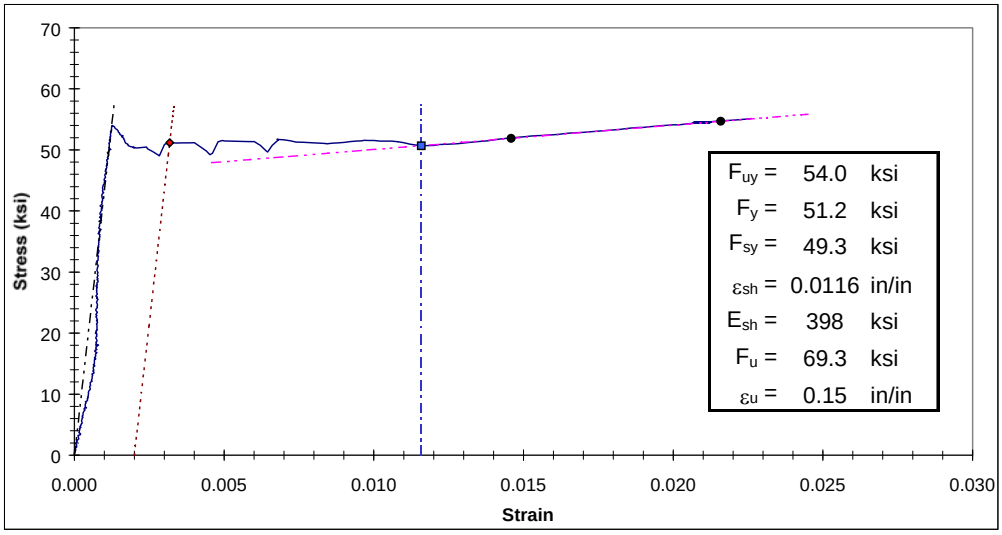

Figure C2.3.2 Yield Plateau and Tensile Test Results for Specimen N3-B

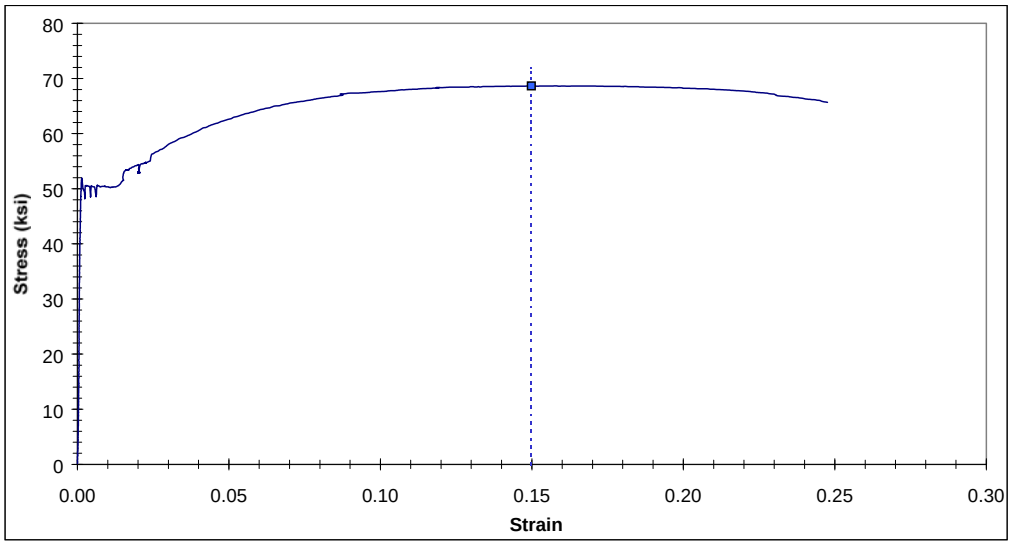

Figure C2.3.3 Complete Stress-strain Curve for Specimen N3-D

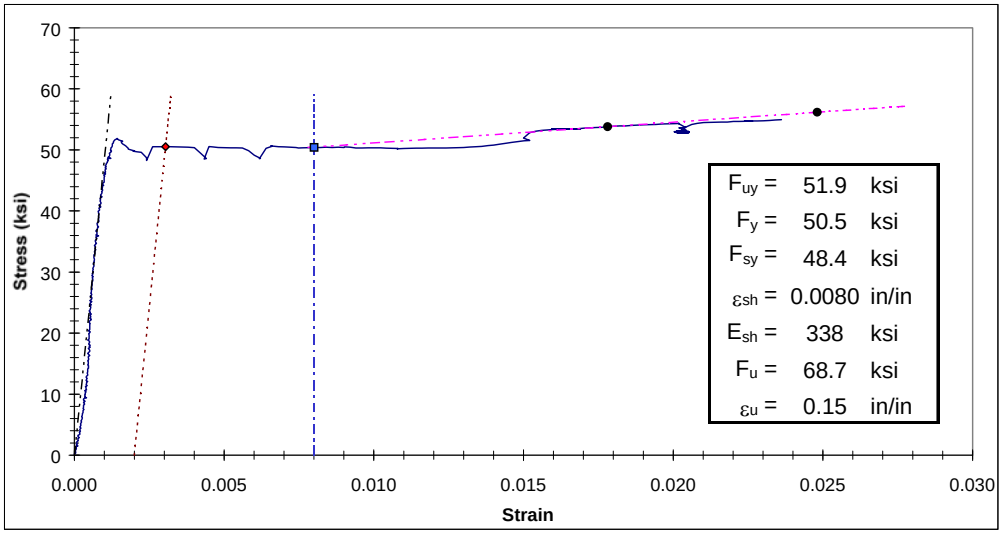

Figure C2.3.4 Yield Plateau and Tensile Test Results for Specimen N3-D

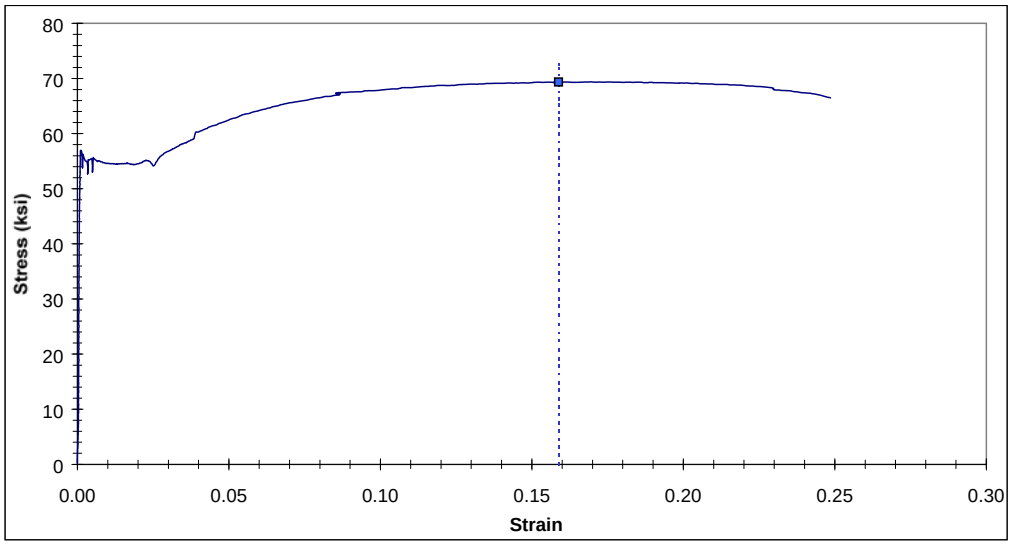

Figure C2.3.5 Complete Stress-strain Curve for Specimen N3-F

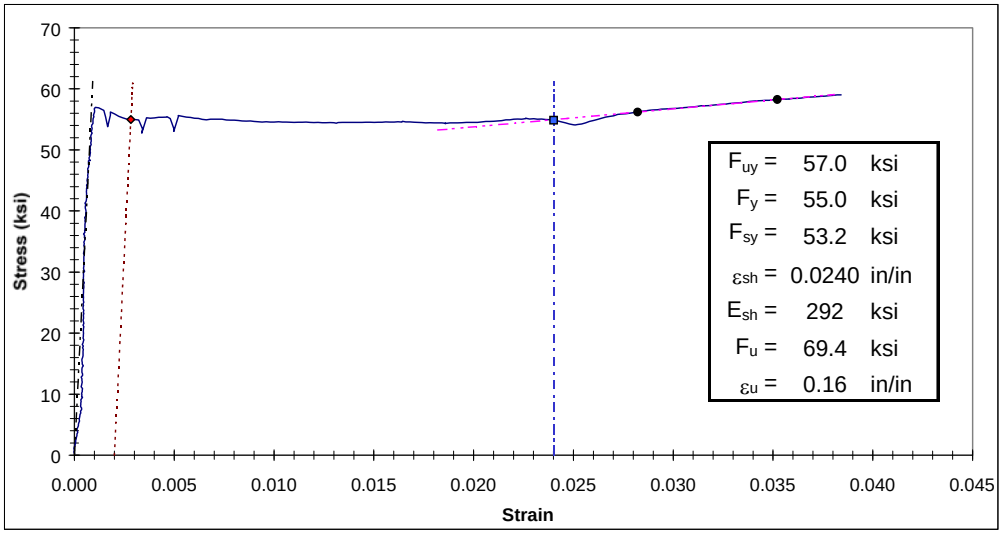

Figure C2.3.6 Yield Plateau and Tensile Test Results for Specimen N3-F

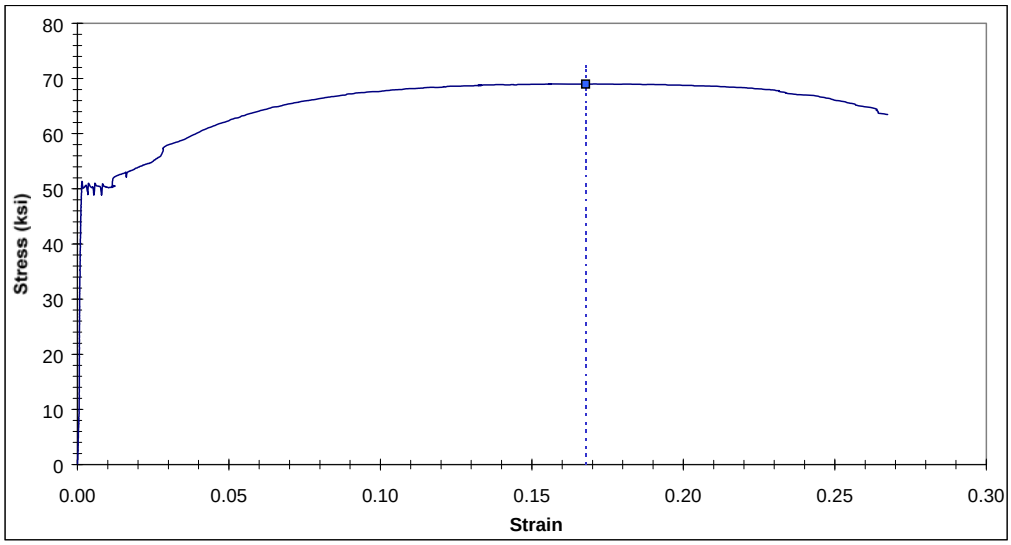

Figure C2.4.1 Complete Stress-strain Curve for Specimen N4-B

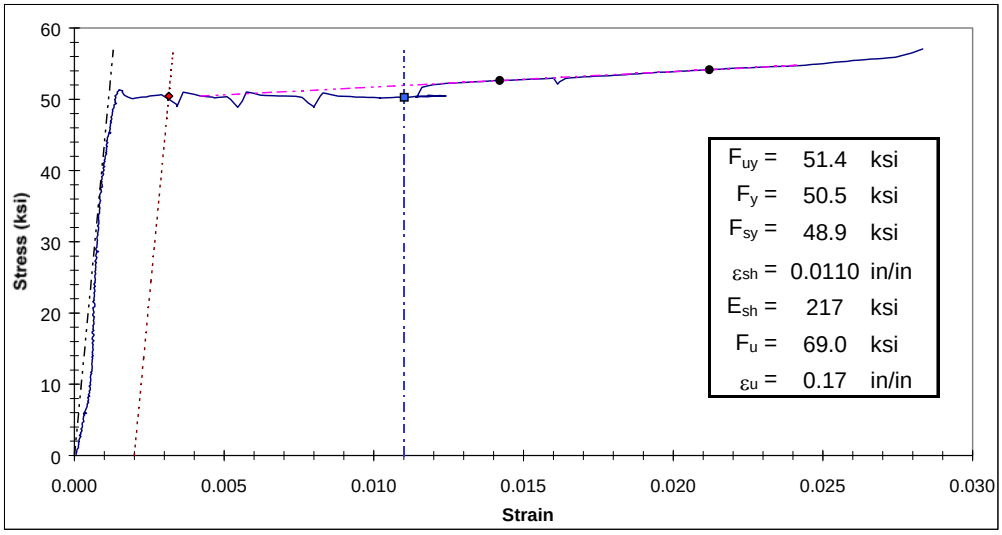

Figure C2.4.2 Yield Plateau and Tensile Test Results for Specimen N4-B

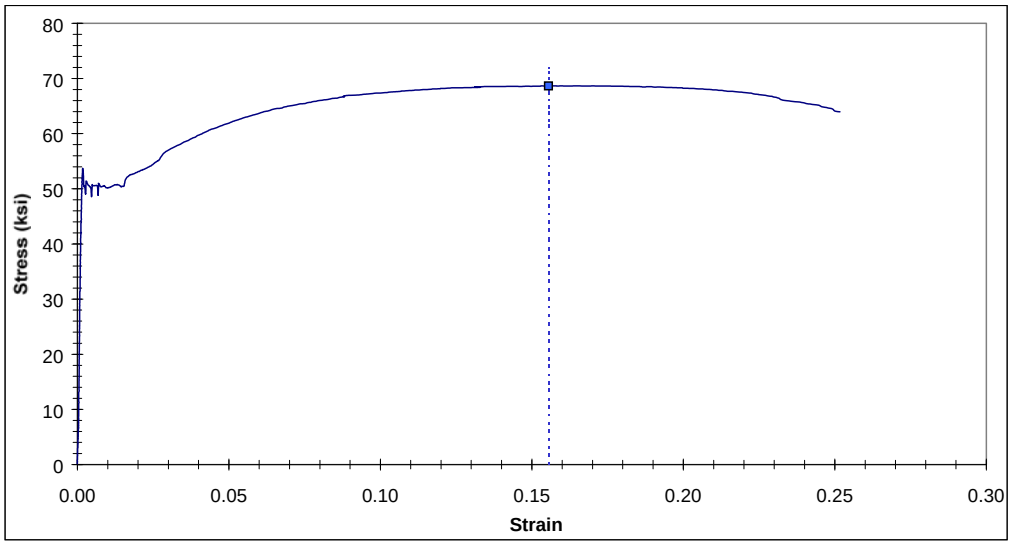

Figure C2.4.3 Complete Stress-strain Curve for Specimen N4-D

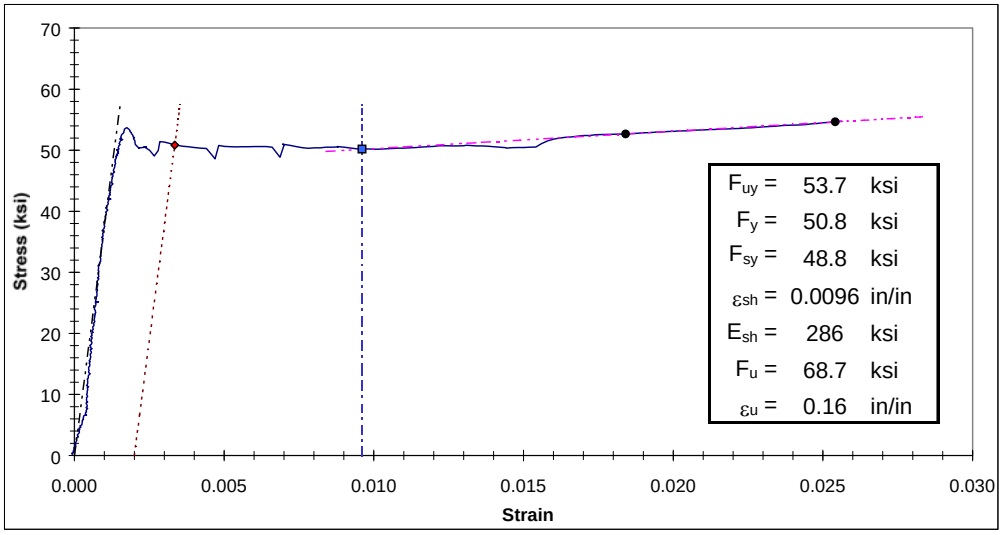

Figure C2.4.4 Yield Plateau and Tensile Test Results for Specimen N4-D

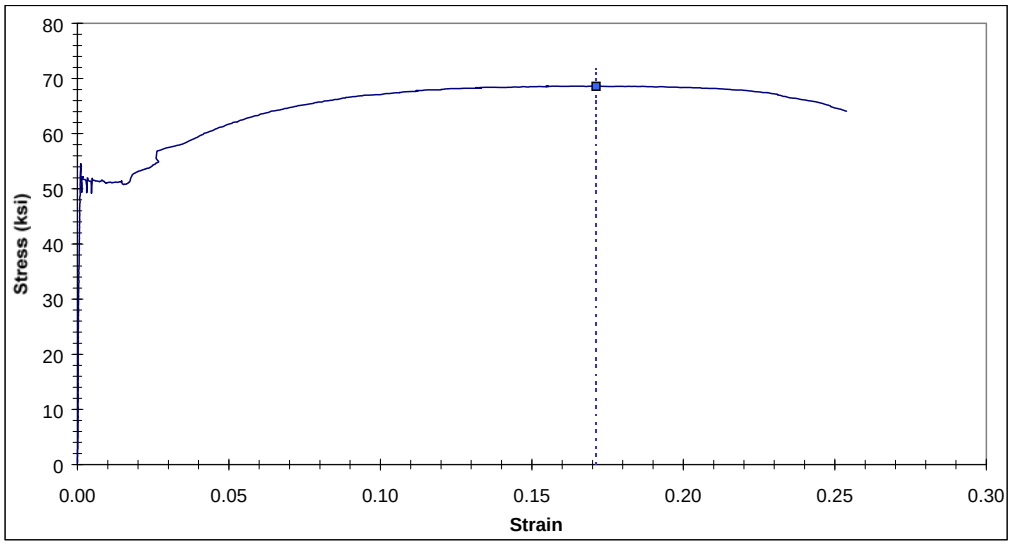

Figure C2.4.5 Complete Stress-strain Curve for Specimen N4-F

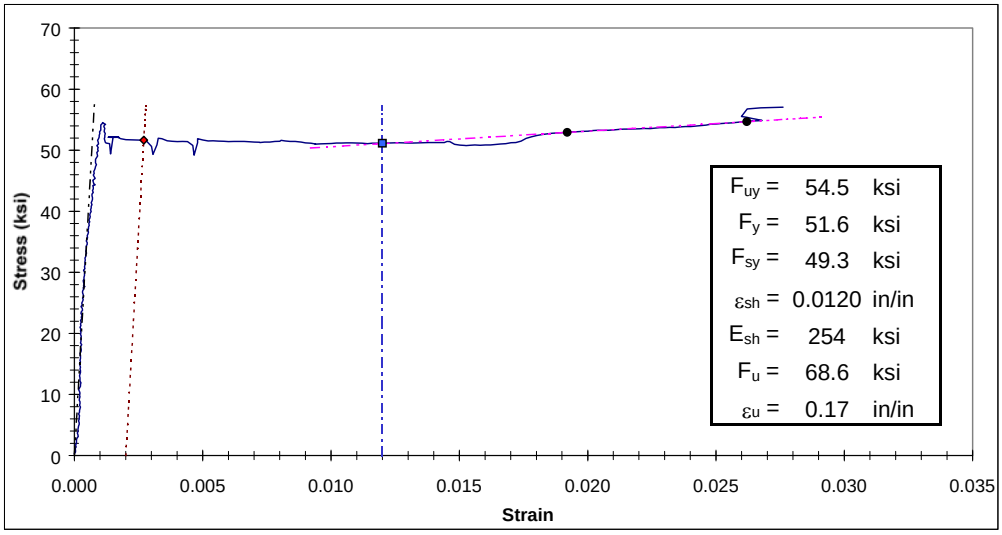

Figure C2.4.6 Yield Plateau and Tensile Test Results for Specimen N4-F

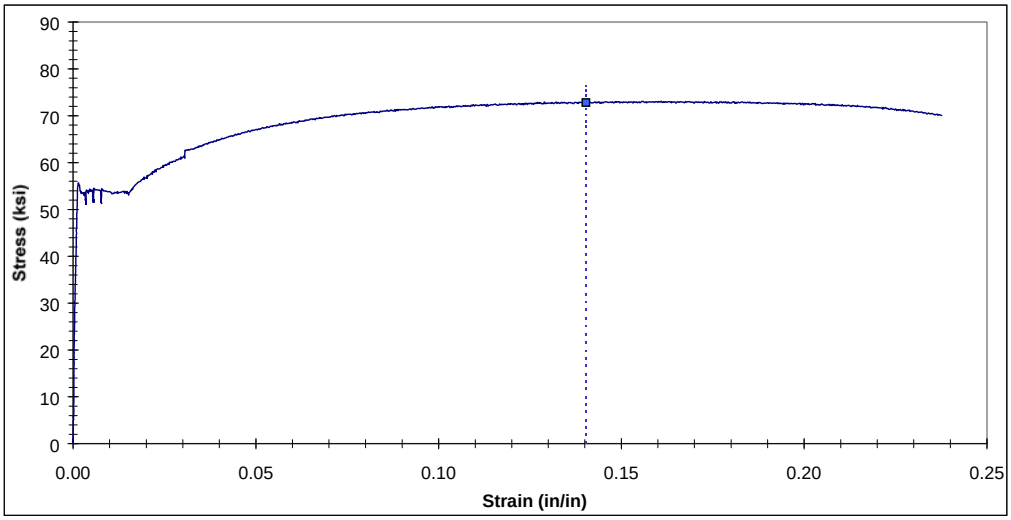

Figure C2.5.1 Complete Stress-strain Curve for Specimen N5-A

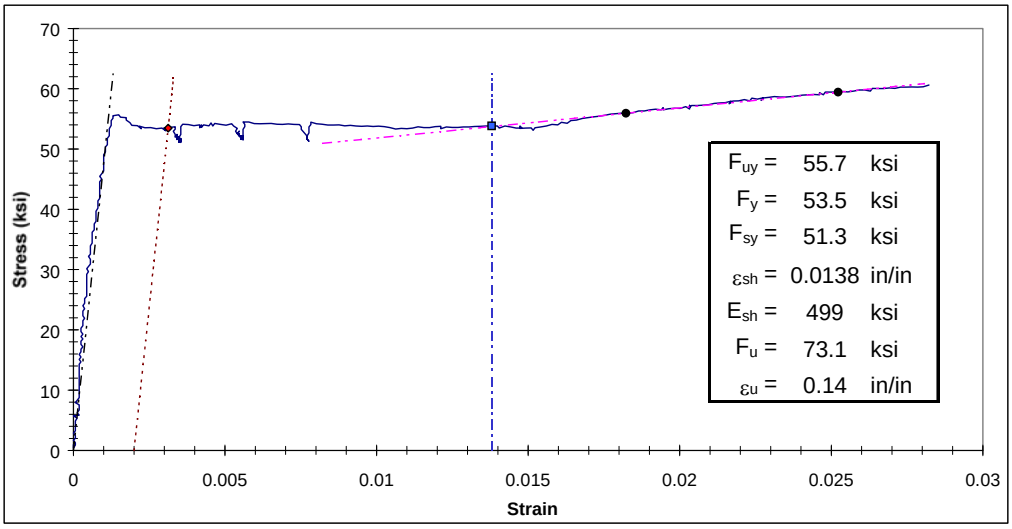

Figure C2.5.2 Yield Plateau and Tensile Test Results for Specimen N5-A

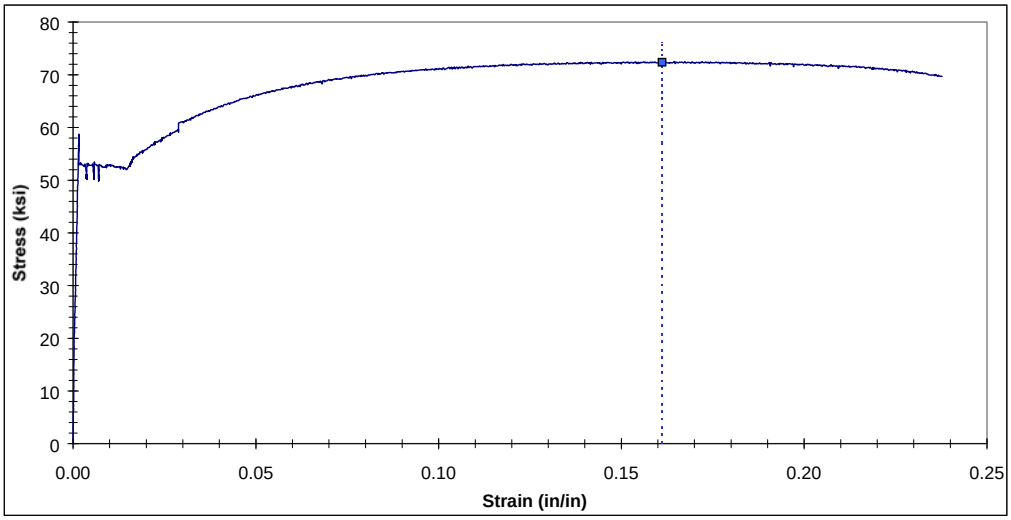

Figure C2.5.3 Complete Stress-strain Curve for Specimen N5-B

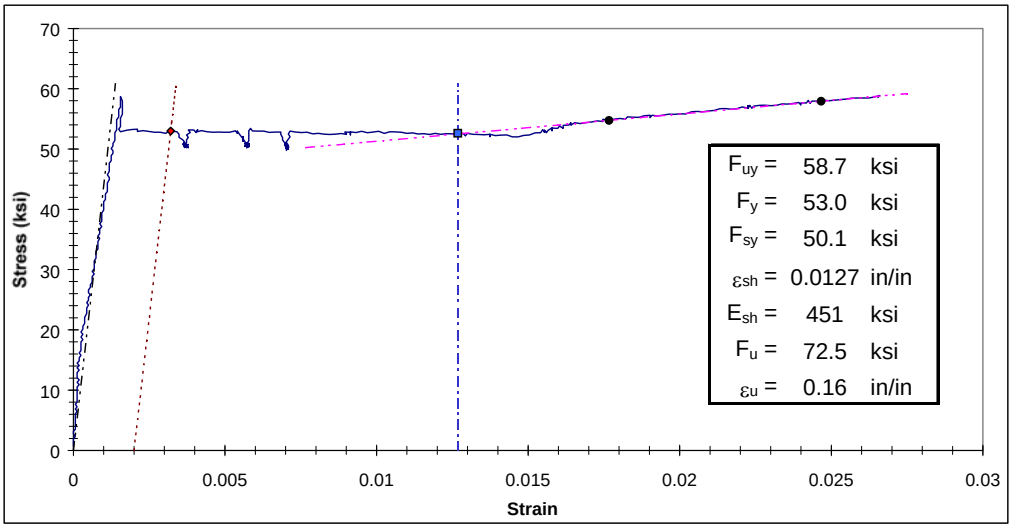

Figure C2.5.4 Yield Plateau and Tensile Test Results for Specimen N5-B

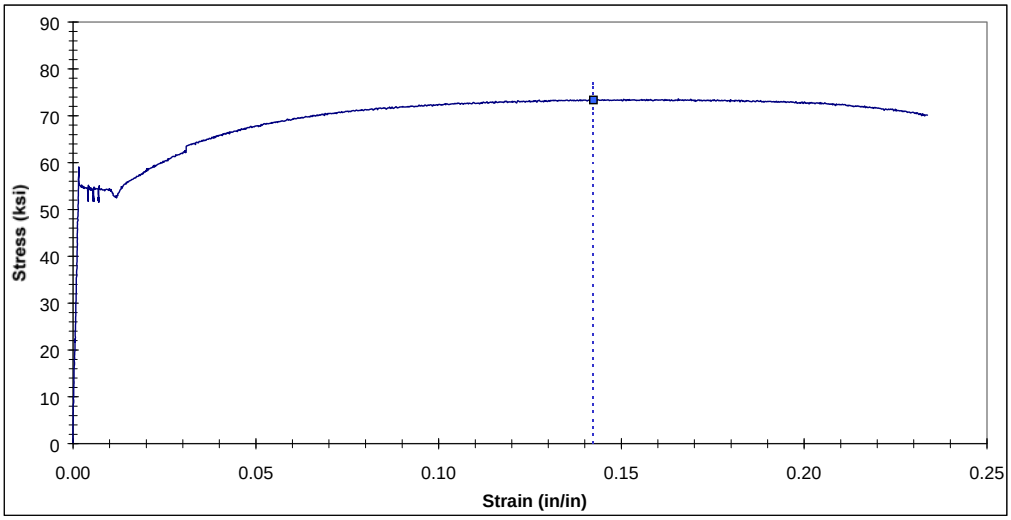

Figure C2.5.5 Complete Stress-strain Curve for Specimen N5-C

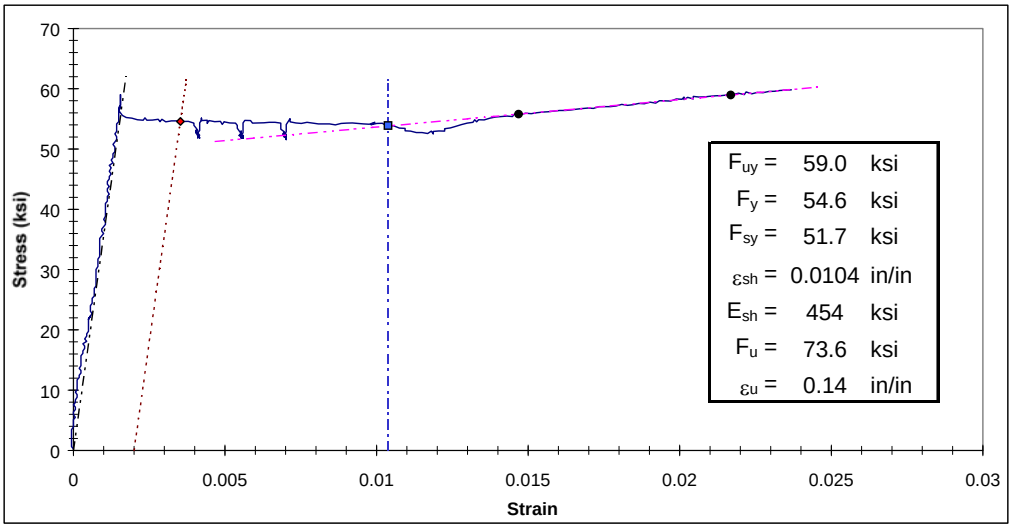

Figure C2.5.6 Yield Plateau and Tensile Test Results for Specimen N5-C

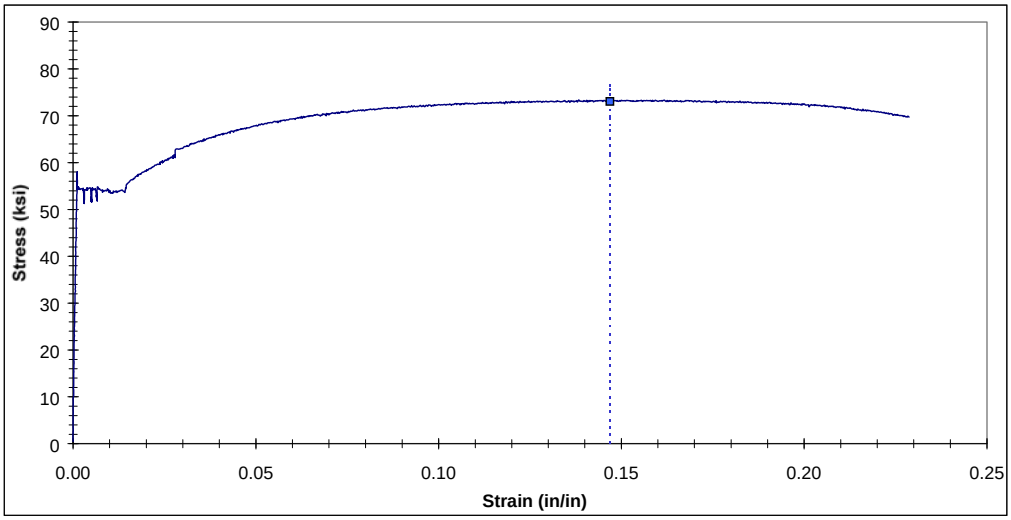

Figure C2.5.7 Complete Stress-strain Curve for Specimen N5-D

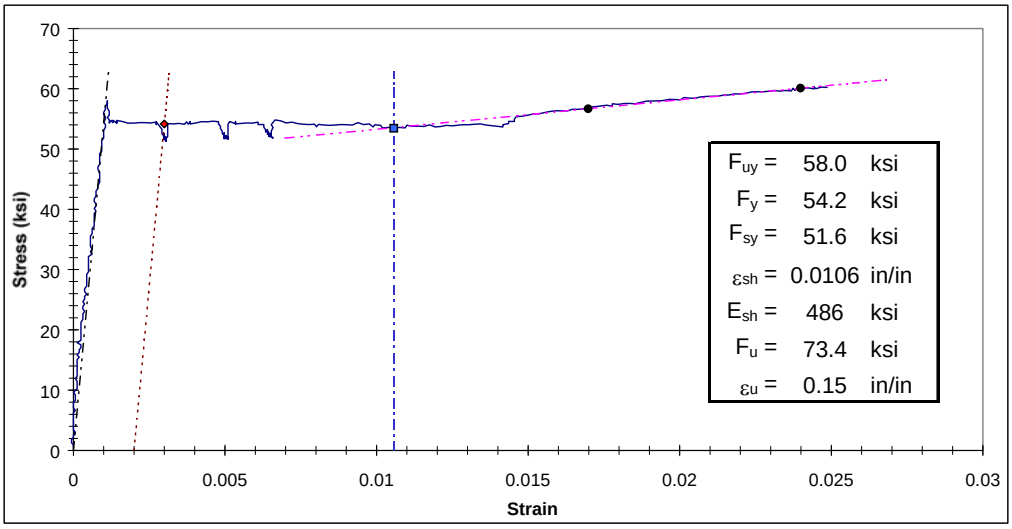

Figure C2.5.8 Yield Plateau and Tensile Test Results for Specimen N5-D

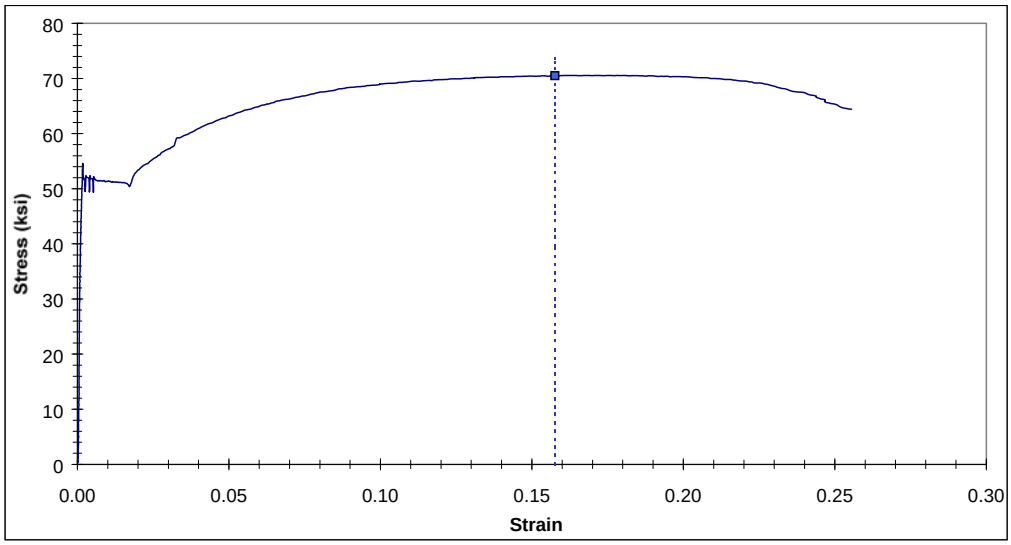

Figure C2.5.9 Complete Stress-strain Curve for Specimen N5-B2

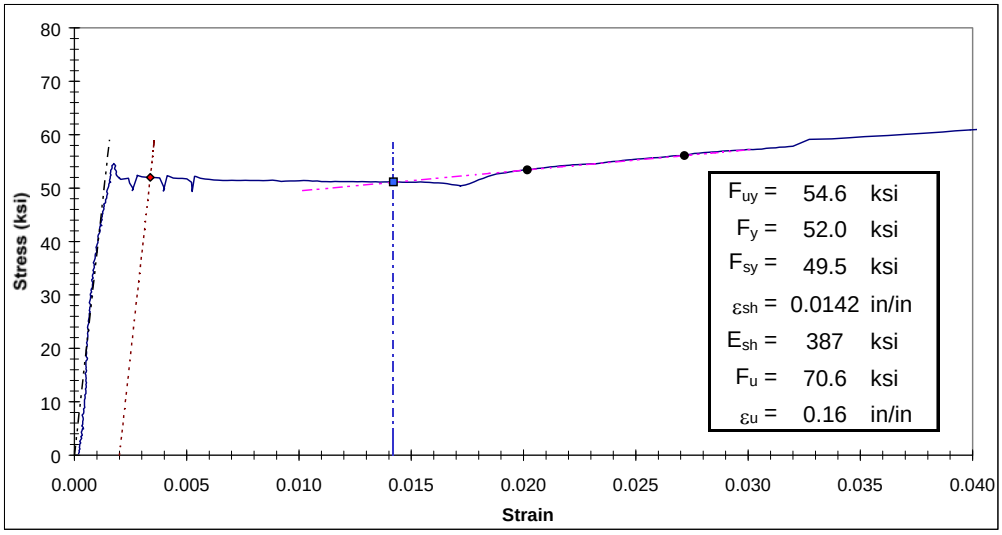

Figure C2.5.10 Yield Plateau and Tensile Test Results for Specimen N5-B2

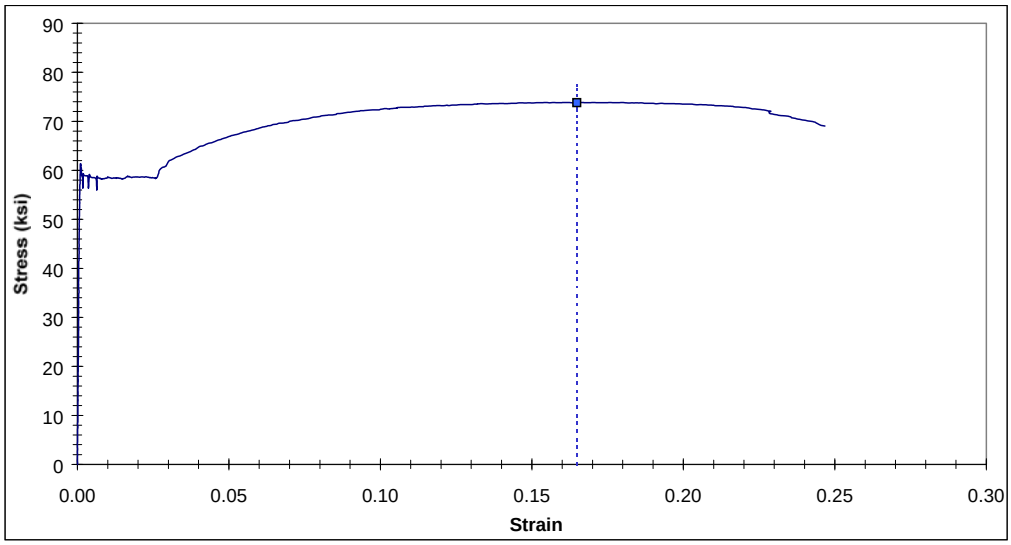

Figure C2.5.11 Complete Stress-strain Curve for Specimen N5-F2

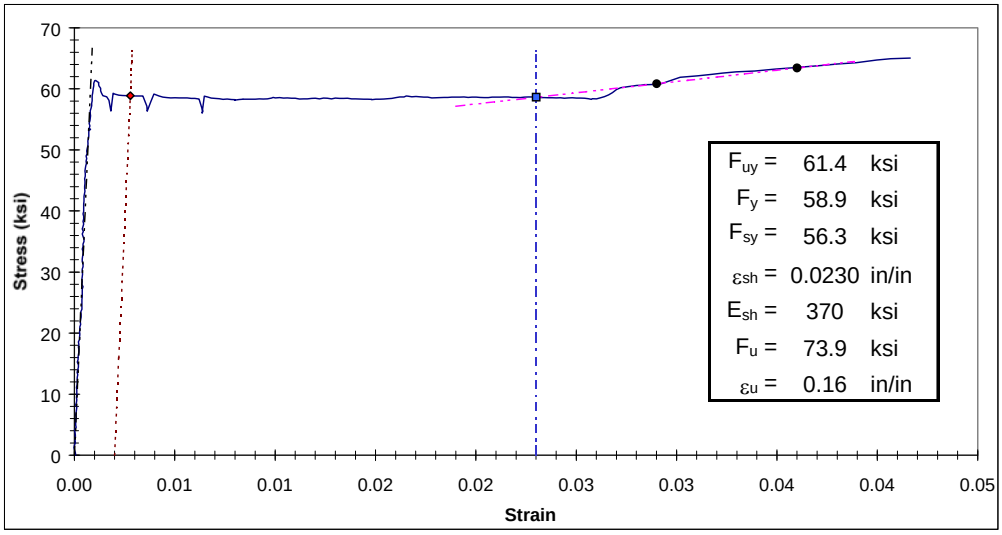

Figure C2.5.12 Yield Plateau and Tensile Test Results for Specimen N5-F2

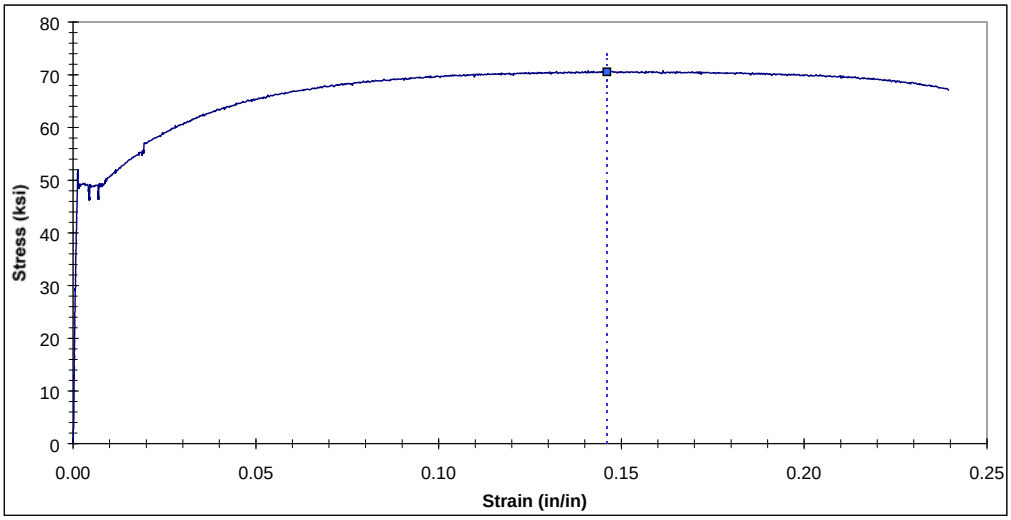

Figure C2.6.1 Complete Stress-strain Curve for Specimen N6-B

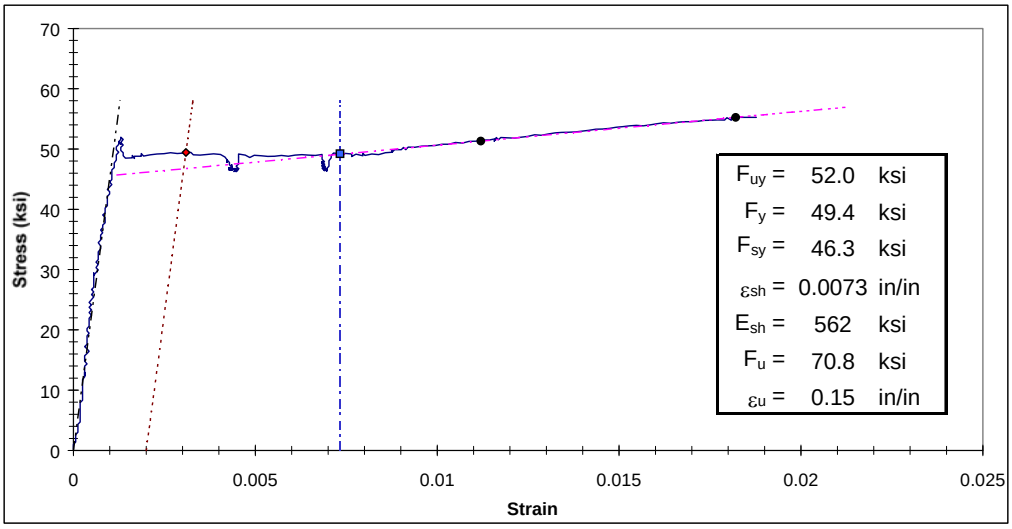

Figure C2.6.2 Yield Plateau and Tensile Test Results for Specimen N6-B

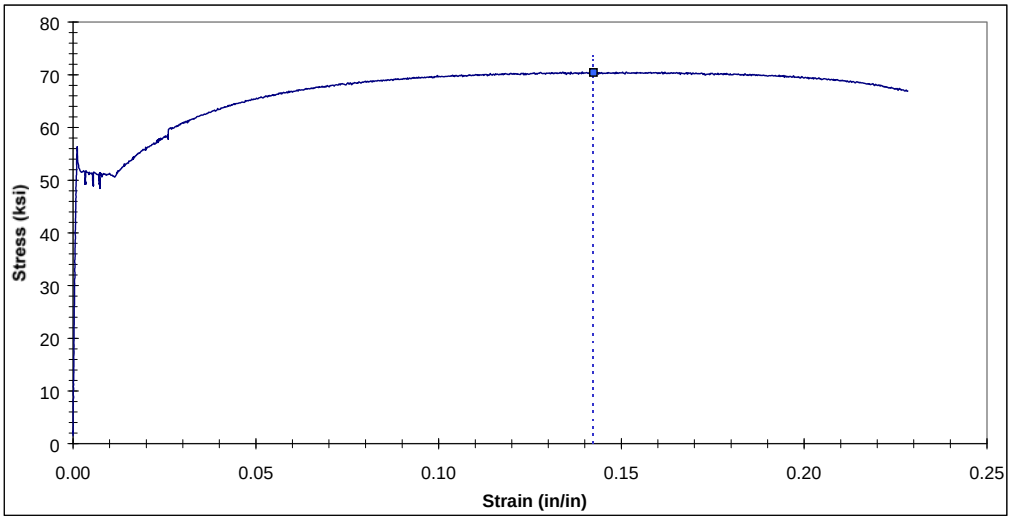

Figure C2.6.3 Complete Stress-strain Curve for Specimen N6-D

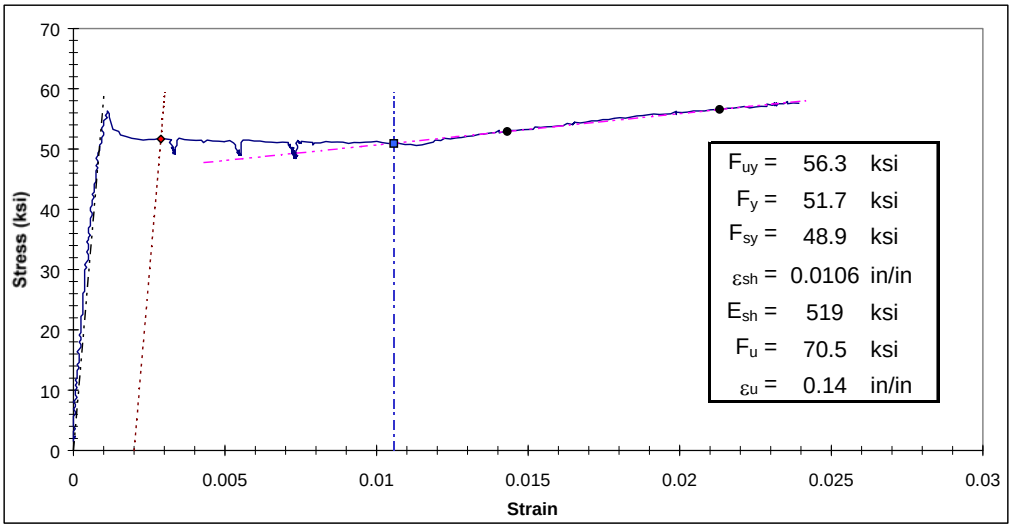

Figure C2.6.4 Yield Plateau and Tensile Test Results for Specimen N6-D

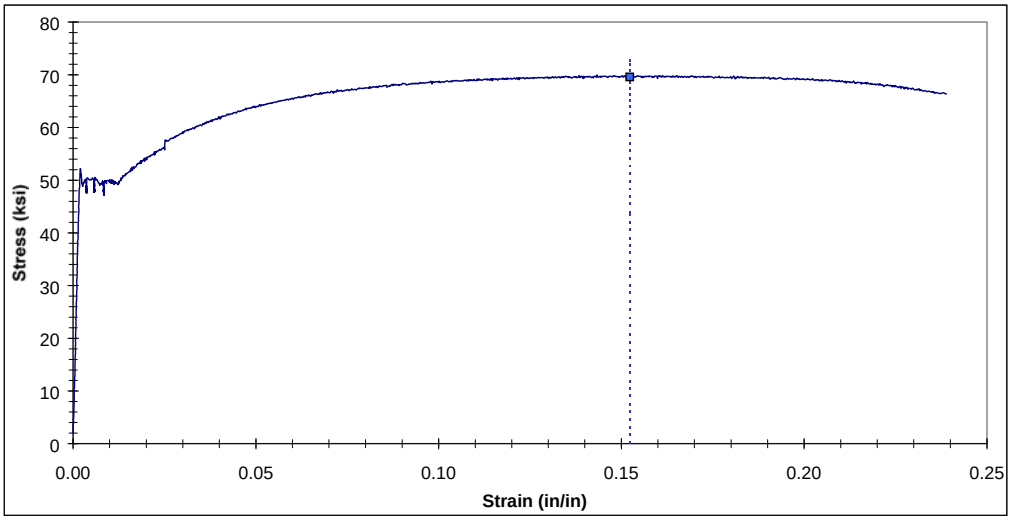

Figure C2.6.5 Complete Stress-strain Curve for Specimen N6-F

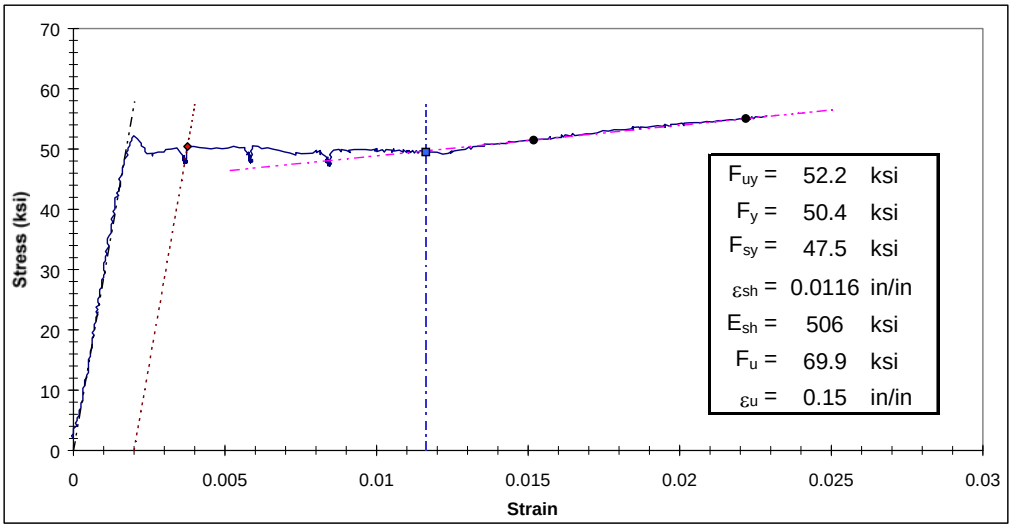

Figure C2.6.6 Yield Plateau and Tensile Test Results for Specimen N6-F

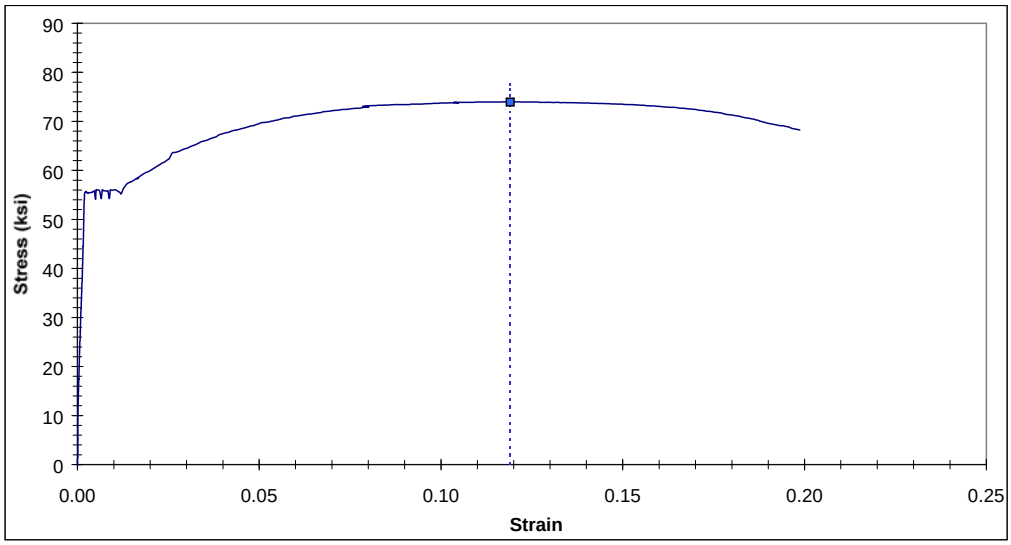

Figure C3.1.1 Complete Stress-strain Curve for Specimen B1-A

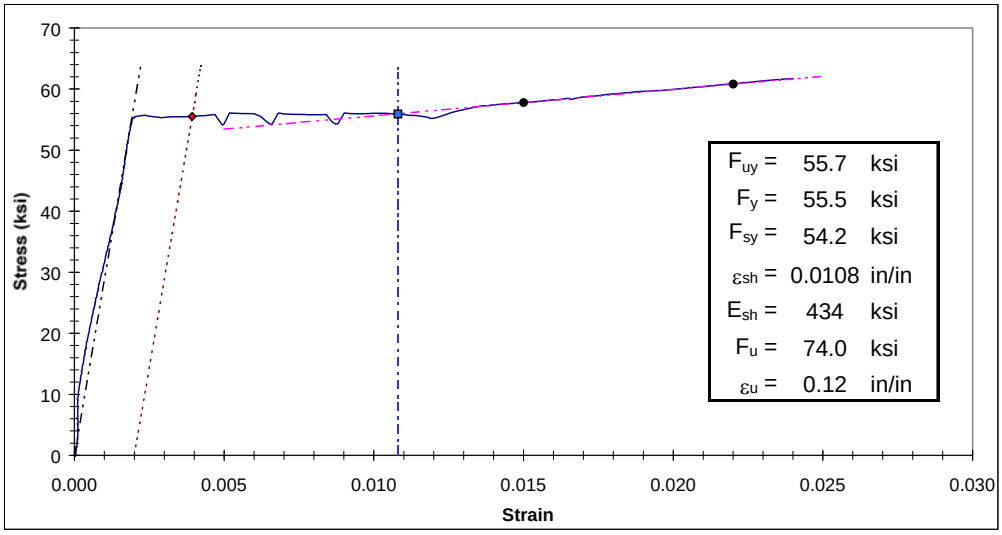

Figure C3.1.2 Yield Plateau and Tensile Test Results for Specimen B1-A

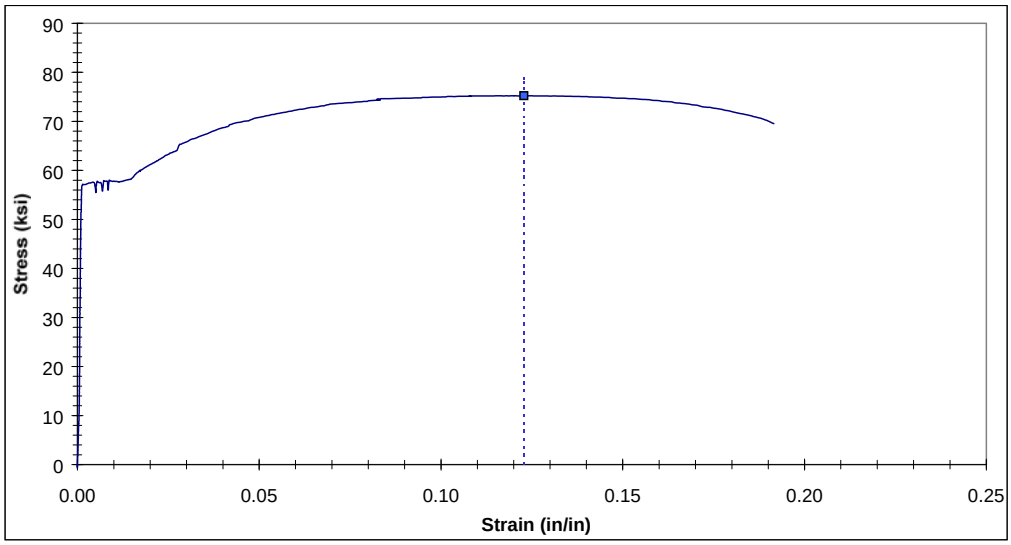

Figure C3.1.3 Complete Stress-strain Curve for Specimen B1-B

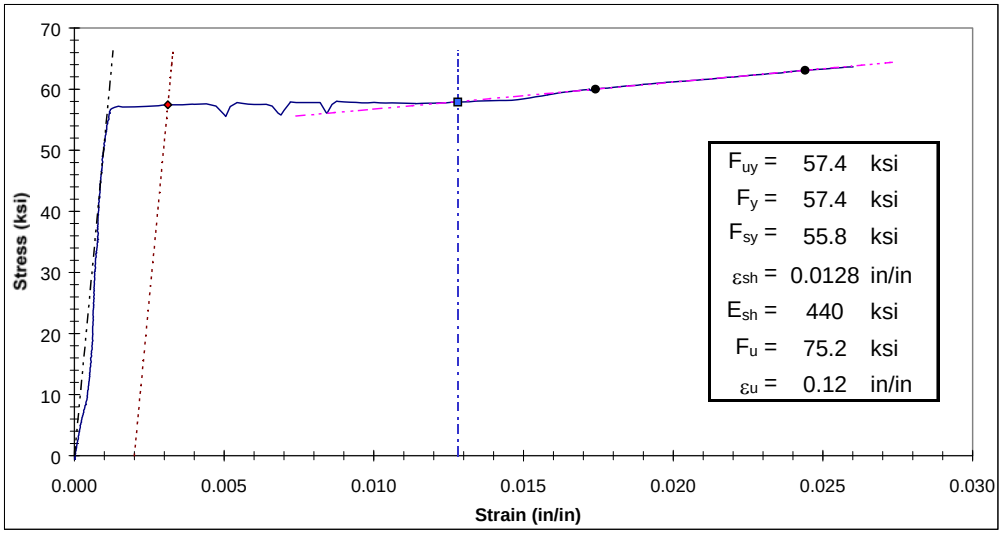

Figure C3.1.4 Yield Plateau and Tensile Test Results for Specimen B1-B

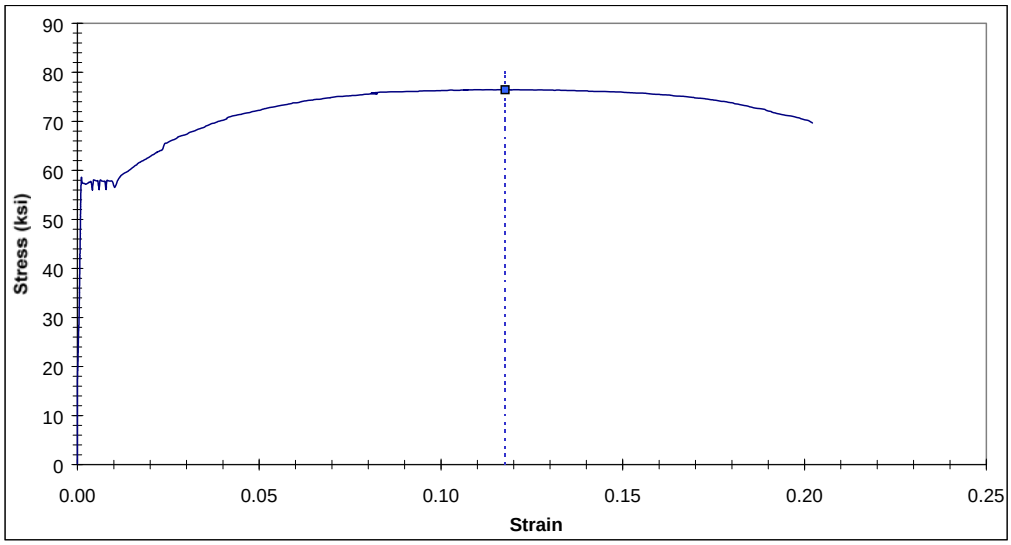

Figure C3.1.5 Complete Stress-strain Curve for Specimen B1-C

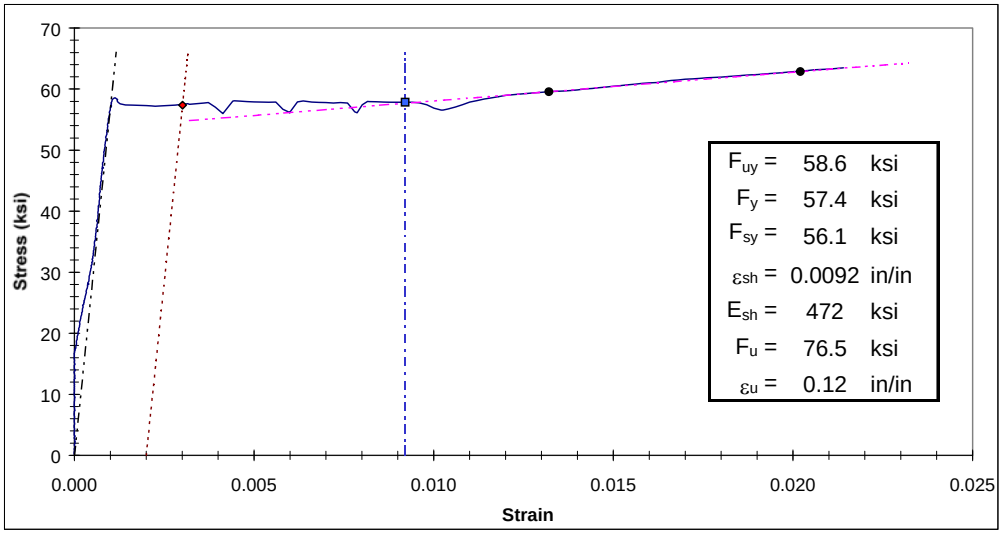

Figure C3.1.6 Yield Plateau and Tensile Test Results for Specimen B1-C

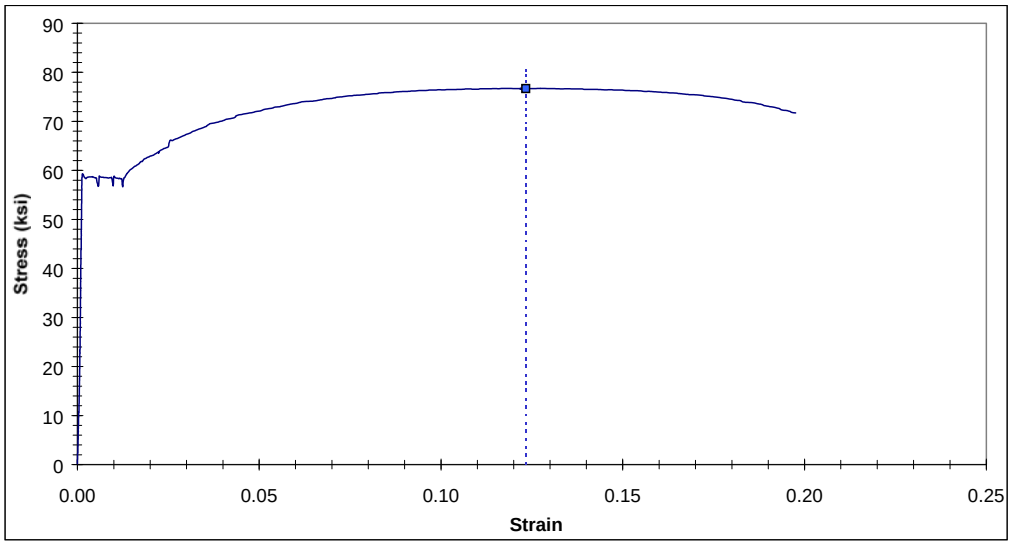

Figure C3.1.7 Complete Stress-strain Curve for Specimen B1-D

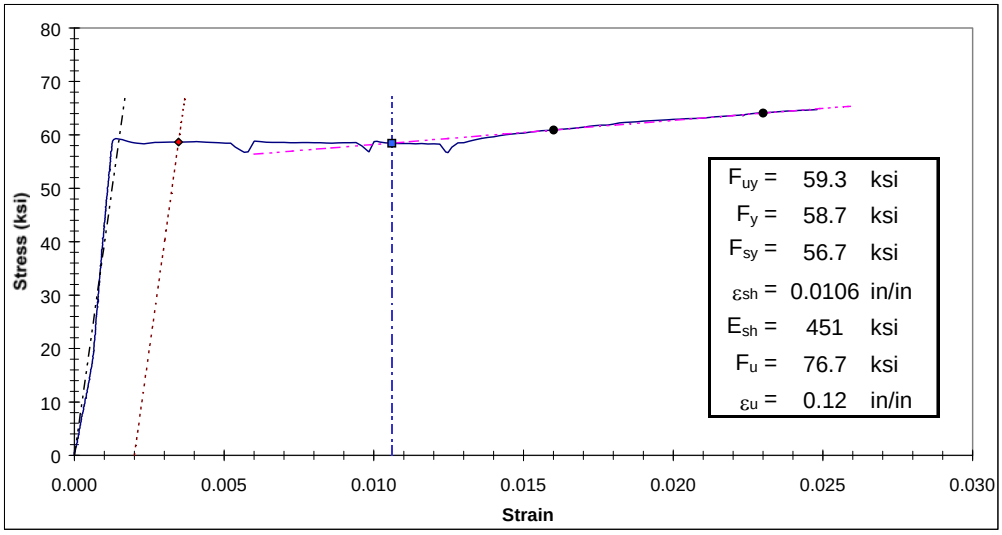

Figure C3.1.8 Yield Plateau and Tensile Test Results for Specimen B1-D

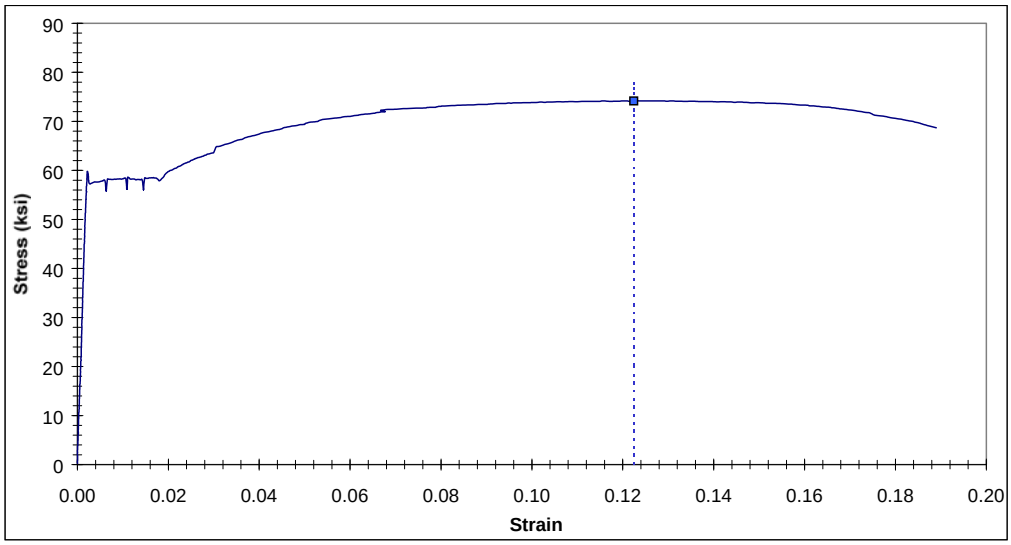

Figure C3.1.9 Complete Stress-strain Curve for Specimen B1-E

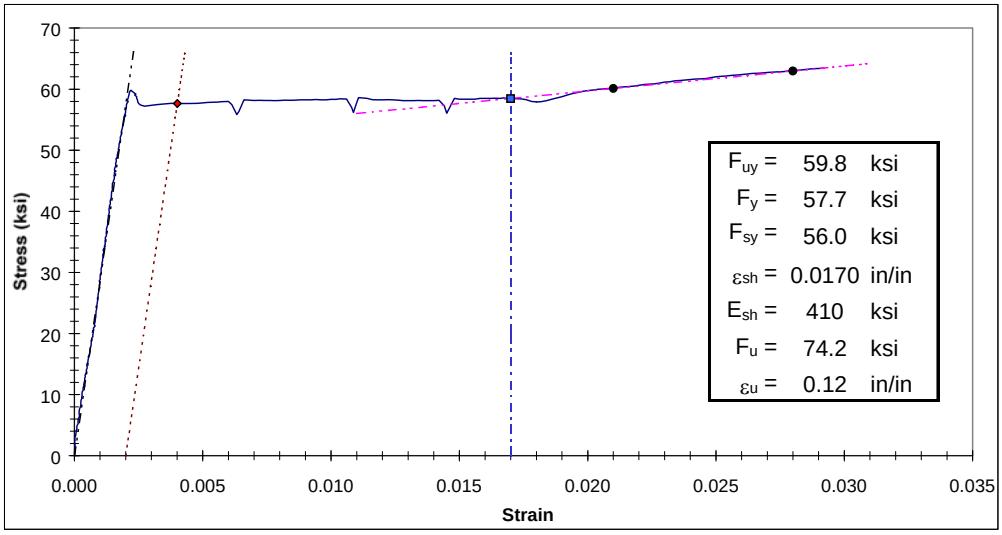

Figure C3.1.10 Yield Plateau and Tensile Test Results for Specimen B1-E

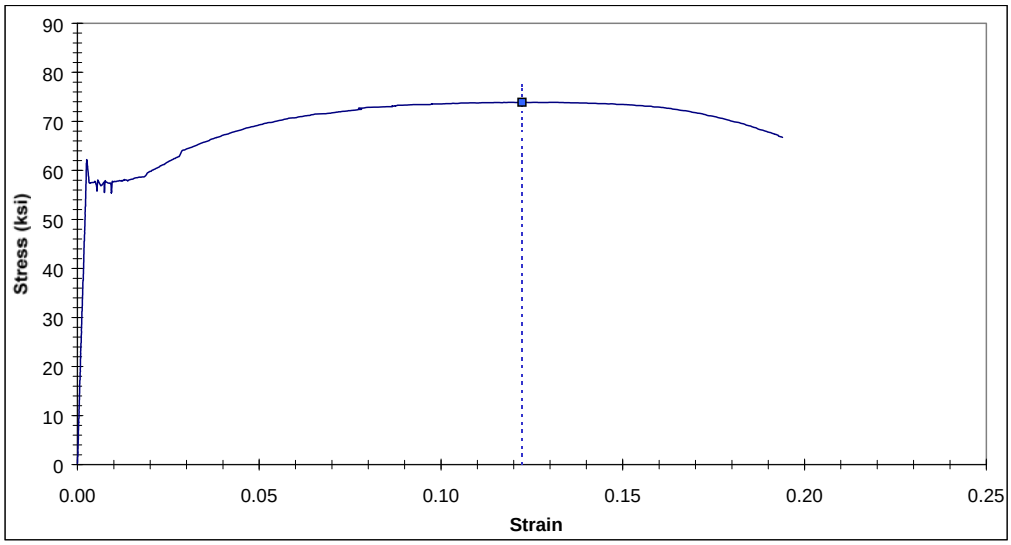

Figure C3.1.11 Complete Stress-strain Curve for Specimen B1-F

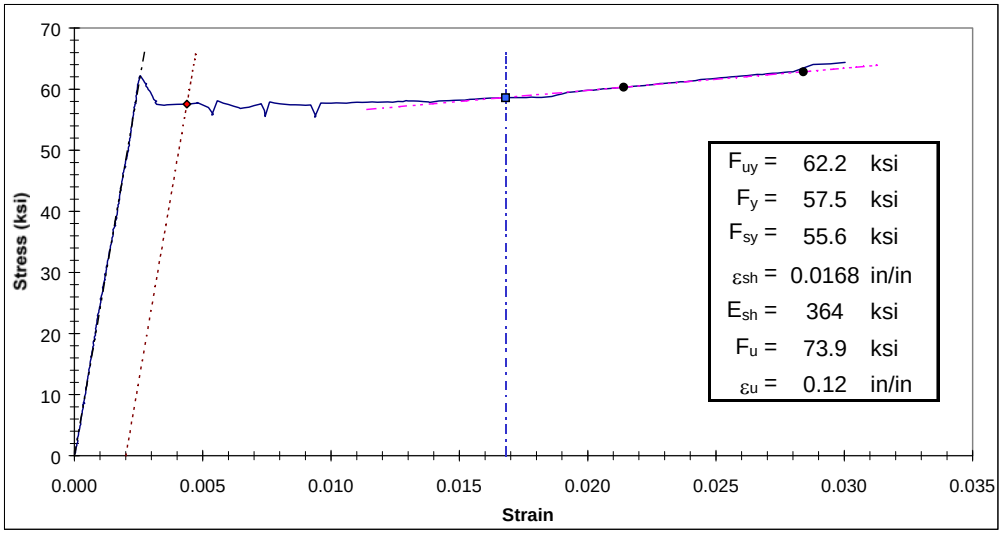

Figure C3.1.12 Yield Plateau and Tensile Test Results for Specimen B1-F

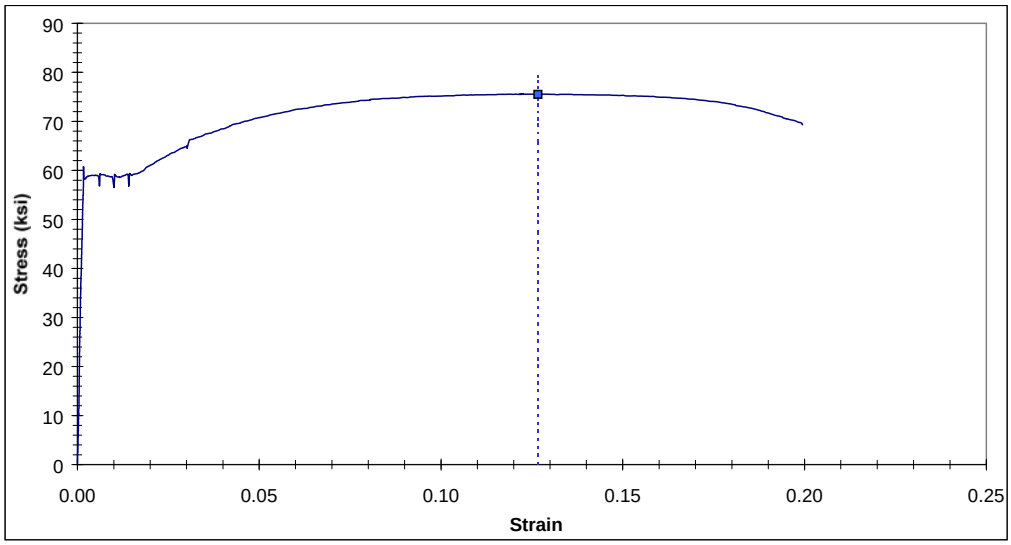

Figure C3.1.13 Complete Stress-strain Curve for Specimen B1-G

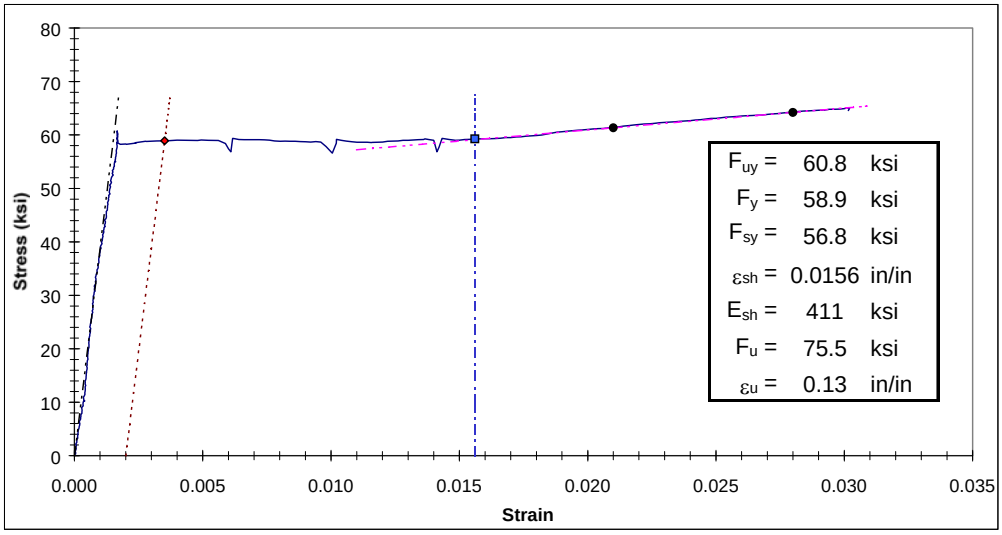

Figure C3.1.14 Yield Plateau and Tensile Test Results for Specimen B1-G

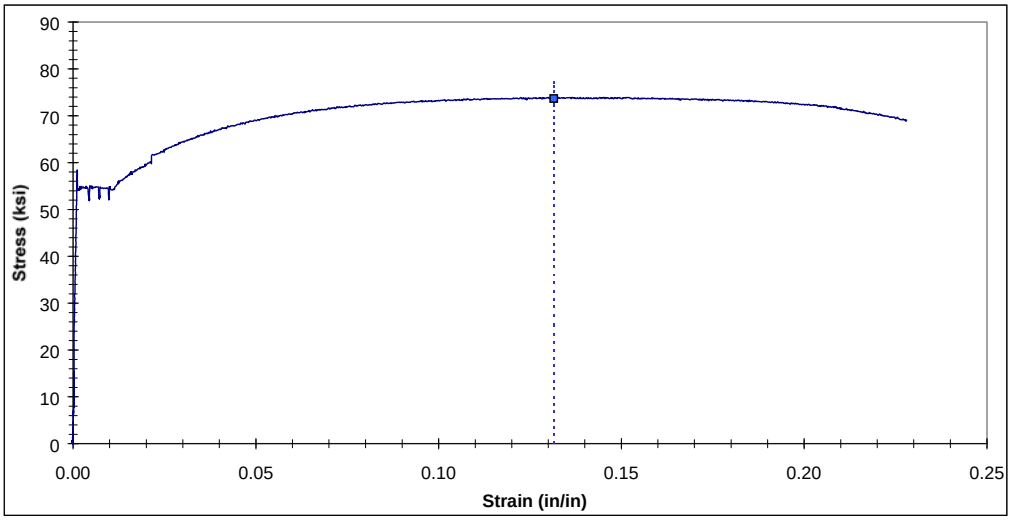

Figure C3.2.1 Complete Stress-strain Curve for Specimen B2-A

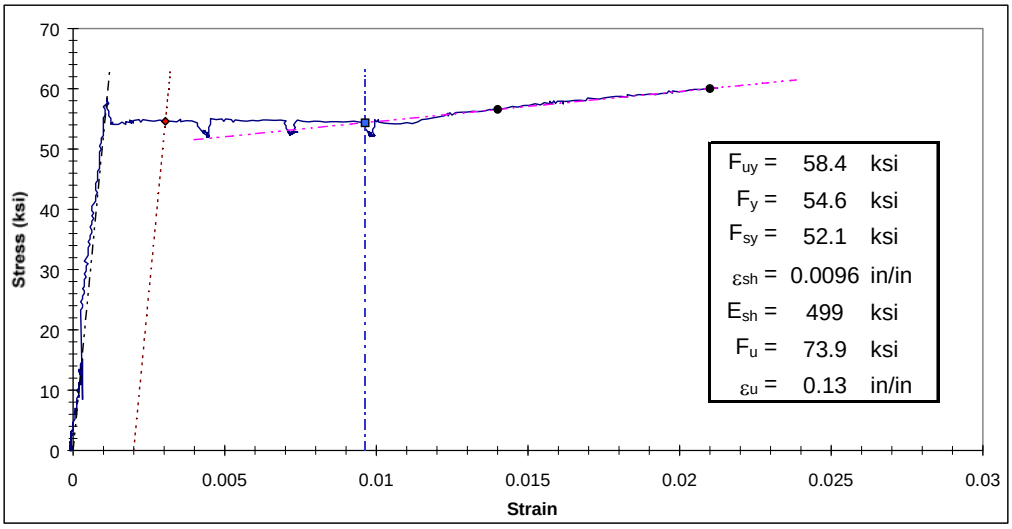

Figure C3.2.2 Yield Plateau and Tensile Test Results for Specimen B2-A

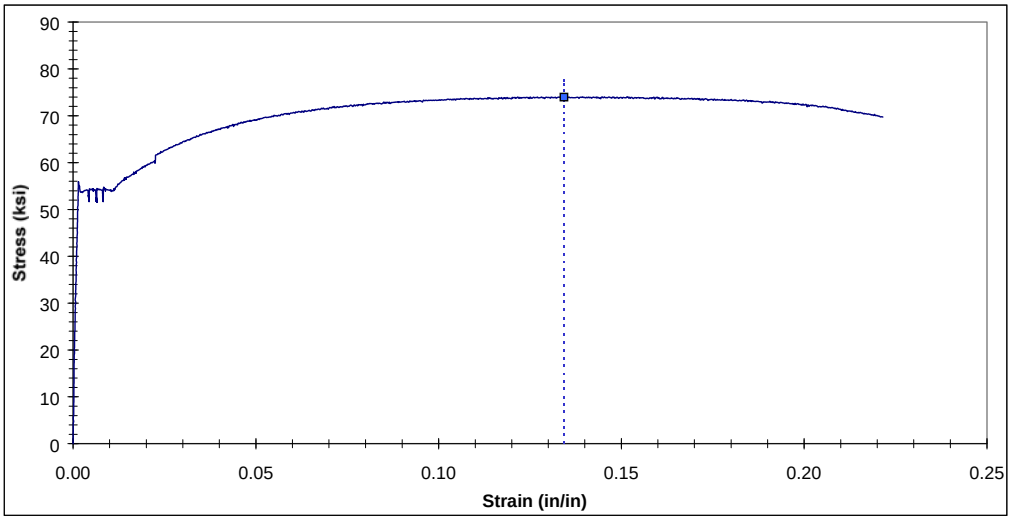

Figure C3.2.3 Complete Stress-strain Curve for Specimen B2-B

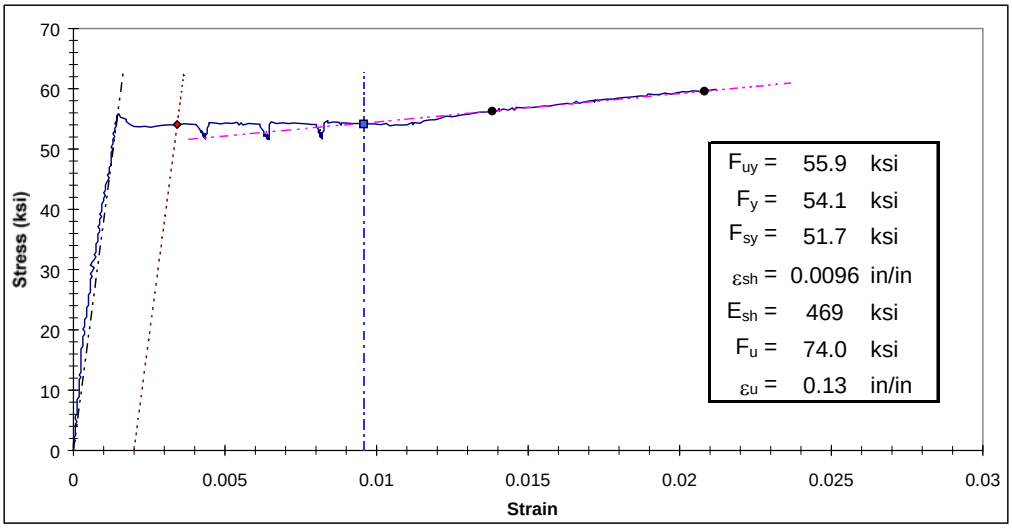

Figure C3.2.4 Yield Plateau and Tensile Test Results for Specimen B2-B

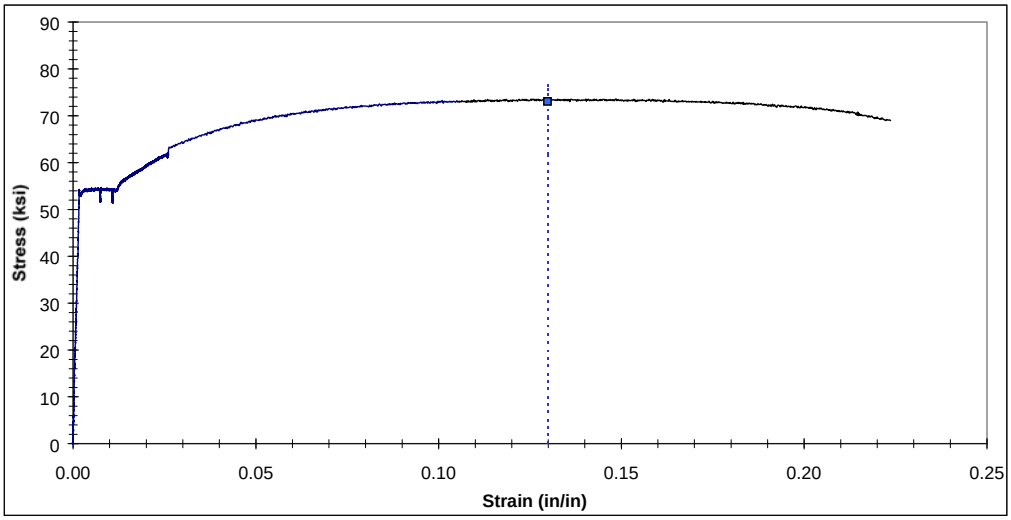

Figure C3.2.5 Complete Stress-strain Curve for Specimen B2-C

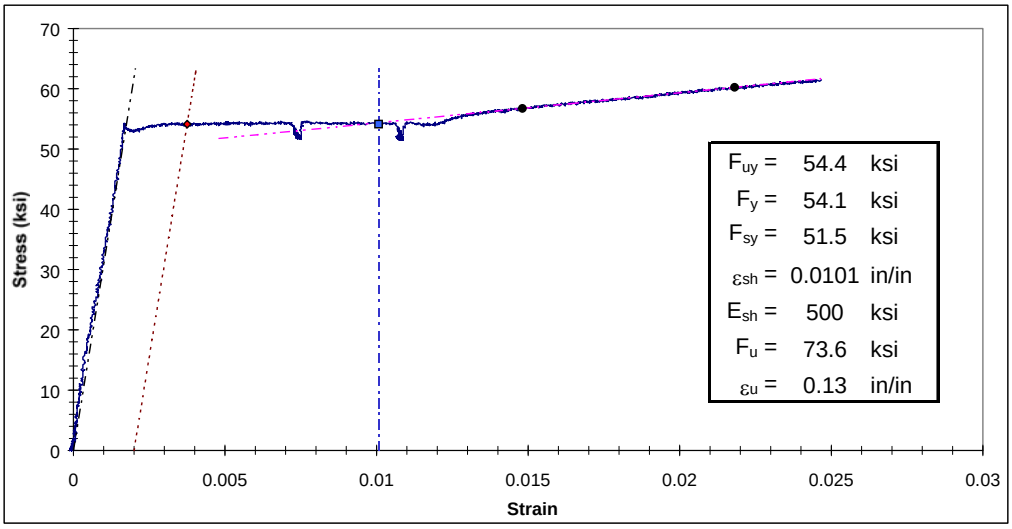

Figure C3.2.6 Yield Plateau and Tensile Test Results for Specimen B2-C

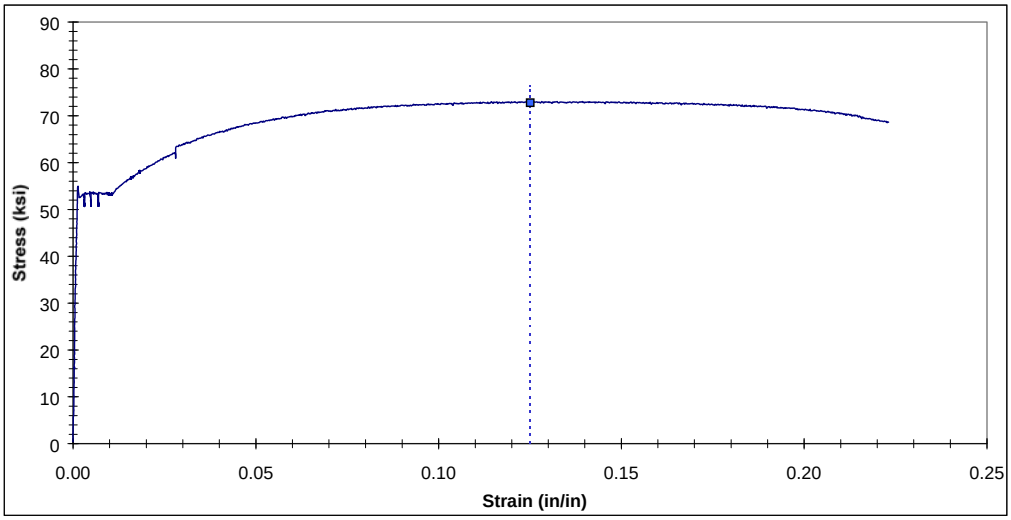

Figure C3.2.7 Complete Stress-strain Curve for Specimen B2-D

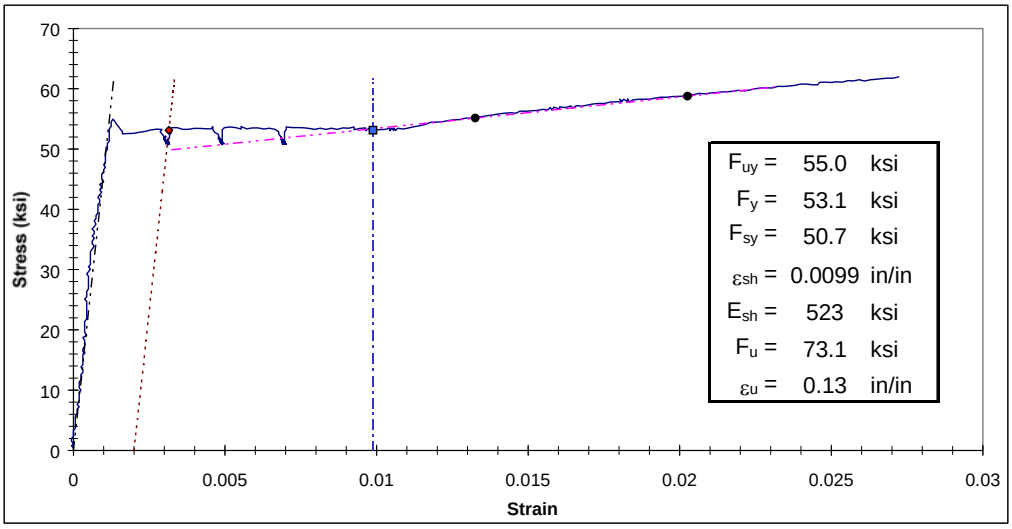

Figure C3.2.8 Yield Plateau and Tensile Test Results for Specimen B2-D

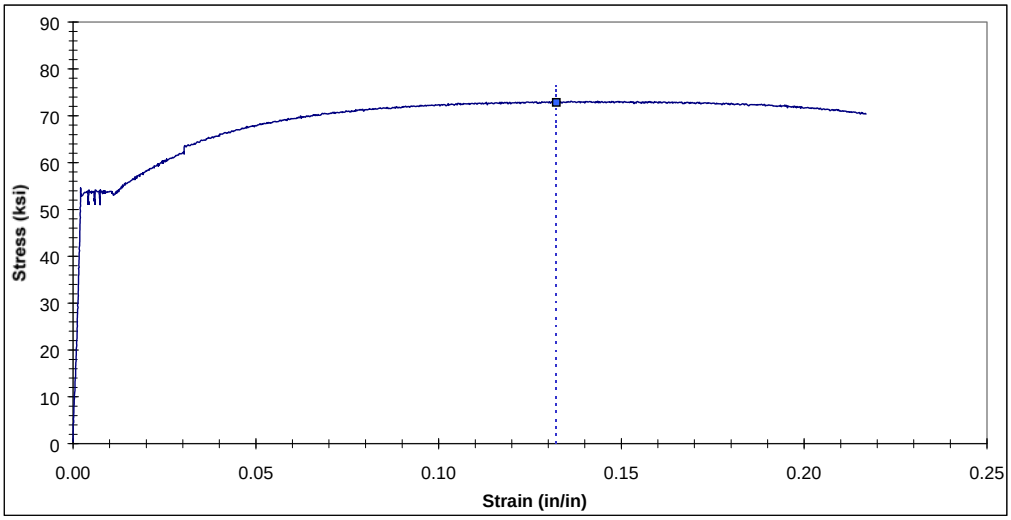

Figure C3.2.9 Complete Stress-strain Curve for Specimen B2-E

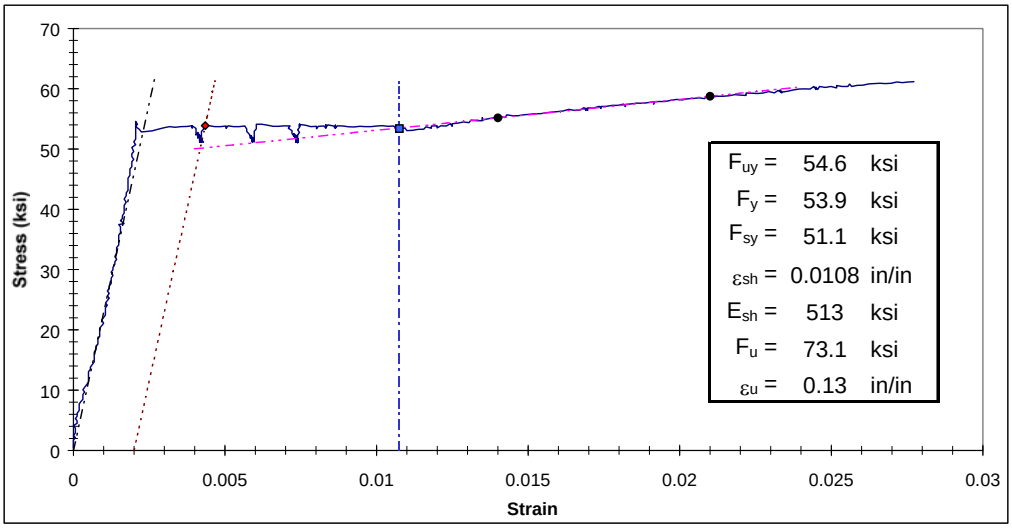

Figure C3.2.10 Yield Plateau and Tensile Test Results for Specimen B2-E

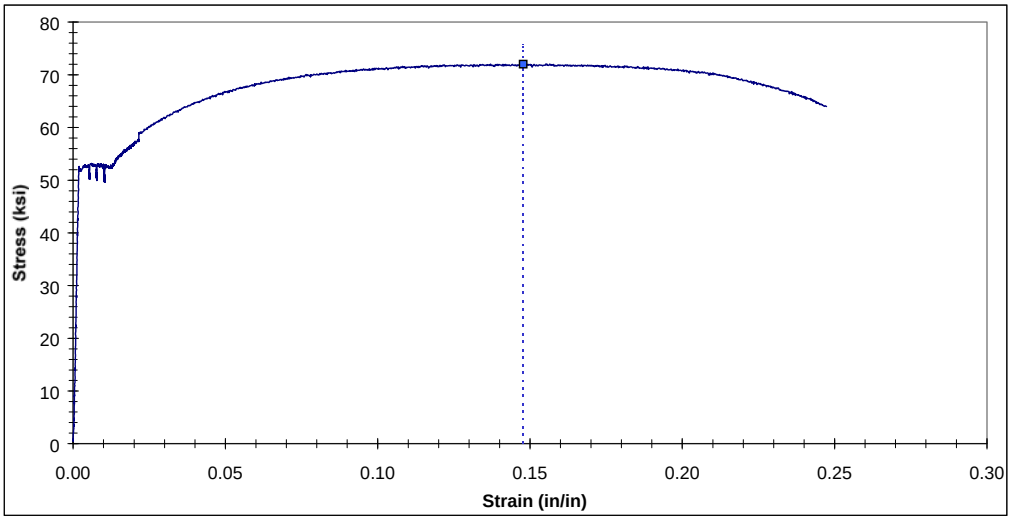

Figure C3.2.11 Complete Stress-strain Curve for Specimen B2-F

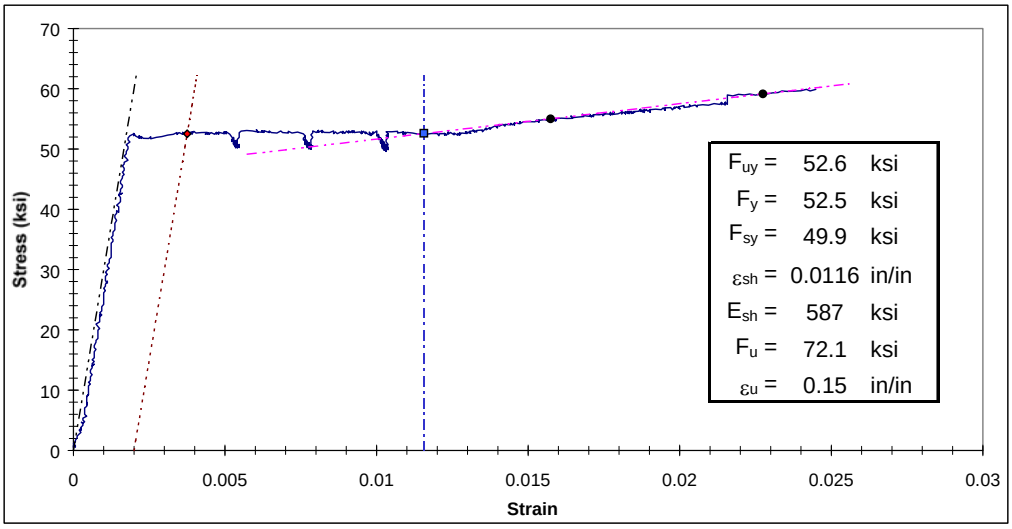

Figure C3.2.12 Yield Plateau and Tensile Test Results for Specimen B2-F

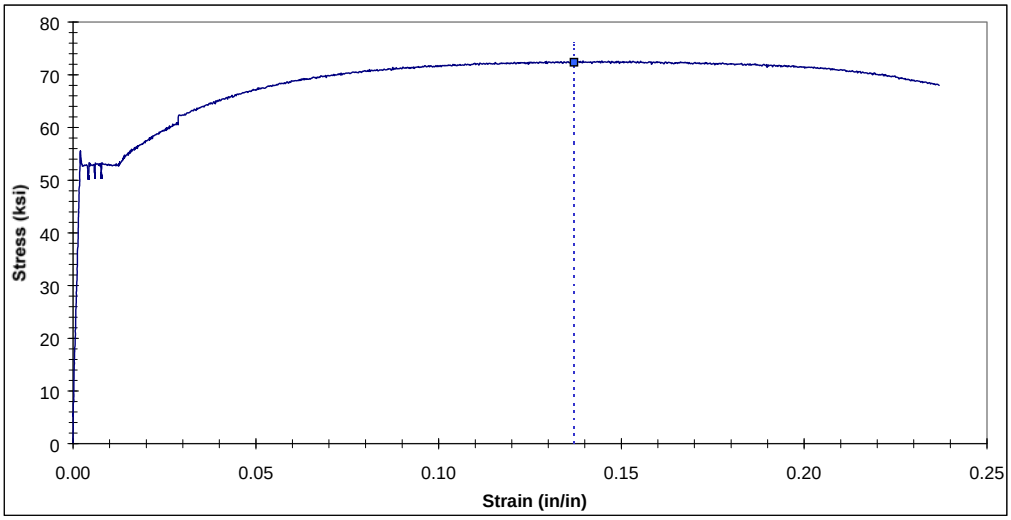

Figure C3.2.13 Complete Stress-strain Curve for Specimen B2-G

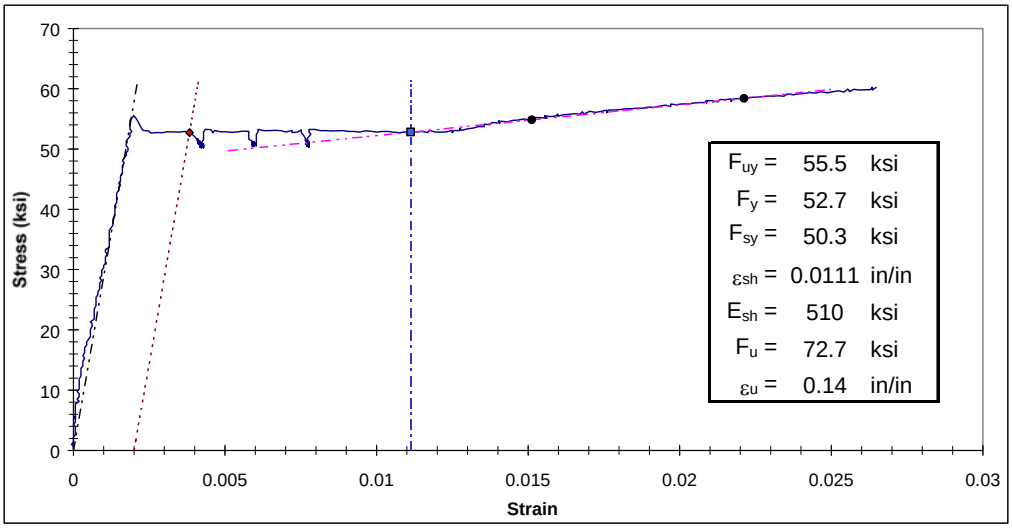

Figure C3.2.14 Yield Plateau and Tensile Test Results for Specimen B2-G

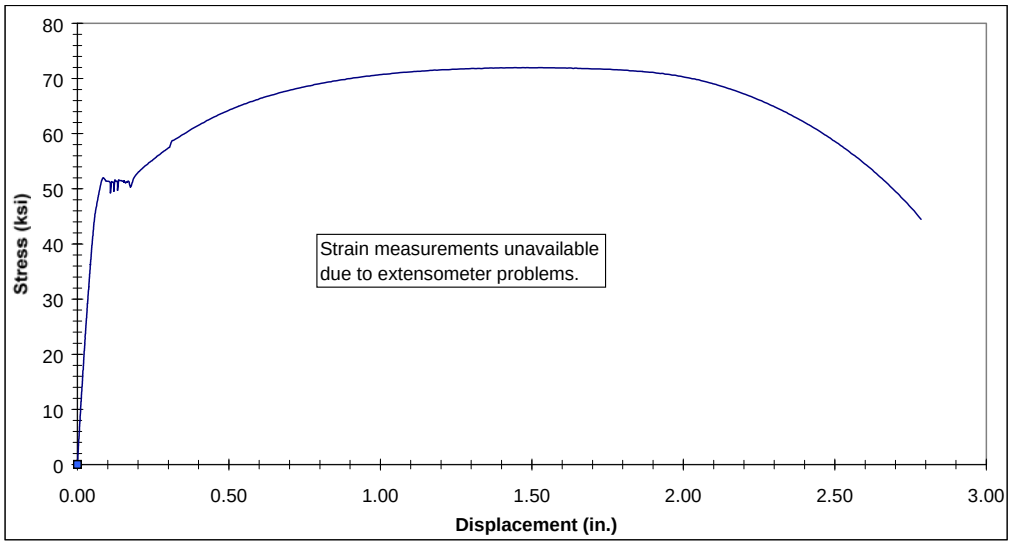

Figure C3.3.1 Complete Stress-strain Curve for Specimen B3-A

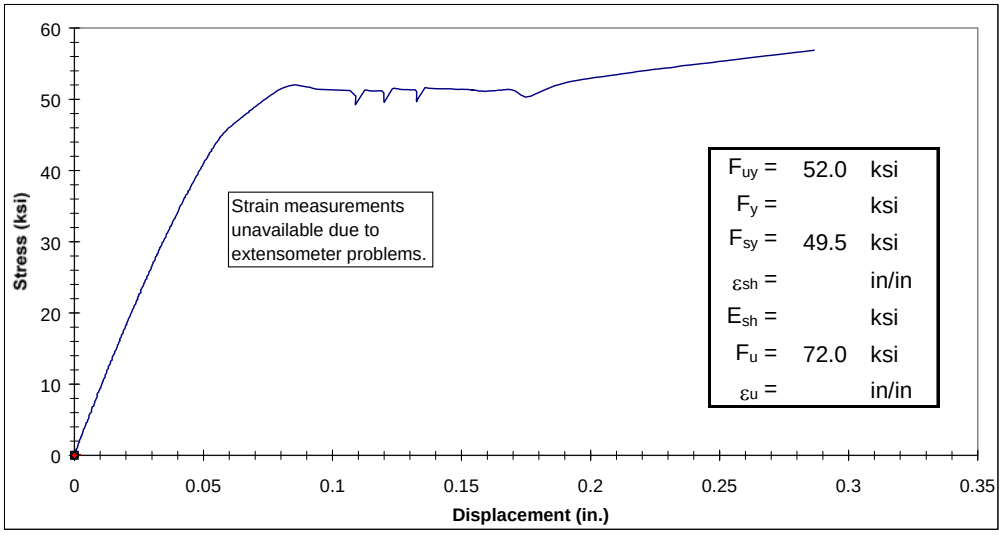

Figure C3.3.2 Yield Plateau and Tensile Test Results for Specimen B3-A

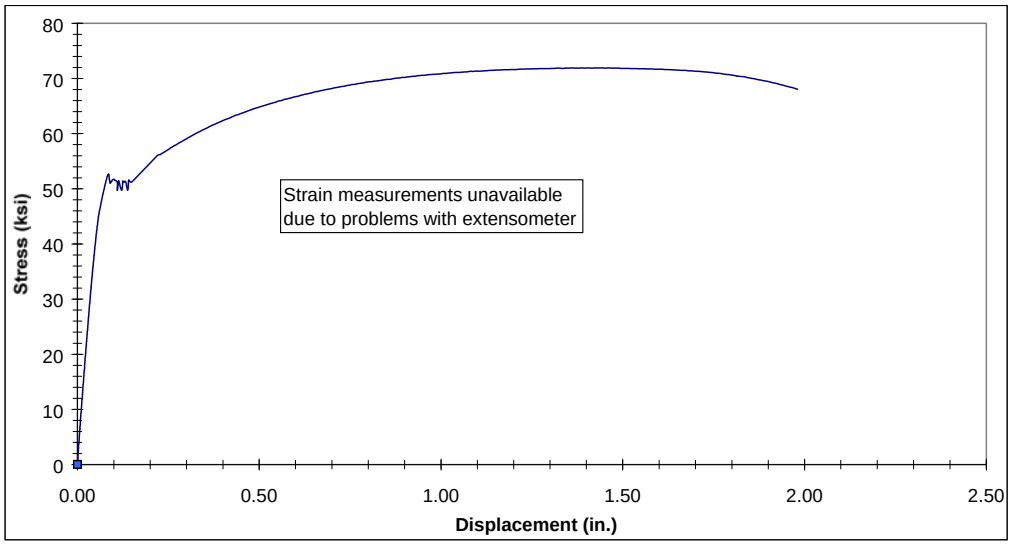

Figure C3.3.3 Complete Stress-strain Curve for Specimen B3-B

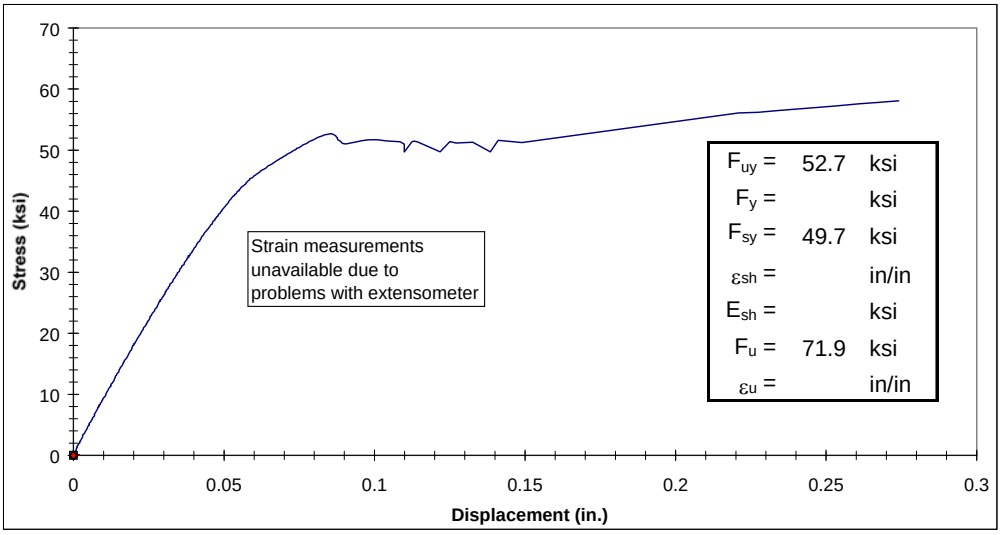

Figure C3.3.4 Yield Plateau and Tensile Test Results for Specimen B3-B

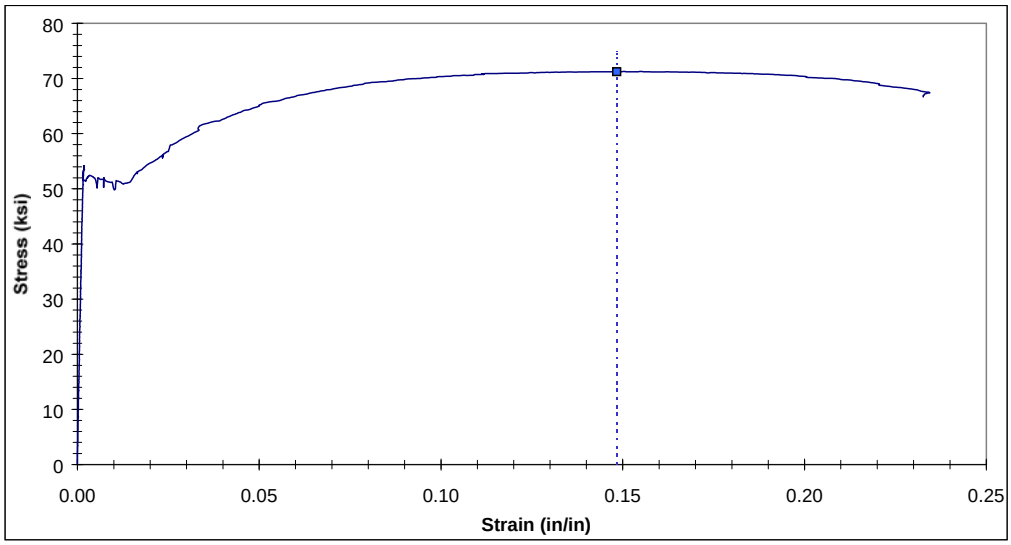

Figure C3.3.5 Complete Stress-strain Curve for Specimen B3-C

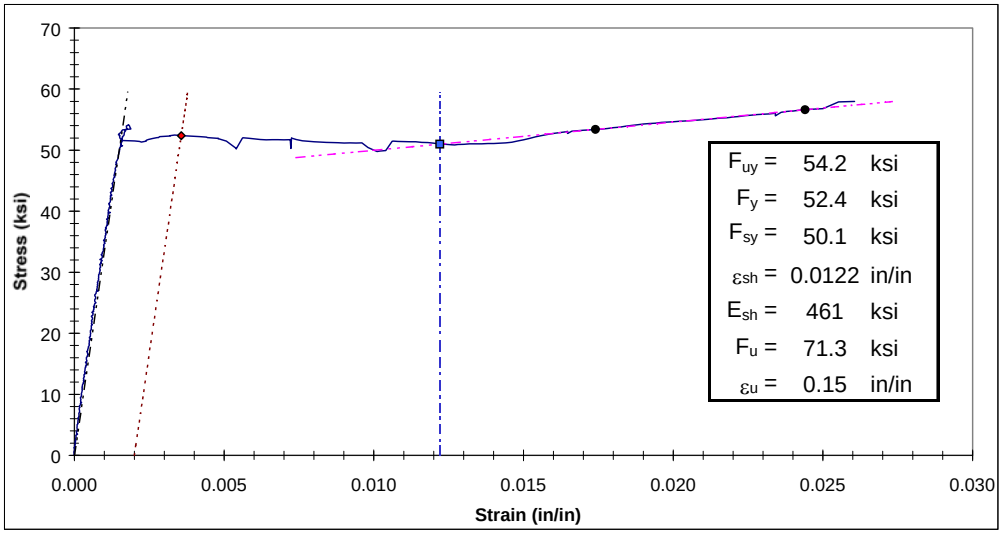

Figure C3.3.6 Yield Plateau and Tensile Test Results for Specimen B3-C

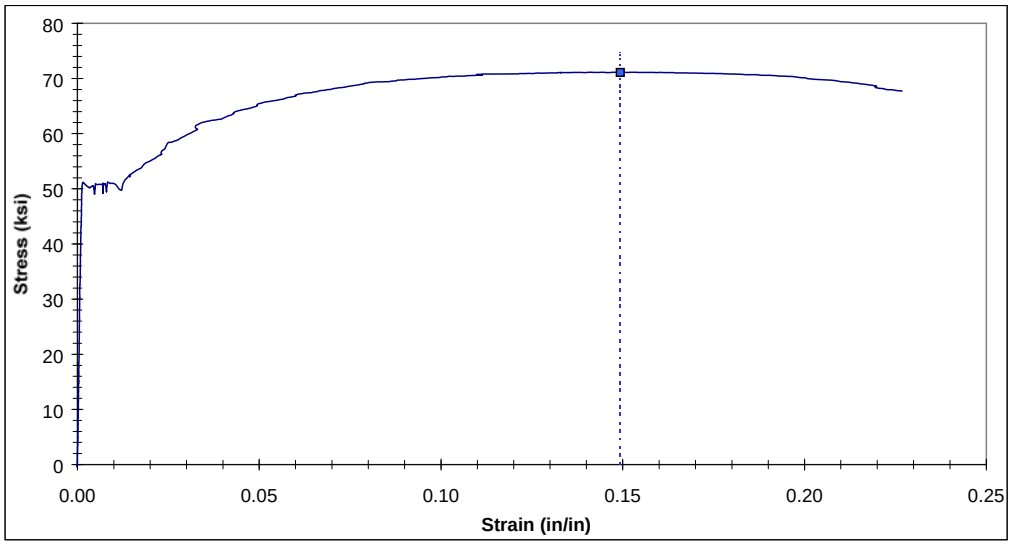

Figure C3.3.7 Complete Stress-strain Curve for Specimen B3-D

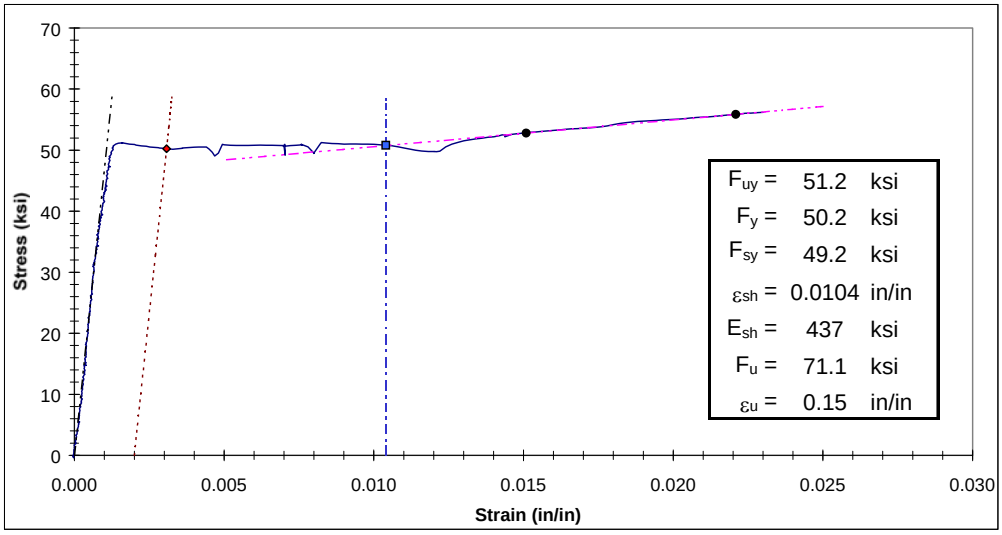

Figure C3.3.8 Yield Plateau and Tensile Test Results for Specimen B3-D

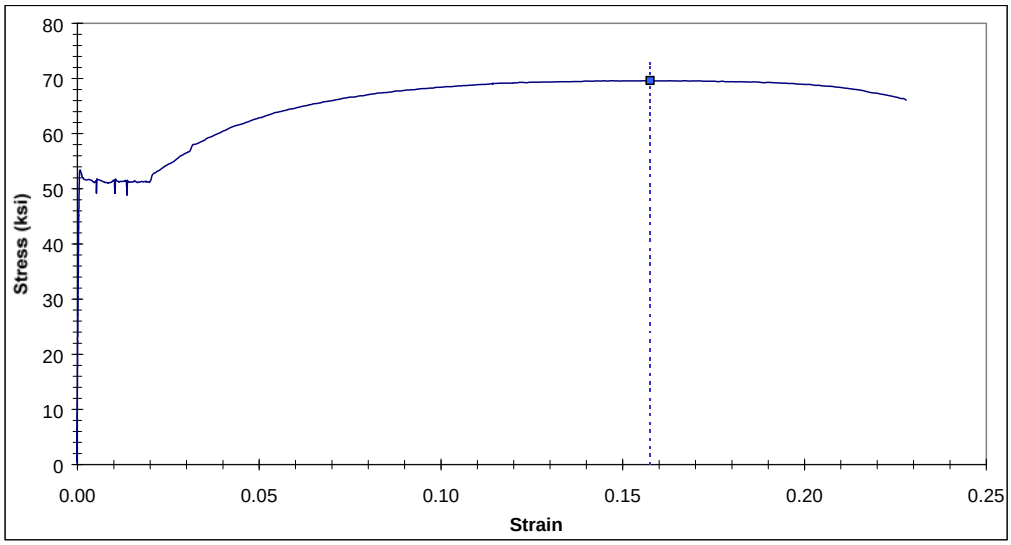

Figure C3.3.9 Complete Stress-strain Curve for Specimen B3-E

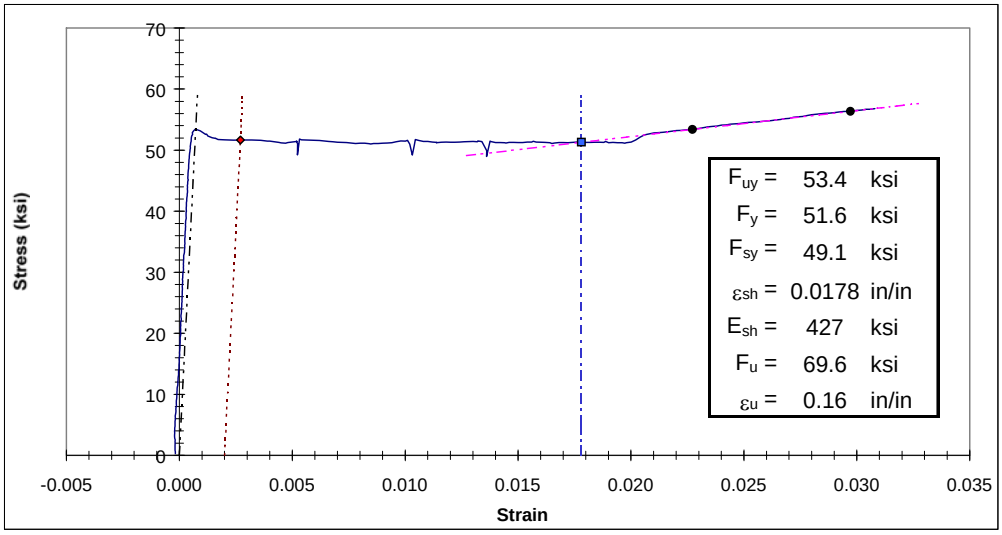

Figure C3.3.10 Yield Plateau and Tensile Test Results for Specimen B3-E

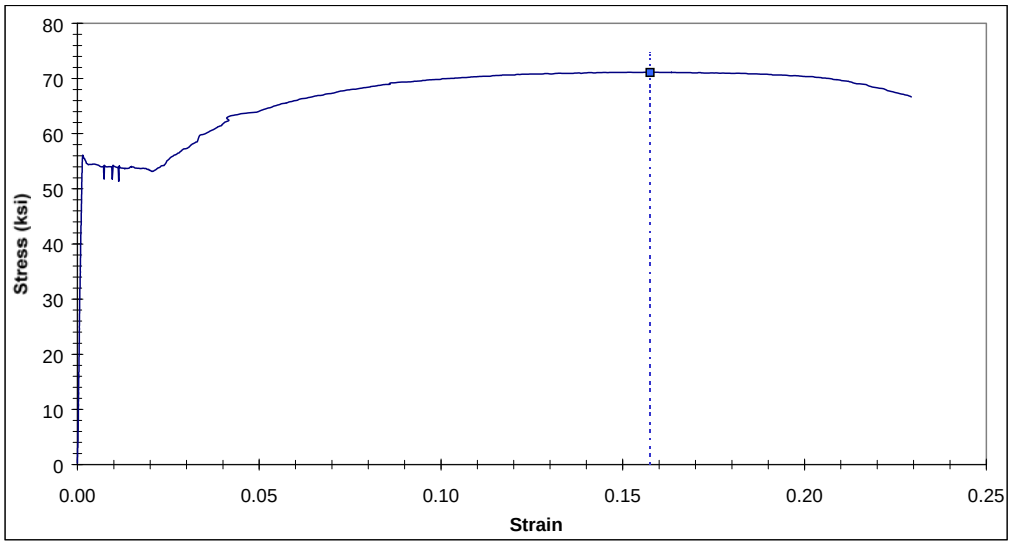

Figure C3.3.11 Complete Stress-strain Curve for Specimen B3-F

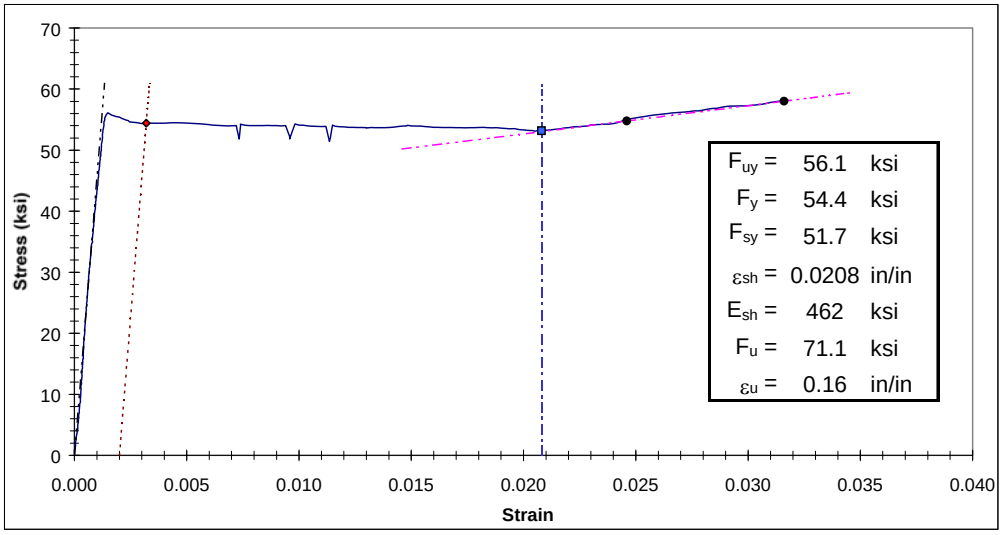

Figure C3.3.12 Yield Plateau and Tensile Test Results for Specimen B3-F

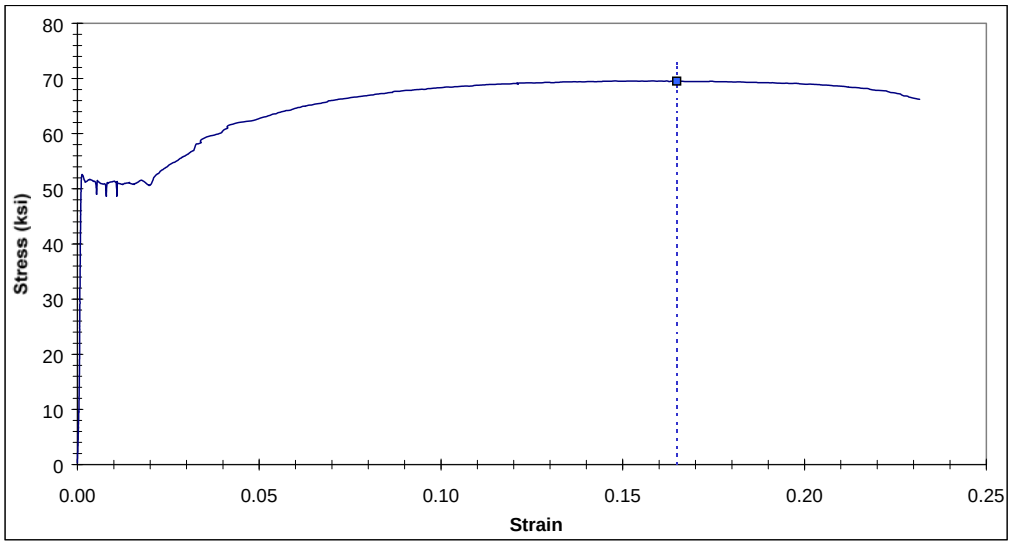

Figure C3.3.13 Complete Stress-strain Curve for Specimen B3-G

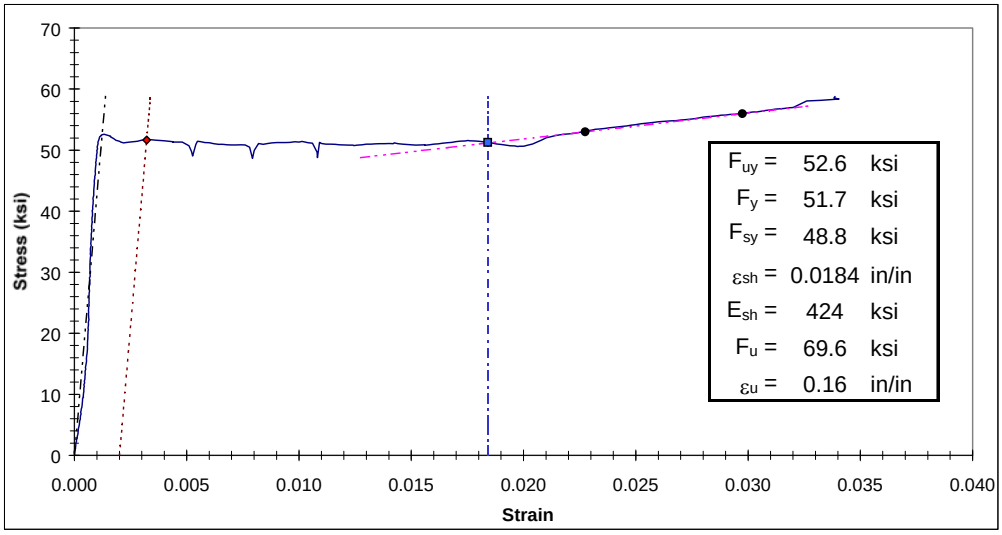

Figure C3.3.14 Yield Plateau and Tensile Test Results for Specimen B3-G

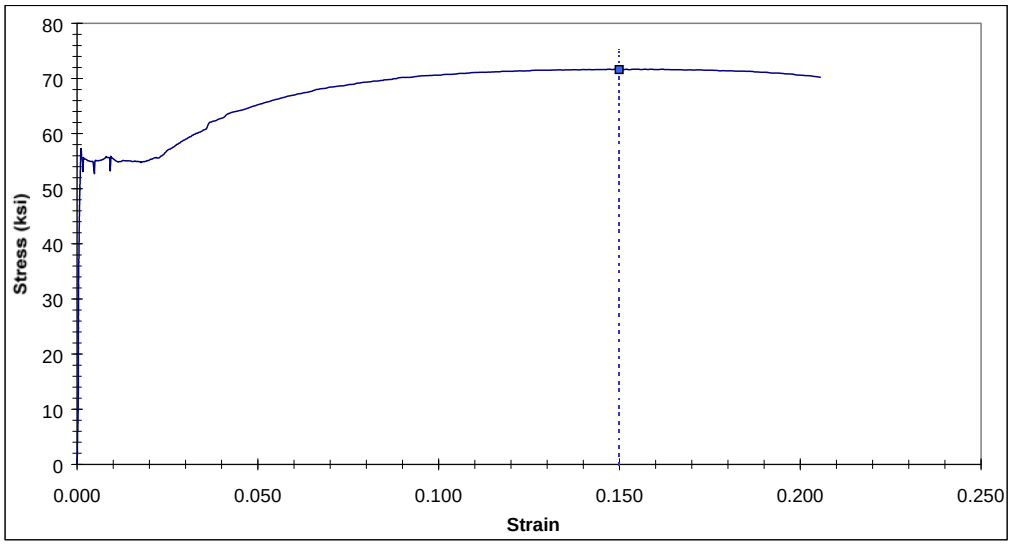

Figure C3.4.1 Complete Stress-strain Curve for Specimen B4-A

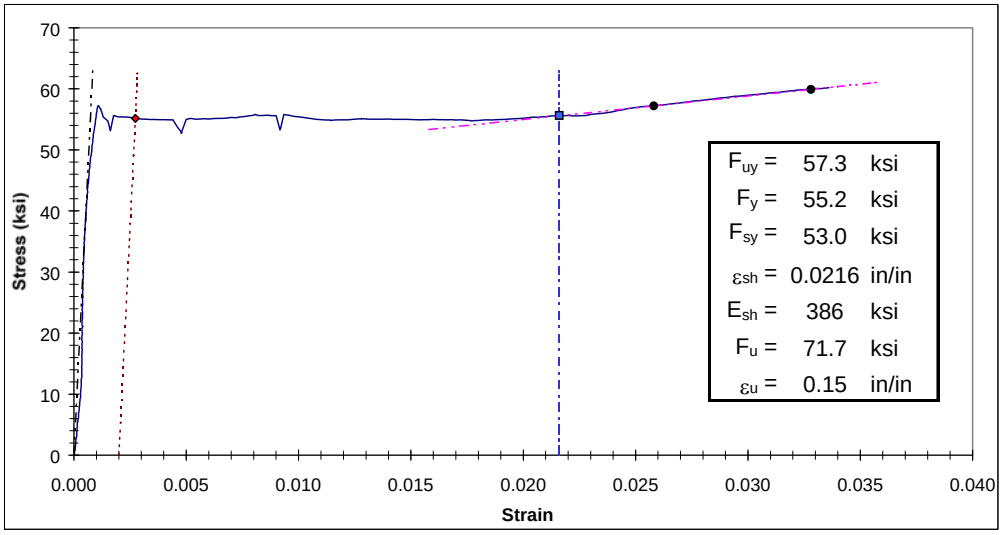

Figure C3.4.2 Yield Plateau and Tensile Test Results for Specimen B4-A

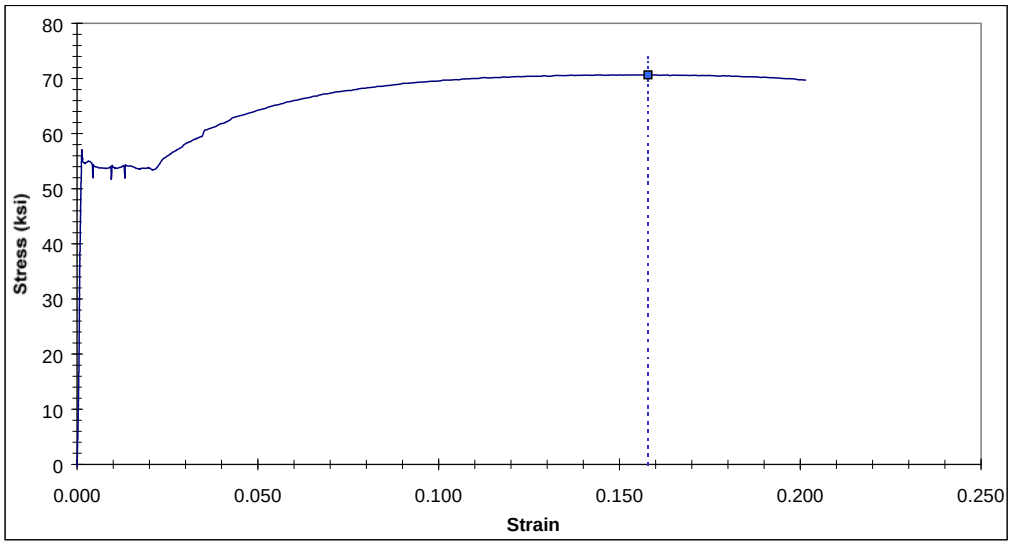

Figure C3.4.3 Complete Stress-strain Curve for Specimen B4-B

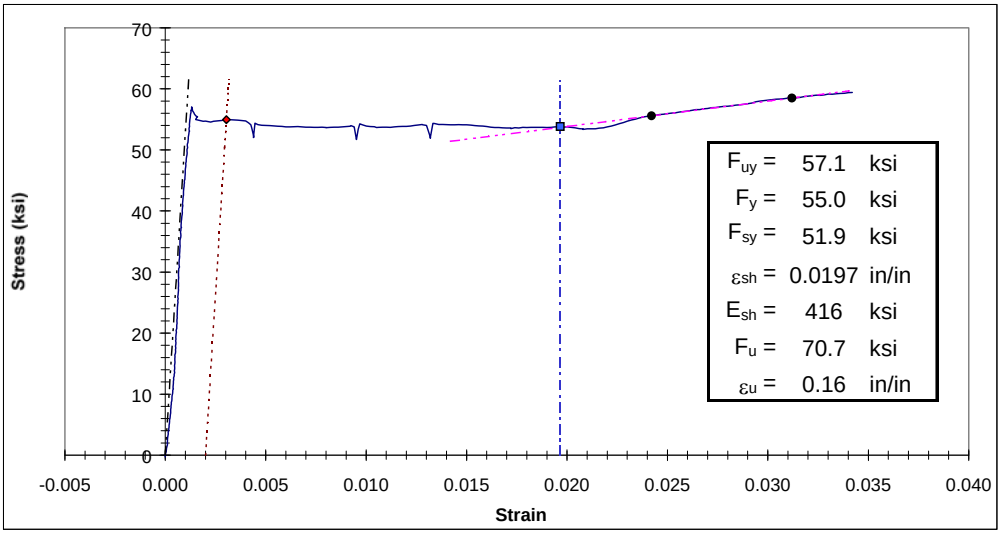

Figure C3.4.4 Yield Plateau and Tensile Test Results for Specimen B4-B

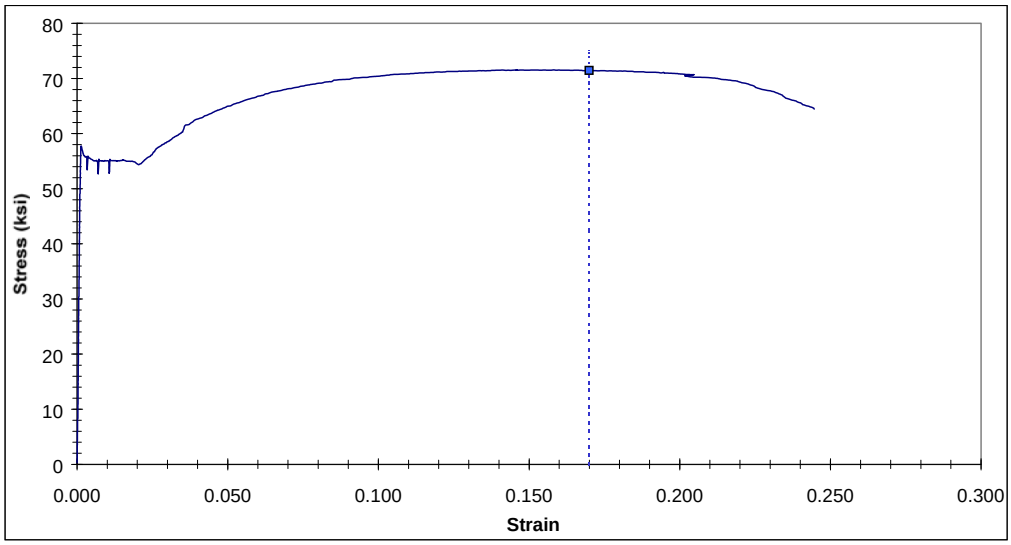

Figure C3.4.5 Complete Stress-strain Curve for Specimen B4-C

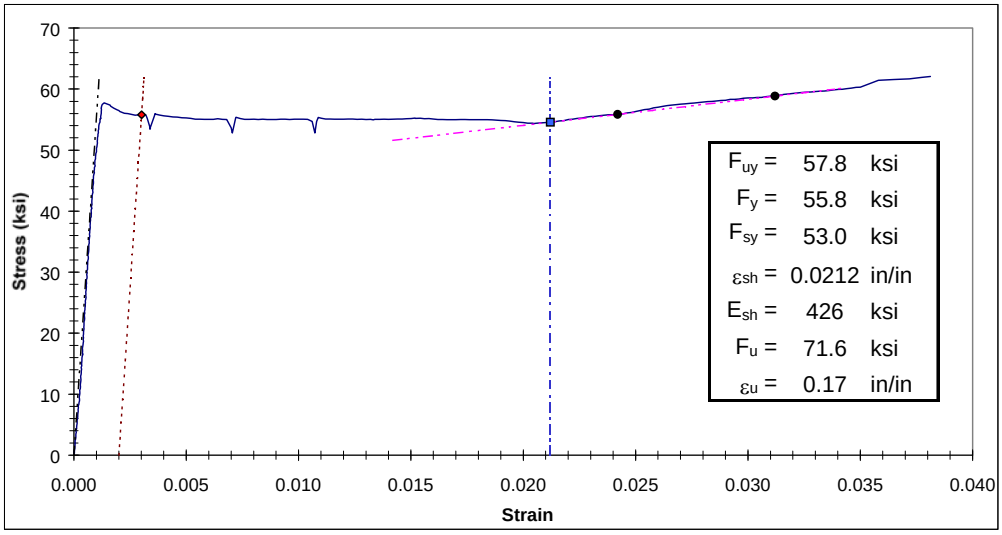

Figure C3.4.6 Yield Plateau and Tensile Test Results for Specimen B4-C

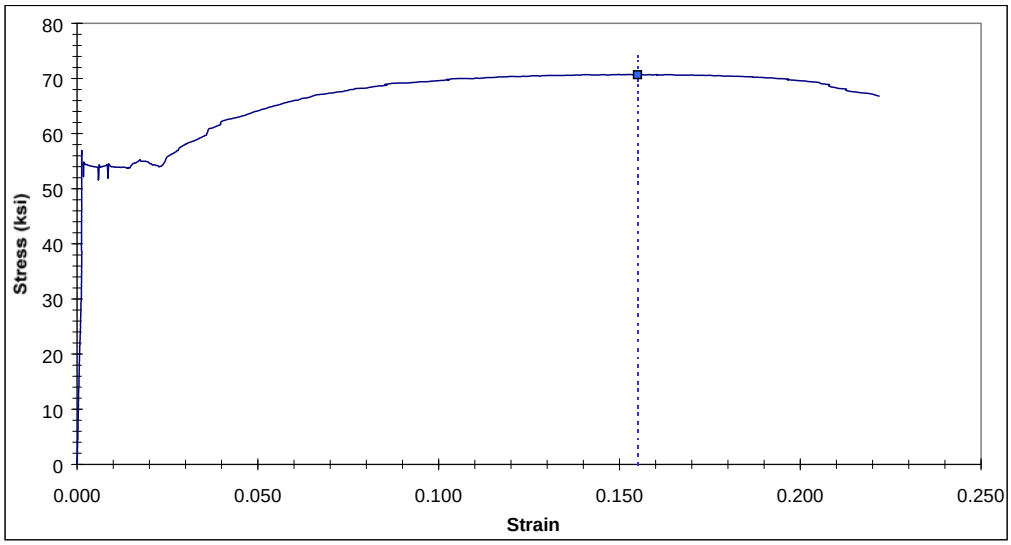

Figure C3.4.7 Complete Stress-strain Curve for Specimen B4-D

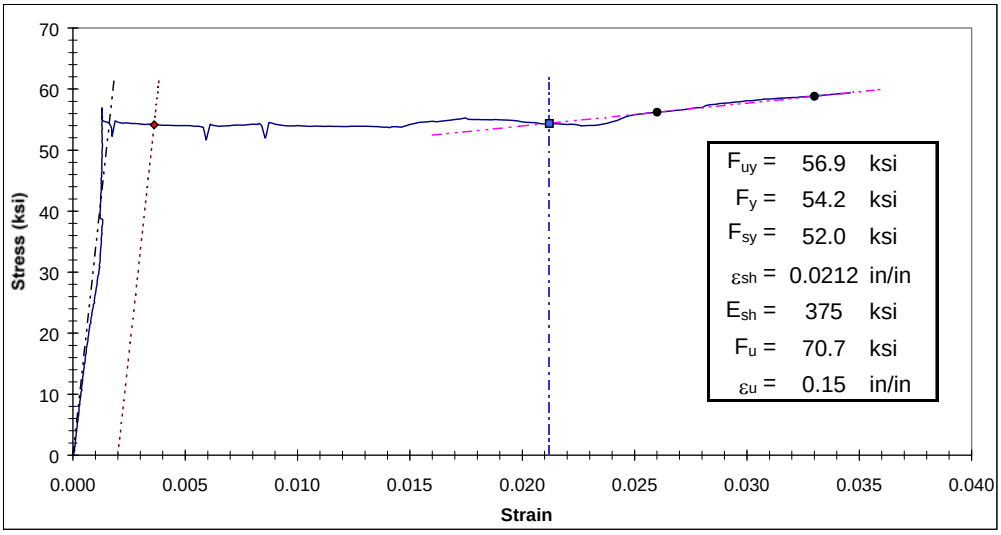

Figure C3.4.8 Yield Plateau and Tensile Test Results for Specimen B4-D

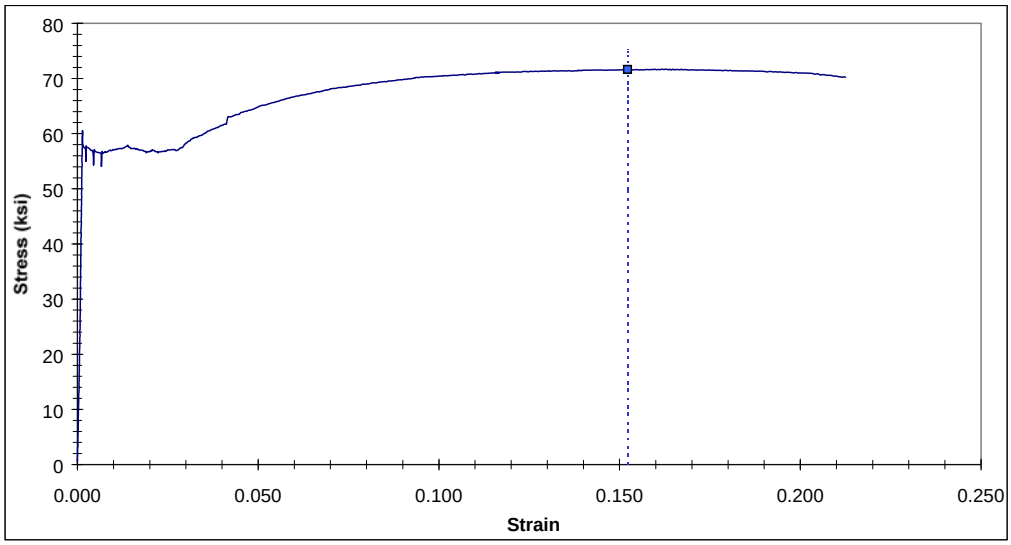

Figure C3.4.9 Complete Stress-strain Curve for Specimen B4-E

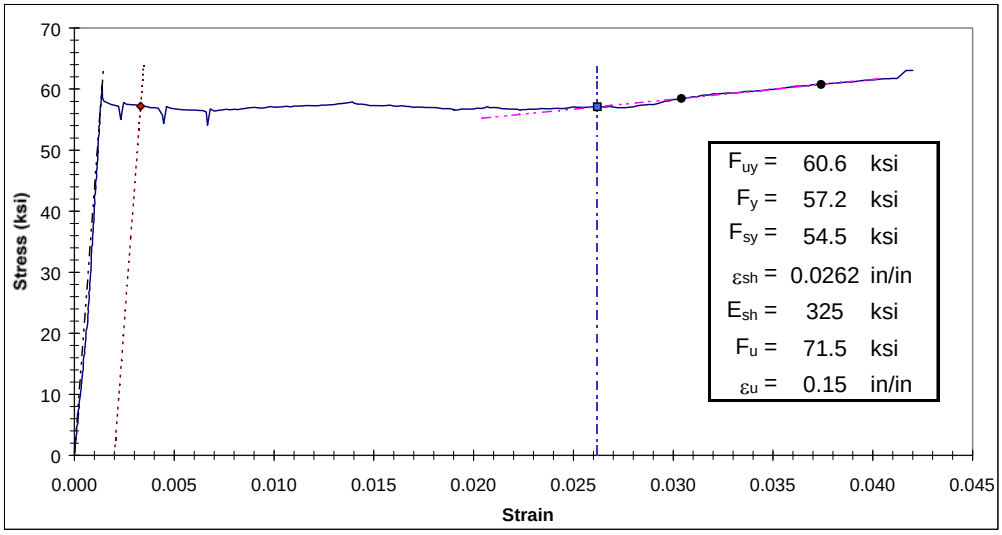

Figure C3.4.10 Yield Plateau and Tensile Test Results for Specimen B4-E

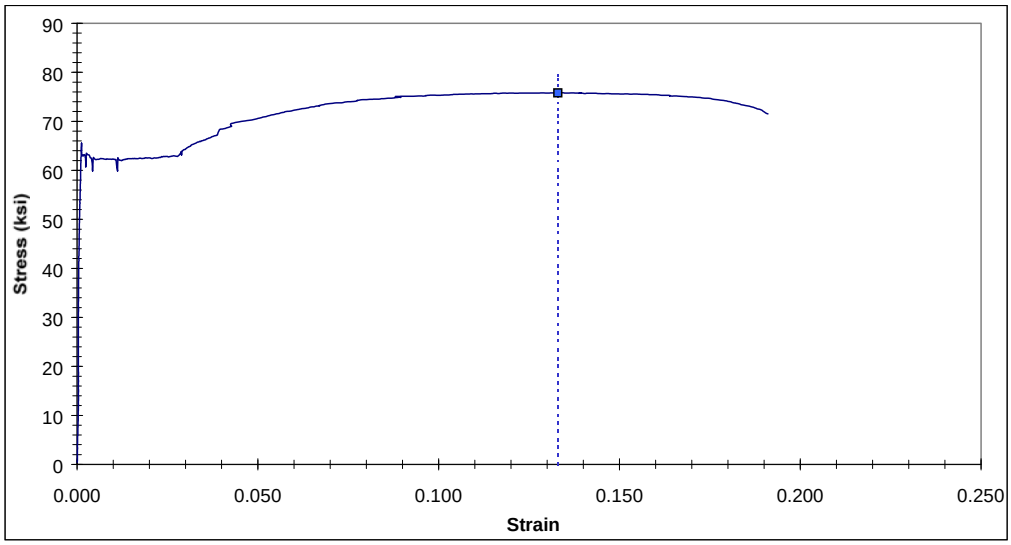

Figure C3.4.11 Complete Stress-strain Curve for Specimen B4-F

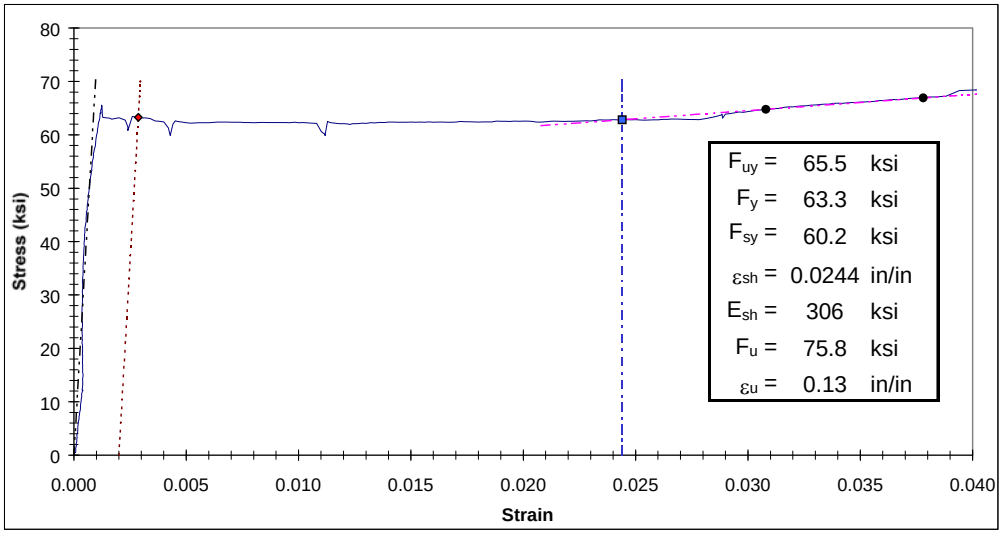

Figure C3.4.12 Yield Plateau and Tensile Test Results for Specimen B4-F

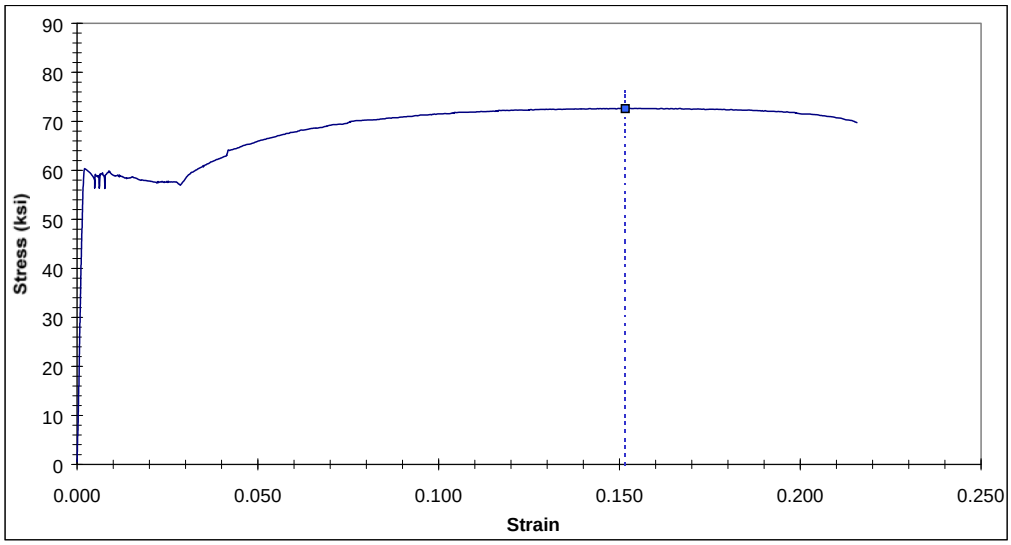

Figure C3.4.13 Complete Stress-strain Curve for Specimen B4-G

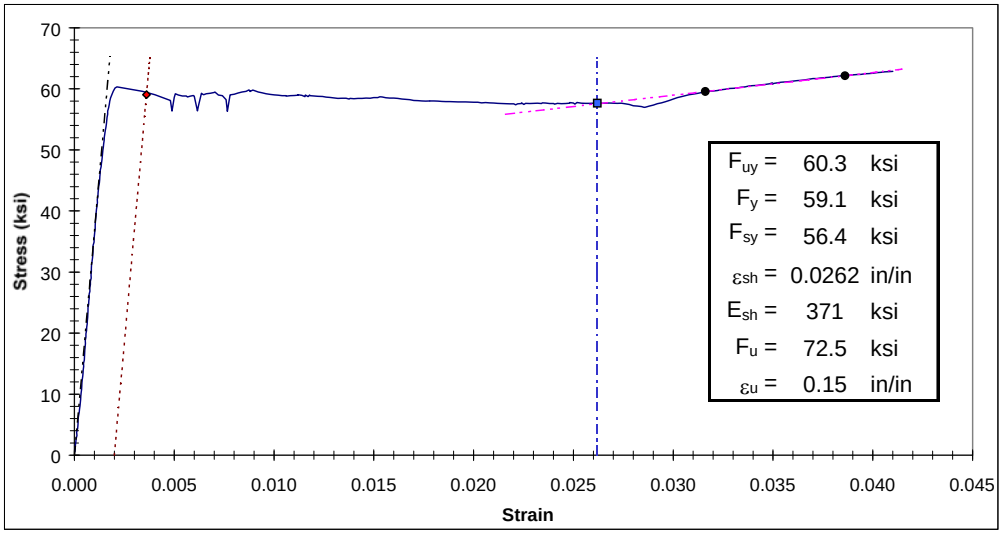

Figure C3.4.14 Yield Plateau and Tensile Test Results for Specimen B4-G

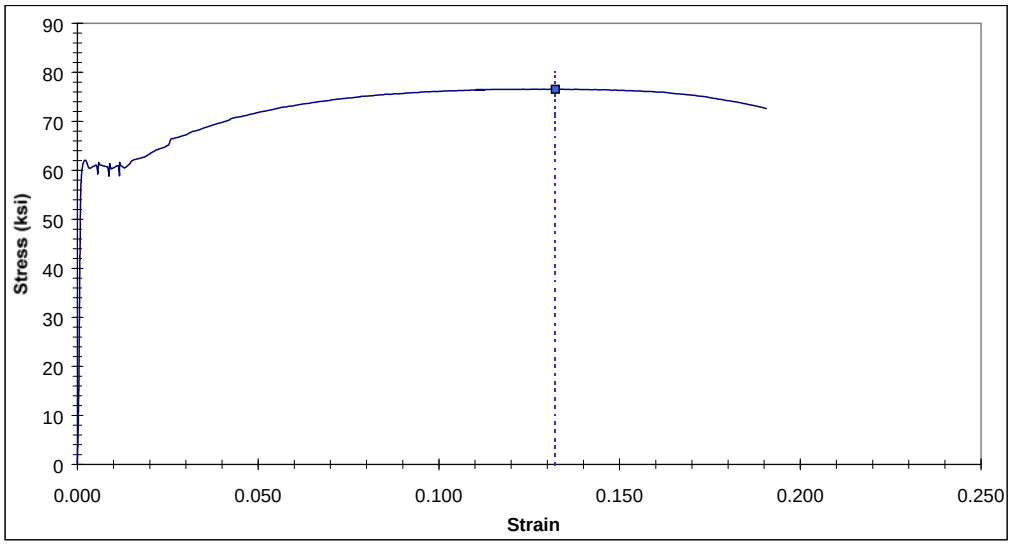

Figure C4.1.1 Complete Stress-strain Curve for Specimen T1-A

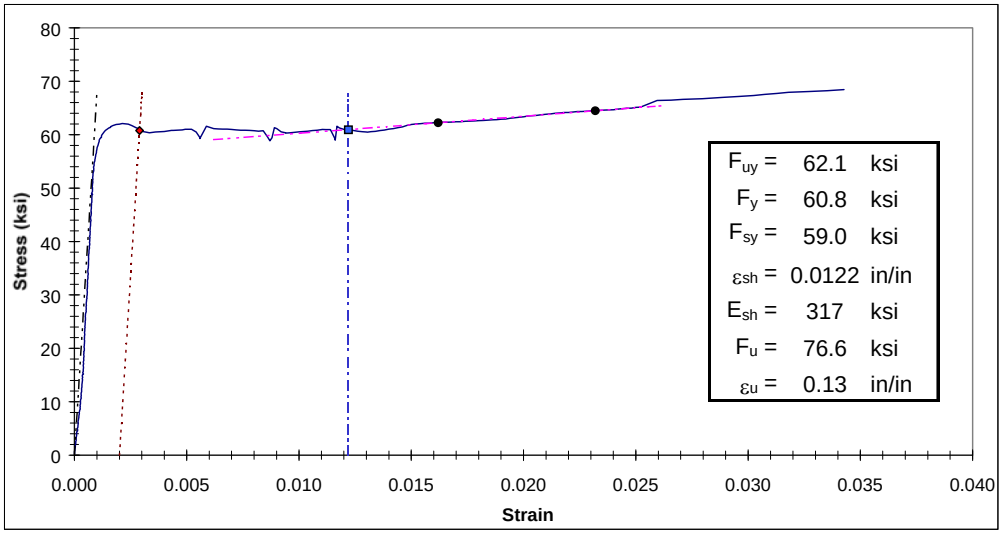

Figure C4.1.2 Yield Plateau and Tensile Test Results for Specimen T1-A

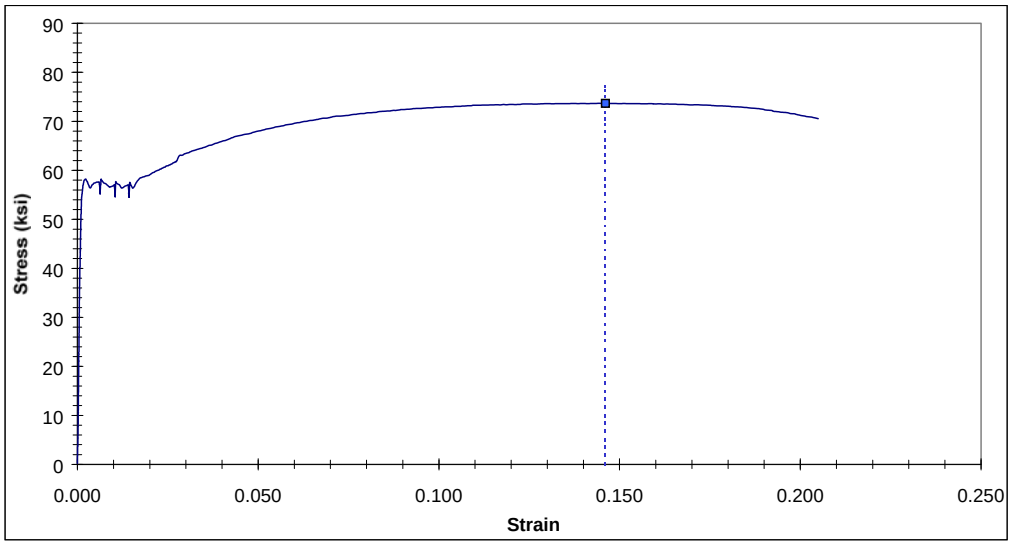

Figure C4.1.3 Complete Stress-strain Curve for Specimen T1-B

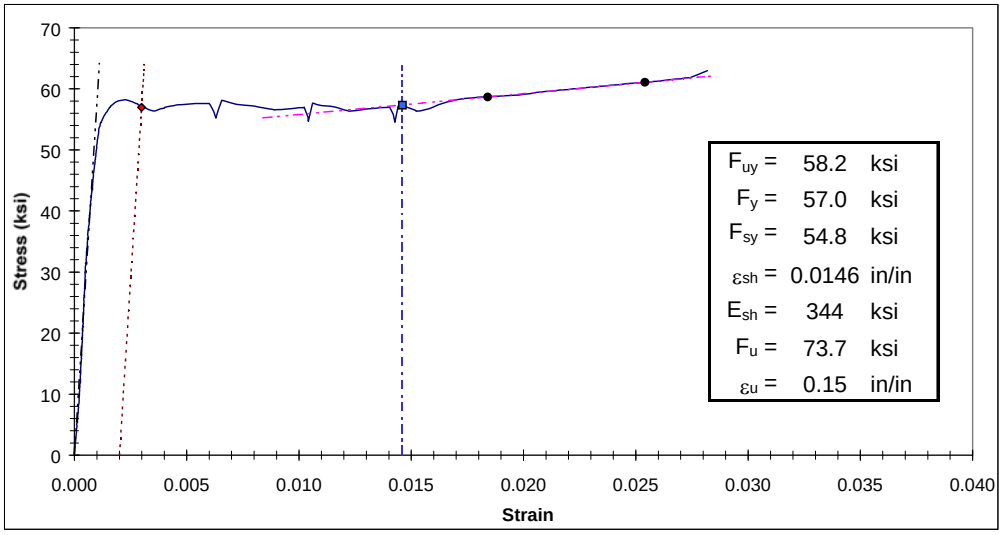

Figure C4.1.4 Yield Plateau and Tensile Test Results for Specimen T1-B

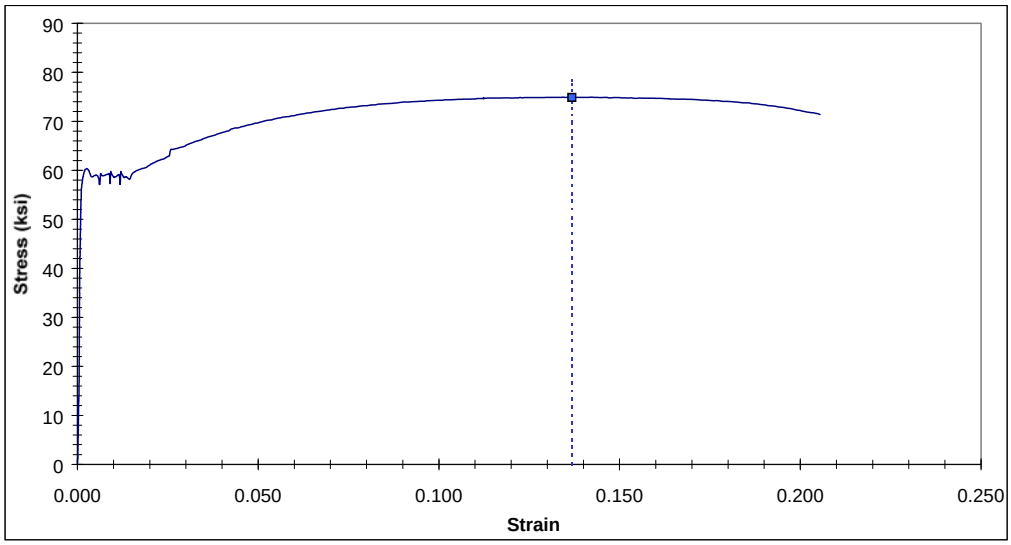

Figure C4.1.5 Complete Stress-strain Curve for Specimen T1-C

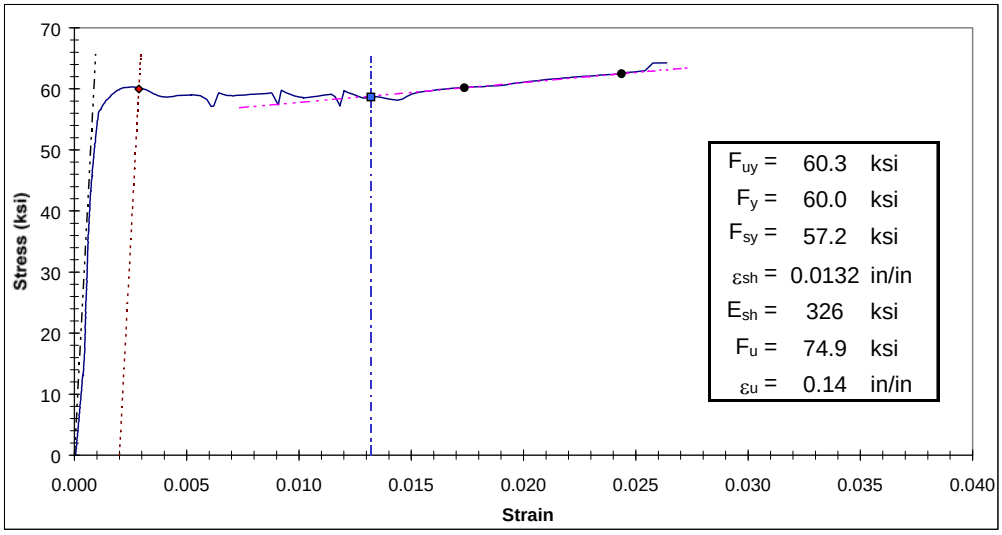

Figure C4.1.6 Yield Plateau and Tensile Test Results for Specimen T1-C

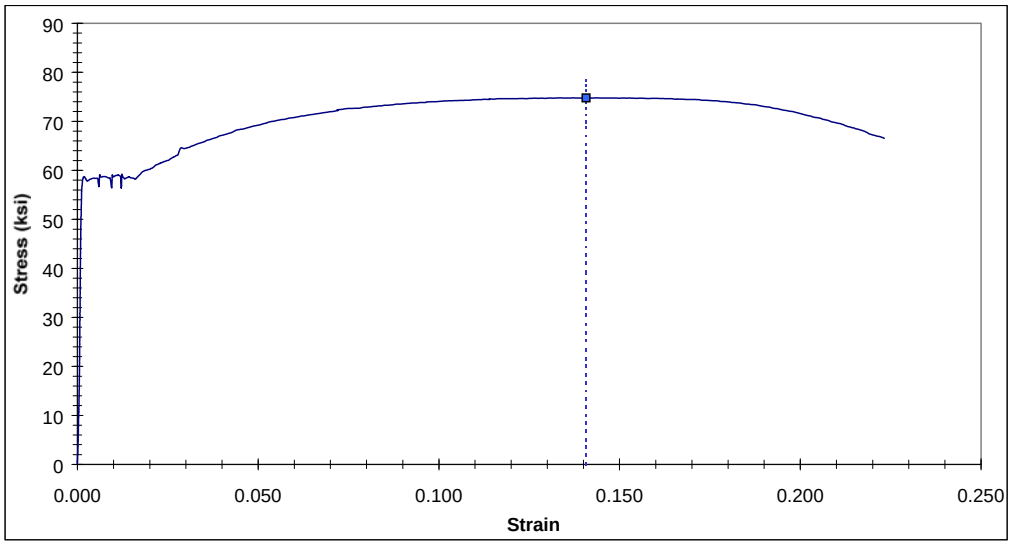

Figure C4.1.7 Complete Stress-strain Curve for Specimen T1-D

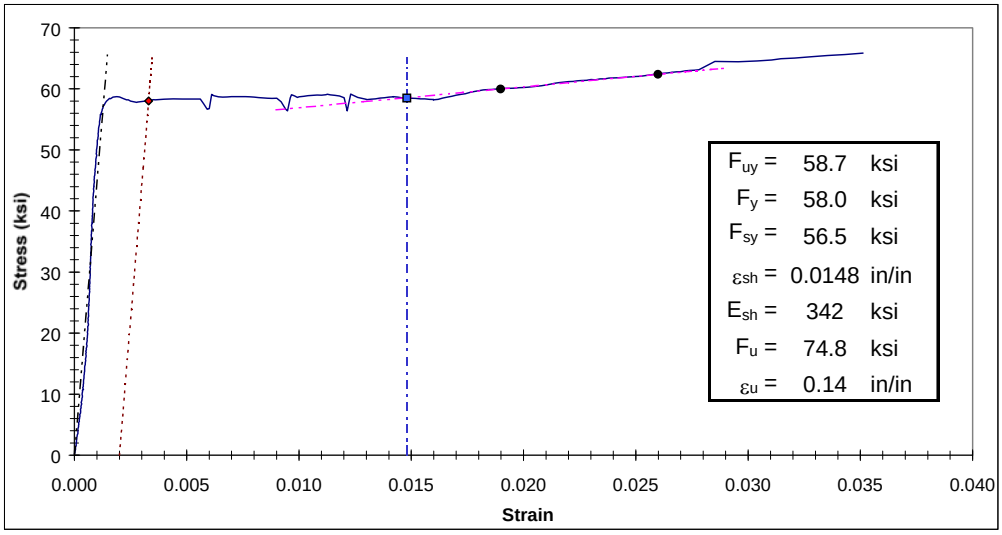

Figure C4.1.8 Yield Plateau and Tensile Test Results for Specimen T1-D

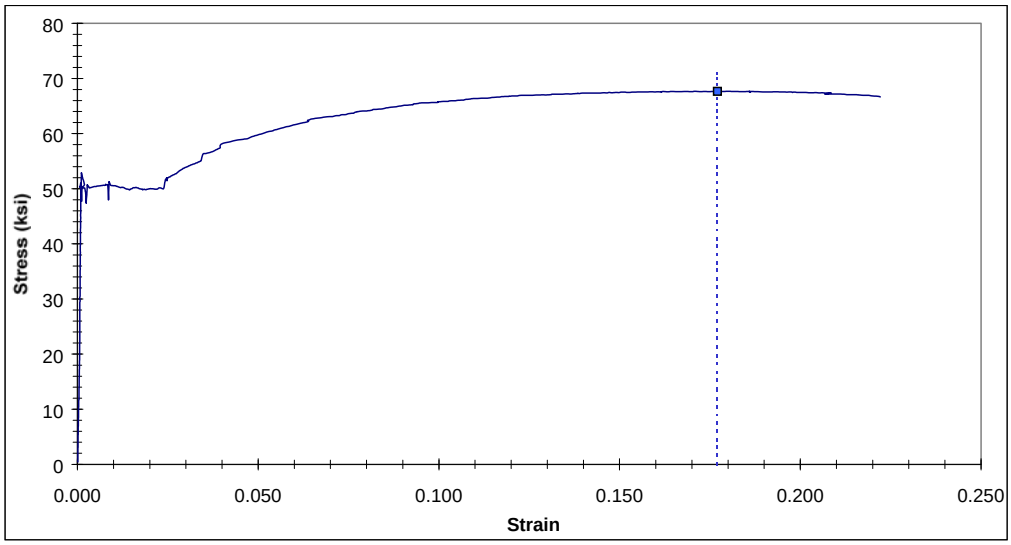

Figure C4.1.9 Complete Stress-strain Curve for Specimen T1-E

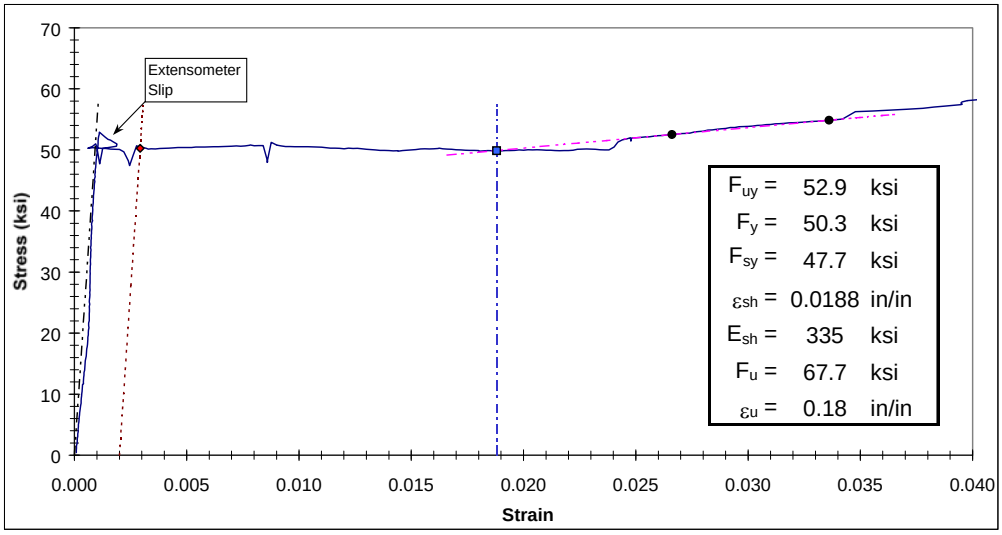

Figure C4.1.10 Yield Plateau and Tensile Test Results for Specimen T1-E

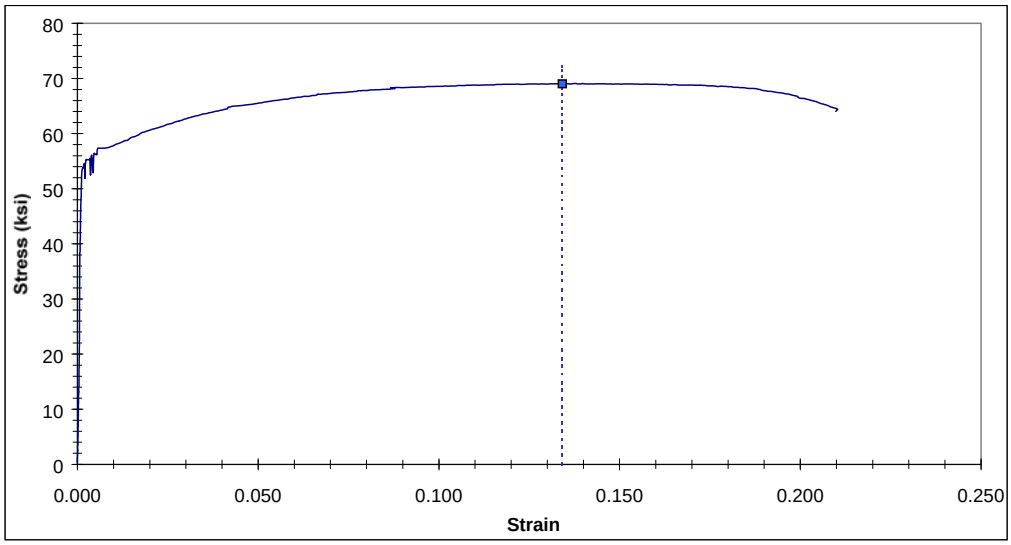

Figure C4.1.11 Complete Stress-strain Curve for Specimen T1-F

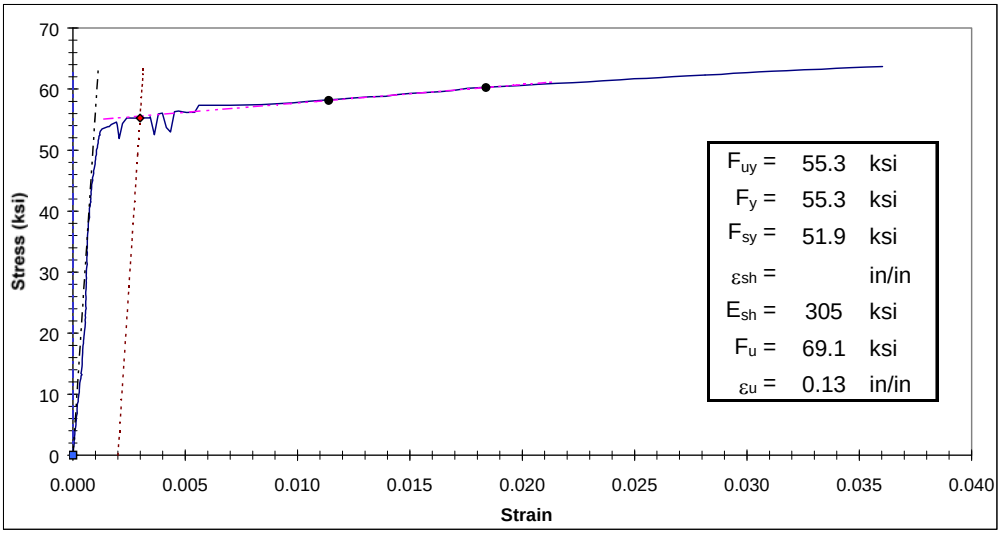

Figure C4.1.12 Yield Plateau and Tensile Test Results for Specimen T1-F

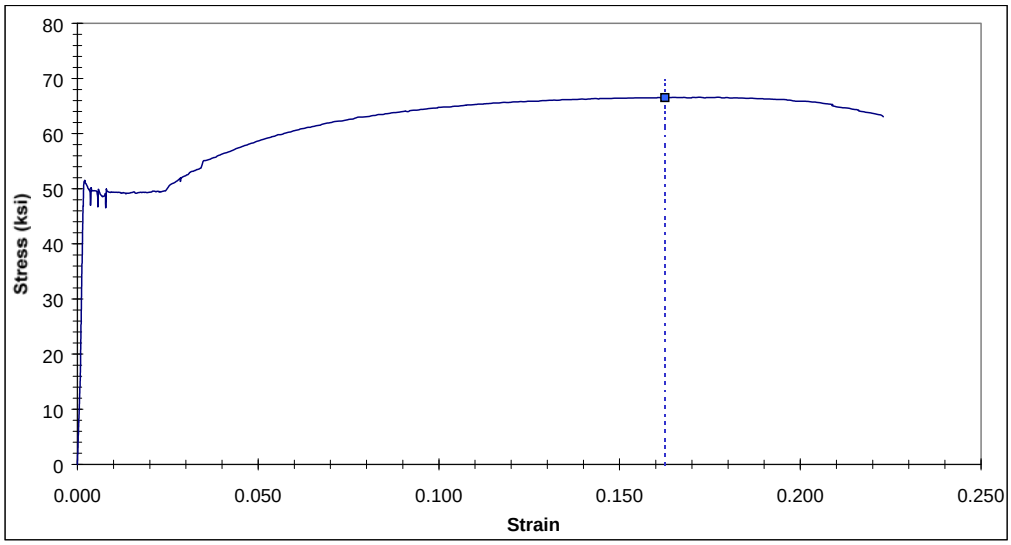

Figure C4.1.13 Complete Stress-strain Curve for Specimen T1-G

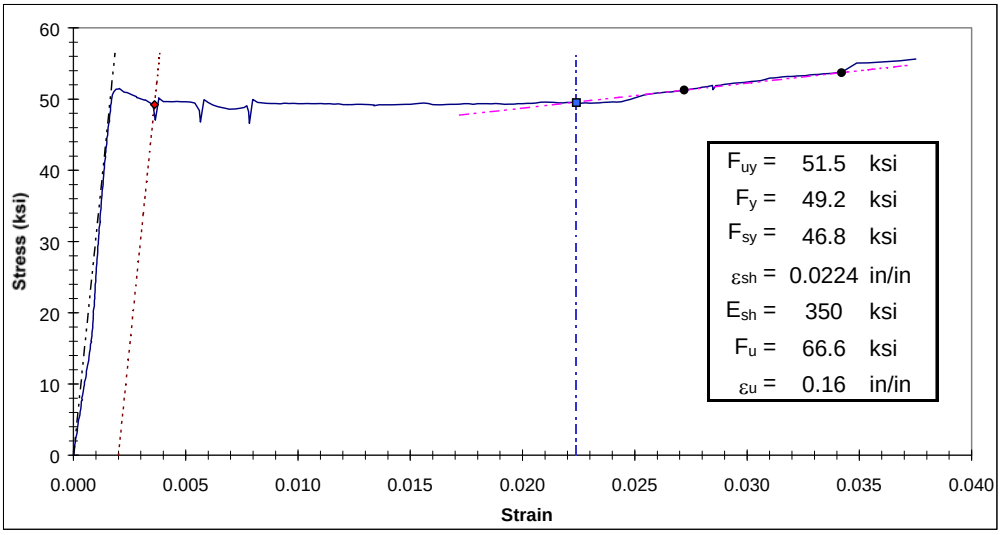

Figure C4.1.14 Yield Plateau and Tensile Test Results for Specimen T1-G

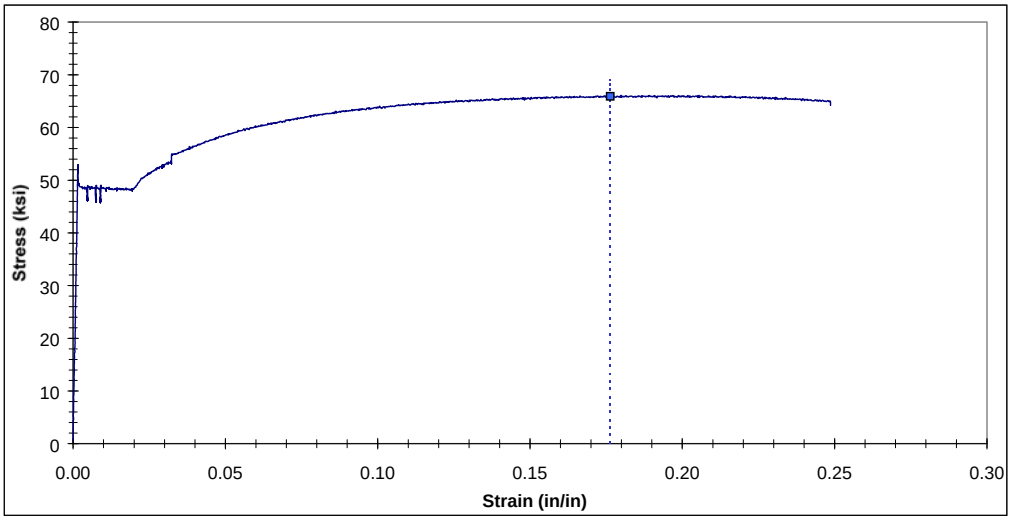

Figure C4.2.1 Complete Stress-strain Curve for Specimen T2-A

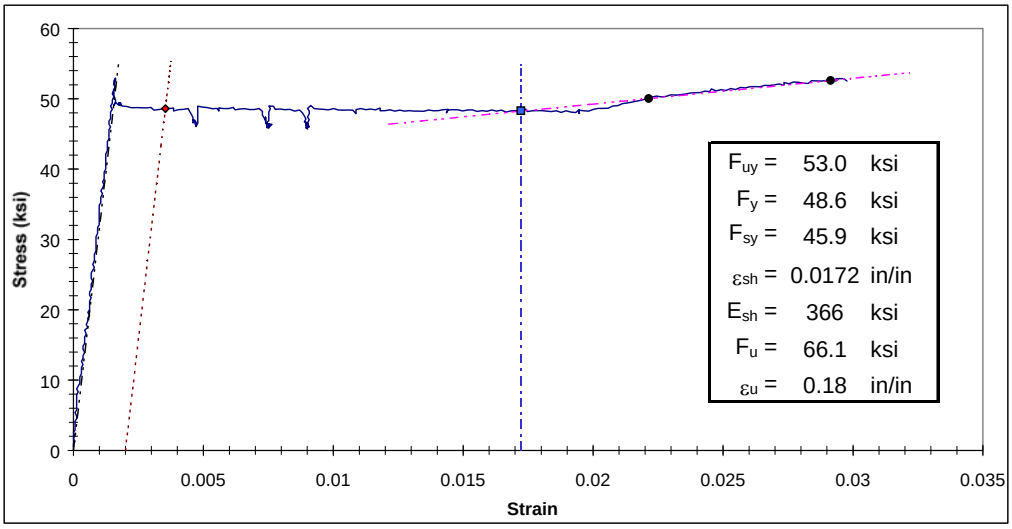

Figure C4.2.2 Yield Plateau and Tensile Test Results for Specimen T2-A

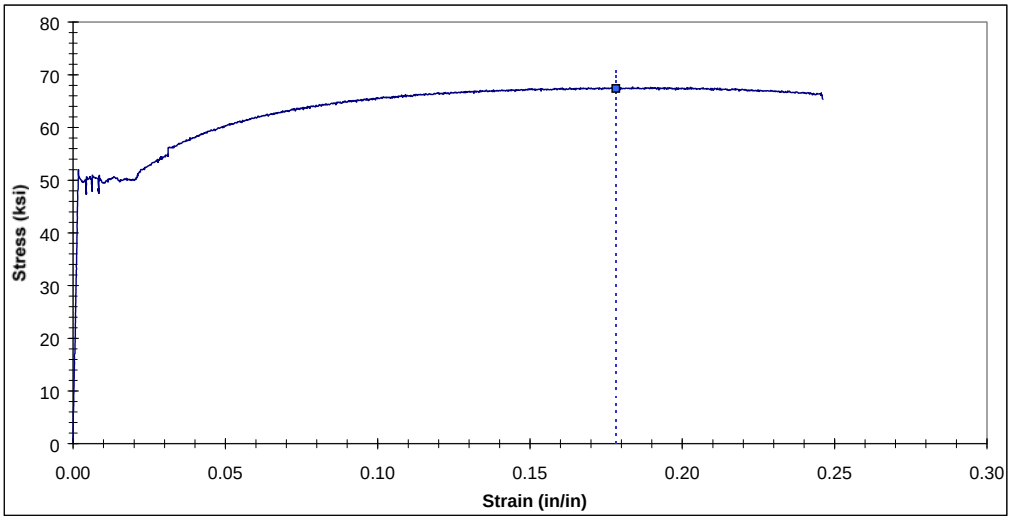

Figure C4.2.3 Complete Stress-strain Curve for Specimen T2-B

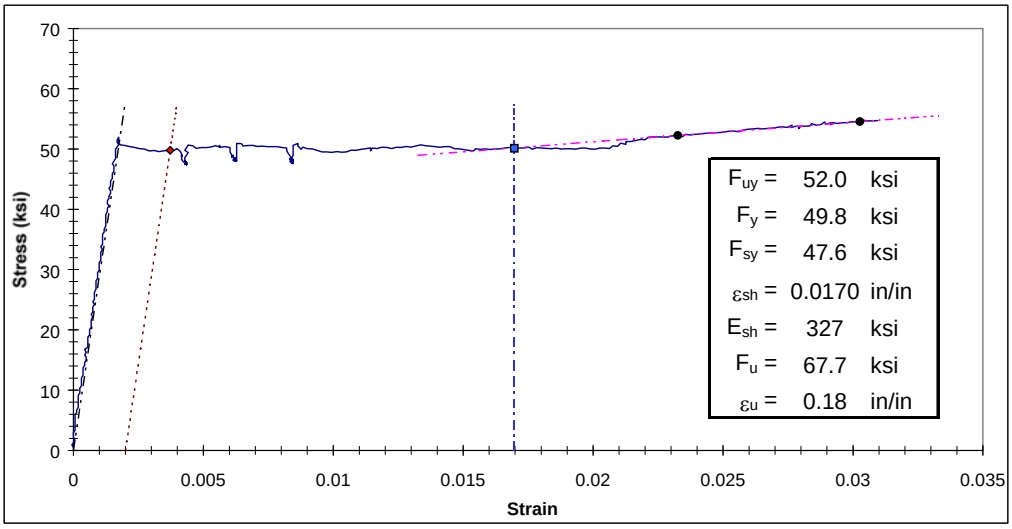

Figure C4.2.4 Yield Plateau and Tensile Test Results for Specimen T2-B

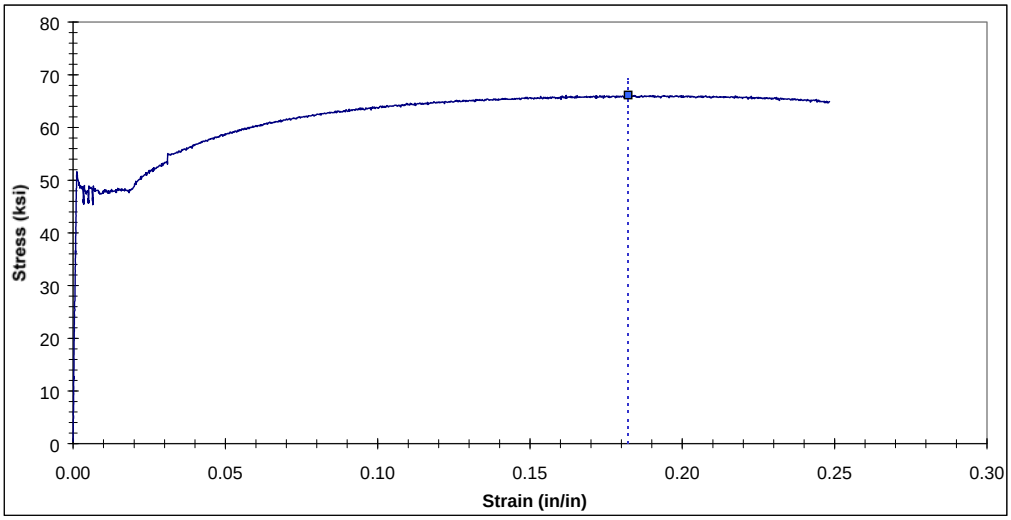

Figure C4.2.5 Complete Stress-strain Curve for Specimen T2-C

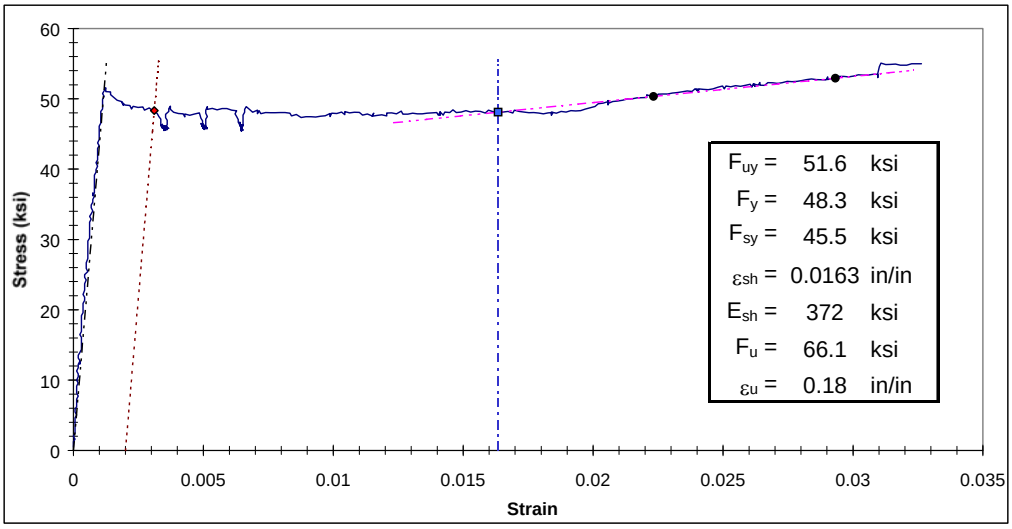

Figure C4.2.6 Yield Plateau and Tensile Test Results for Specimen T2-C

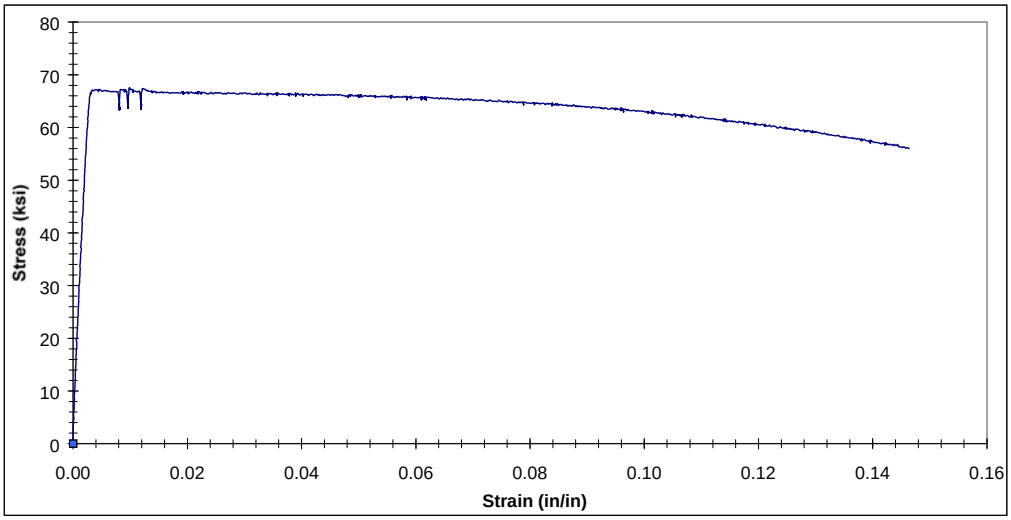

Figure C4.2.7 Complete Stress-strain Curve for Specimen T2-D

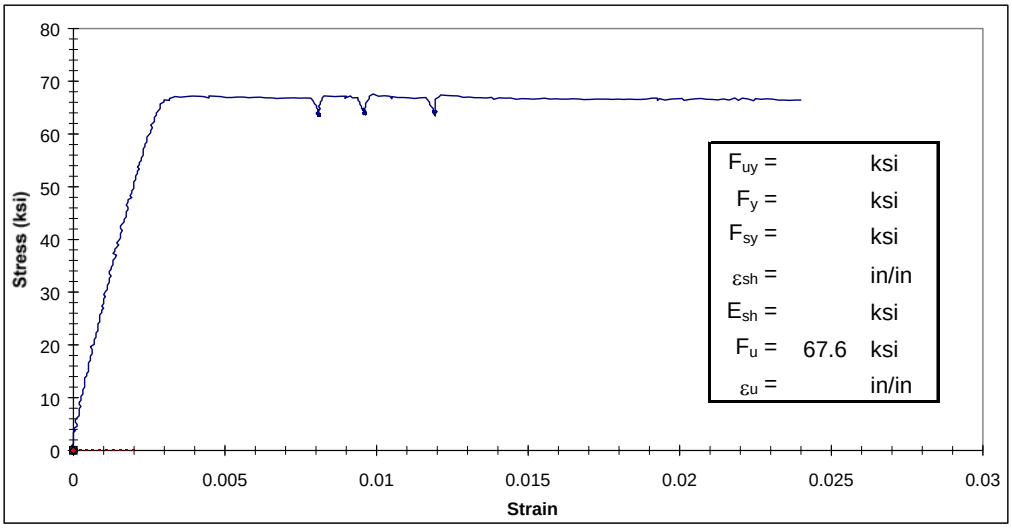

Figure C4.2.8 Yield Plateau and Tensile Test Results for Specimen T2-D

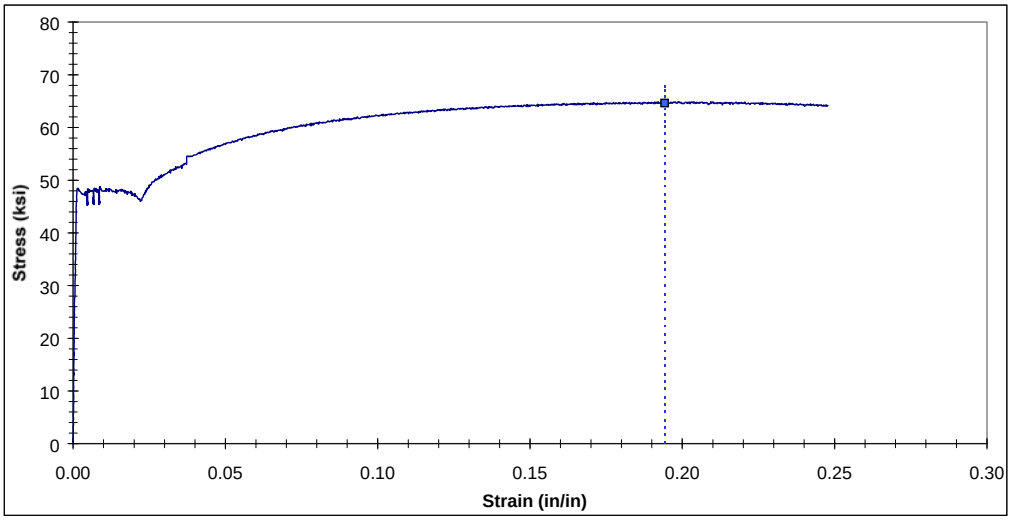

Figure C4.2.9 Complete Stress-strain Curve for Specimen T2-E

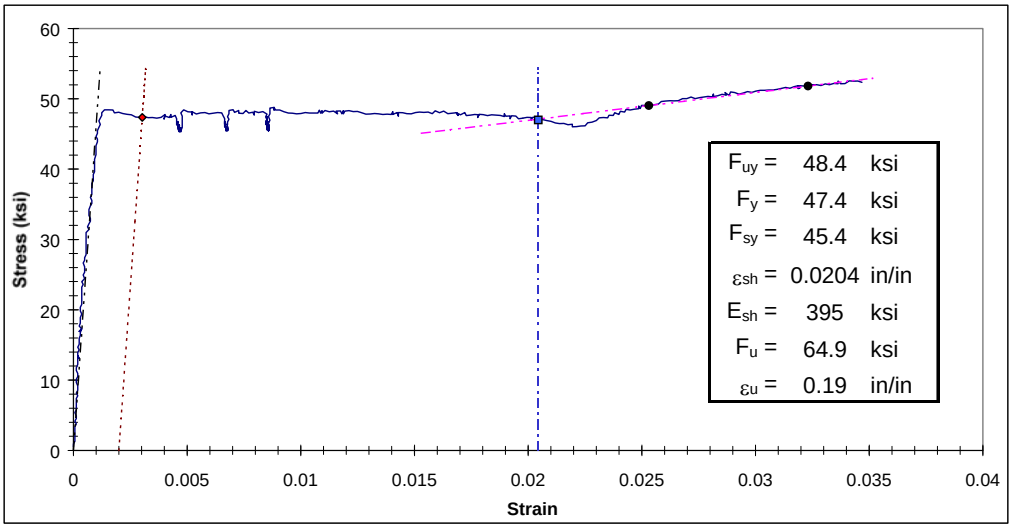

Figure C4.2.10 Yield Plateau and Tensile Test Results for Specimen T2-E

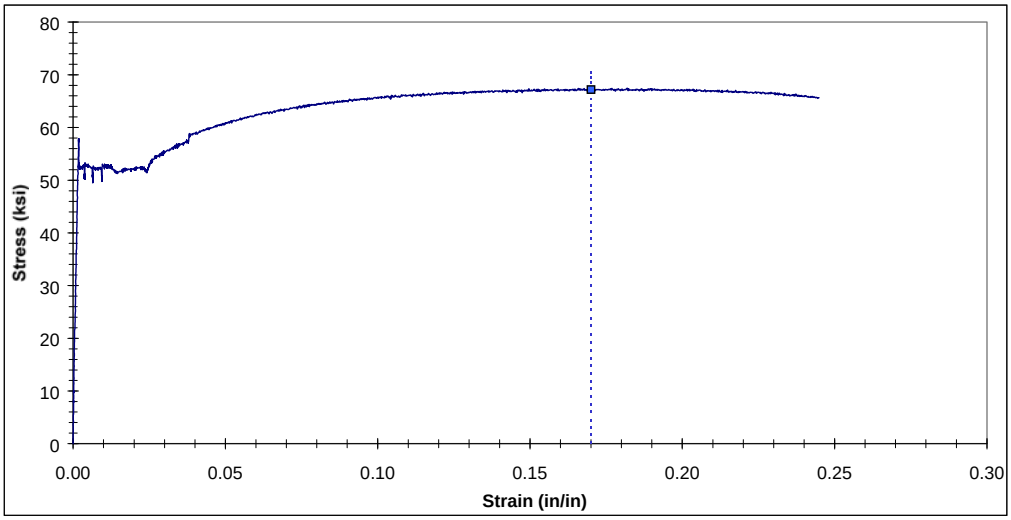

Figure C4.2.11 Complete Stress-strain Curve for Specimen T2-F

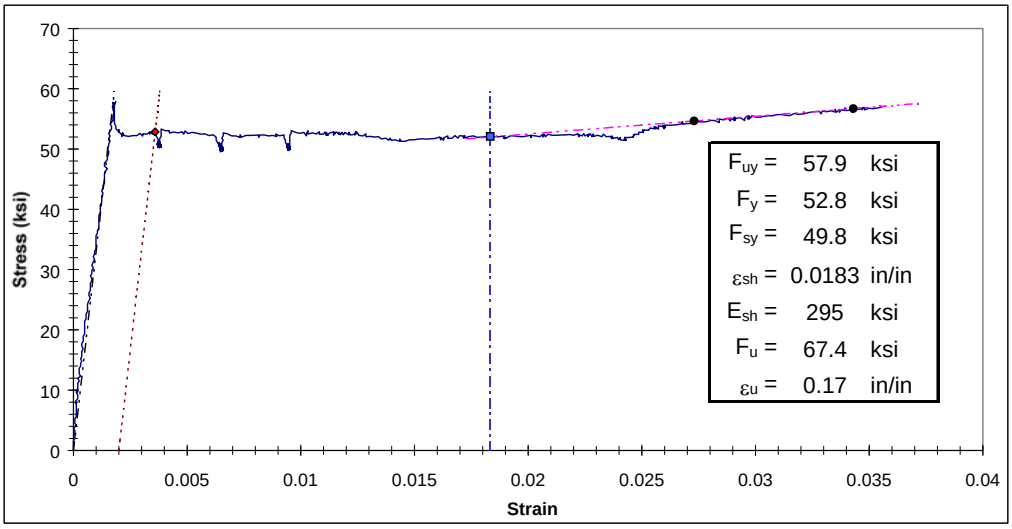

Figure C4.2.12 Yield Plateau and Tensile Test Results for Specimen T2-F

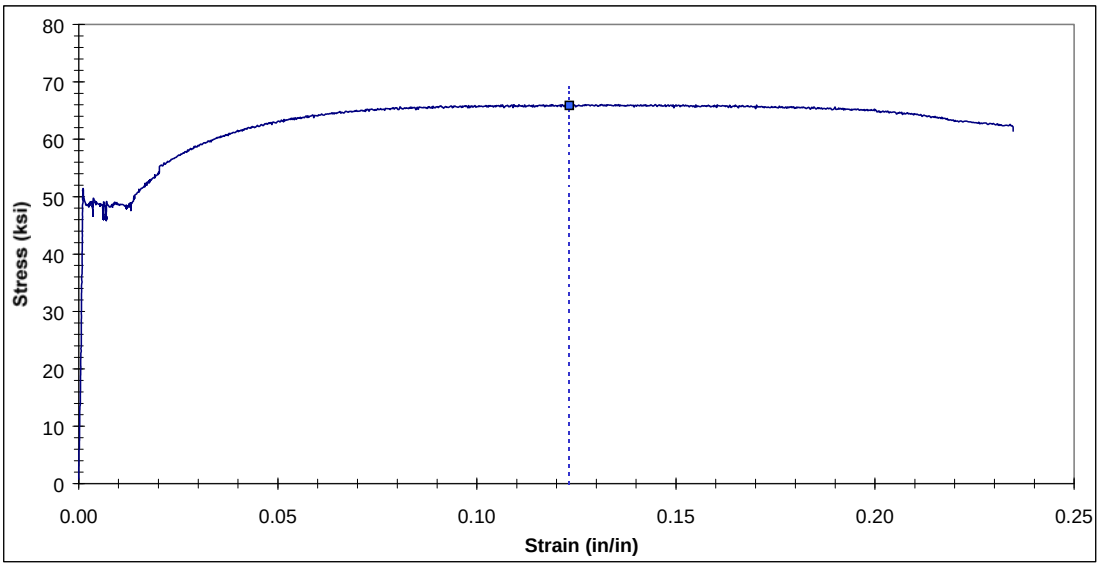

Figure C4.2.13 Complete Stress-strain Curve for Specimen T2-G

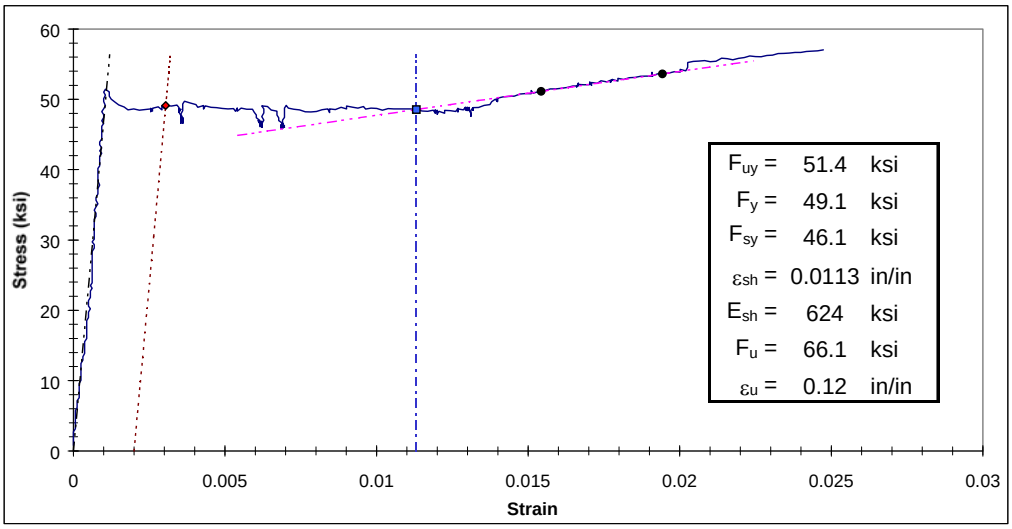

Figure C4.2.14 Yield Plateau and Tensile Test Results for Specimen T2-G

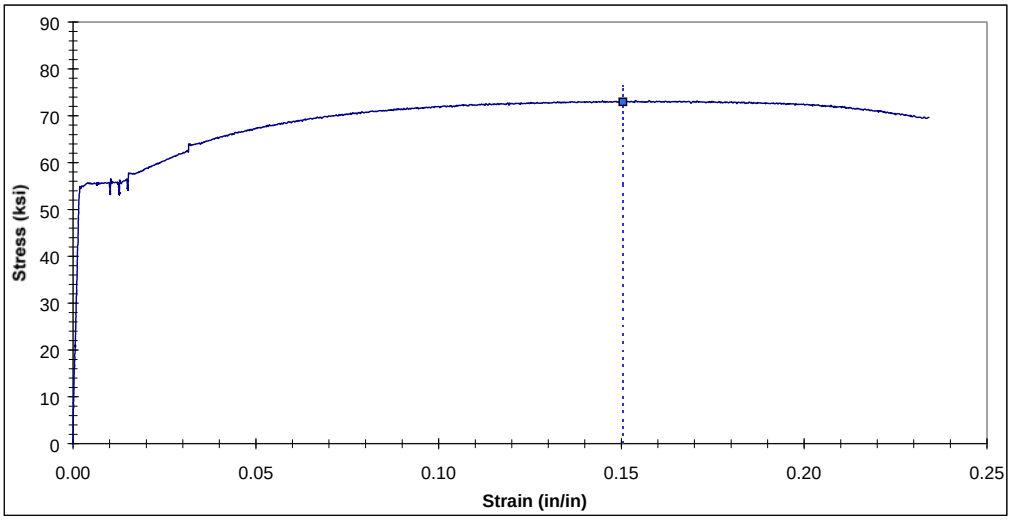

Figure C4.3.1 Complete Stress-strain Curve for Specimen T3-A

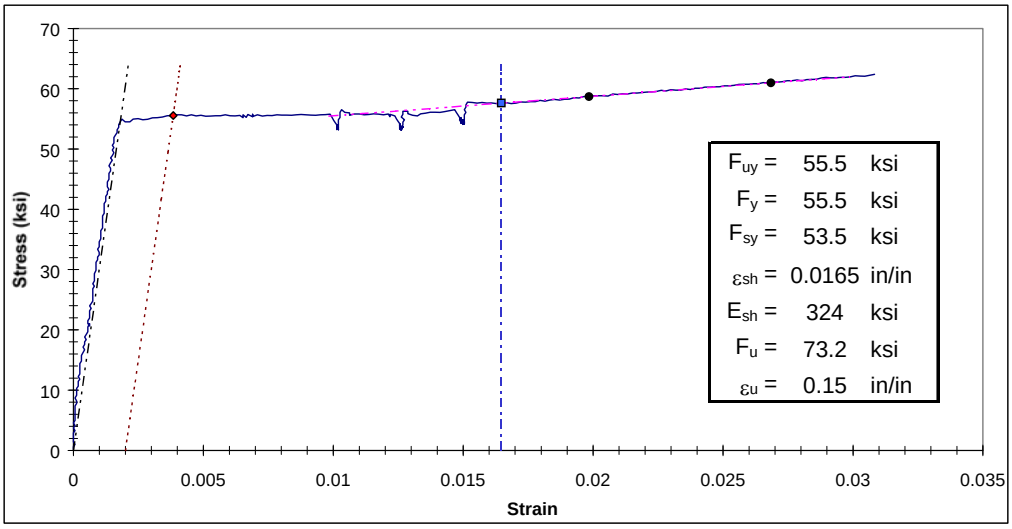

Figure C4.3.2 Yield Plateau and Tensile Test Results for Specimen T3-A

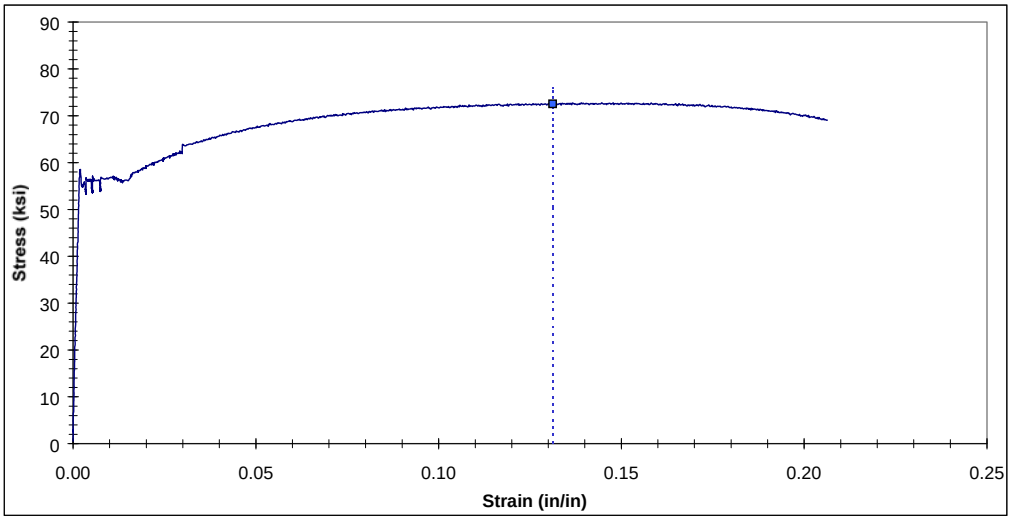

Figure C4.3.3 Complete Stress-strain Curve for Specimen T3-B

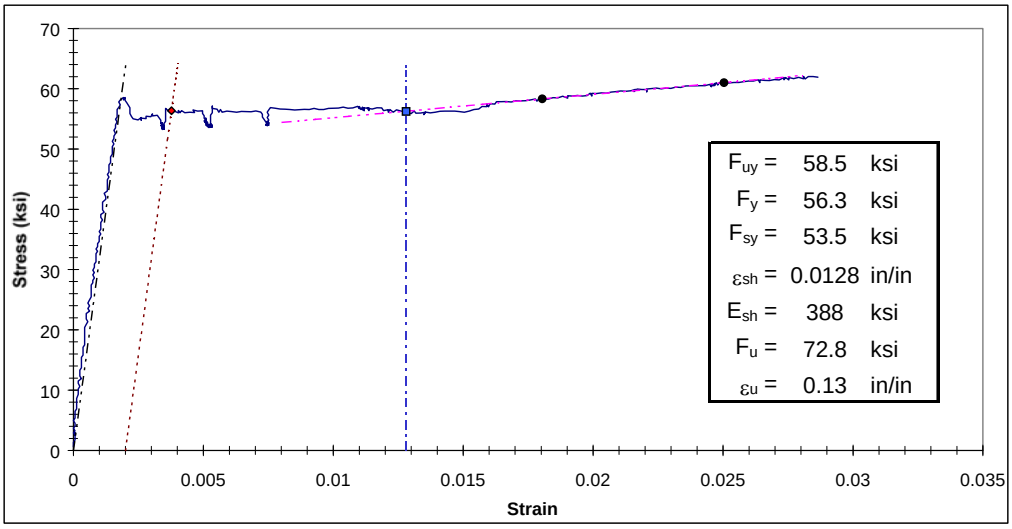

Figure C4.3.4 Yield Plateau and Tensile Test Results for Specimen T3-B

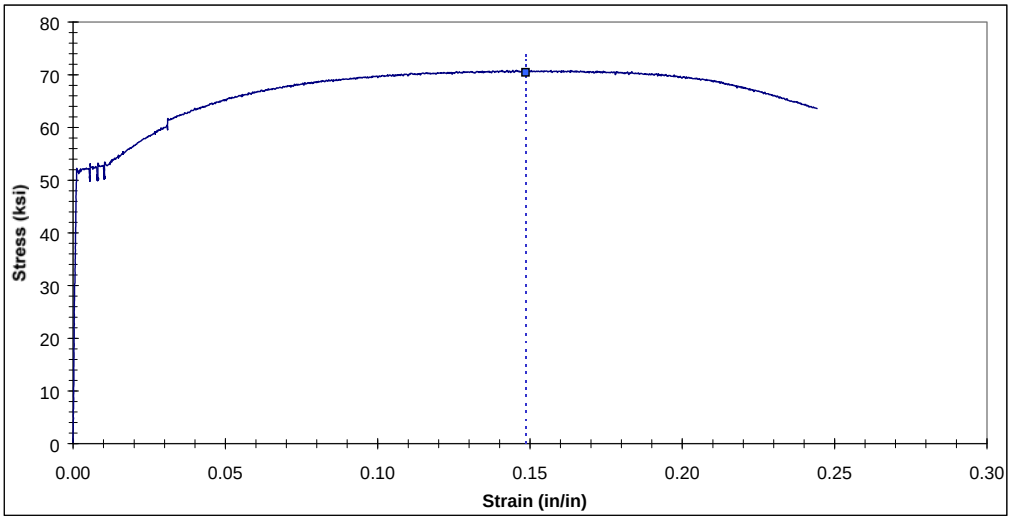

Figure C4.3.5 Complete Stress-strain Curve for Specimen T3-C

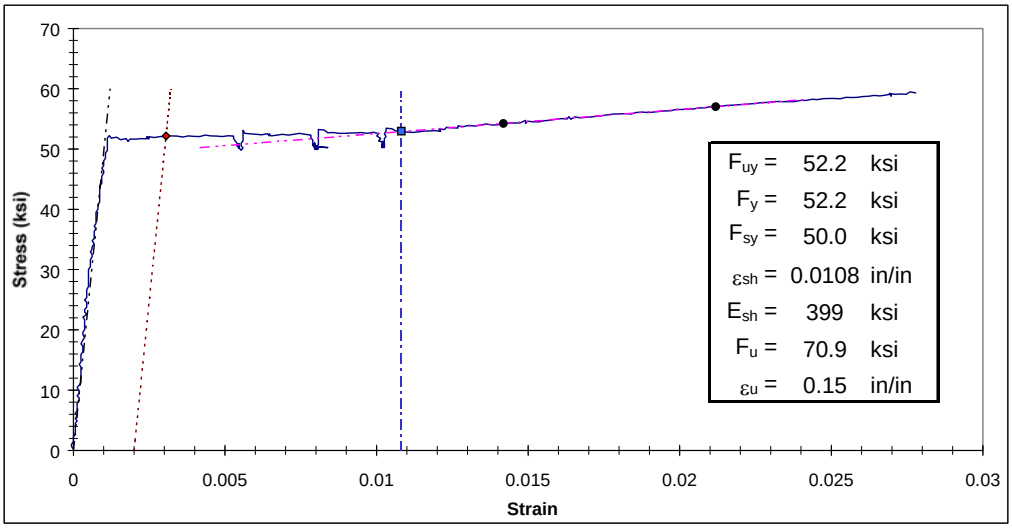

Figure C4.3.6 Yield Plateau and Tensile Test Results for Specimen T3-C

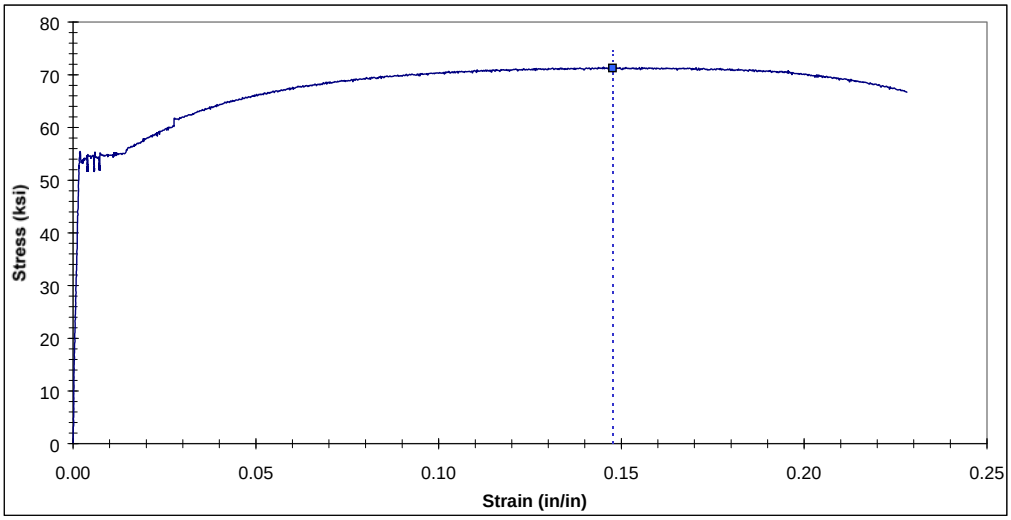

Figure C4.3.7 Complete Stress-strain Curve for Specimen T3-D

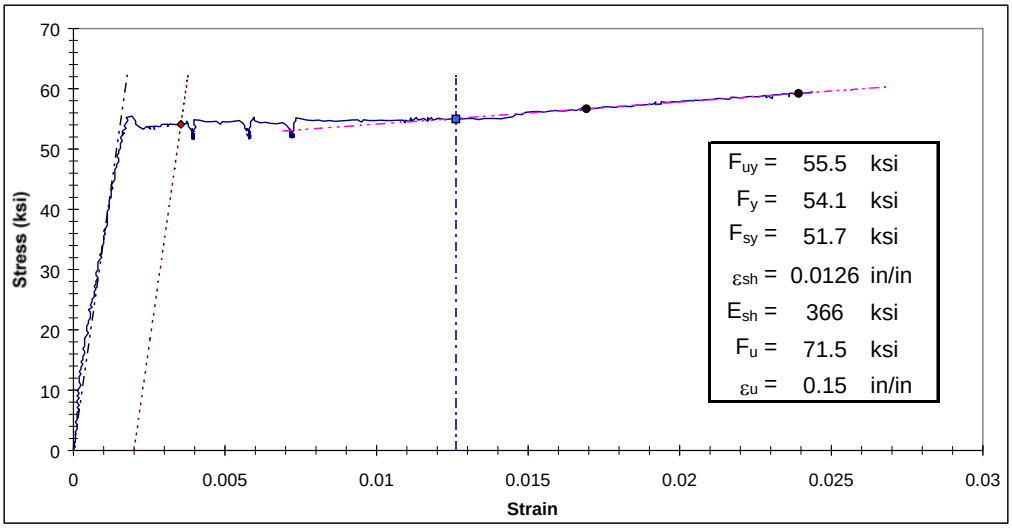

Figure C4.3.8 Yield Plateau and Tensile Test Results for Specimen T3-D

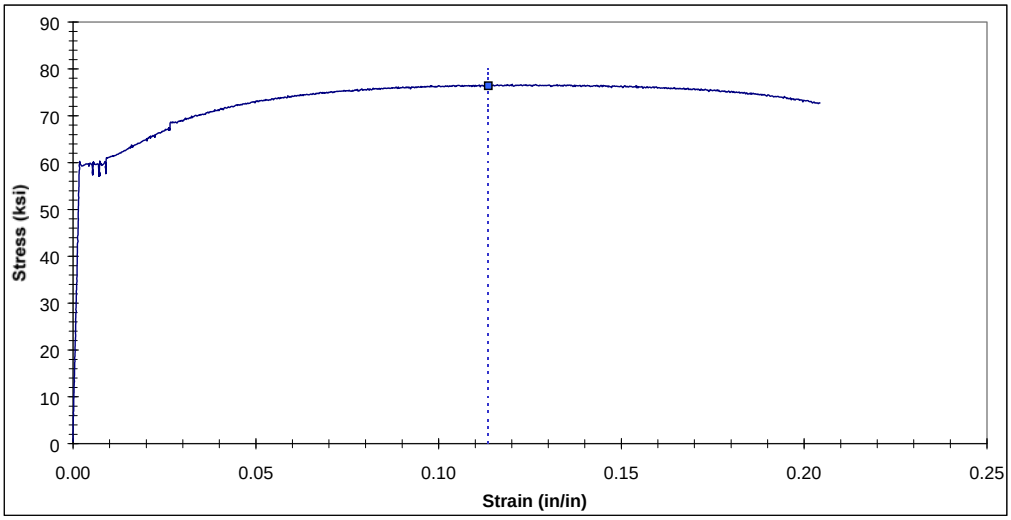

Figure C4.3.9 Complete Stress-strain Curve for Specimen T3-E

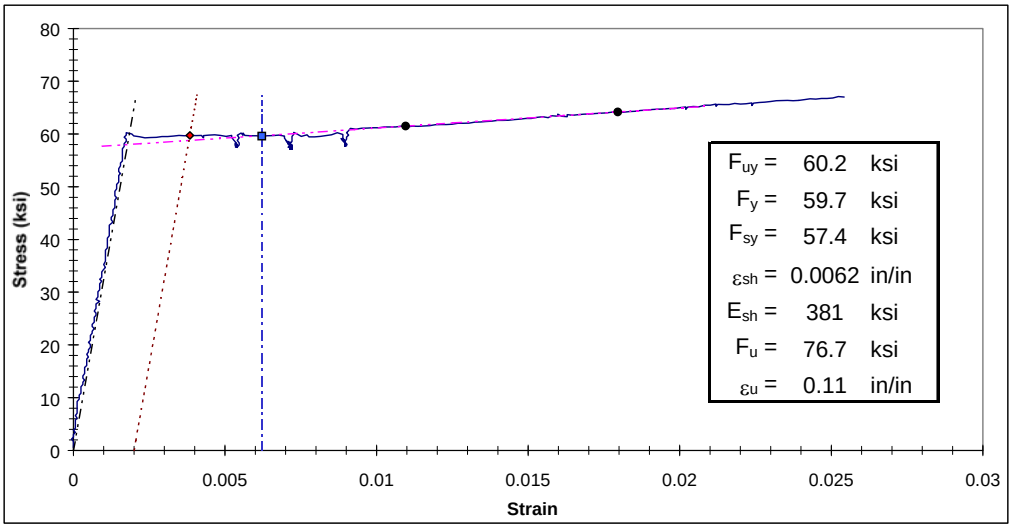

Figure C4.3.10 Yield Plateau and Tensile Test Results for Specimen T3-E

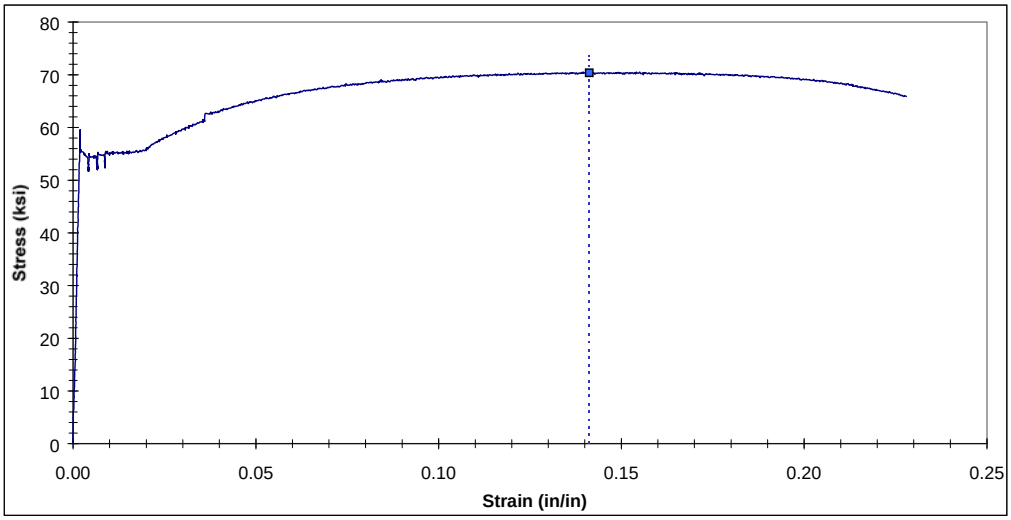

Figure C4.3.11 Complete Stress-strain Curve for Specimen T3-F

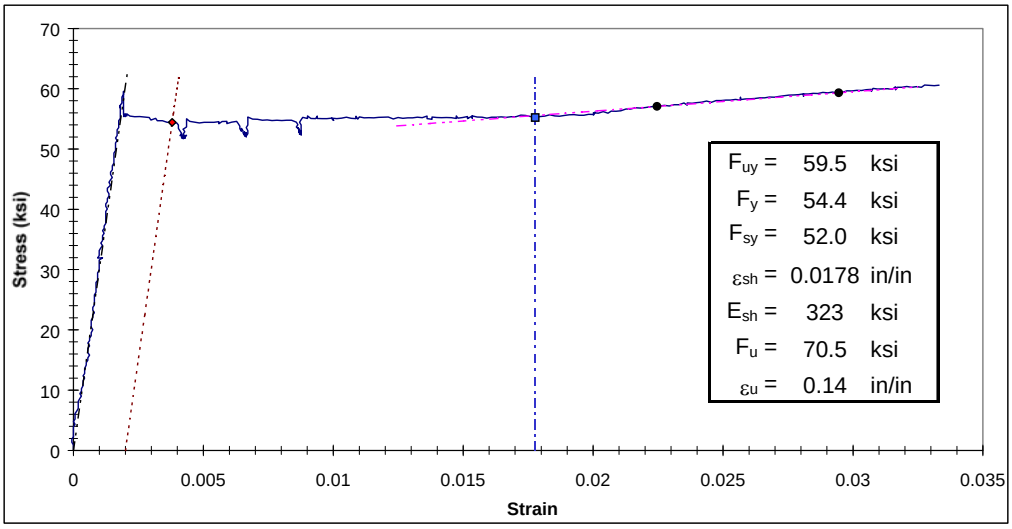

Figure C4.3.12 Yield Plateau and Tensile Test Results for Specimen T3-F

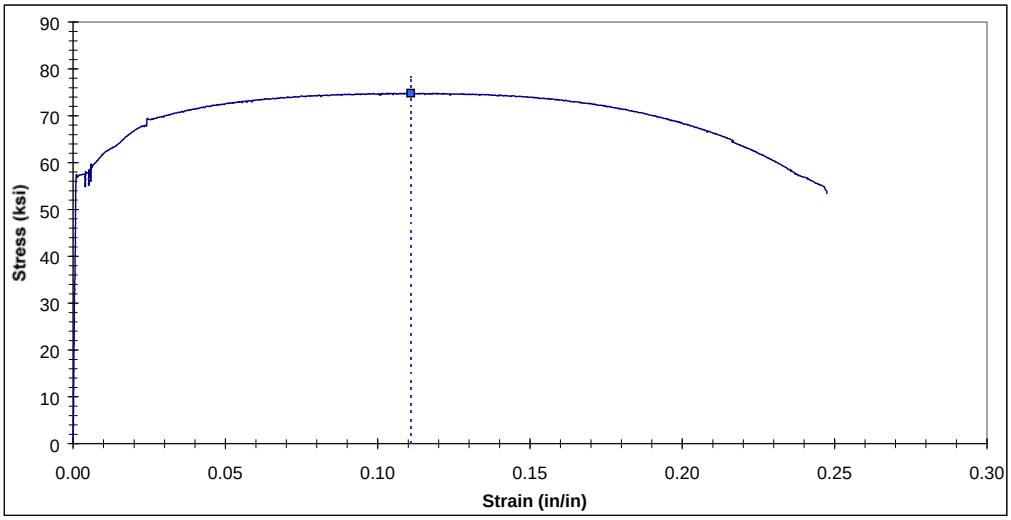

Figure C4.3.13 Complete Stress-strain Curve for Specimen T3-G

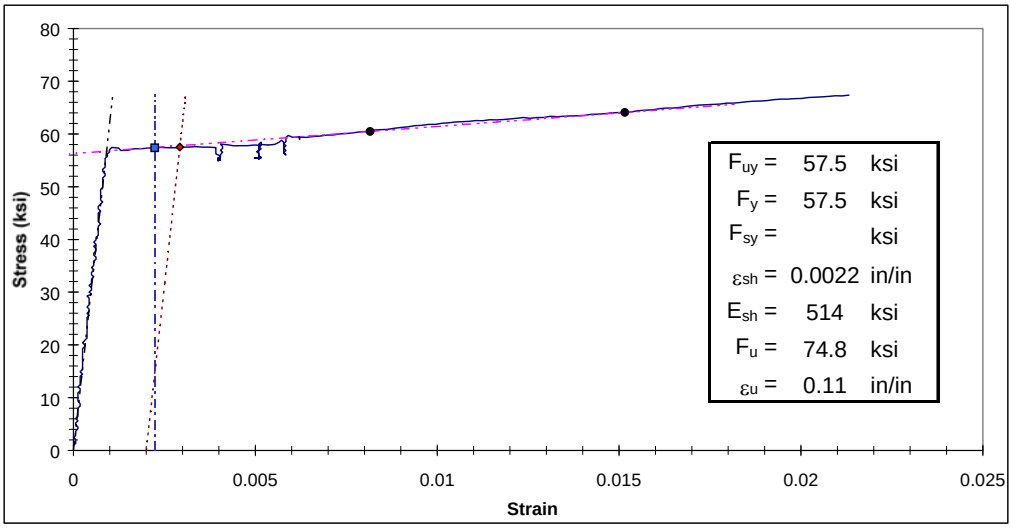

Figure C4.3.14 Yield Plateau and Tensile Test Results for Specimen T3-G

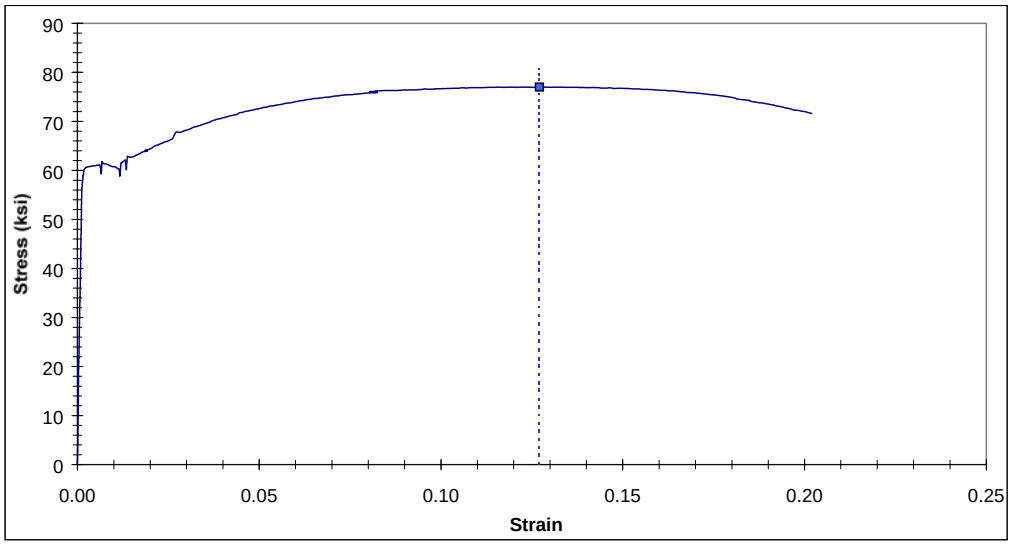

Figure C4.4.1 Complete Stress-strain Curve for Specimen T4-A

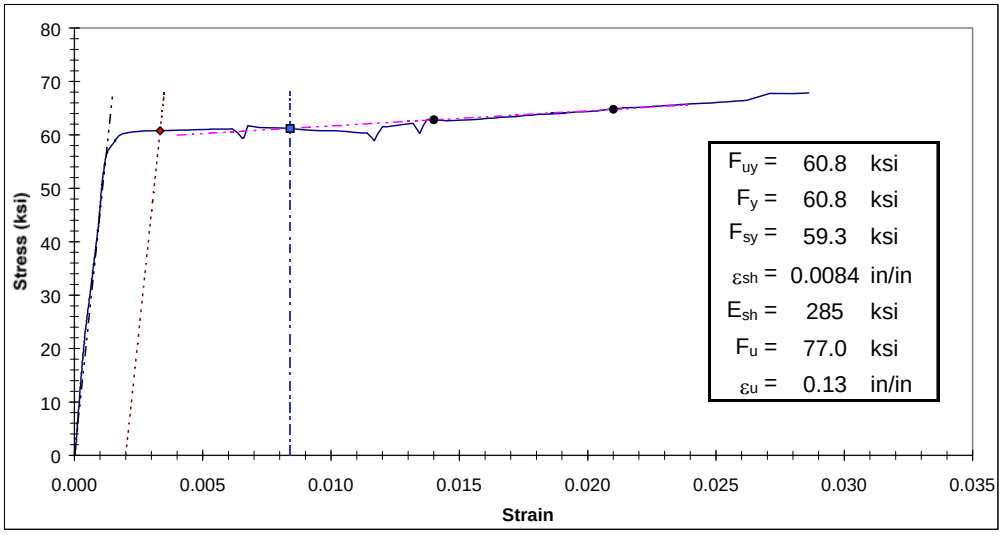

Figure C4.4.2 Yield Plateau and Tensile Test Results for Specimen T4-A

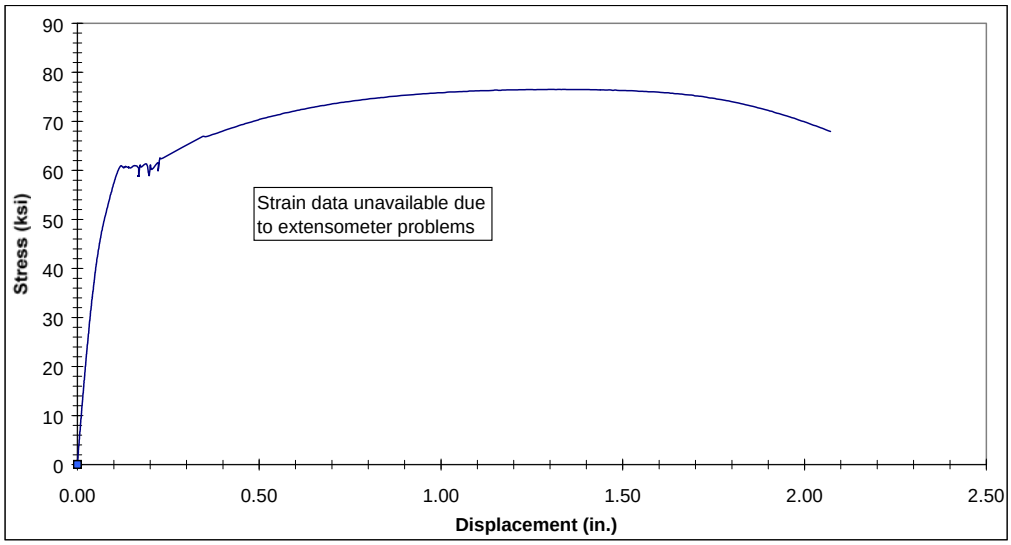

Figure C4.4.3 Complete Stress-strain Curve for Specimen T4-B

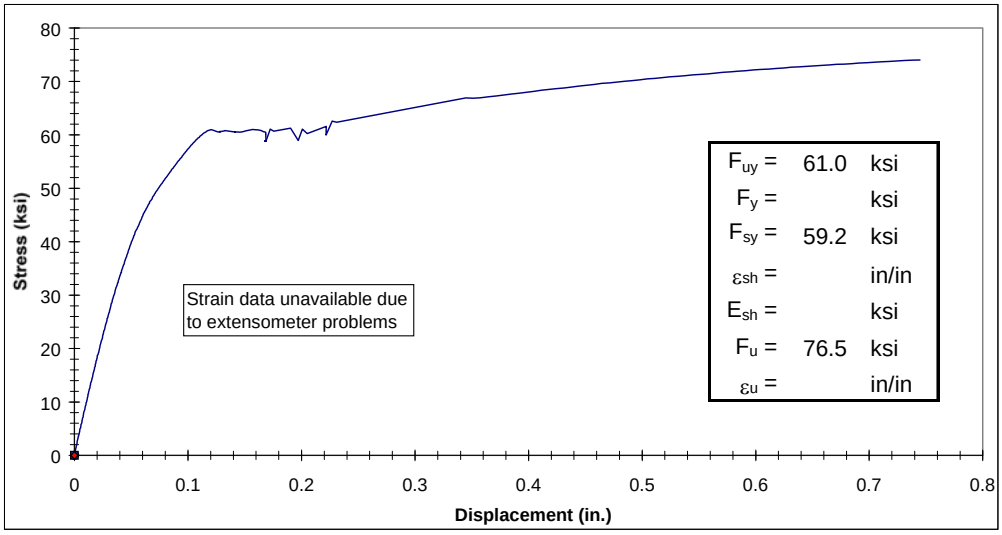

Figure C4.4.4 Yield Plateau and Tensile Test Results for Specimen T4-B

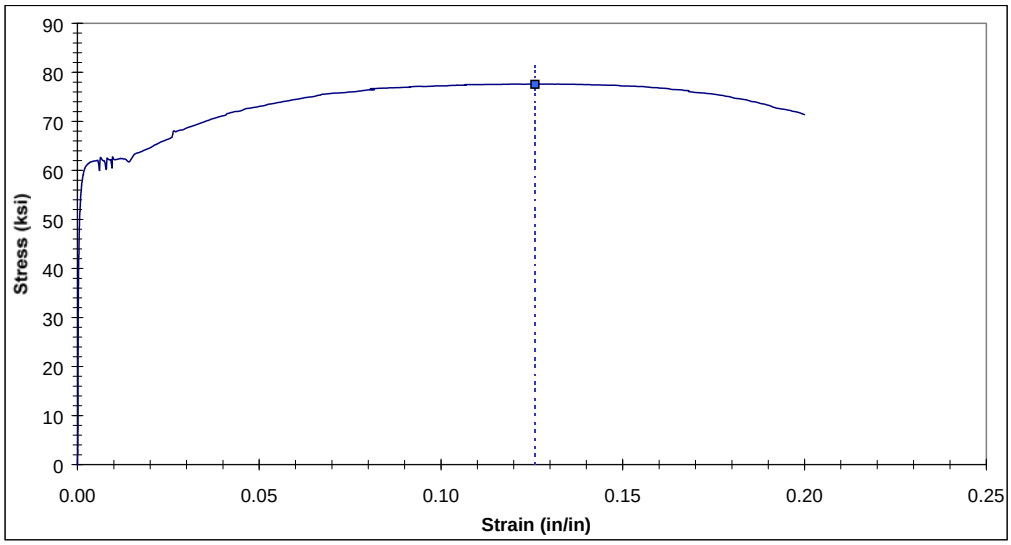

Figure C4.4.5 Complete Stress-strain Curve for Specimen T4-C

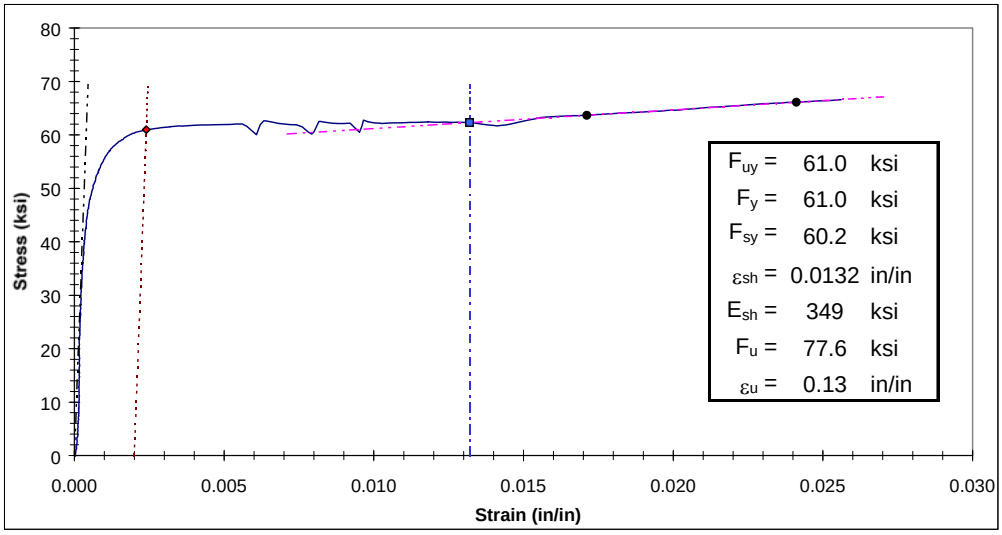

Figure C4.4.6 Yield Plateau and Tensile Test Results for Specimen T4-C

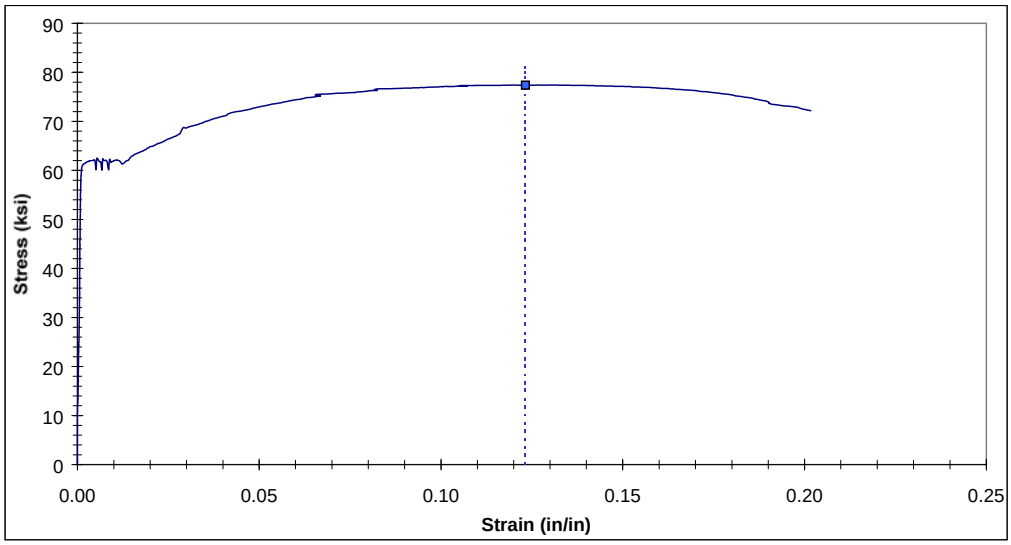

Figure C4.4.7 Complete Stress-strain Curve for Specimen T4-D

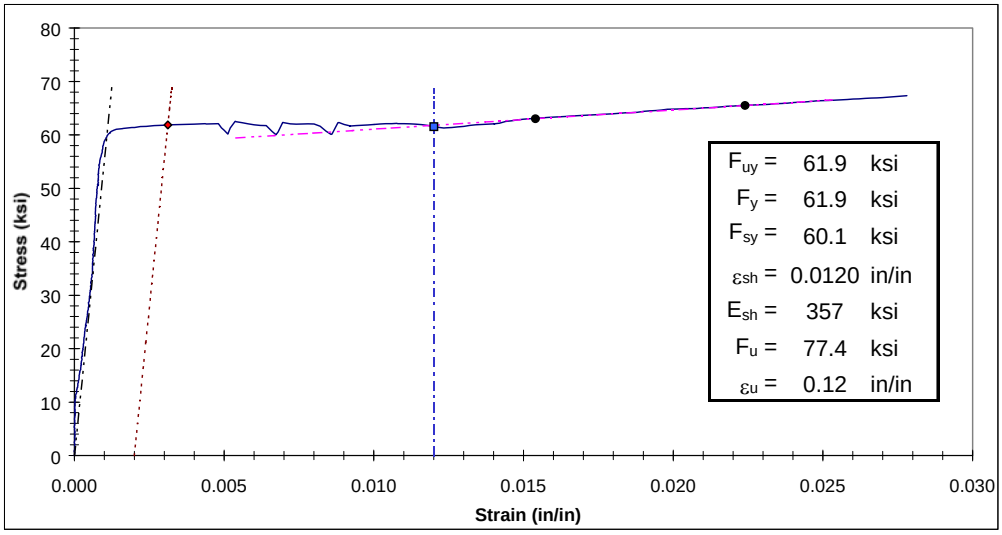

Figure C4.4.8 Yield Plateau and Tensile Test Results for Specimen T4-D

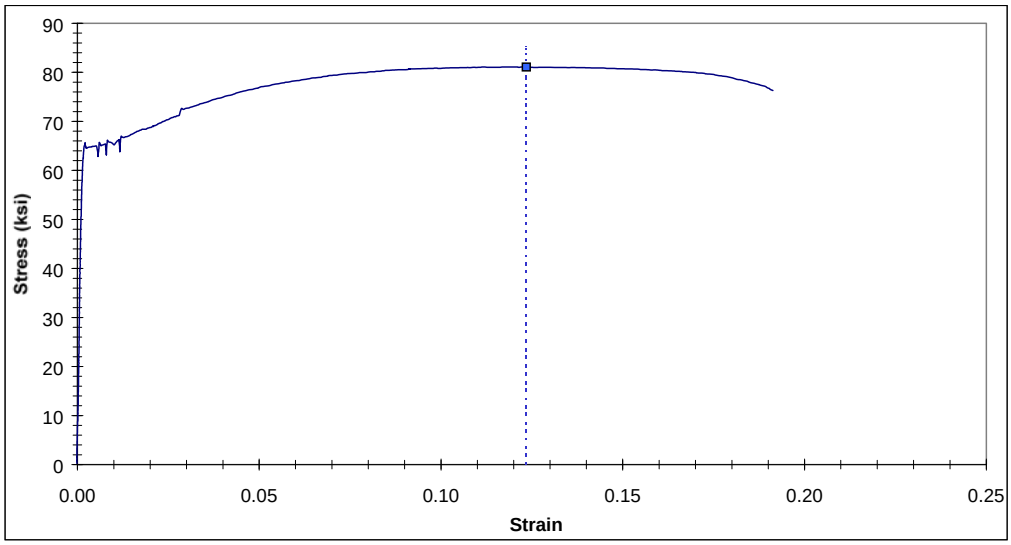

Figure C4.4.9 Complete Stress-strain Curve for Specimen T4-E

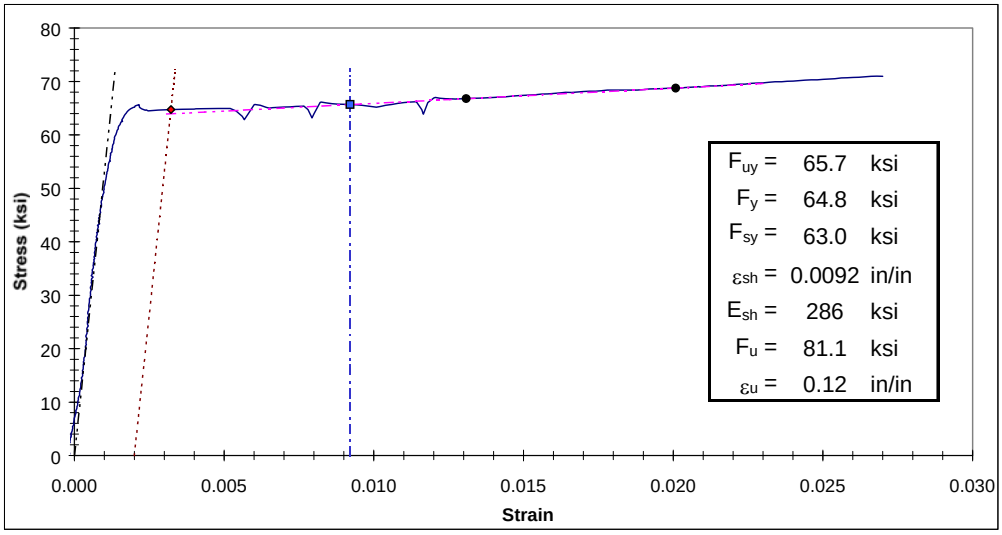

Figure C4.4.10 Yield Plateau and Tensile Test Results for Specimen T4-E

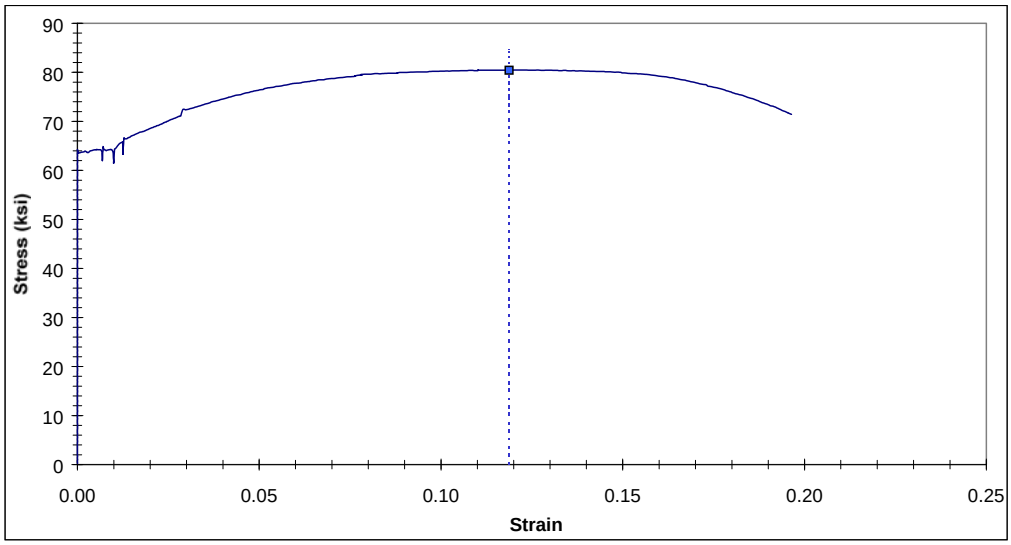

Figure C4.4.11 Complete Stress-strain Curve for Specimen T4-F

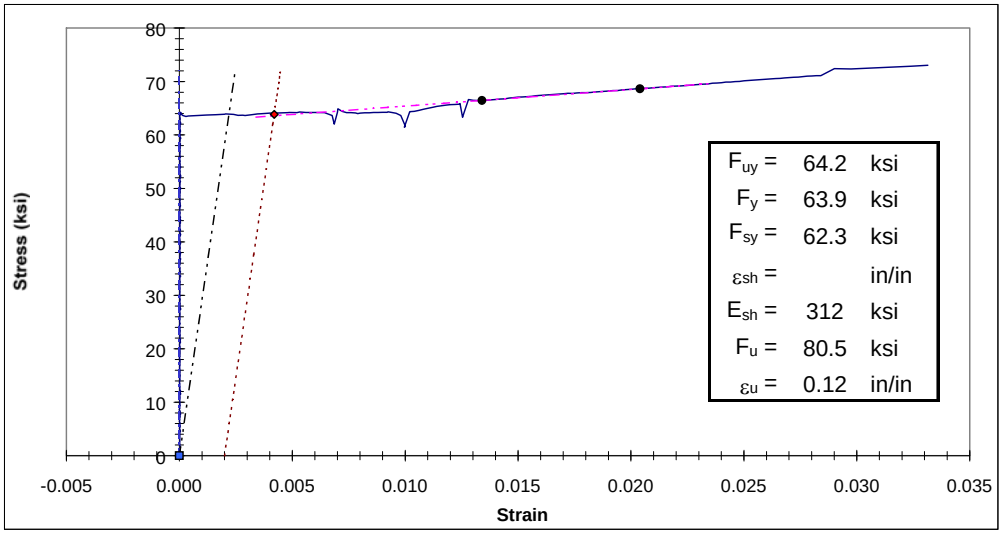

Figure C4.4.12 Yield Plateau and Tensile Test Results for Specimen T4-F

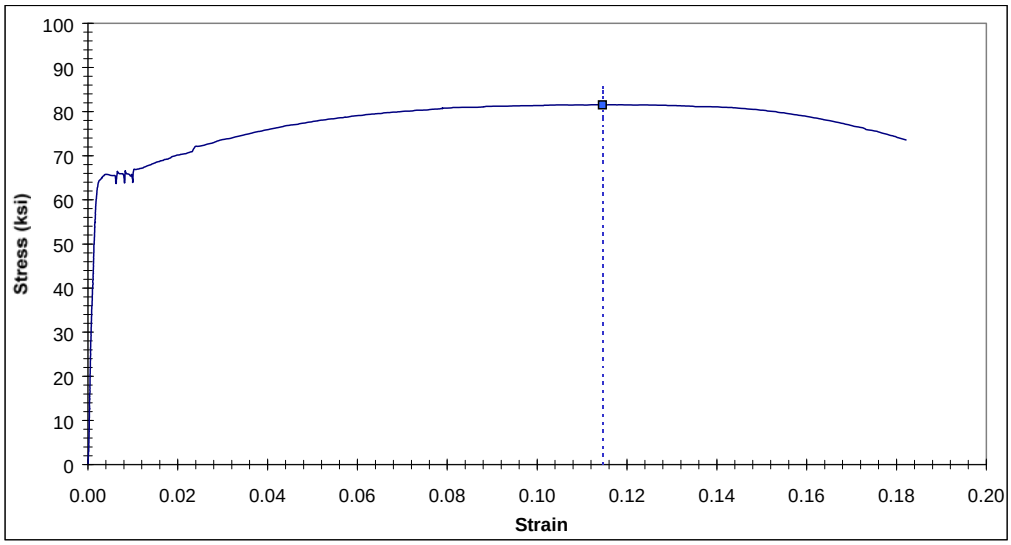

Figure C4.4.13 Complete Stress-strain Curve for Specimen T4-G

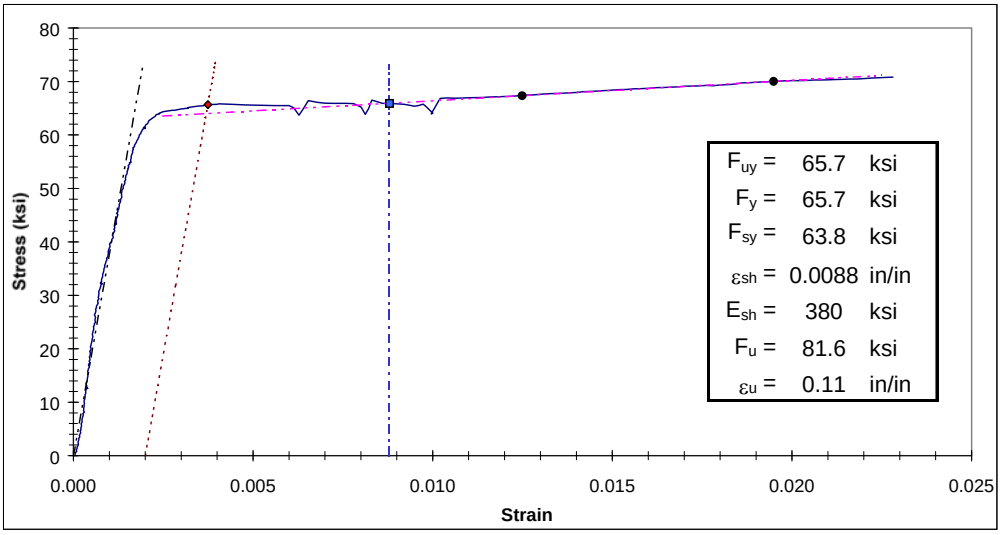

Figure C4.4.14 Yield Plateau and Tensile Test Results for Specimen T4-G

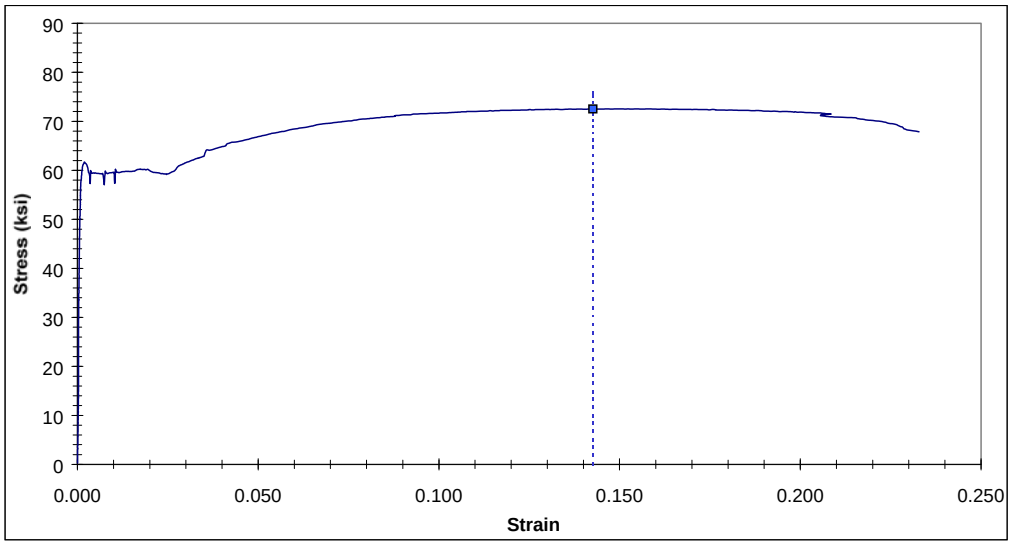

Figure C4.5.1 Complete Stress-strain Curve for Specimen T5-A

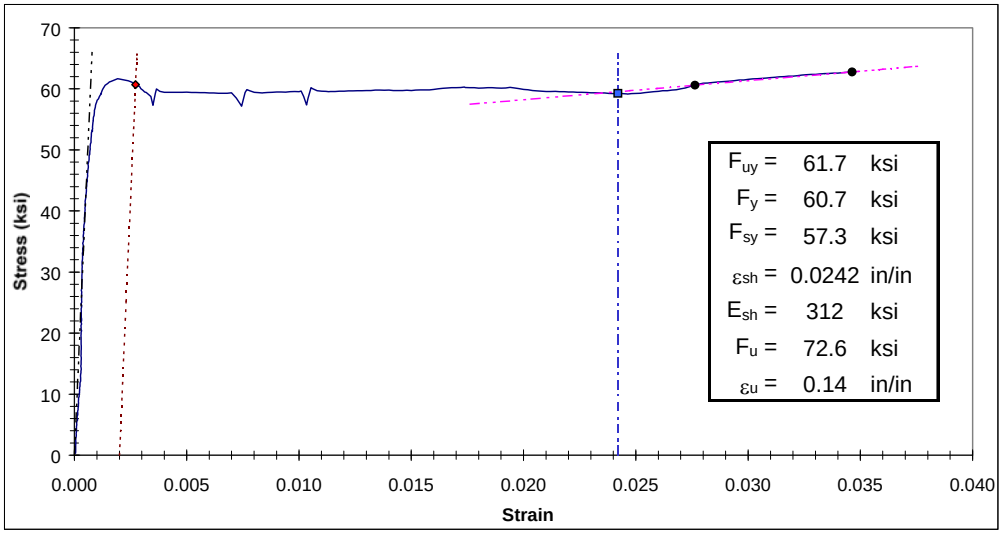

Figure C4.5.2 Yield Plateau and Tensile Test Results for Specimen T5-A

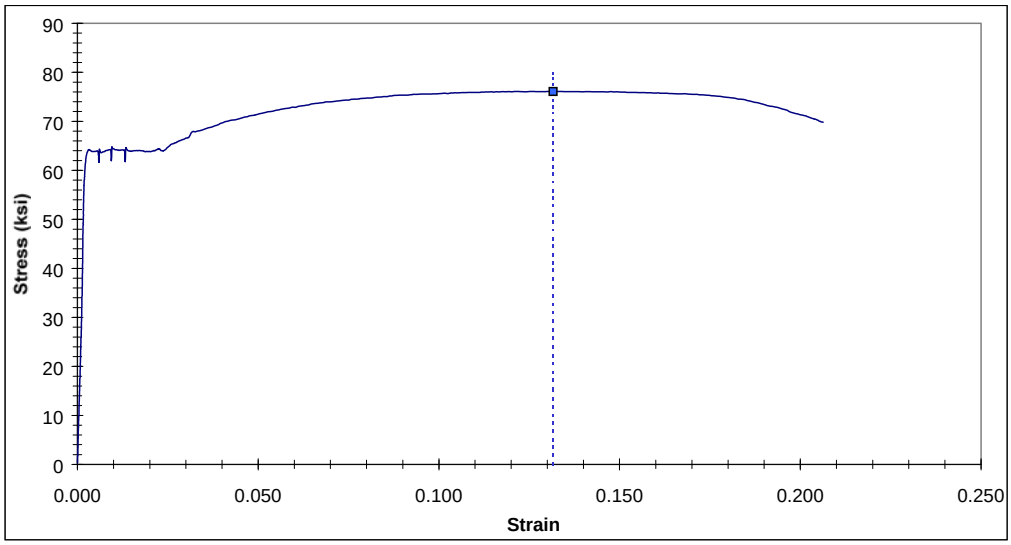

Figure C4.5.3 Complete Stress-strain Curve for Specimen T5-B

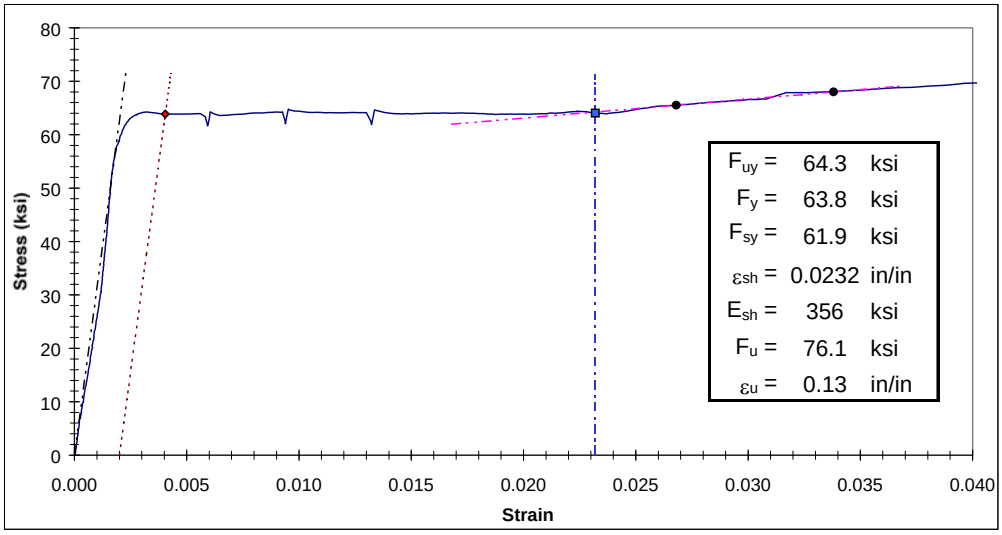

Figure C4.5.4 Yield Plateau and Tensile Test Results for Specimen T5-B

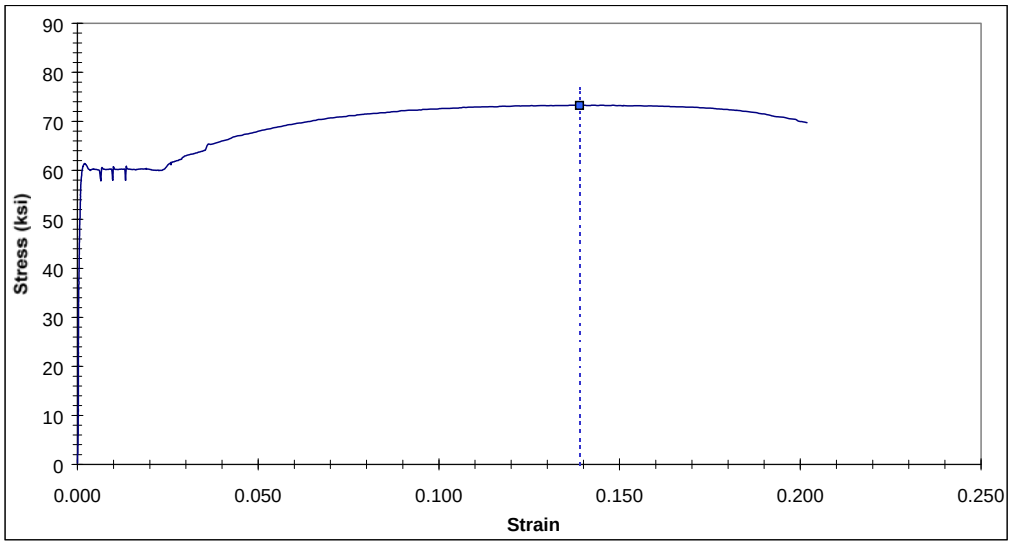

Figure C4.5.5 Complete Stress-strain Curve for Specimen T5-C

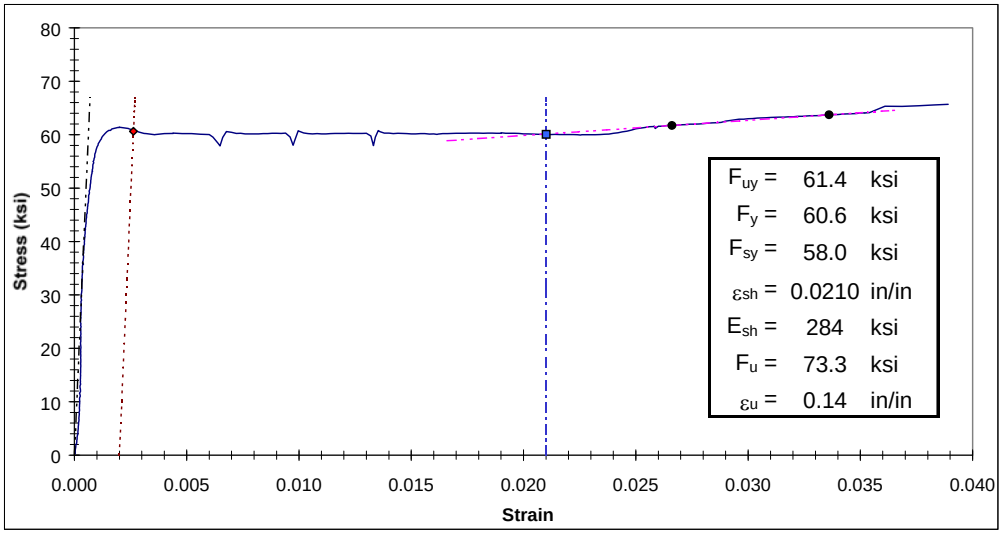

Figure C4.5.6 Yield Plateau and Tensile Test Results for Specimen T5-C

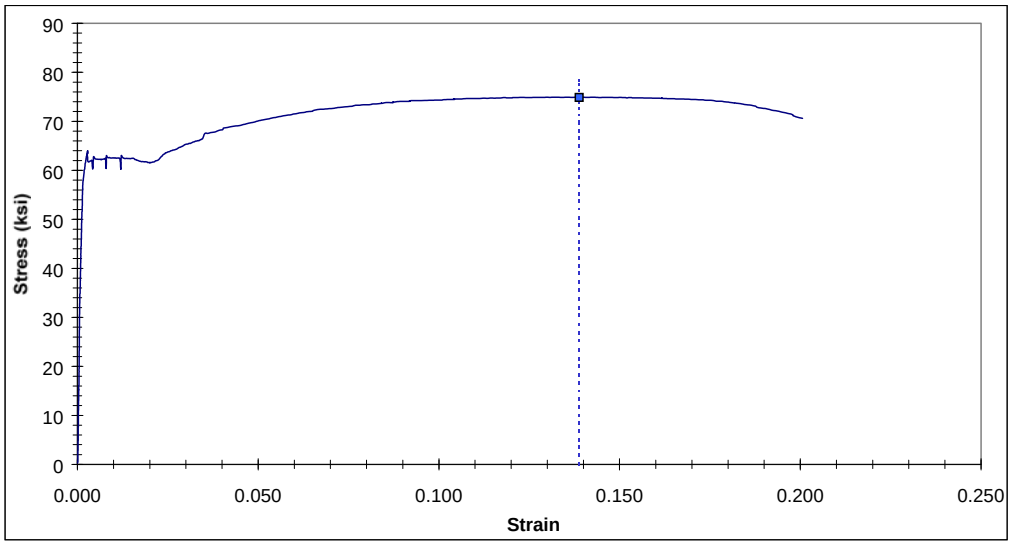

Figure C4.5.7 Complete Stress-strain Curve for Specimen T5-D

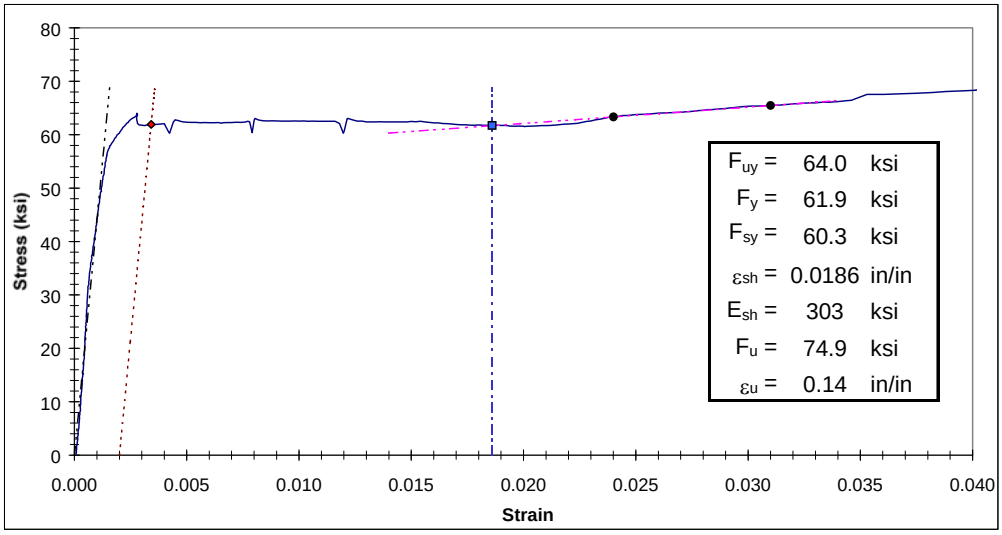

Figure C4.5.8 Yield Plateau and Tensile Test Results for Specimen T5-D

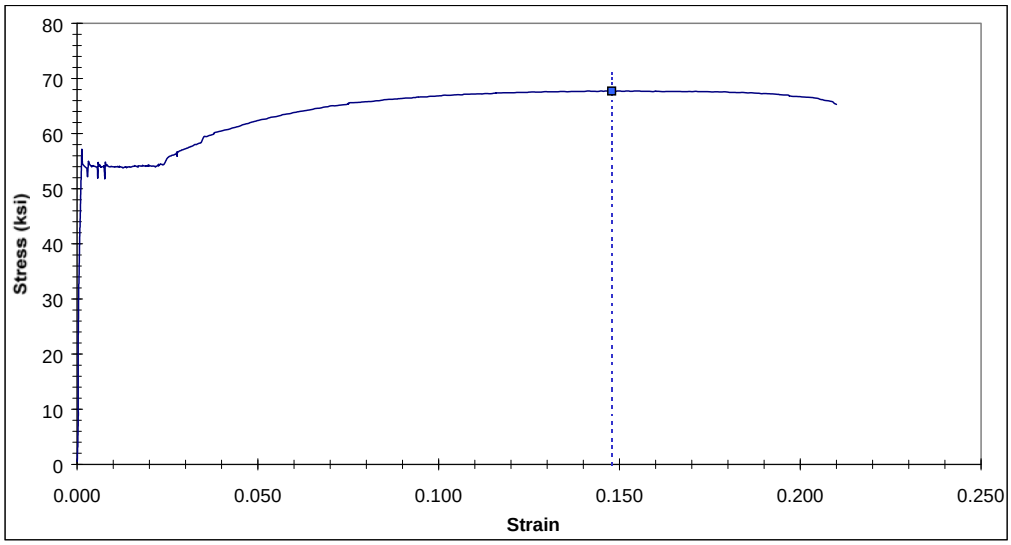

Figure C4.5.9 Complete Stress-strain Curve for Specimen T5-E

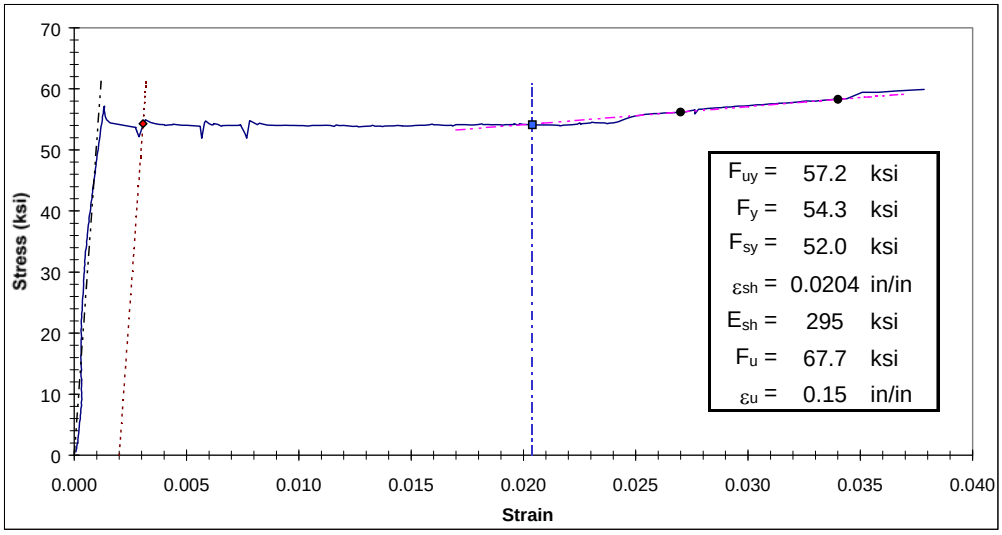

Figure C4.5.10 Yield Plateau and Tensile Test Results for Specimen T5-E

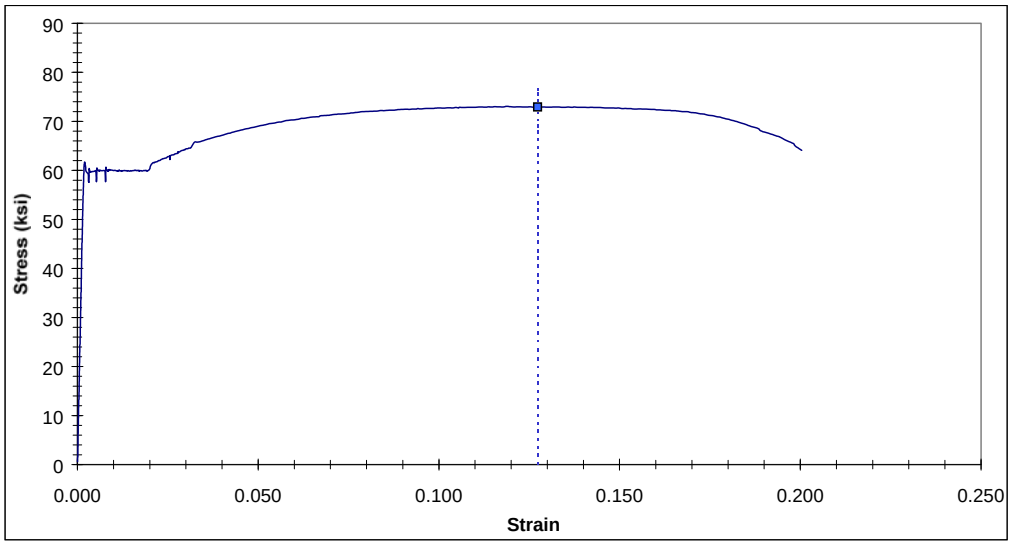

Figure C4.5.11 Complete Stress-strain Curve for Specimen T5-F

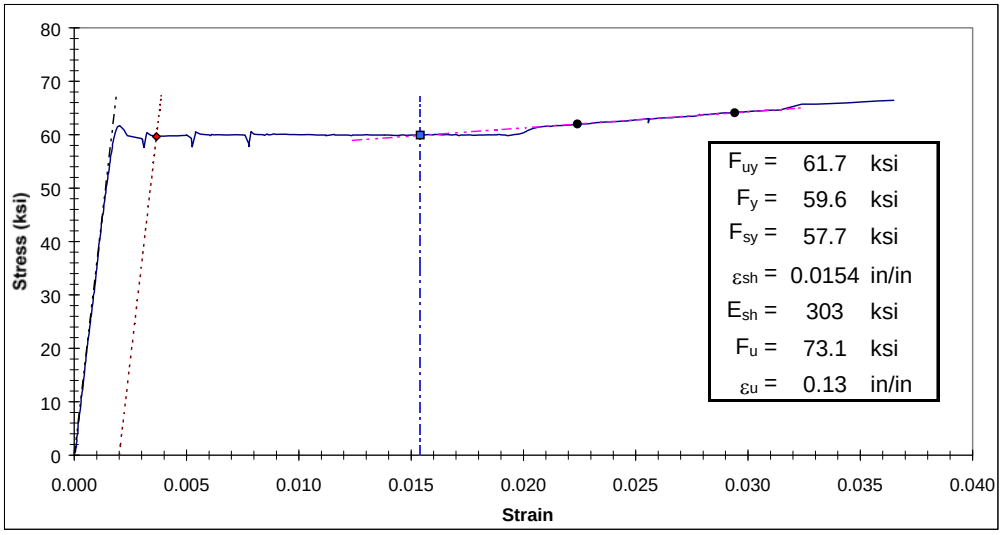

Figure C4.5.12 Yield Plateau and Tensile Test Results for Specimen T5-F

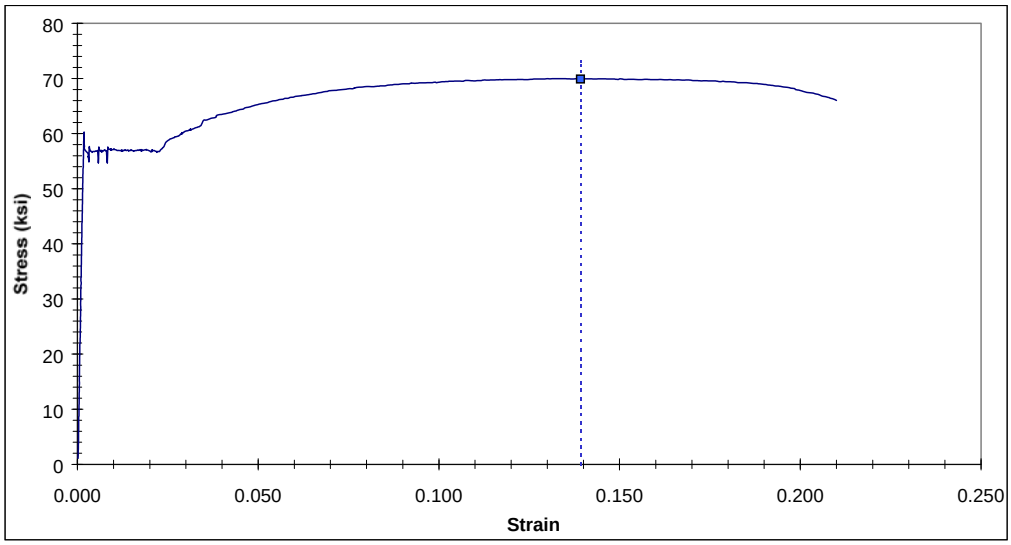

Figure C4.5.13 Complete Stress-strain Curve for Specimen T5-G

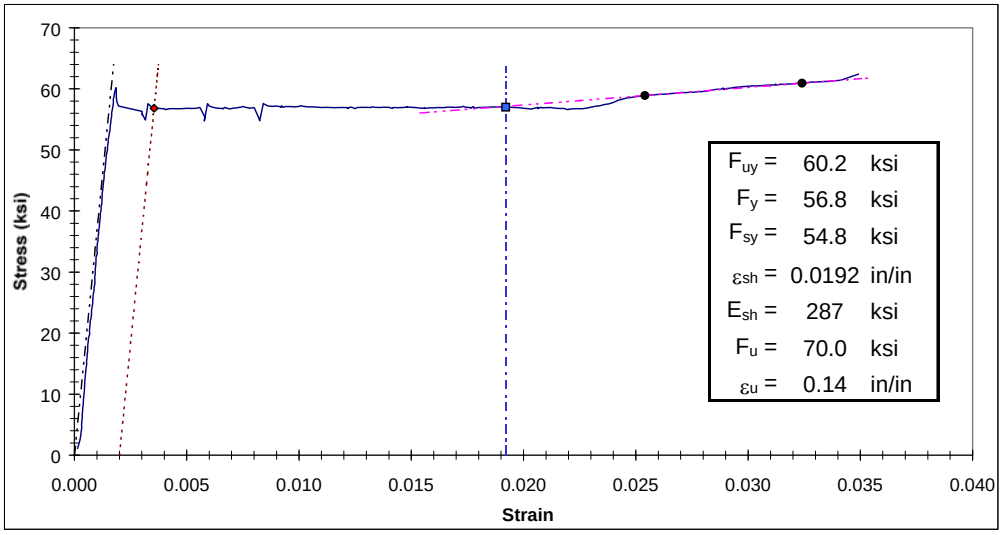

Figure C4.5.14 Yield Plateau and Tensile Test Results for Specimen T5-G

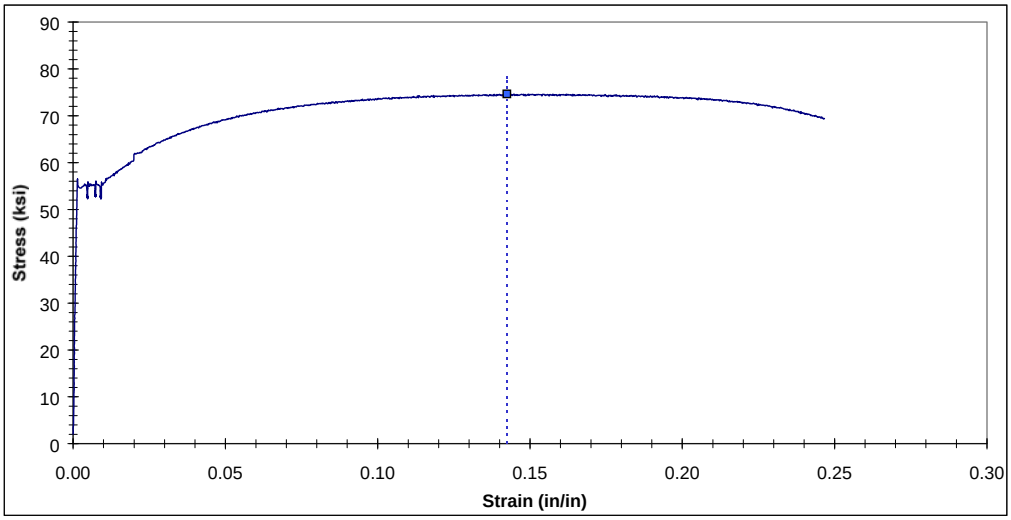

Figure C4.6.1 Complete Stress-strain Curve for Specimen T6-A

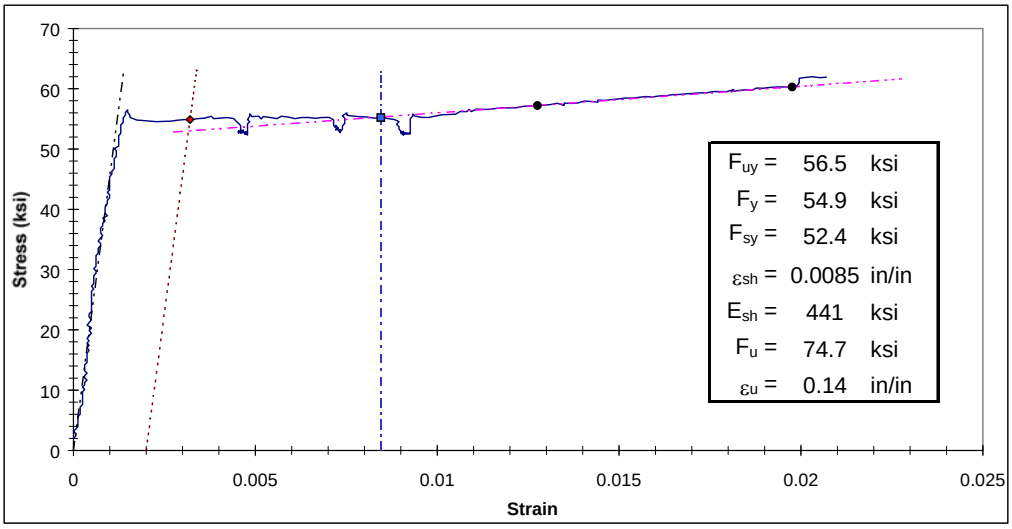

Figure C4.6.2 Yield Plateau and Tensile Test Results for Specimen T6-A

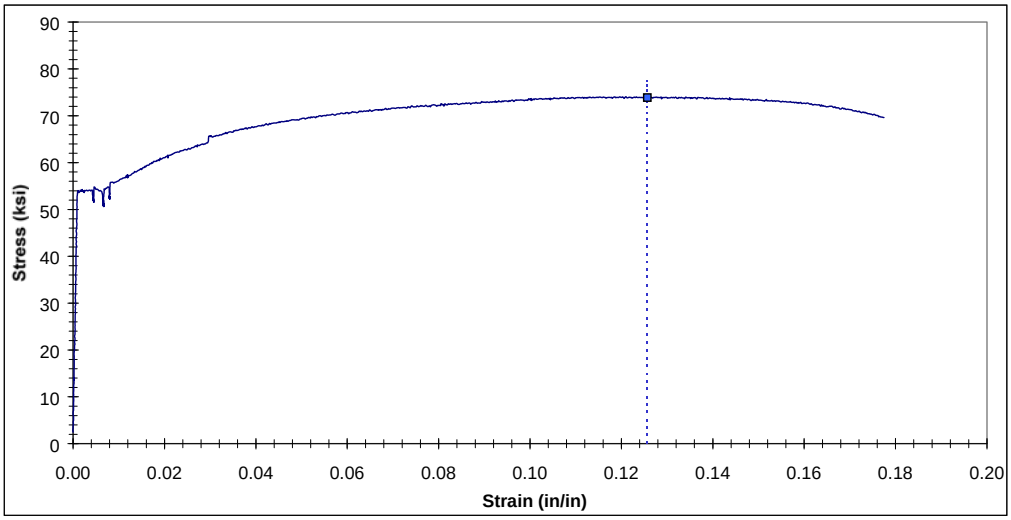

Figure C4.6.3 Complete Stress-strain Curve for Specimen T6-B

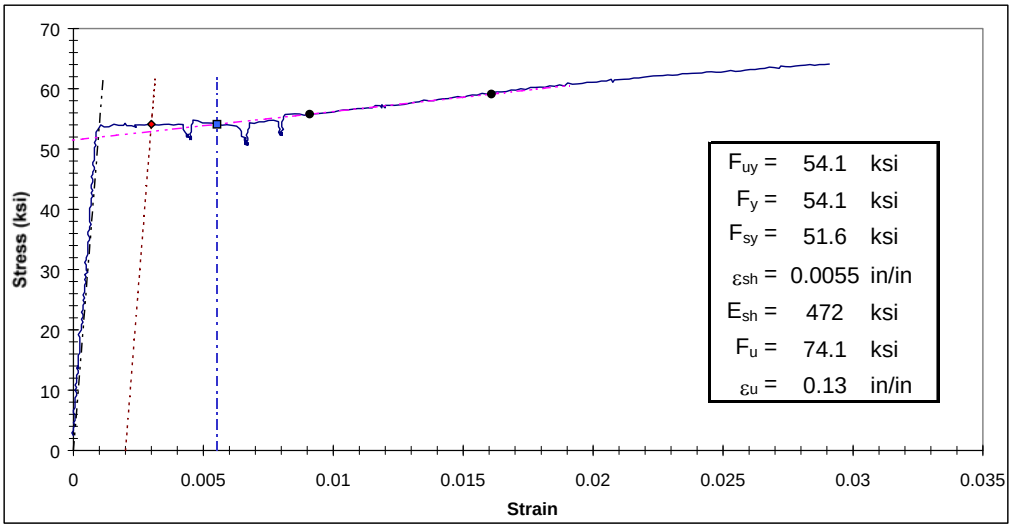

Figure C4.6.4 Yield Plateau and Tensile Test Results for Specimen T6-B

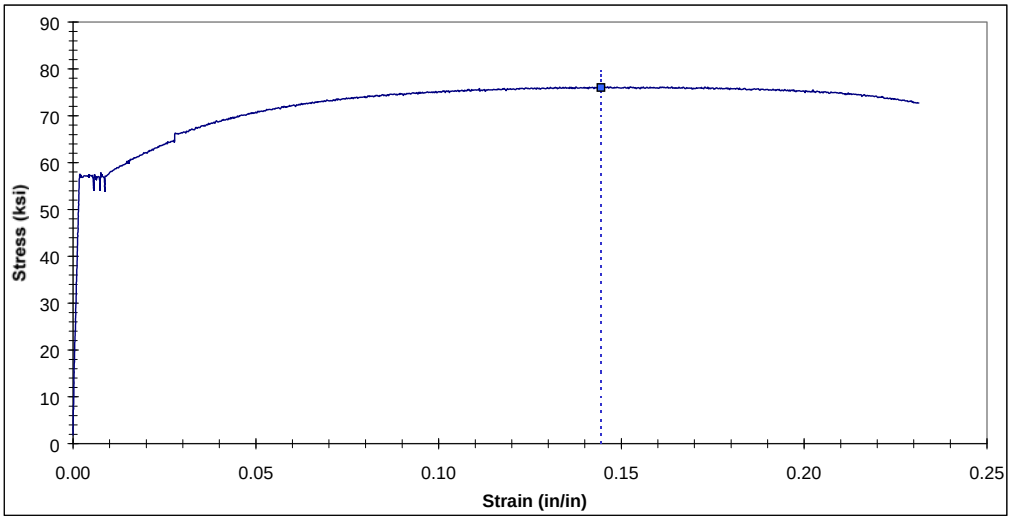

Figure C4.6.5 Complete Stress-strain Curve for Specimen T6-C

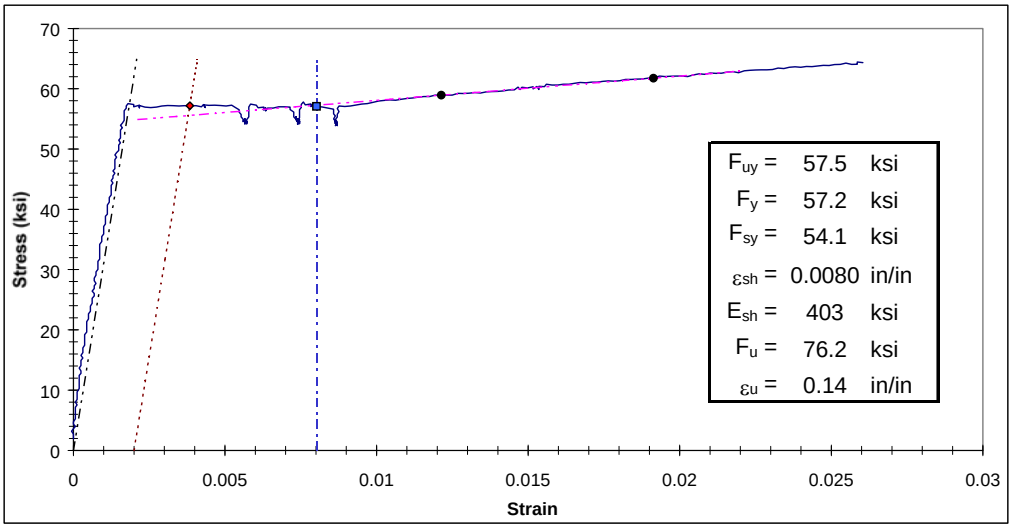

Figure C4.6.6 Yield Plateau and Tensile Test Results for Specimen T6-C

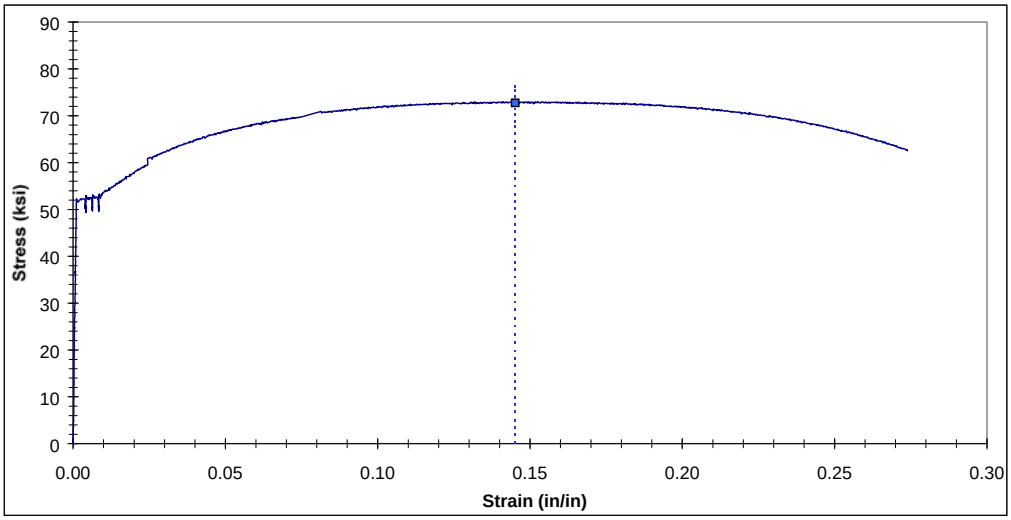

Figure C4.6.7 Complete Stress-strain Curve for Specimen T6-D

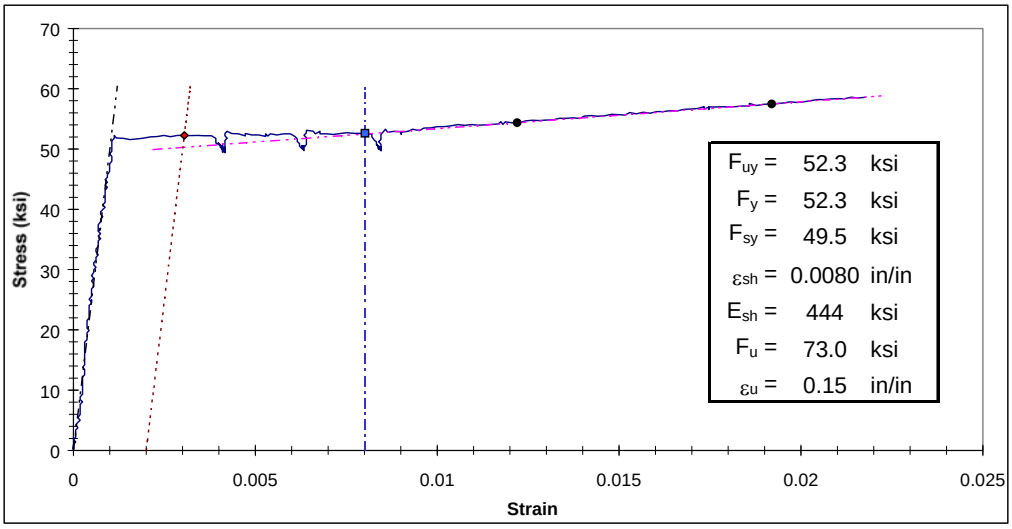

Figure C4.6.8 Yield Plateau and Tensile Test Results for Specimen T6-D

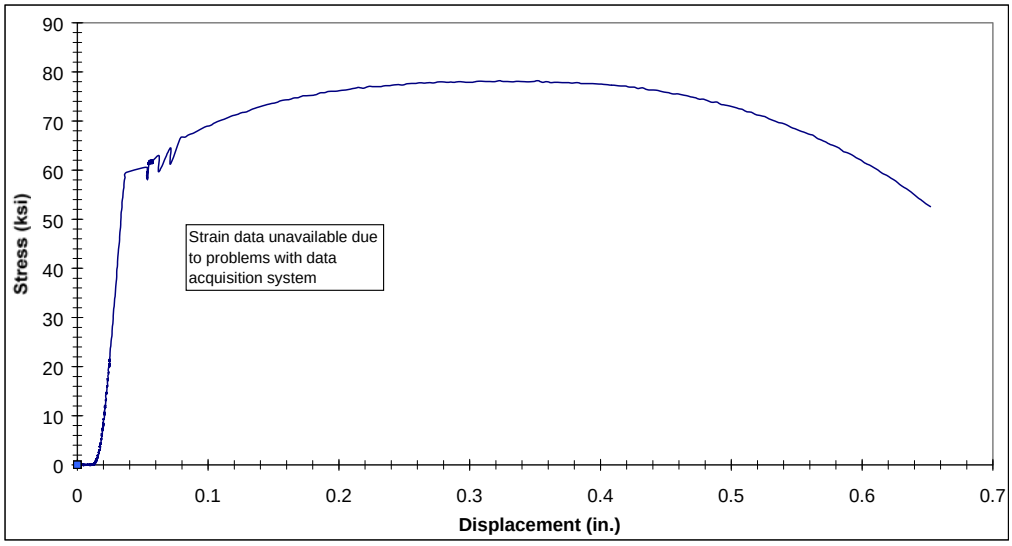

Figure C4.6.9 Complete Stress-strain Curve for Specimen T6-E

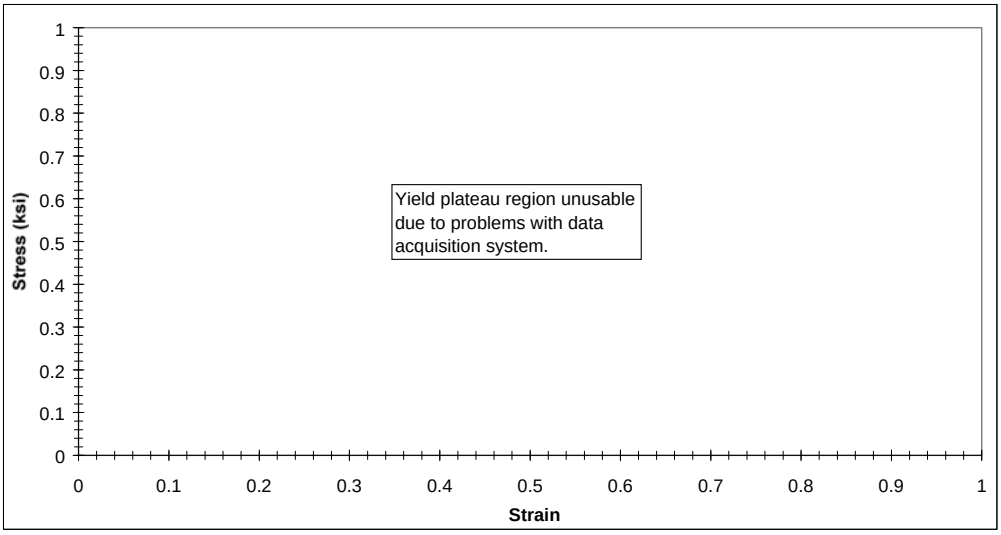

Figure C4.6.10 Yield Plateau and Tensile Test Results for Specimen T6-E

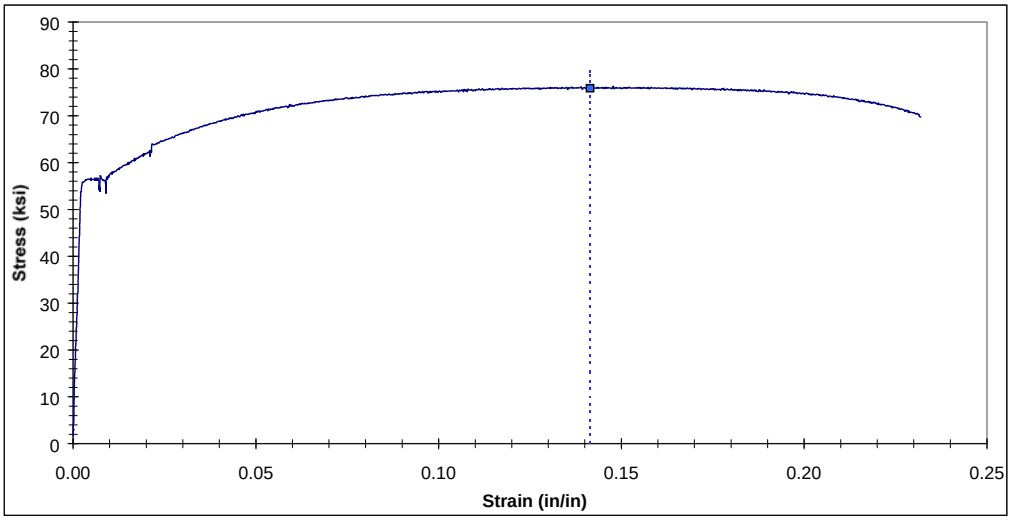

Figure C4.6.11 Complete Stress-strain Curve for Specimen T6-F

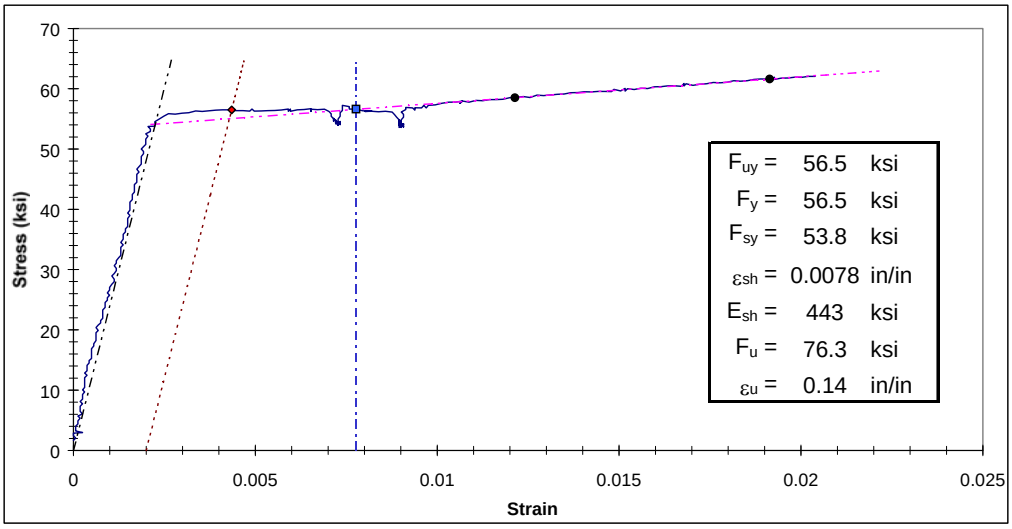

Figure C4.6.12 Yield Plateau and Tensile Test Results for Specimen T6-F

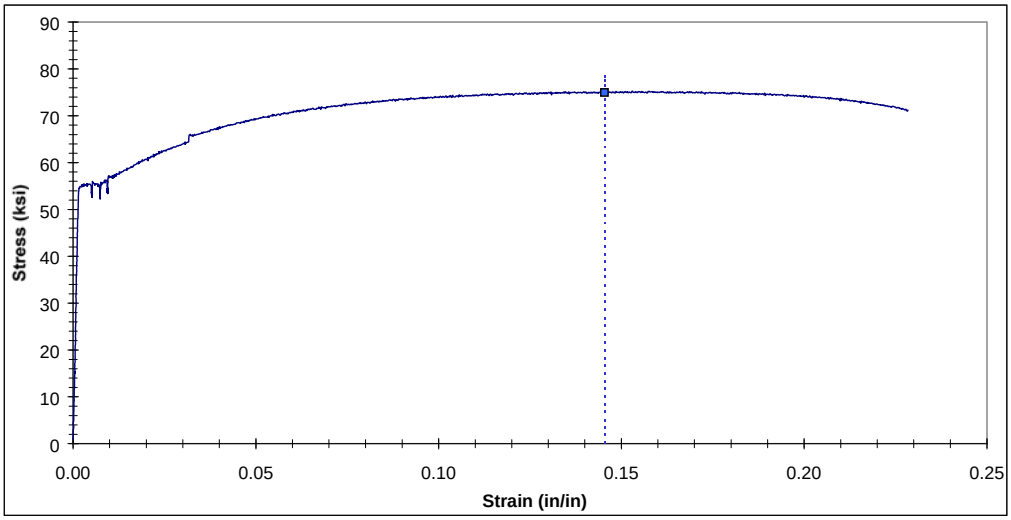

Figure C4.6.13 Complete Stress-strain Curve for Specimen T6-G

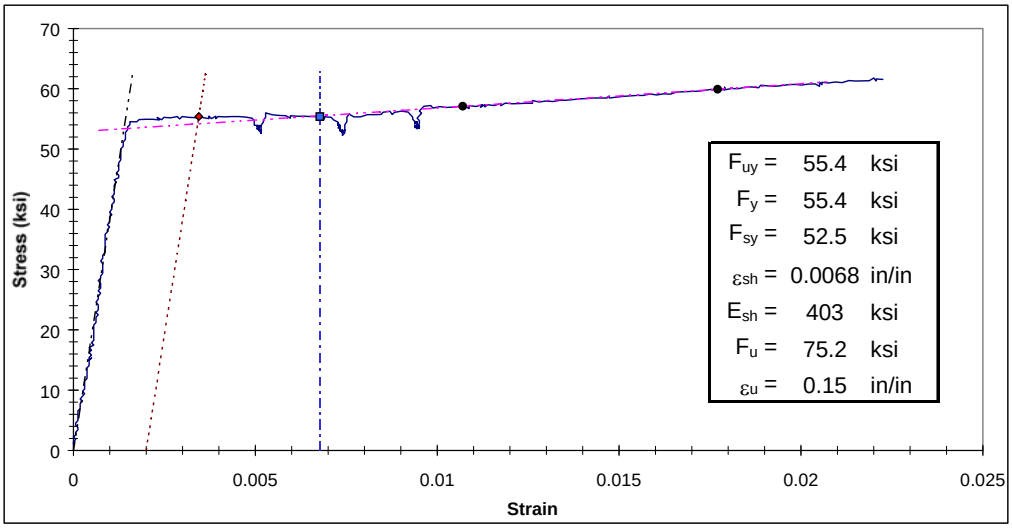

Figure C4.6.14 Yield Plateau and Tensile Test Results for Specimen T6-G

Appendix D: Charpy Impact Test Results

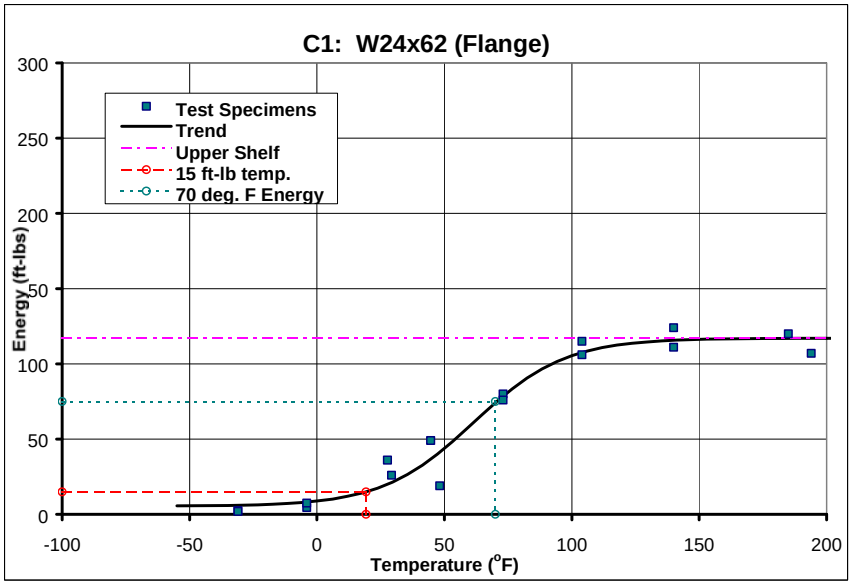

β_1=	61
β_2=	56
β_3=	0.028
β_4=	62

Shelf Energy	
Upper	Lower
117	5

Energy	Temp.
10	5
15	19
20	28
25	34

Temp.	Energy
60	60
70	75
80	90
90	100

* Round to nearest 5 ft-lbs

Figure D.1.1: Flange Region Charpy Impact Test Results for Member C1

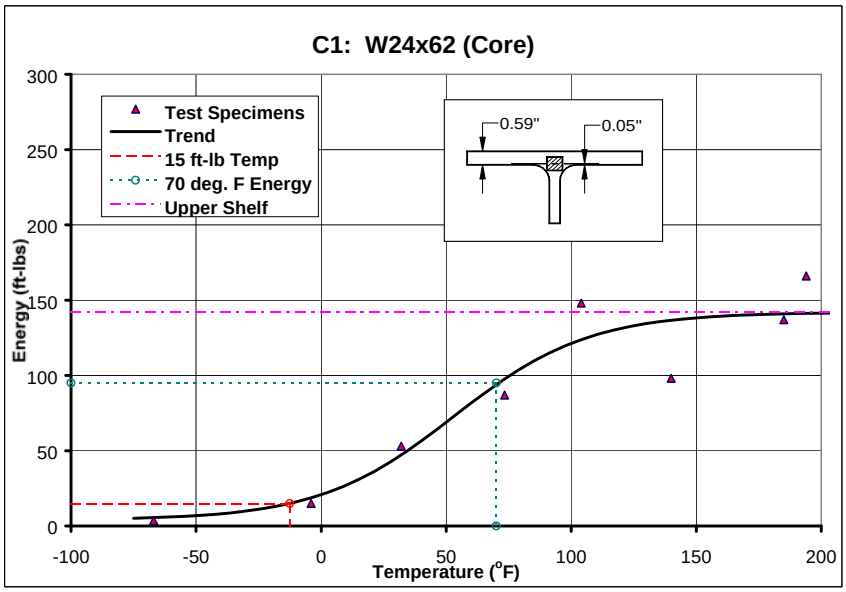

β_1=	73
β_2=	69
β_3=	0.019
β_4=	53

Shelf Energy	
Upper	Lower
142	4

Energy	Temp.
10	-30
15	-13
20	-1
25	7

Temp.	Energy*
60	80
70	95
80	105
90	115

* Round to nearest 5 ft-lbs

Figure D.1.2: Core Region Charpy Impact Test Results for Member C1

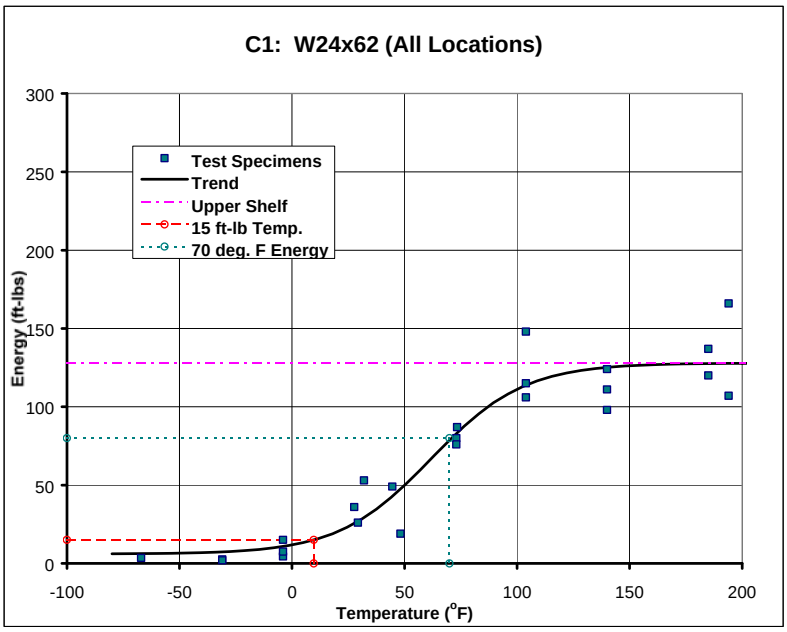

β_1= 67
β_2= 61
β_3= 0.024
β_4= 62

Shelf Energy	
Upper	Lower
128	6

Energy	Temp.
10	-8
15	10
20	20
25	27

Temp.	Energy*
60	65
70	80
80	90
90	105

* Round to nearest 5 ft-lbs

Figure D.1.3: All Charpy Impact Test Results for Member C1

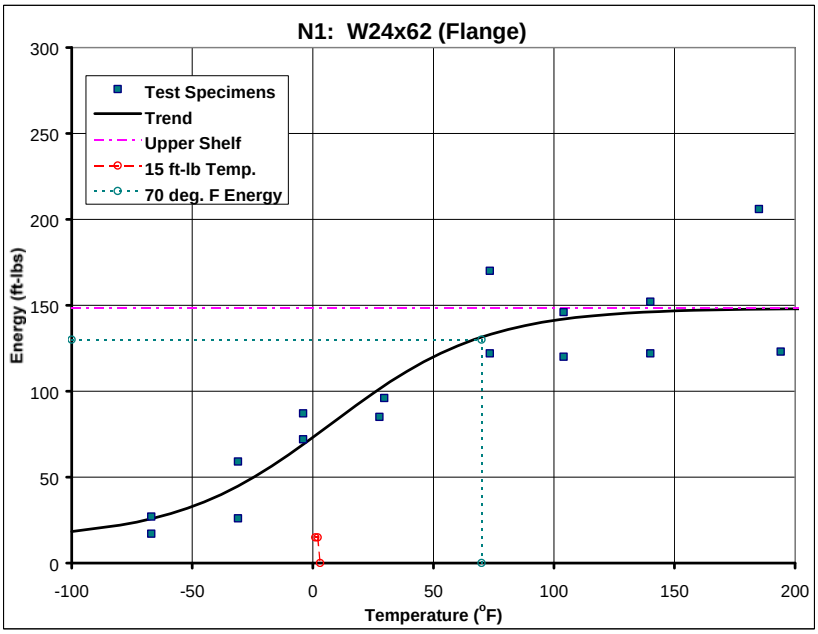

β_1= 81
β_2= 67
β_3= 0.016
β_4= 8

Shelf Energy	
Upper	Lower
148	14

Energy	Temp.
10	<-70
15	<-70
20	<-70
25	<-70

Temp.	Energy
60	125
70	130
80	135
90	140

* Round to nearest 5 ft-lbs

Figure D.2.1: Flange Region Charpy Impact Test Results for Member N1

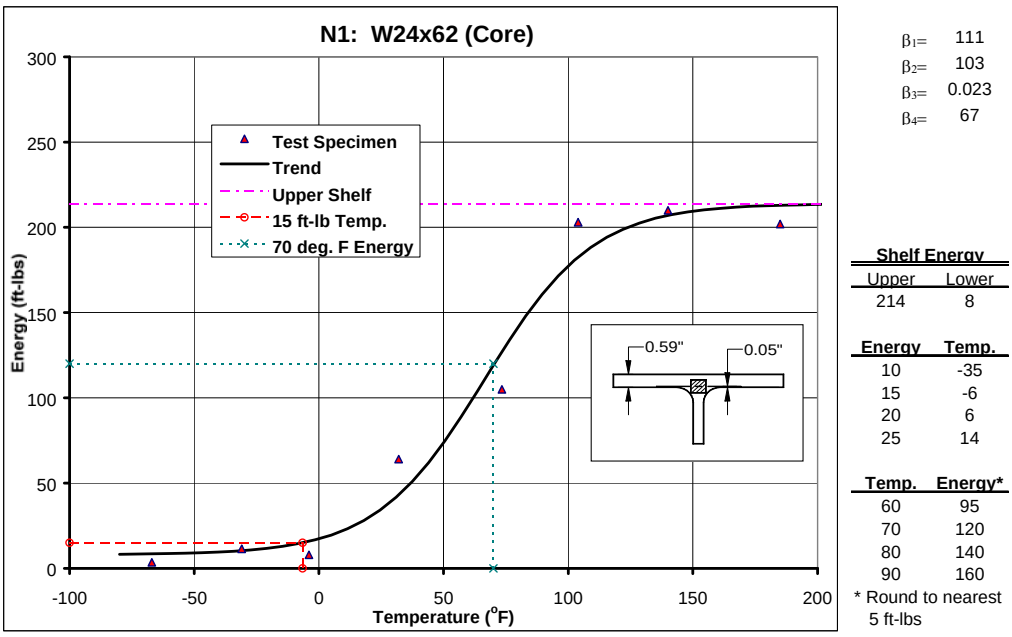

Figure D.2.2: Core Region Charpy Impact Test Results for Member N1

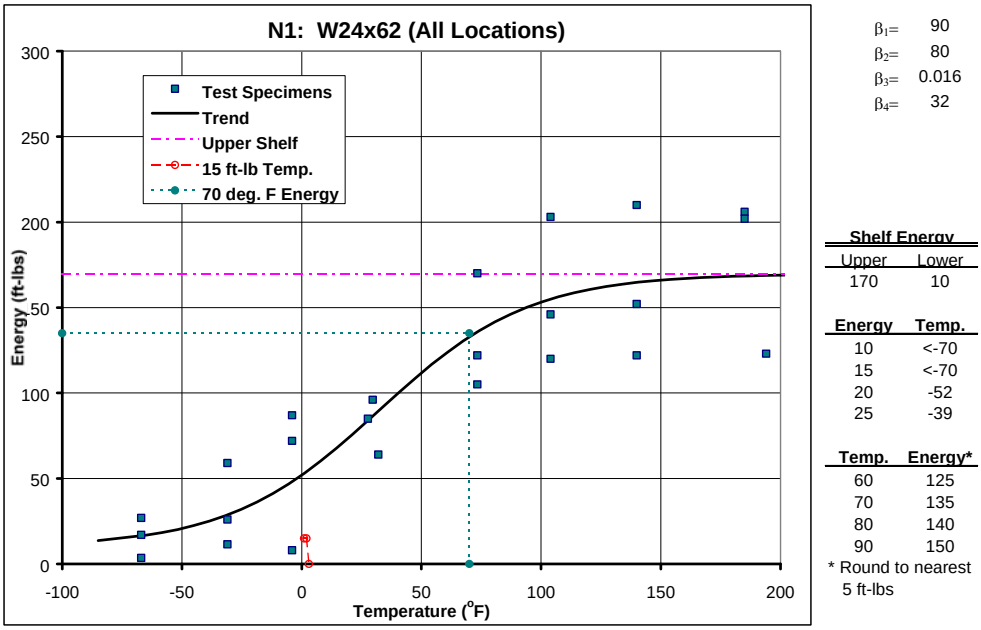

Figure D.2.3: All Charpy Impact Test Results for Member N1

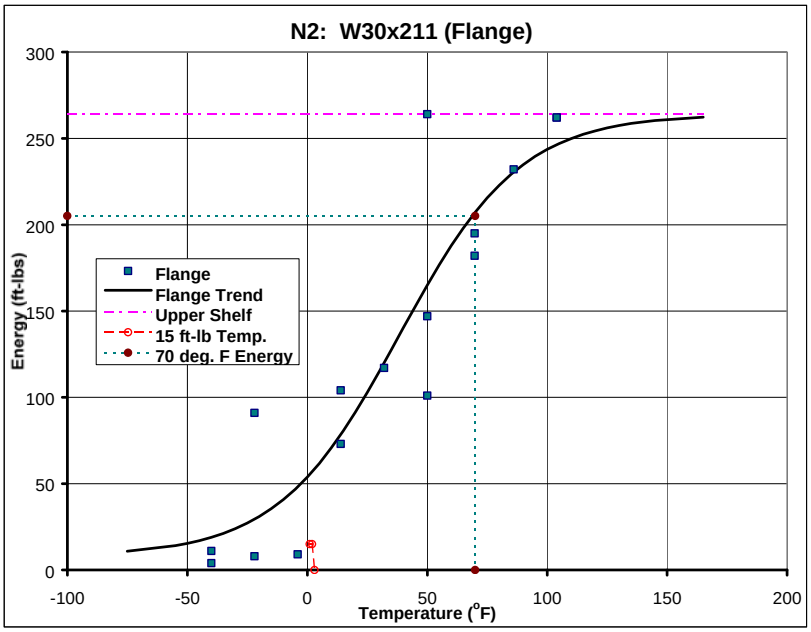

β_1= 136
β_2= 128
β_3= 0.020
β_4= 38

Shelf Energy	
Upper	Lower
264	8

Energy	Temp.
10	<-40
15	<-40
20	-38
25	-28

Temp.	Energy
60	190
70	205
80	225
90	235

* Round to nearest 5 ft-lbs

Figure D.3.1: Flange Region Charpy Impact Test Results for Member N2

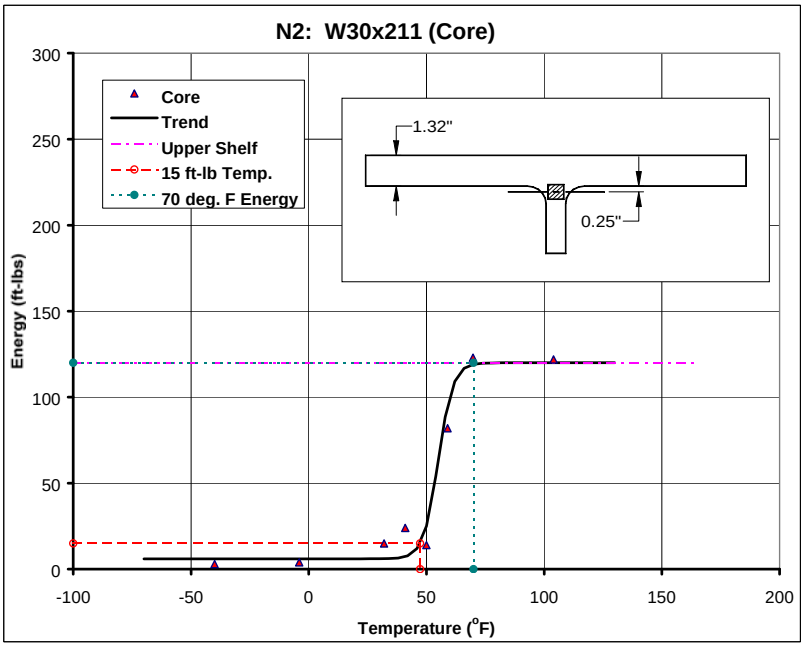

β_1= 63
β_2= 57
β_3= 0.161
β_4= 55

Shelf Energy	
Upper	Lower
120	6

Energy	Temp.
10	45
15	47
20	49
25	50

Temp.	Energy*
60	100
70	120
80	120
90	120

* Round to nearest 5 ft-lbs

Figure D.3.2: Core Region Charpy Impact Test Results for Member N2

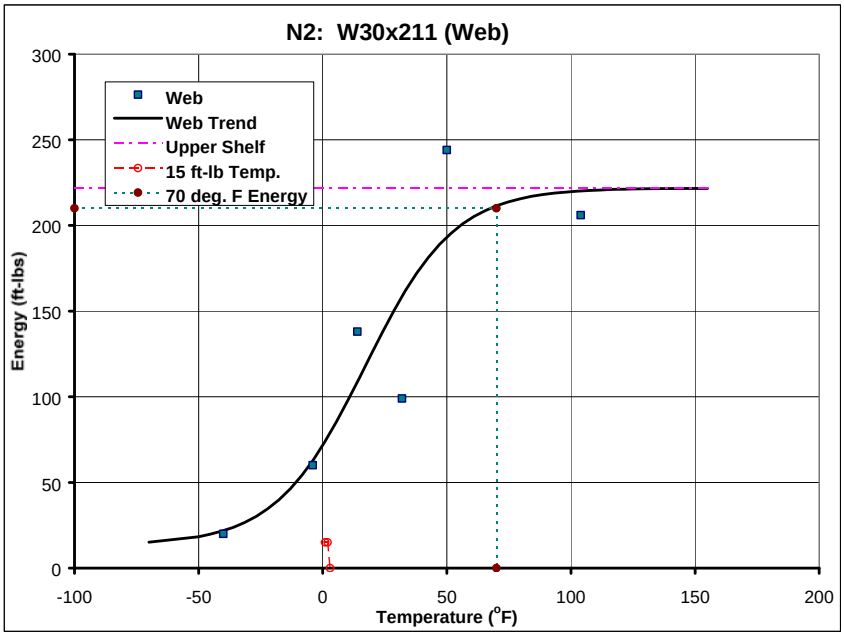

β_1= 118
β_2= 104
β_3= 0.028
β_4= 17

Shelf Energy	
Upper	Lower
222	14

Energy	Temp.
10	<-40
15	<-40
20	<-40
25	-34

Temp.	Energy
60	205
70	210
80	215
90	220

* Round to nearest 5 ft-lbs

Figure D.3.3: Web Region Charpy Impact Test Results for Member N2

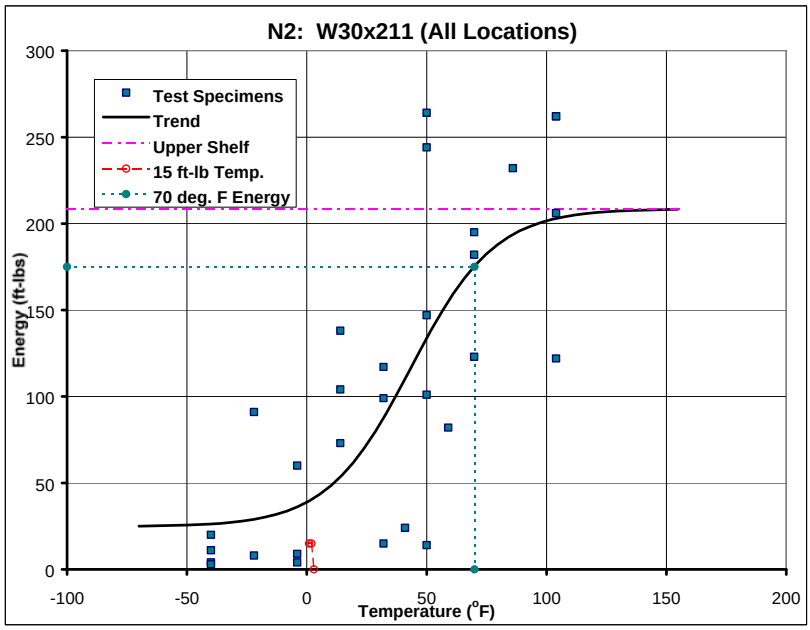

β_1= 117
β_2= 92
β_3= 0.029
β_4= 43

Shelf Energy	
Upper	Lower
209	25

Energy	Temp.
10	<-40
15	<-40
20	<-40
25	<-40

Temp.	Energy*
60	155
70	175
80	190
90	195

* Round to nearest 5 ft-lbs

Figure D.3.4: All Charpy Impact Test Results for Member N2

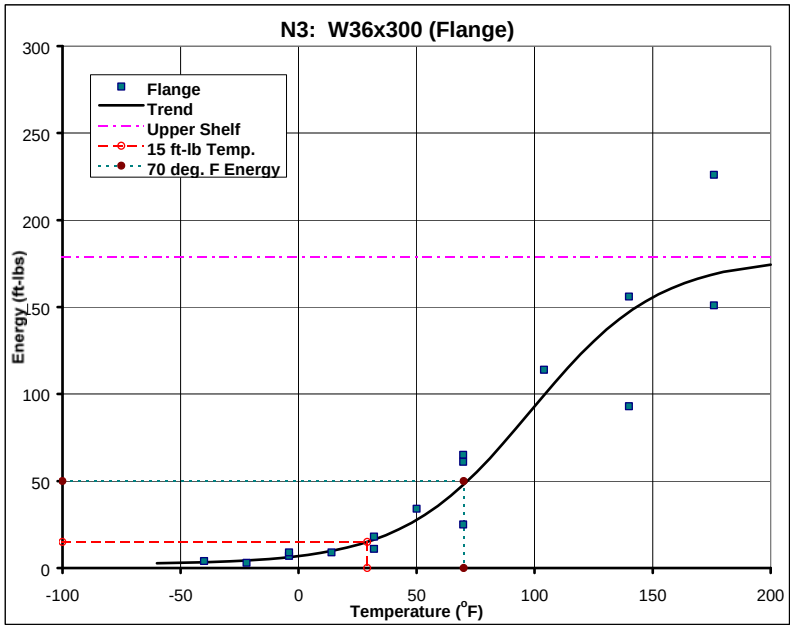

β_1= 90
β_2= 88
β_3= 0.018
β_4= 98

Shelf Energy	
Upper	Lower
179	2

Energy	Temp.
10	15
15	29
20	39
25	47

Temp.	Energy
60	35
70	50
80	60
90	75

* Round to nearest 5 ft-lbs

Figure D.4.1: Flange Region Charpy Impact Test Results for Member N3

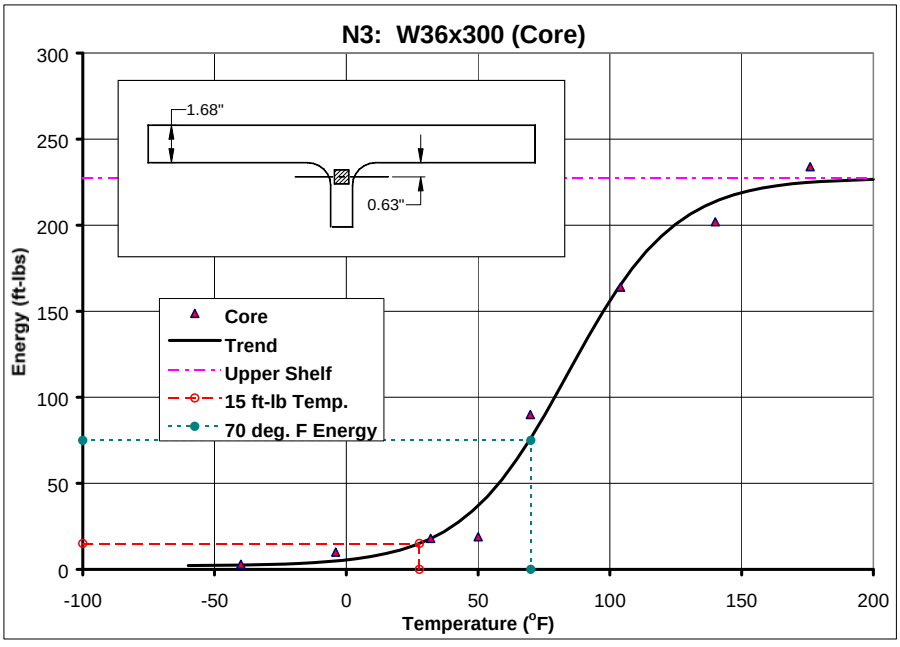

β_1= 115
β_2= 113
β_3= 0.025
β_4= 84

Shelf Energy	
Upper	Lower
227	2

Energy	Temp.
10	17
15	28
20	35
25	40

Temp.	Energy*
60	55
70	75
80	105
90	130

* Round to nearest 5 ft-lbs

Figure D.4.2: Core Region Charpy Impact Test Results for Member N3

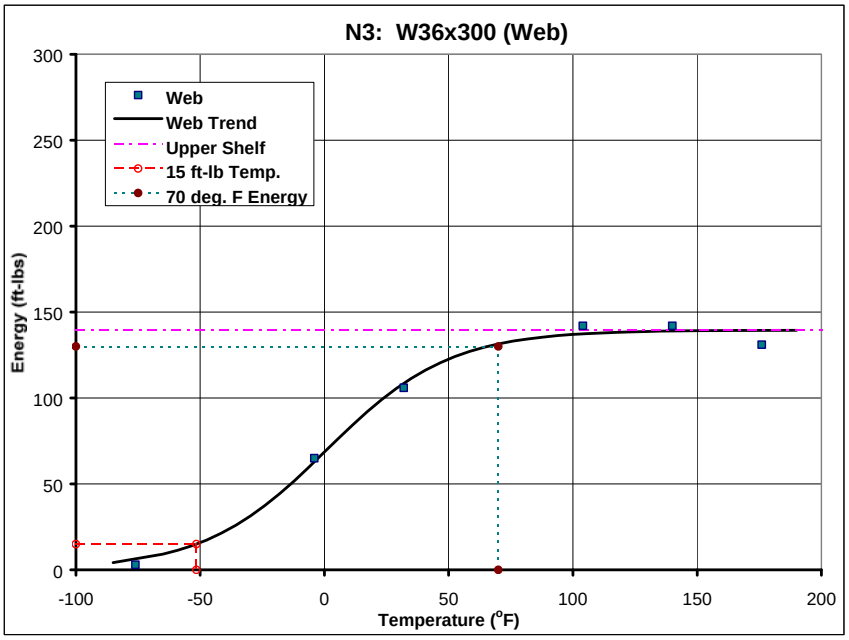

β_1=	70
β_2=	70
β_3=	0.020
β_4=	1

Shelf Energy	
Upper	Lower
139	0

Energy	Temp.
10	-63
15	-52
20	-43
25	-37

Temp.	Energy
60	130
70	130
80	135
90	135

* Round to nearest 5 ft-lbs

Figure D.4.3: Web Region Charpy Impact Test Results for Member N3

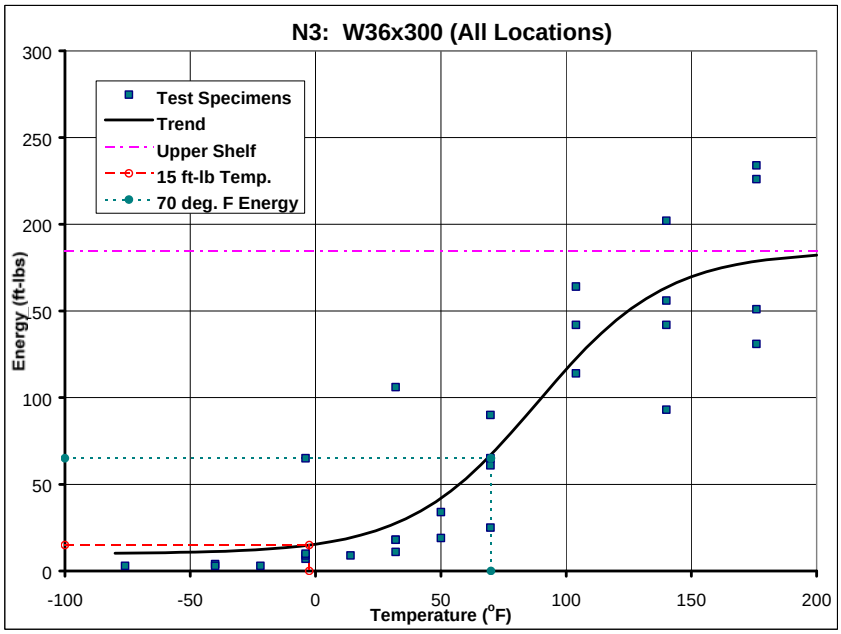

β_1=	97
β_2=	87
β_3=	0.019
β_4=	89

Shelf Energy	
Upper	Lower
184	10

Energy	Temp.
10	<-75
15	-3
20	16
25	28

Temp.	Energy*
60	55
70	65
80	85
90	100

* Round to nearest 5 ft-lbs

Figure D.4.4: All Charpy Impact Test Results for Member N3

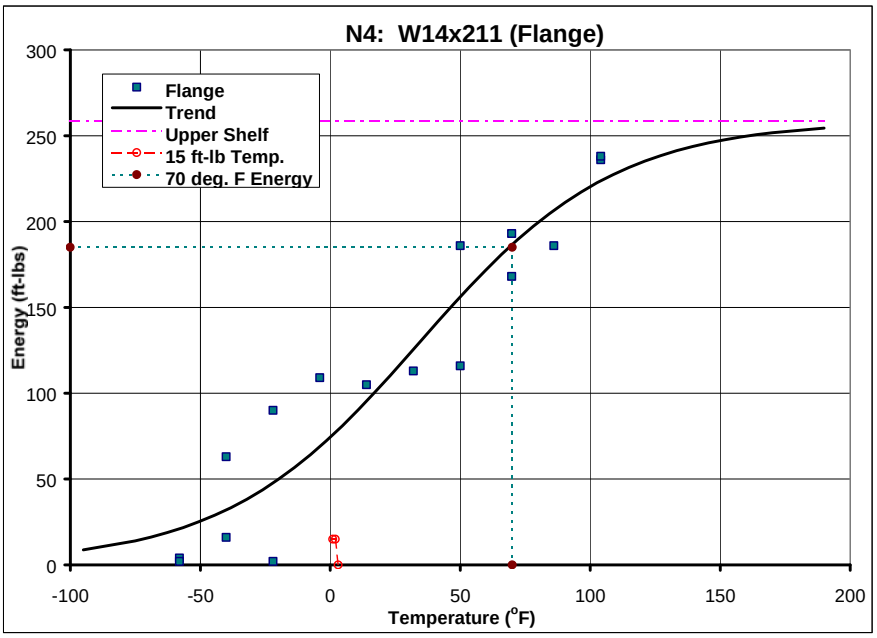

β_1=	130
β_2=	129
β_3=	0.013
β_4=	34

Shelf Energy	
Upper	Lower
258	1

Energy	Temp.
10	<-60
15	<-60
20	-60
25	-51

Temp.	Energy
60	170
70	185
80	200
90	210

* Round to nearest 5 ft-lbs

Figure D.5.1: Flange Region Charpy Impact Test Results for Member N4

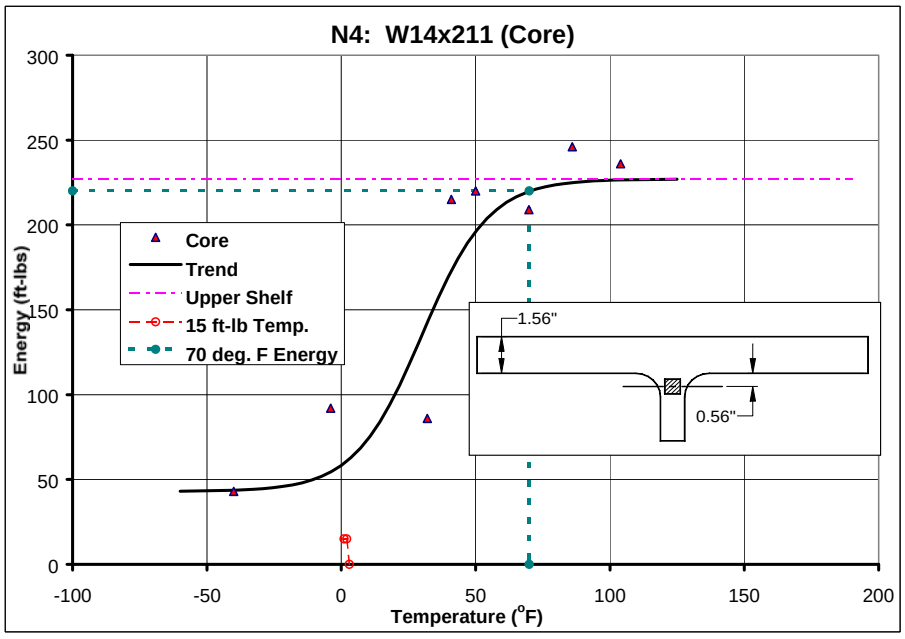

β_1=	135
β_2=	92
β_3=	0.040
β_4=	30

Shelf Energy	
Upper	Lower
227	43

Energy	Temp.
10	<-40
15	<-40
20	<-40
25	<-40

Temp.	Energy*
60	210
70	220
80	225
90	225

* Round to nearest 5 ft-lbs

Figure D.5.2: Core Region Charpy Impact Test Results for Member N4

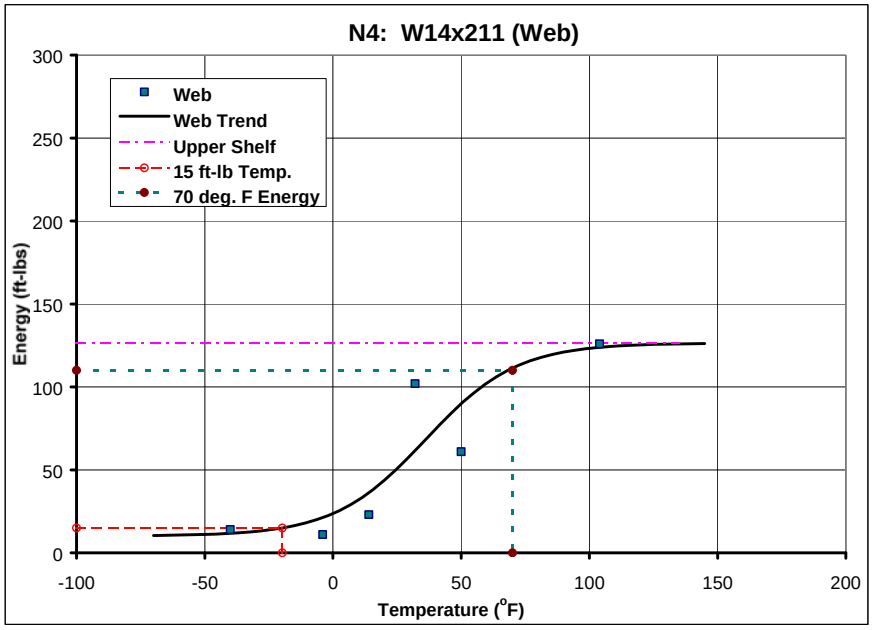

β_1=	68
β_2=	58
β_3=	0.028
β_4=	36

Shelf Energy	
Upper	Lower
126	10

Energy	Temp.
10	<-40
15	-20
20	-6
25	2

Temp.	Energy
60	100
70	110
80	115
90	120

* Round to nearest 5 ft-lbs

Figure D.5.3: Web Region Charpy Impact Test Results for Member N4

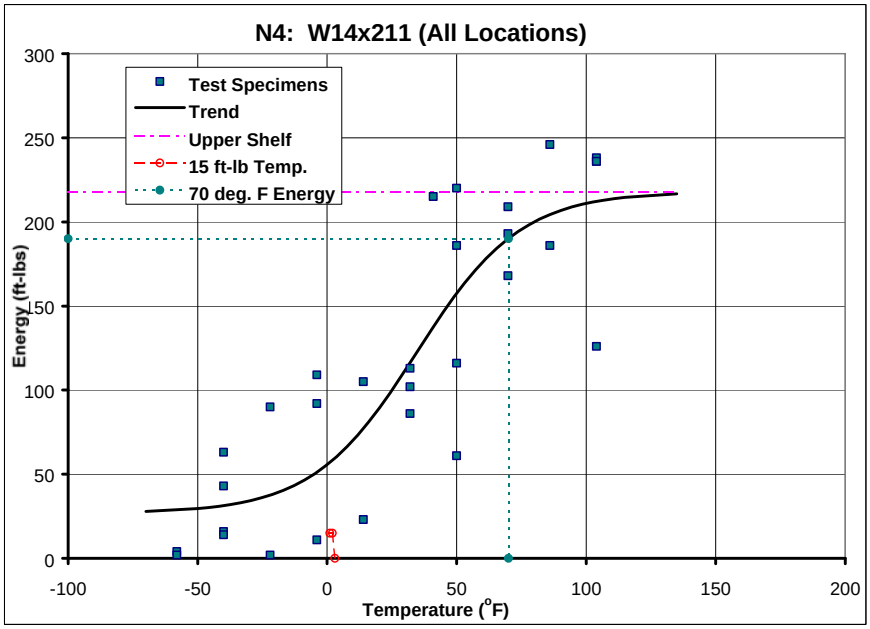

β_1=	122
β_2=	96
β_3=	0.025
β_4=	35

Shelf Energy	
Upper	Lower
218	27

Energy	Temp.
10	<-70
15	<-70
20	<-70
25	<-70

Temp.	Energy*
60	175
70	190
80	200
90	205

* Round to nearest 5 ft-lbs

Figure D.5.4: All Charpy Impact Test Results for Member N4

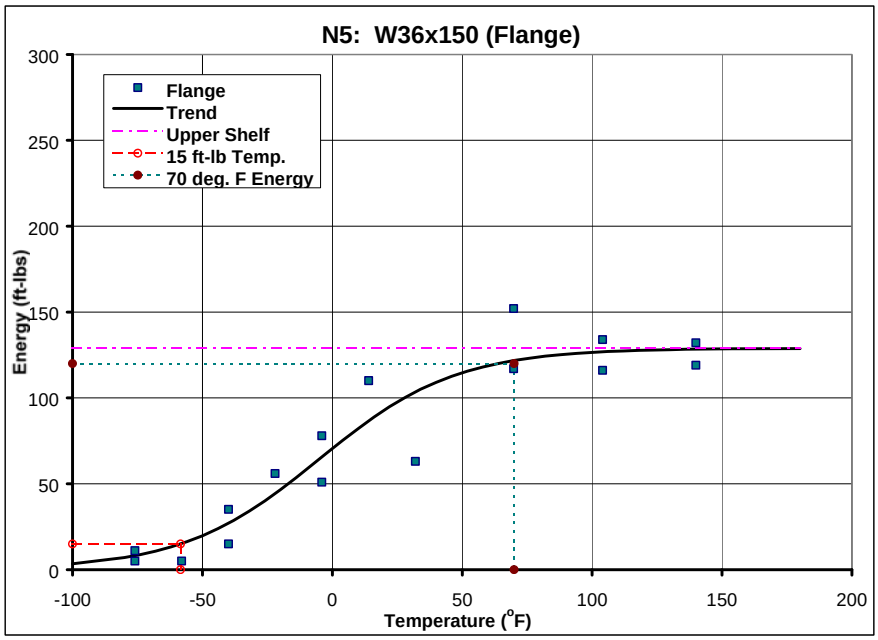

β_1=	64
β_2=	64
β_3=	0.019
β_4=	-5

Shelf Energy	
Upper	Lower
129	0

Energy	Temp.
10	-70
15	-58
20	-50
25	-43

Temp.	Energy
60	120
70	120
80	125
90	125

* Round to nearest 5 ft-lbs

Figure D.6.1: Flange Region Charpy Impact Test Results for Member N5

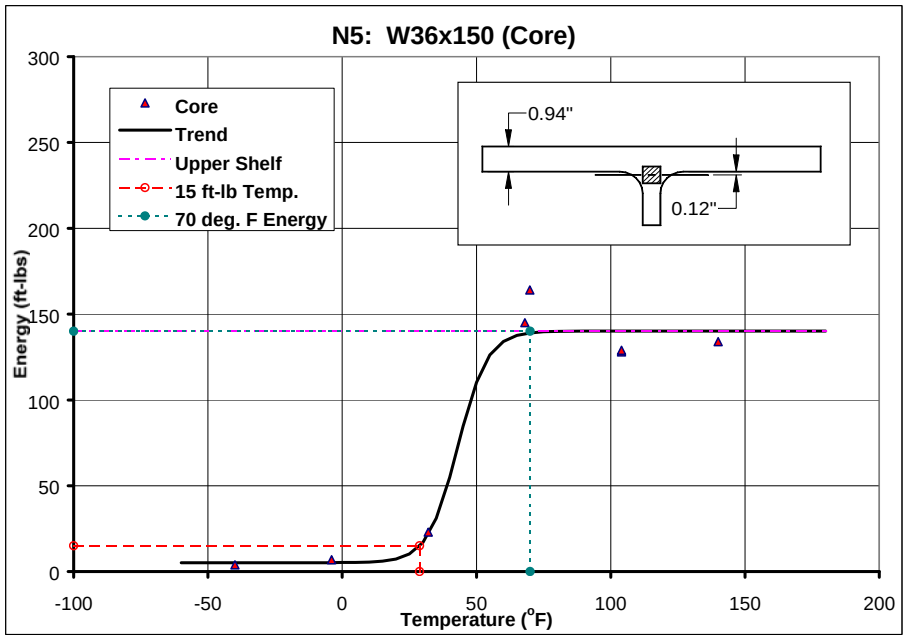

β_1=	73
β_2=	67
β_3=	0.090
β_4=	43

Shelf Energy	
Upper	Lower
140	5

Energy	Temp.
10	25
15	29
20	31
25	33

Temp.	Energy*
60	135
70	140
80	140
90	140

* Round to nearest 5 ft-lbs

Figure D.6.2: Core Region Charpy Impact Test Results for Member N5

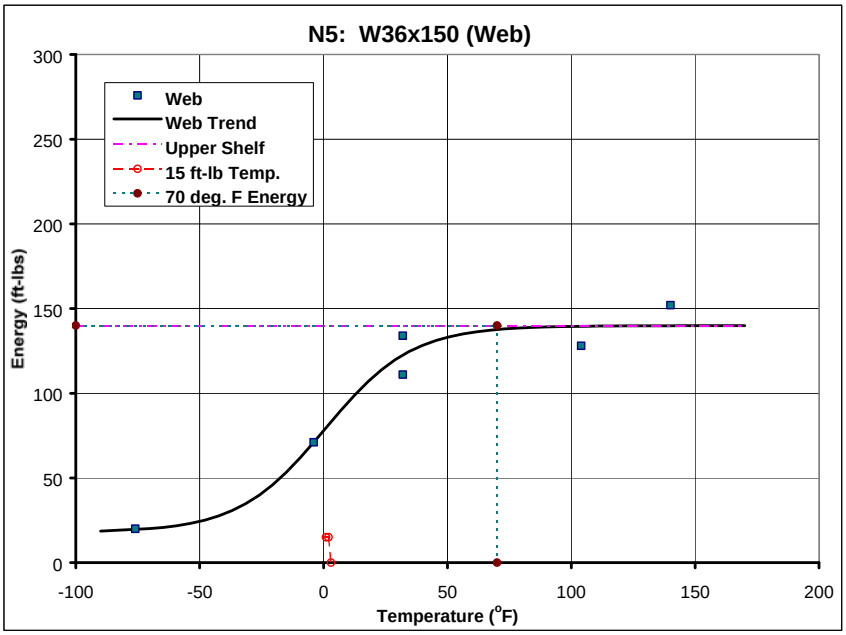

β_1=	79
β_2=	61
β_3=	0.029
β_4=	1

Shelf Energy	
Upper	Lower
140	18

Energy	Temp.
10	<-75
15	<-75
20	-70
25	-48

Temp.	Energy
60	135
70	140
80	140
90	140

* Round to nearest 5 ft-lbs

Figure D.6.3: Web Region Charpy Impact Test Results for Member N5

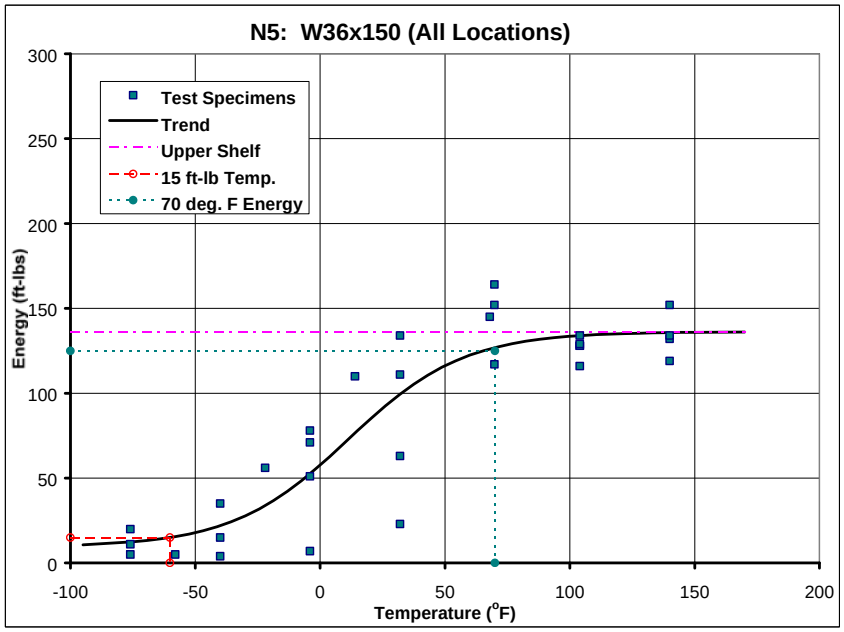

β_1=	73
β_2=	63
β_3=	0.022
β_4=	11

Shelf Energy	
Upper	Lower
136	9

Energy	Temp.
10	<-75
15	-60
20	-44
25	-34

Temp.	Energy*
60	120
70	125
80	130
90	130

* Round to nearest 5 ft-lbs

Figure D.6.4: All Charpy Impact Test Results for Member N5

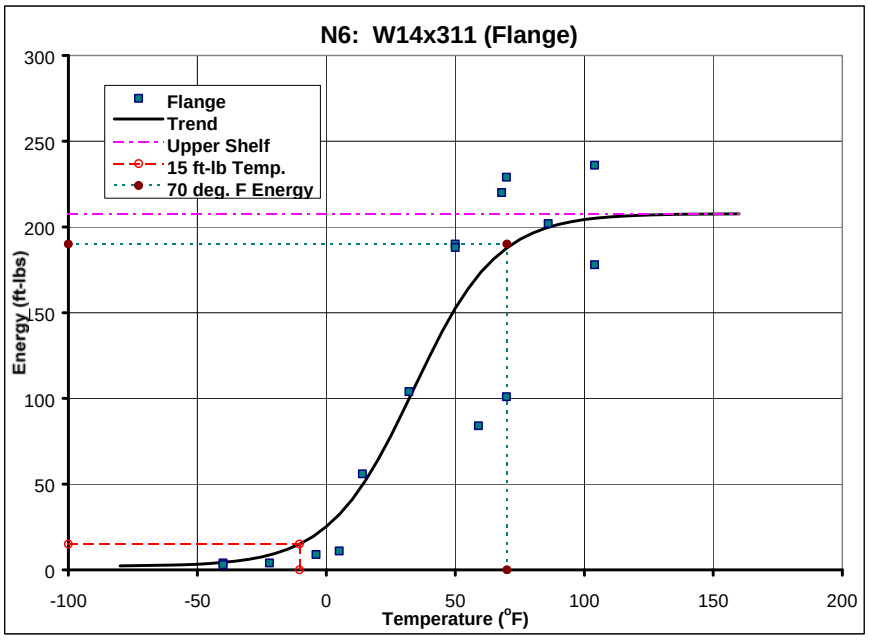

β_1= 105
β_2= 103
β_3= 0.031
β_4= 34

Shelf Energy	
Upper	Lower
208	2

Energy	Temp.
10	-19
15	-10
20	-5
25	0

Temp.	Energy
60	175
70	190
80	195
90	200

* Round to nearest 5 ft-lbs

Figure D.7.1: Flange Region Charpy Impact Test Results for Member N6

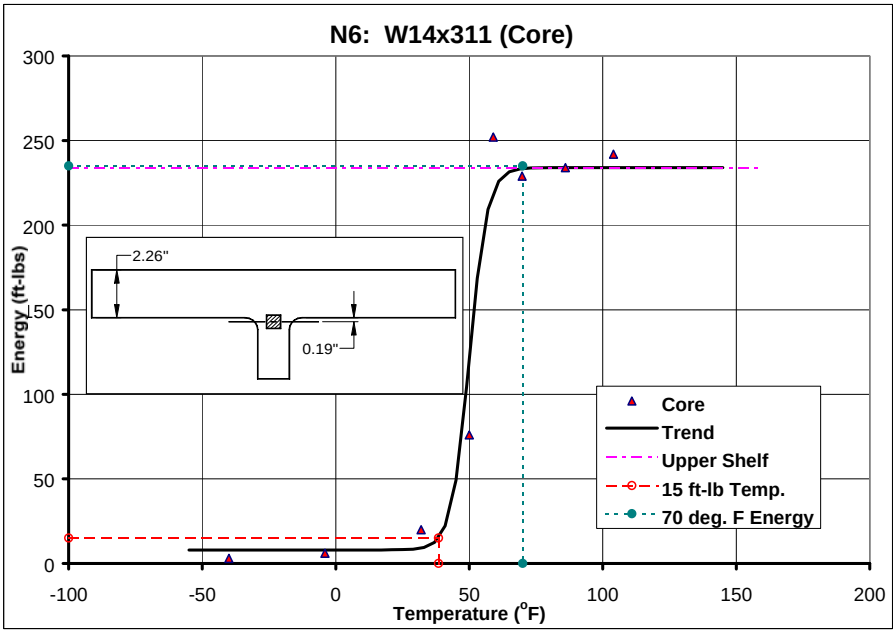

β_1= 121
β_2= 113
β_3= 0.150
β_4= 50

Shelf Energy	
Upper	Lower
234	8

Energy	Temp.
10	34
15	39
20	40
25	42

Temp.	Energy*
60	225
70	235
80	235
90	235

* Round to nearest 5 ft-lbs

Figure D.7.2: Core Region Charpy Impact Test Results for Member N6

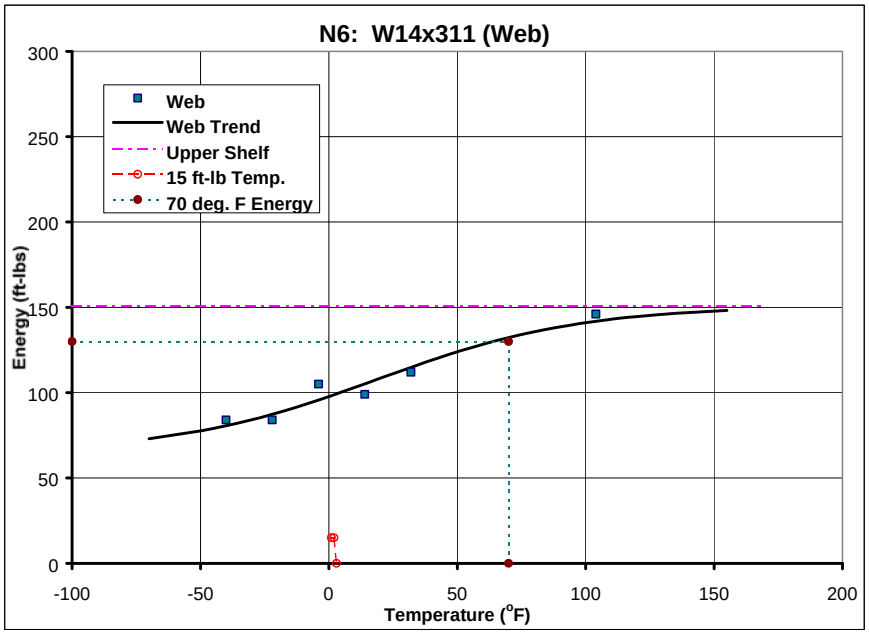

β_1=	108
β_2=	43
β_3=	0.013
β_4=	19

Shelf Energy	
Upper	Lower
151	65

Energy	Temp.
10	<-40
15	<-40
20	<-40
25	<-40

Temp.	Energy
60	130
70	130
80	135
90	140

* Round to nearest 5 ft-lbs

Figure D.7.3: Web Region Charpy Impact Test Results for Member N6

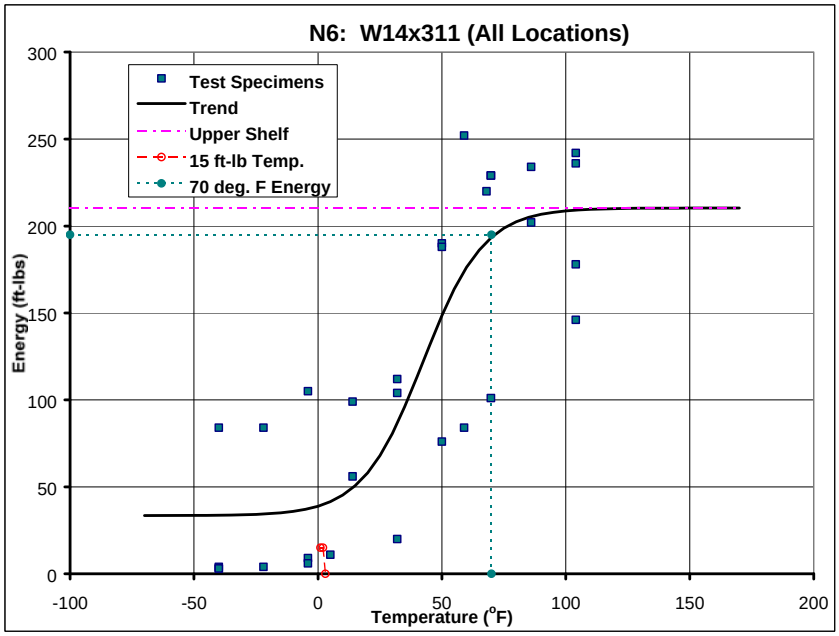

β_1=	122
β_2=	88
β_3=	0.041
β_4=	42

Shelf Energy	
Upper	Lower
210	33

Energy	Temp.
10	<-40
15	<-40
20	<-40
25	<-40

Temp.	Energy*
60	175
70	195
80	200
90	205

* Round to nearest 5 ft-lbs

Figure D.7.4: All Charpy Impact Test Results for Member N6

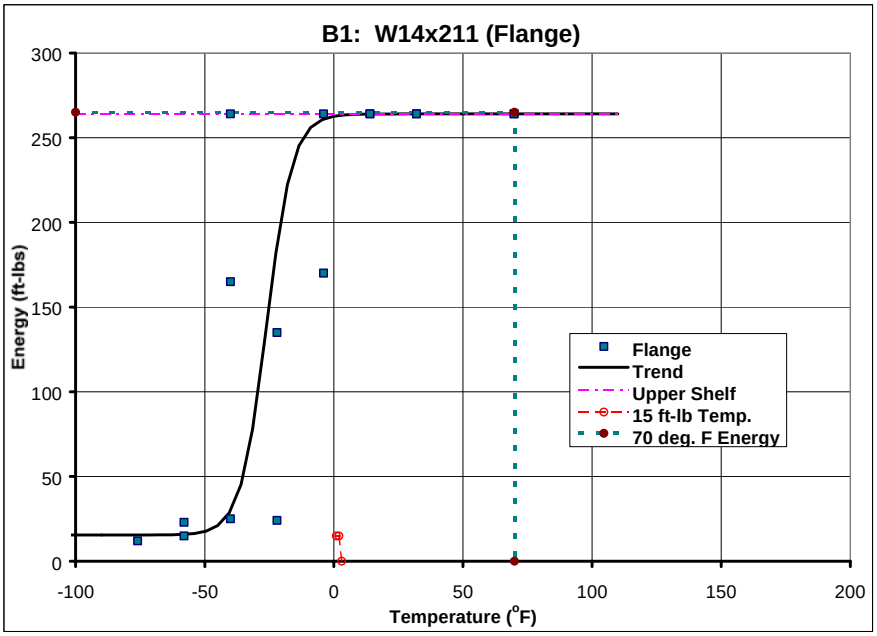

β_1=	140
β_2=	124
β_3=	0.10
β_4=	-26

Shelf Energy	
Upper	Lower
264	15

Energy	Temp.
10	<-75
15	<-75
20	-46
25	-42

Temp.	Energy
60	265
70	265
80	265
90	265

* Round to nearest 5 ft-lbs

Figure D.8.1: Flange Region Charpy Impact Test Results for Member B1

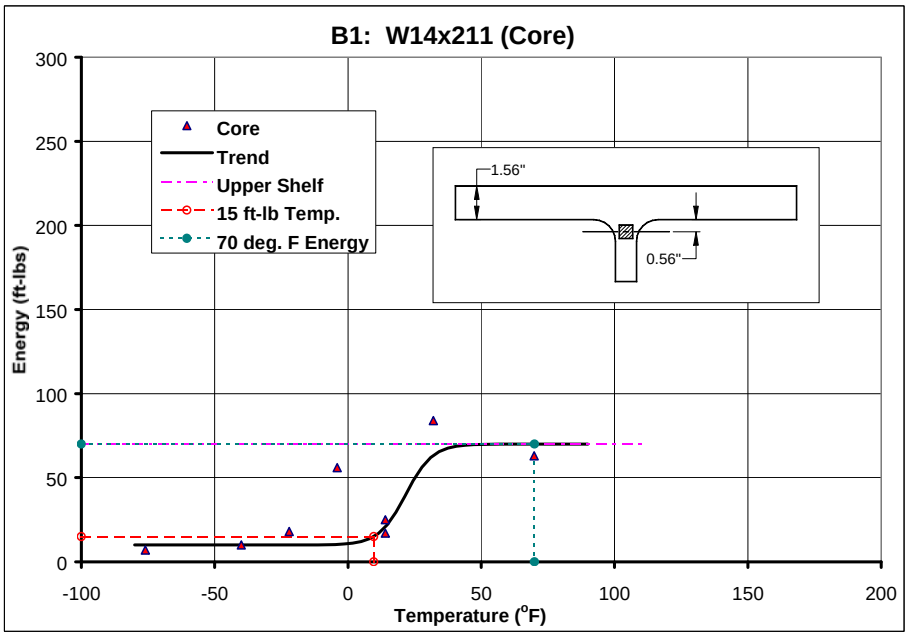

β_1=	40
β_2=	30
β_3=	0.10
β_4=	22

Shelf Energy	
Upper	Lower
70	10

Energy	Temp.
10	<-75
15	10
20	14
25	16

Temp.	Energy*
60	70
70	70
80	70
90	70

* Round to nearest 5 ft-lbs

Figure D.8.2: Core Region Charpy Impact Test Results for Member B1

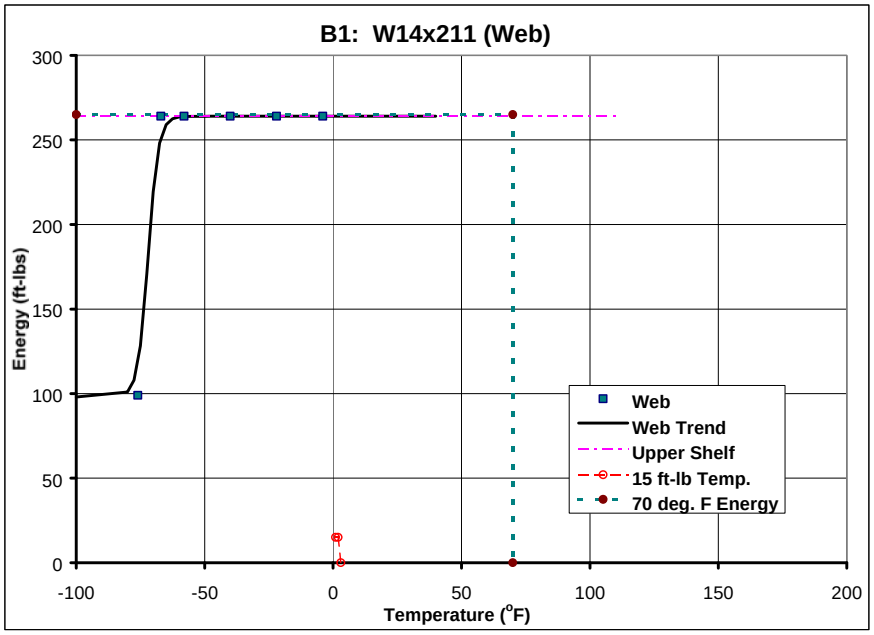

β_1= 181
β_2= 83
β_3= 0.25
β_4= -72

Shelf Energy	
Upper	Lower
264	98

Energy	Temp.
10	<-75
15	<-75
20	<-75
25	<-75

Temp.	Energy
60	265
70	265
80	265
90	265

* Round to nearest 5 ft-lbs

Figure D.8.3: Web Region Charpy Impact Test Results for Member B1

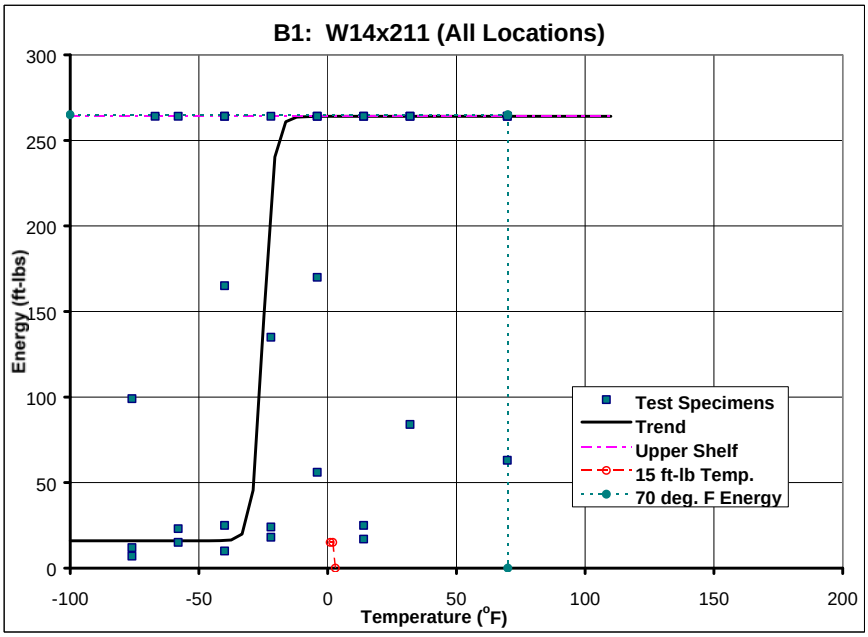

β_1= 140
β_2= 124
β_3= 0.25
β_4= -25

Shelf Energy	
Upper	Lower
264	16

Energy	Temp.
10	<-75
15	<-75
20	-33
25	-32

Temp.	Energy*
60	265
70	265
80	265
90	265

* Round to nearest 5 ft-lbs

Figure D.8.4: All Charpy Impact Test Results for Member B1

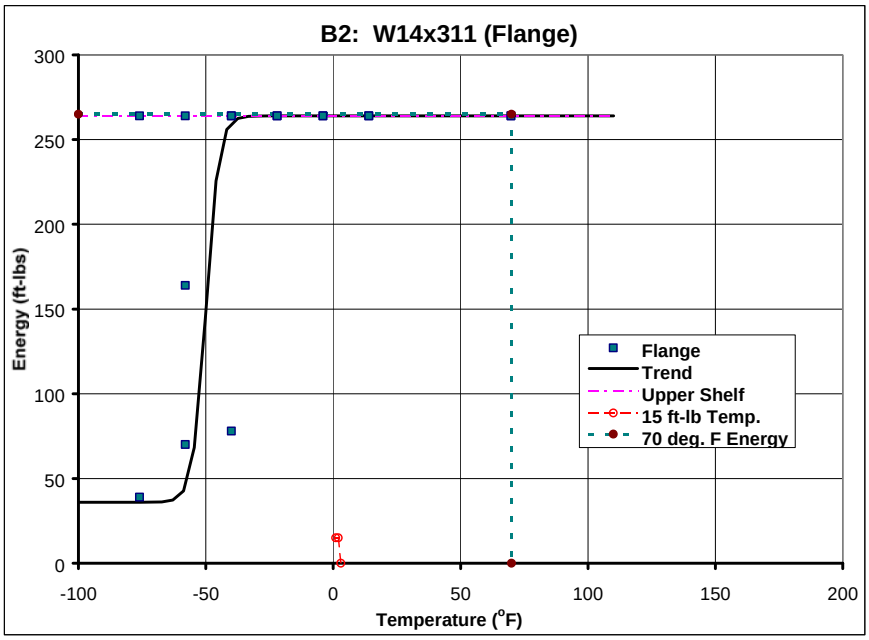

β_1= 150
β_2= 114
β_3= 0.20
β_4= -50

Shelf Energy	
Upper	Lower
264	36

Energy	Temp.
10	<-75
15	<-75
20	<-75
25	<-75

Temp.	Energy
60	265
70	265
80	265
90	265

* Round to nearest 5 ft-lbs

Figure D.9.1: Flange Region Charpy Impact Test Results for Member B2

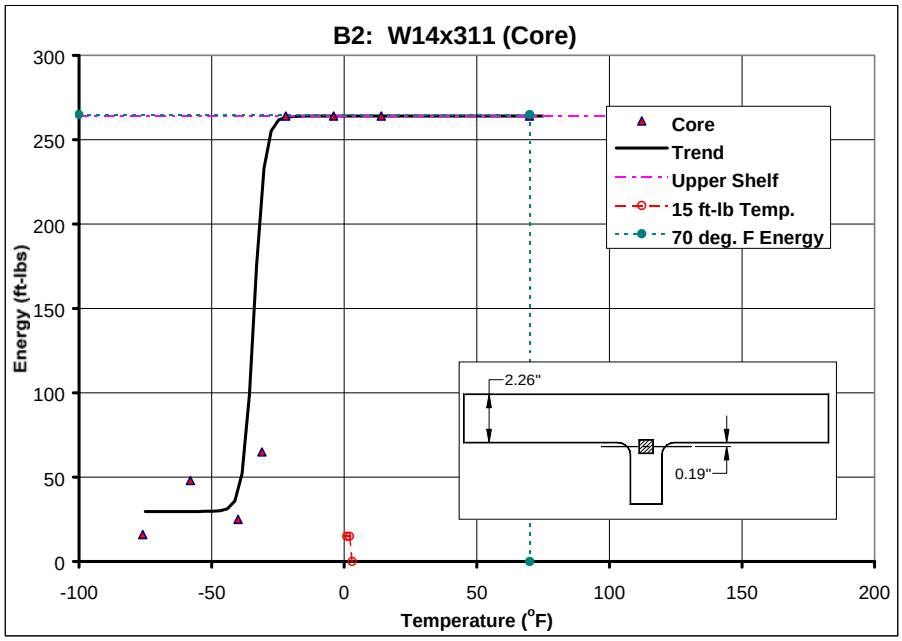

β_1= 147
β_2= 117
β_3= 0.25
β_4= -34

Shelf Energy	
Upper	Lower
264	30

Energy	Temp.
10	<-60
15	<-60
20	<-60
25	<-60

Temp.	Energy*
60	265
70	265
80	265
90	265

* Round to nearest 5 ft-lbs

Figure D.9.2: Core Region Charpy Impact Test Results for Member B2

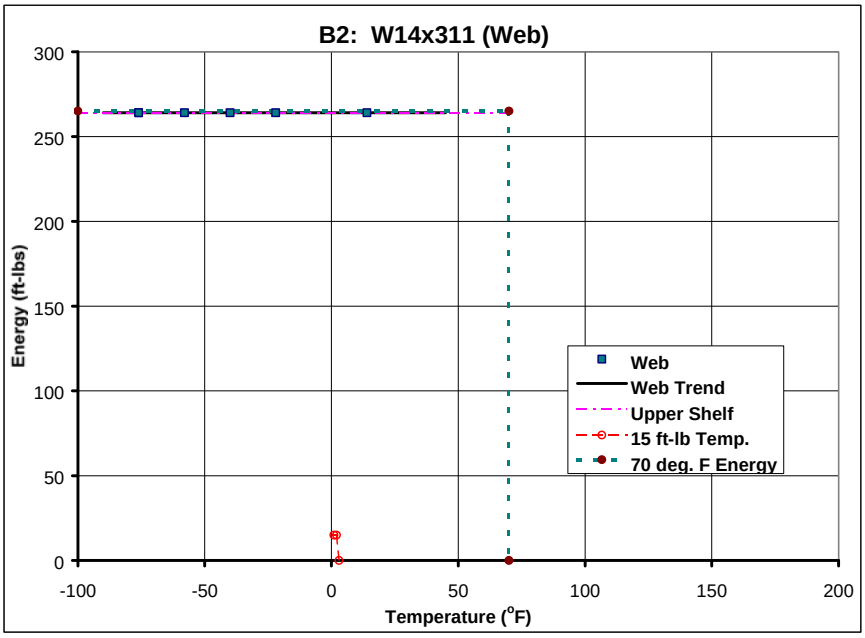

β_1=	264
β_2=	0.00
β_3=	0.00
β_4=	-75

Shelf Energy	
Upper	Lower
264	264

Energy	Temp.
10	<-75
15	<-75
20	<-75
25	<-75

Temp.	Energy
60	265
70	265
80	265
90	265

* Round to nearest 5 ft-lbs

Figure D.9.3: Web Region Charpy Impact Test Results for Member B2

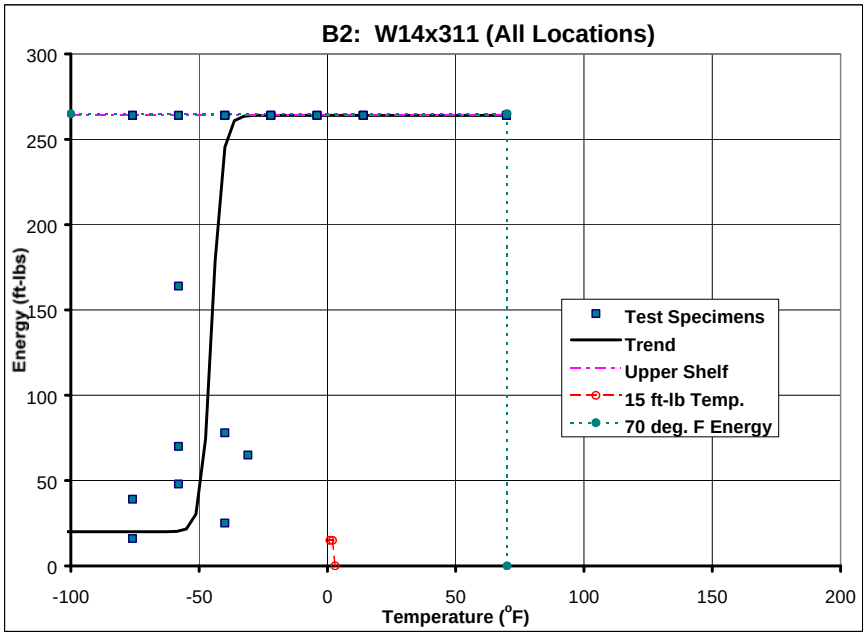

β_1=	142
β_2=	122
β_3=	0.25
β_4=	-45

Shelf Energy	
Upper	Lower
264	20

Energy	Temp.
10	<-75
15	<-75
20	<-75
25	-53

Temp.	Energy*
60	265
70	265
80	265
90	265

* Round to nearest 5 ft-lbs

Figure D.9.4: All Charpy Impact Test Results for Member B2

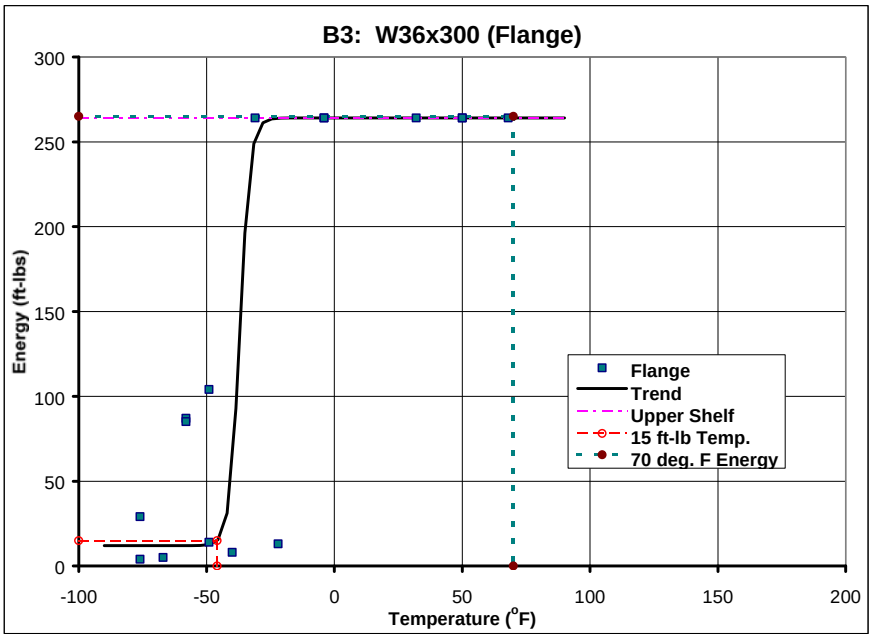

β_1=	138
β_2=	126
β_3=	0.25
β_4=	-37

Shelf Energy	
Upper	Lower
264	12

Energy	Temp.
10	<-75
15	-46
20	-44
25	-43

Temp.	Energy
60	265
70	265
80	265
90	265

* Round to nearest 5 ft-lbs

Figure D.10.1: Flange Region Charpy Impact Test Results for Member B3

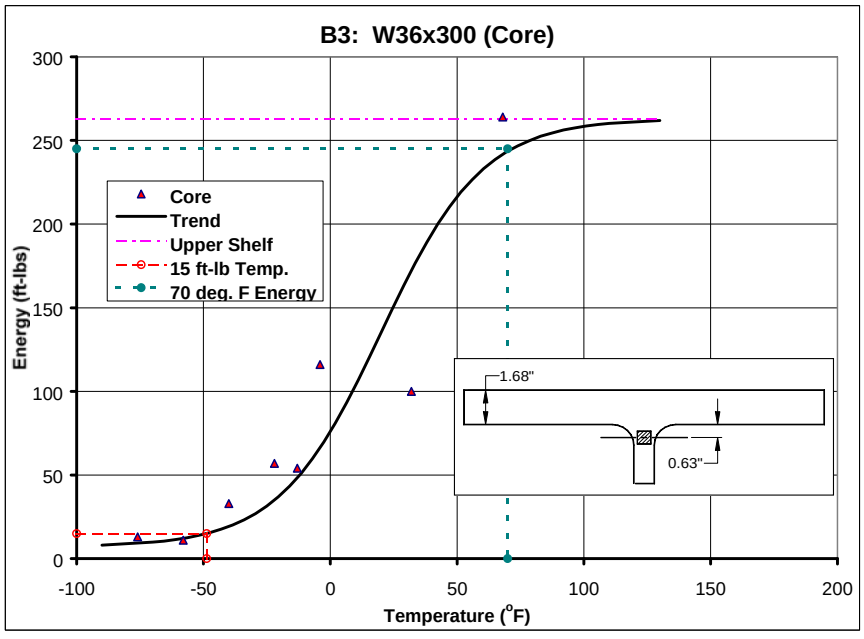

β_1=	135
β_2=	128
β_3=	0.025
β_4=	20

Shelf Energy	
Upper	Lower
263	7

Energy	Temp.
10	-69
15	-49
20	-39
25	-32

Temp.	Energy*
60	230
70	245
80	250
90	255

* Round to nearest 5 ft-lbs

Figure D.10.2: Core Region Charpy Impact Test Results for Member B3

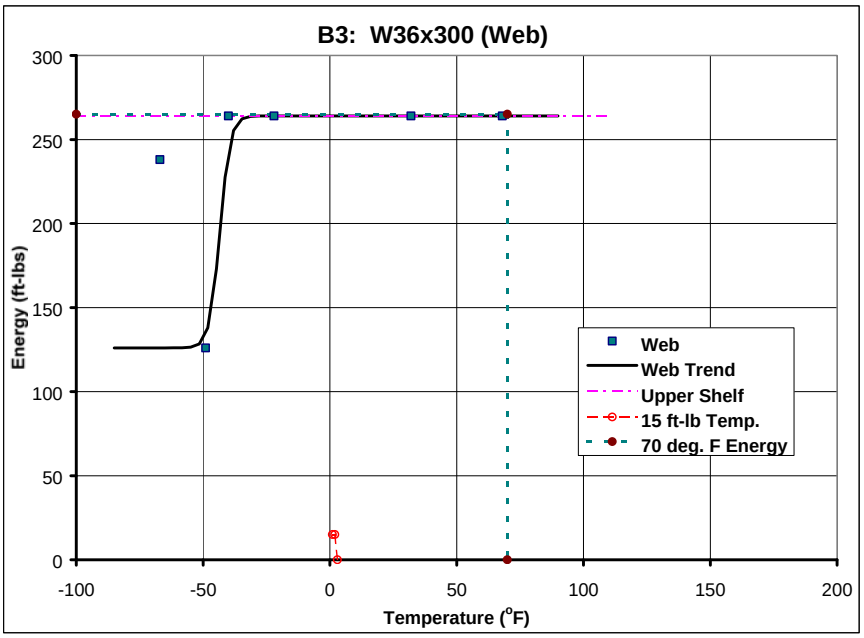

β_1=	195
β_2=	69
β_3=	0.25
β_4=	-43

Shelf Energy	
Upper	Lower
264	126

Energy	Temp.
10	<-70
15	<-70
20	<-70
25	<-70

Temp.	Energy
60	265
70	265
80	265
90	265

* Round to nearest 5 ft-lbs

Figure D.10.3: Web Region Charpy Impact Test Results for Member B3

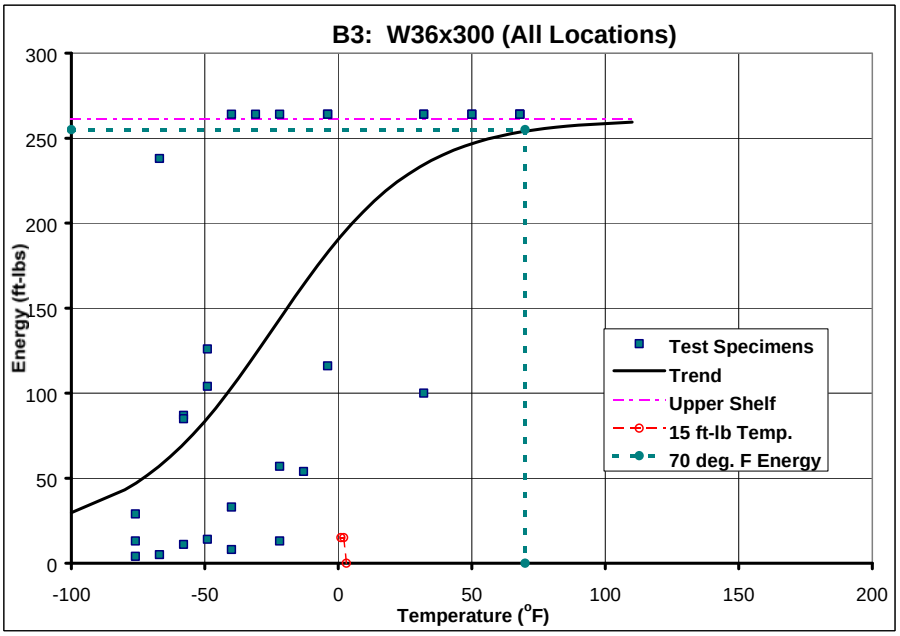

β_1=	139
β_2=	122
β_3=	0.019
β_4=	-24

Shelf Energy	
Upper	Lower
261	16

Energy	Temp.
10	<-75
15	<-75
20	<-75
25	<-75

Temp.	Energy*
60	250
70	255
80	255
90	260

* Round to nearest 5 ft-lbs

Figure D.10.4: All Charpy Impact Test Results for Member B3

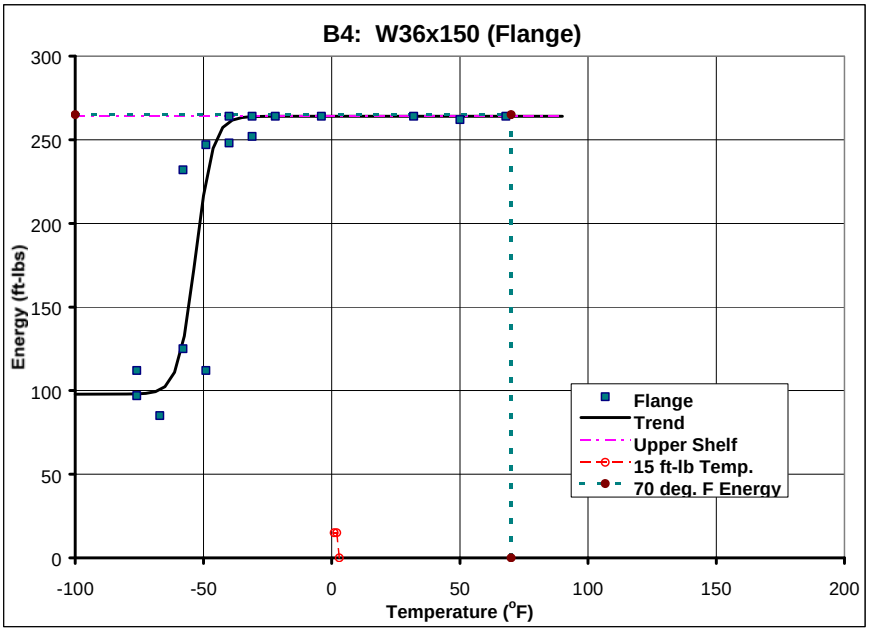

β_1= 181
β_2= 83
β_3= 0.15
β_4= -53

Shelf Energy	
Upper	Lower
264	98

Energy	Temp.
10	<-75
15	<-75
20	<-75
25	<-75

Temp.	Energy
60	265
70	265
80	265
90	265

* Round to nearest 5 ft-lbs

Figure D.11.1: Flange Region Charpy Impact Test Results for Member B4

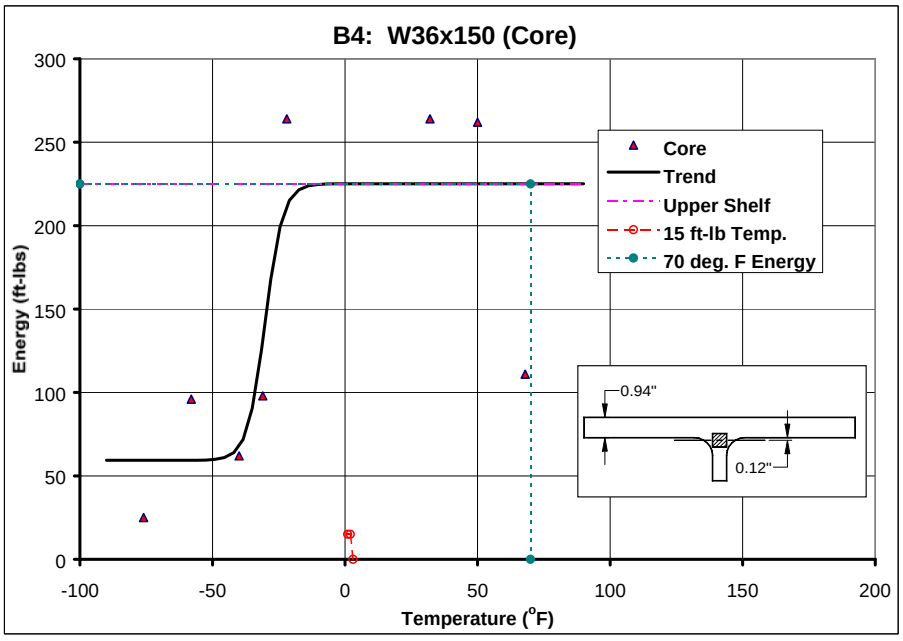

β_1= 142
β_2= 83
β_3= 0.15
β_4= -30

Shelf Energy	
Upper	Lower
225	59

Energy	Temp.
10	<-75
15	<-75
20	<-75
25	<-75

Temp.	Energy*
60	225
70	225
80	225
90	225

* Round to nearest 5 ft-lbs

Figure D.11.2: Core Region Charpy Impact Test Results for Member B4

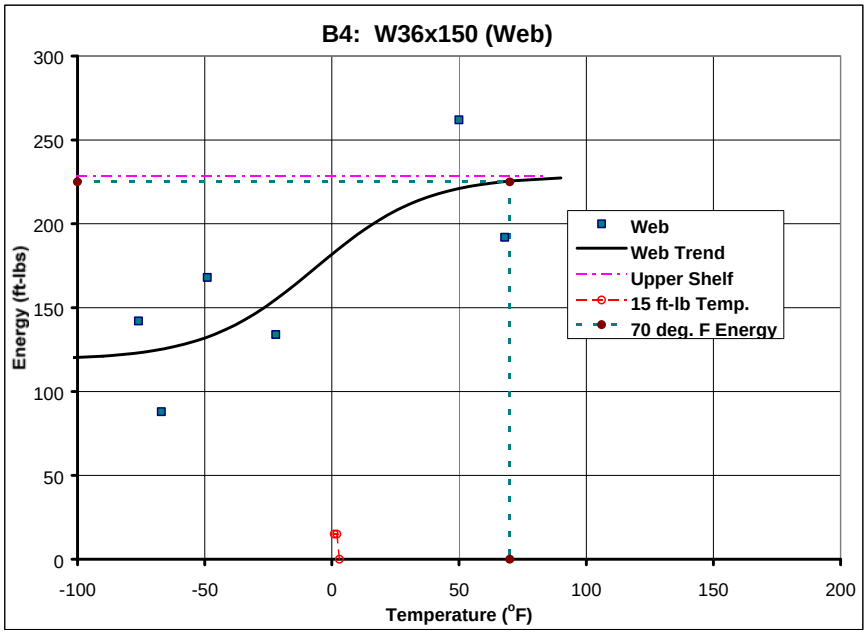

β_1=	174
β_2=	55
β_3=	0.023
β_4=	-6

Shelf Energy	
Upper	Lower
229	119

Energy	Temp.
10	<-75
15	<-75
20	<-75
25	<-75

Temp.	Energy
60	225
70	225
80	225
90	225

* Round to nearest 5 ft-lbs

Figure D.11.3: Web Region Charpy Impact Test Results for Member B4

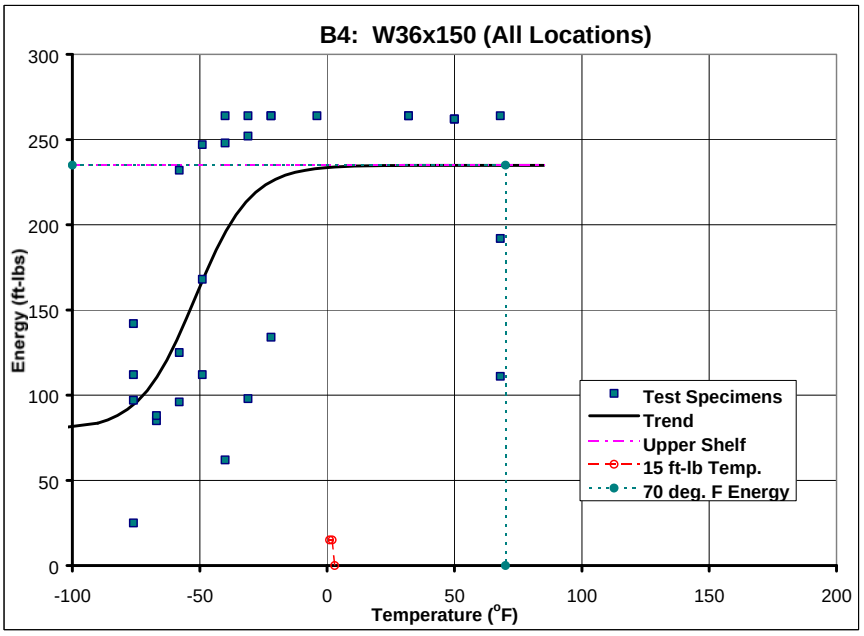

β_1=	157
β_2=	78
β_3=	0.046
β_4=	-52

Shelf Energy	
Upper	Lower
235	79

Energy	Temp.
10	<-75
15	<-75
20	<-75
25	<-75

Temp.	Energy*
60	235
70	235
80	235
90	235

* Round to nearest 5 ft-lbs

Figure D.11.4: All Charpy Impact Test Results for Member B4

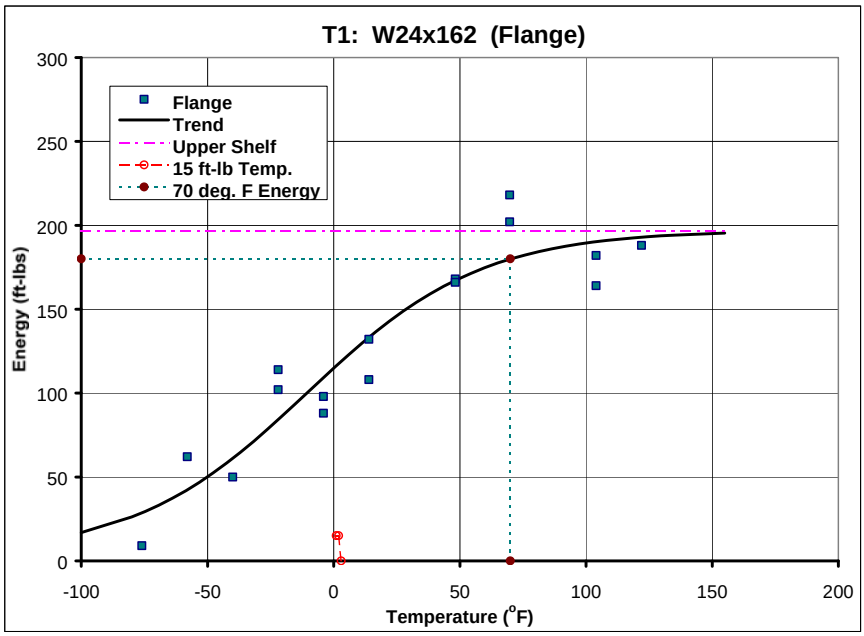

β_1=	100
β_2=	97
β_3=	0.015
β_4=	-10

Shelf Energy	
Upper	Lower
197	4

Energy	Temp.
10	<-75
15	<-75
20	<-75
25	<-75

Temp.	Energy
60	175
70	180
80	185
90	185

* Round to nearest 5 ft-lbs

Figure D.12.1: Flange Region Charpy Impact Test Results for Member T1

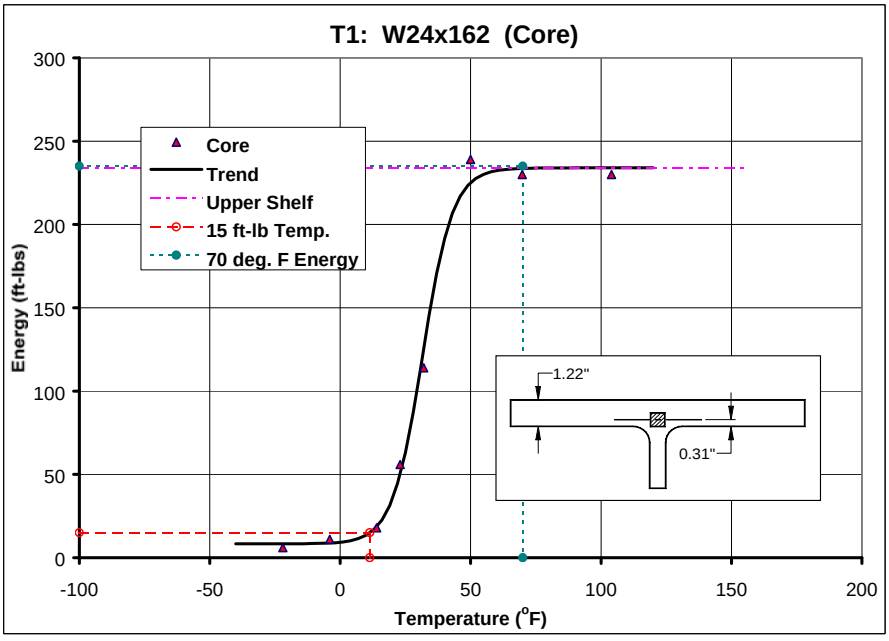

β_1=	121
β_2=	113
β_3=	0.087
β_4=	32

Shelf Energy	
Upper	Lower
234	8

Energy	Temp.
10	3
15	11
20	15
25	17

Temp.	Energy*
60	230
70	235
80	235
90	235

* Round to nearest 5 ft-lbs

Figure D.12.2: Core Region Charpy Impact Test Results for Member T1

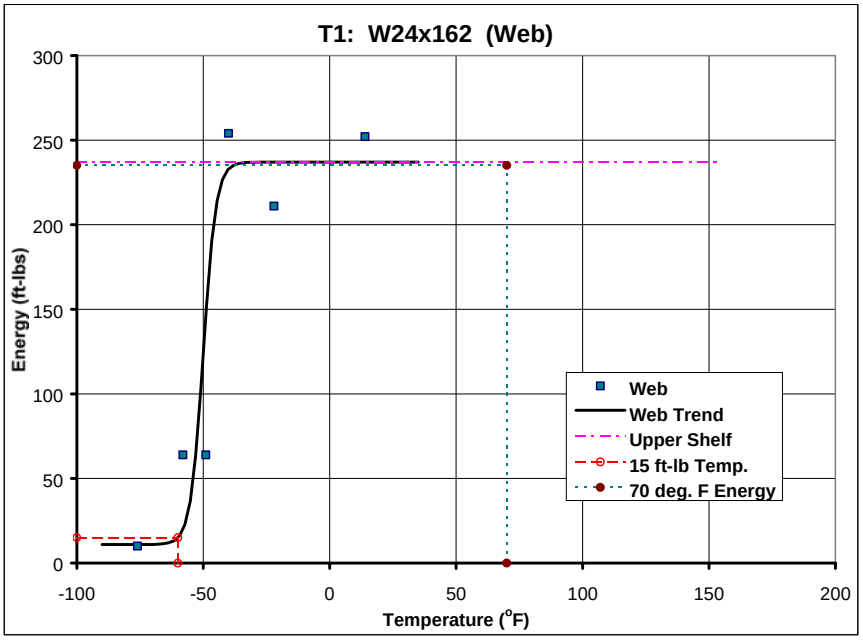

β_1=	124
β_2=	113
β_3=	0.20
β_4=	-50

Shelf Energy	
Upper	Lower
237	11

Energy	Temp.
10	<-75
15	-60
20	-58
25	-57

Temp.	Energy
60	235
70	235
80	235
90	235

* Round to nearest 5 ft-lbs

Figure D.12.3: Web Region Charpy Impact Test Results for Member T1

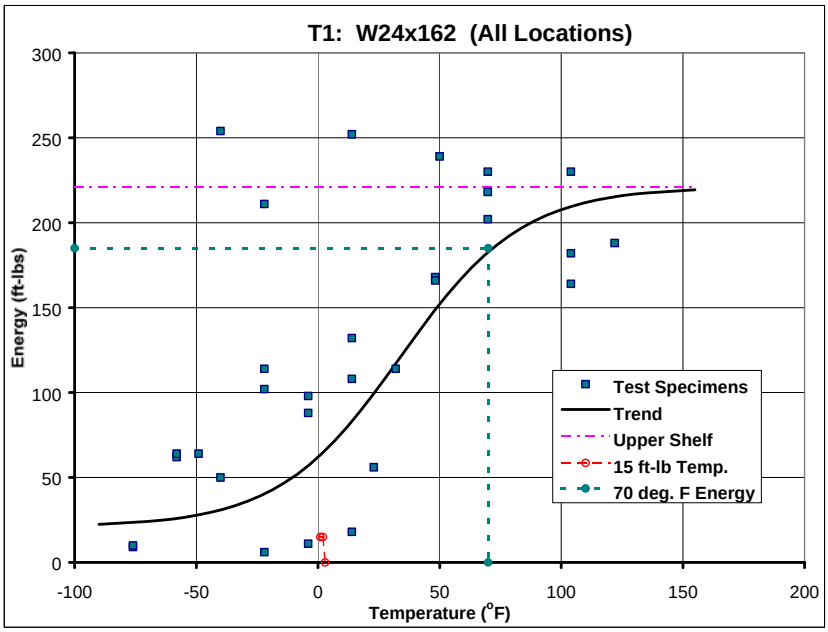

β_1=	121
β_2=	100
β_3=	0.02
β_4=	34

Shelf Energy	
Upper	Lower
221	21

Energy	Temp.
10	<-75
15	<-75
20	<-75
25	-63

Temp.	Energy*
60	170
70	185
80	195
90	200

* Round to nearest 5 ft-lbs

Figure D.12.4: All Charpy Impact Test Results for Member T1

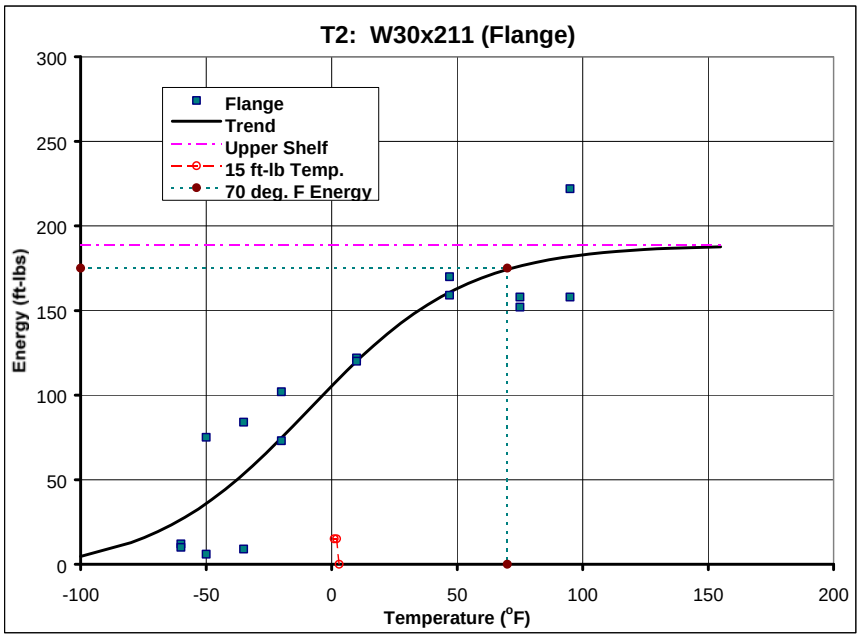

β_1=	92
β_2=	97
β_3=	0.016
β_4=	-9

Shelf Energy	
Upper	Lower
189	-5

Energy	Temp.
10	<-60
15	<-60
20	-68
25	-62

Temp.	Energy
60	170
70	175
80	180
90	180

* Round to nearest 5 ft-lbs

Figure D.13.1: Flange Region Charpy Impact Test Results for Member T2

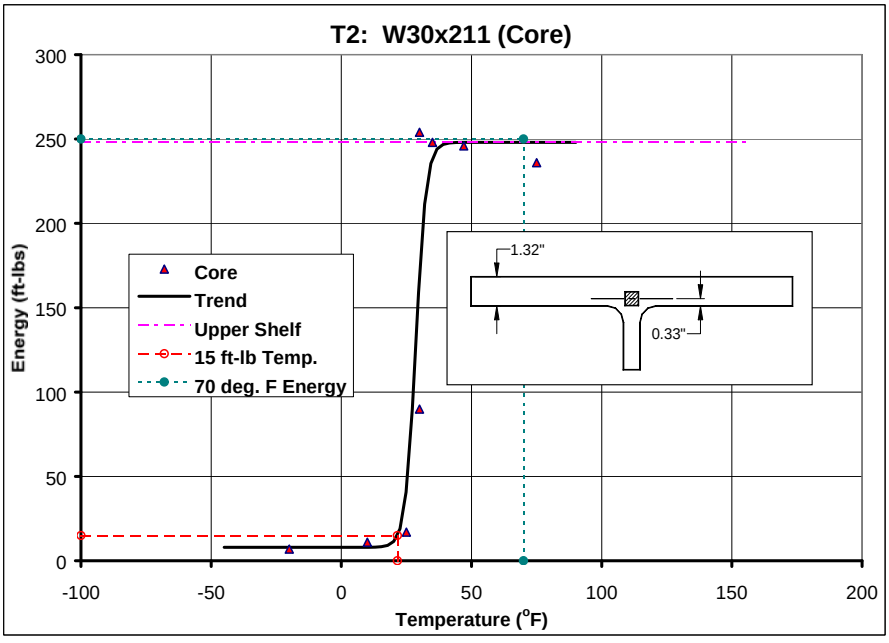

β_1=	128
β_2=	120
β_3=	0.25
β_4=	29

Shelf Energy	
Upper	Lower
248	8

Energy	Temp.
10	19
15	22
20	23
25	23

Temp.	Energy*
60	250
70	250
80	250
90	250

* Round to nearest 5 ft-lbs

Figure D.13.2: Core Region Charpy Impact Test Results for Member T2

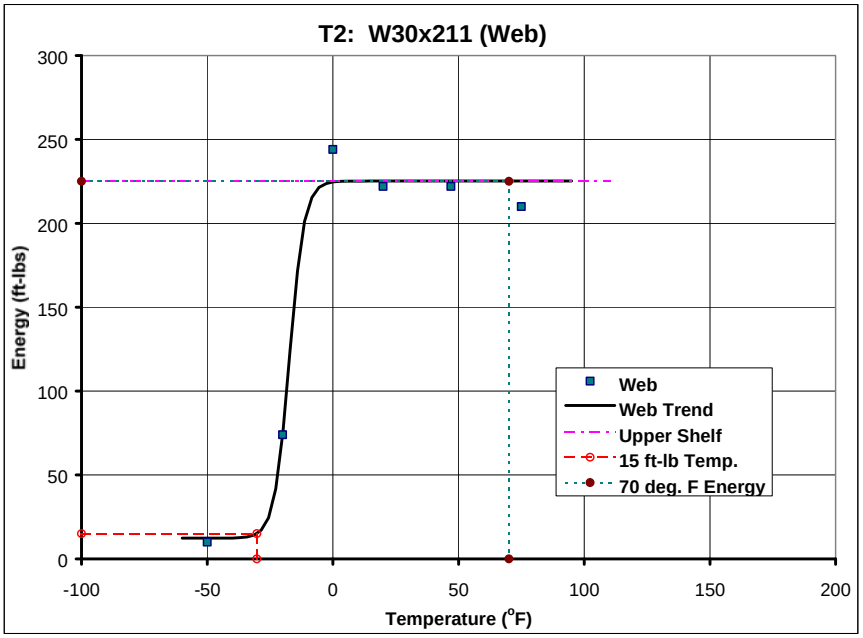

β_1=	119
β_2=	106
β_3=	0.17
β_4=	-17

Shelf Energy	
Upper	Lower
225	12

Energy	Temp.
10	<-75
15	-30
20	-27
25	-25

Temp.	Energy
60	225
70	225
80	225
90	225

* Round to nearest 5 ft-lbs

Figure D.13.3: Web Region Charpy Impact Test Results for Member T2

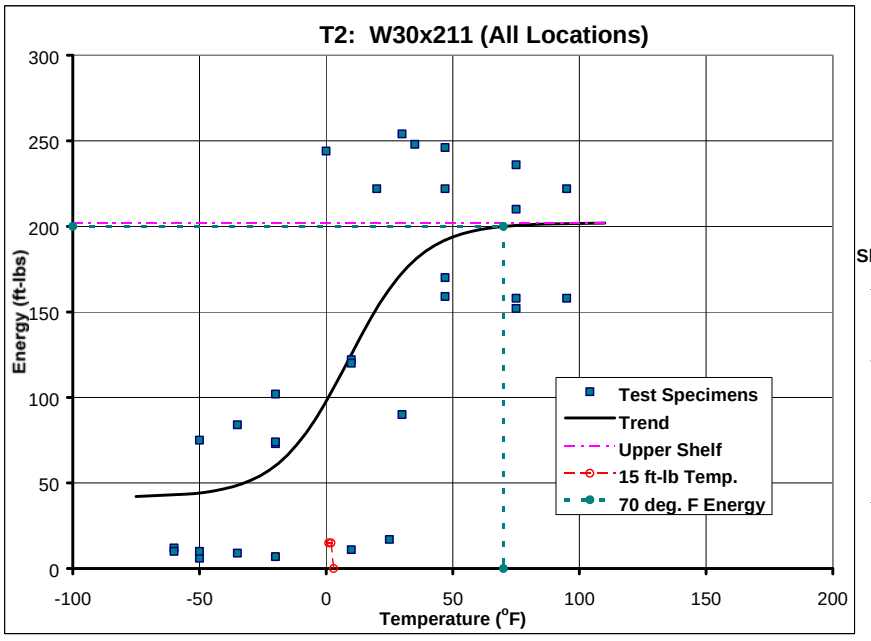

β_1=	122
β_2=	80
β_3=	0.035
β_4=	9

Shelf Energy	
Upper	Lower
202	42

Energy	Temp.
10	<-75
15	<-75
20	<-75
25	<-75

Temp.	Energy*
60	200
70	200
80	200
90	200

* Round to nearest 5 ft-lbs

Figure D.13.4: All Charpy Impact Test Results for Member T2

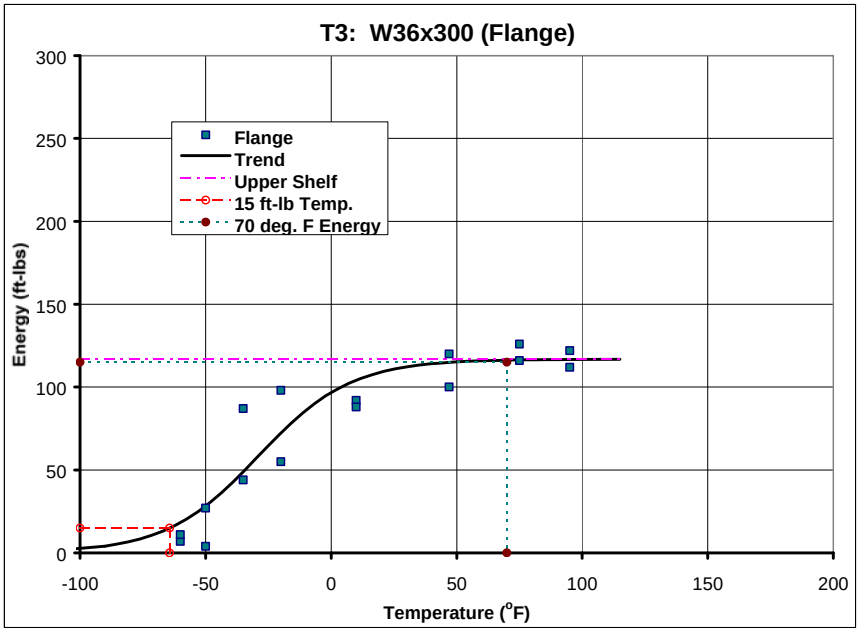

β_1= 58
β_2= 58
β_3= 0.027
β_4= -29

Shelf Energy	
Upper	Lower
117	0

Energy	Temp.
10	-73
15	-64
20	-58
25	-53

Temp.	Energy
60	115
70	115
80	115
90	115

* Round to nearest 5 ft-lbs

Figure D.14.1: Flange Region Charpy Impact Test Results for Member T3

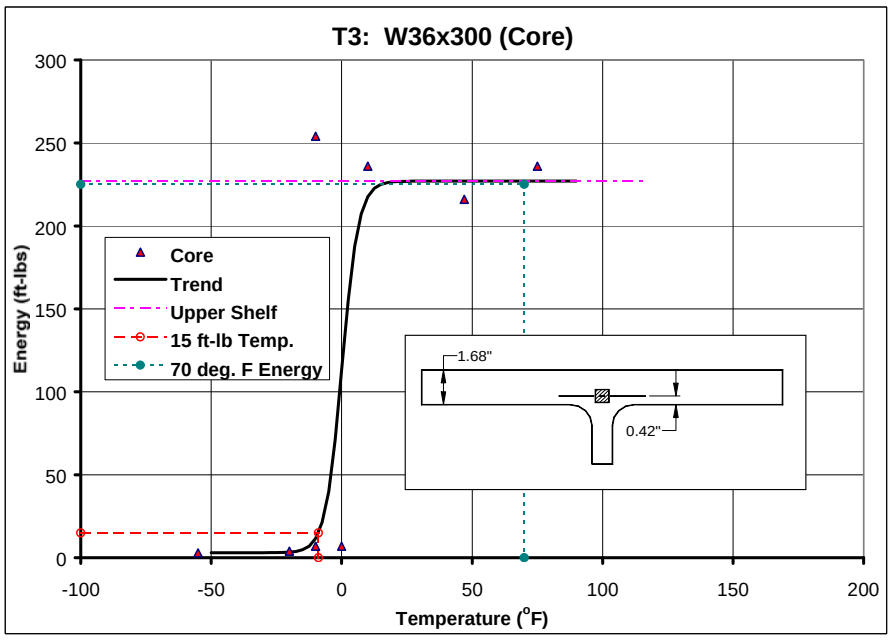

β_1= 115
β_2= 112
β_3= 0.16
β_4= 0

Shelf Energy	
Upper	Lower
227	3

Energy	Temp.
10	-11
15	-9
20	-8
25	-7

Temp.	Energy*
60	225
70	225
80	225
90	225

* Round to nearest 5 ft-lbs

Figure D.14.2: Core Region Charpy Impact Test Results for Member T3

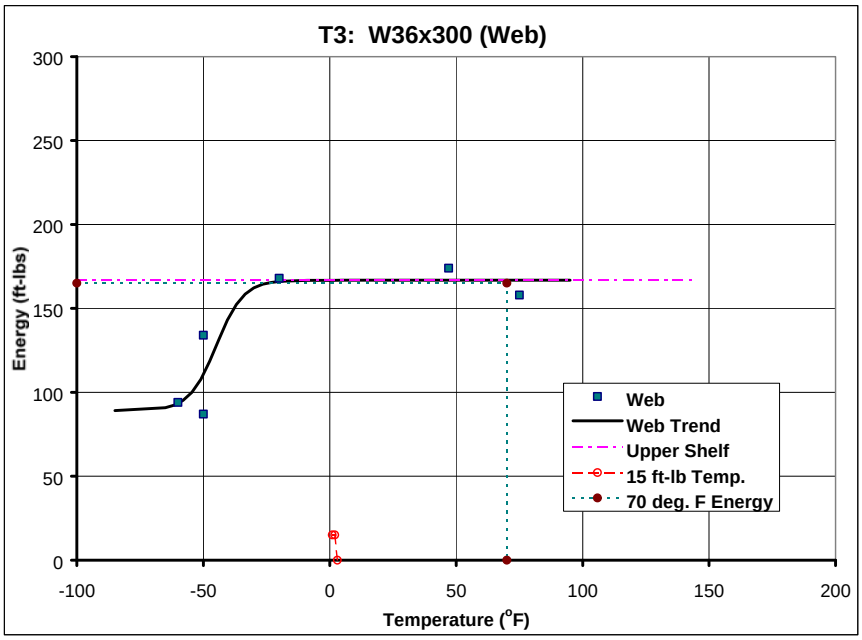

β_1=	128
β_2=	39
β_3=	0.094
β_4=	-45

Shelf Energy	
Upper	Lower
167	89

Energy	Temp.
10	<-60
15	<-60
20	<-60
25	<-60

Temp.	Energy
60	165
70	165
80	165
90	165

* Round to nearest 5 ft-lbs

Figure D.14.3: Web Region Charpy Impact Test Results for Member T3

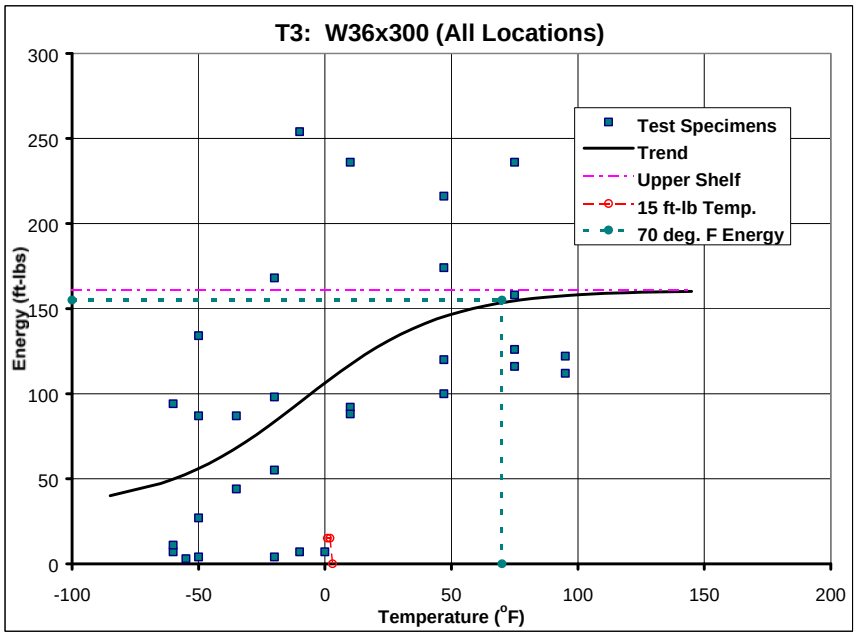

β_1=	96
β_2=	64
β_3=	0.018
β_4=	-9

Shelf Energy	
Upper	Lower
161	32

Energy	Temp.
10	<-60
15	<-60
20	<-60
25	<-60

Temp.	Energy*
60	150
70	155
80	155
90	155

* Round to nearest 5 ft-lbs

Figure D.14.4: All Charpy Impact Test Results for Member T3

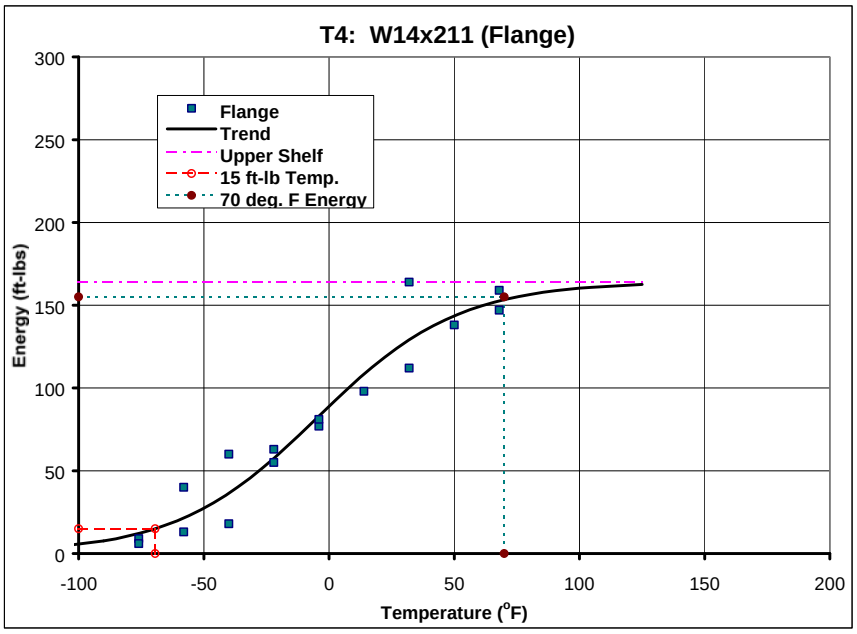

β_1=	82
β_2=	82
β_3=	0.018
β_4=	-5

Shelf Energy	
Upper	Lower
164	0

Energy	Temp.
10	<-75
15	-69
20	-60
25	-53

Temp.	Energy
60	150
70	155
80	155
90	160

* Round to nearest 5 ft-lbs

Figure D.15.1: Flange Region Charpy Impact Test Results for Member T4

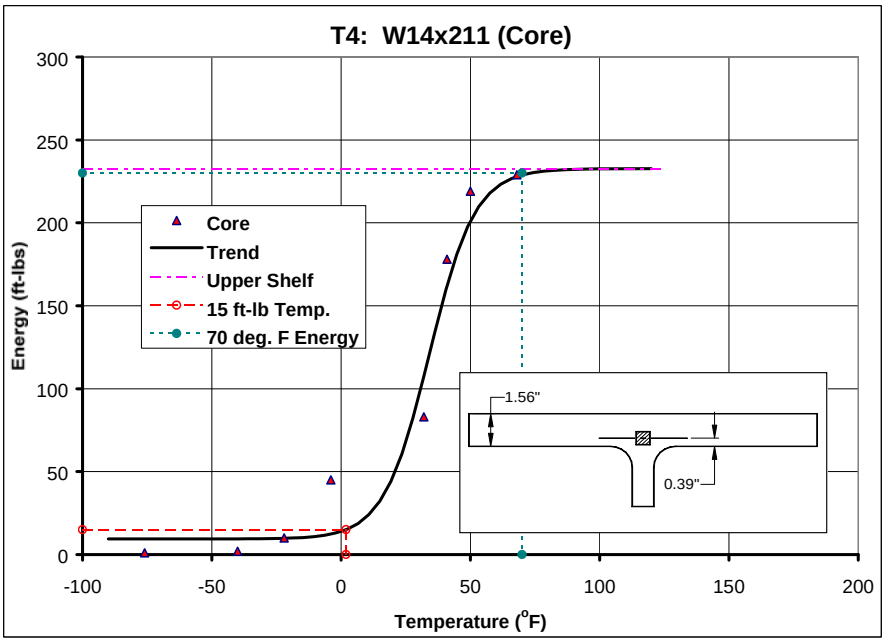

β_1=	121
β_2=	112
β_3=	0.057
β_4=	34

Shelf Energy	
Upper	Lower
233	9

Energy	Temp.
10	-18
15	2
20	8
25	11

Temp.	Energy*
60	220
70	230
80	230
90	230

* Round to nearest 5 ft-lbs

Figure D.15.2: Core Region Charpy Impact Test Results for Member T4

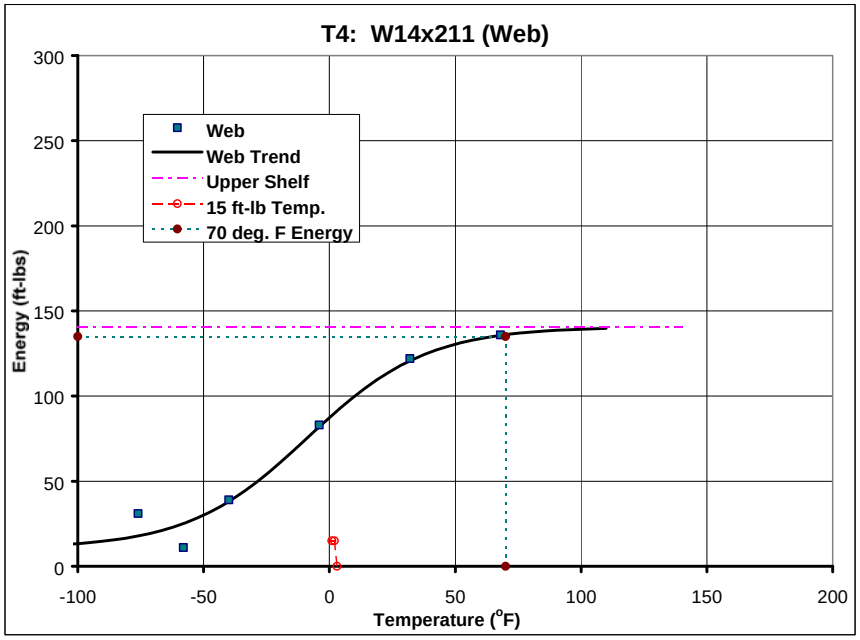

β_1=	76
β_2=	65
β_3=	0.021
β_4=	-9

Shelf Energy	
Upper	Lower
141	11

Energy	Temp.
10	<-75
15	<-75
20	-69
25	-58

Temp.	Energy
60	135
70	135
80	140
90	140

* Round to nearest 5 ft-lbs

Figure D.15.3: Web Region Charpy Impact Test Results for Member T4

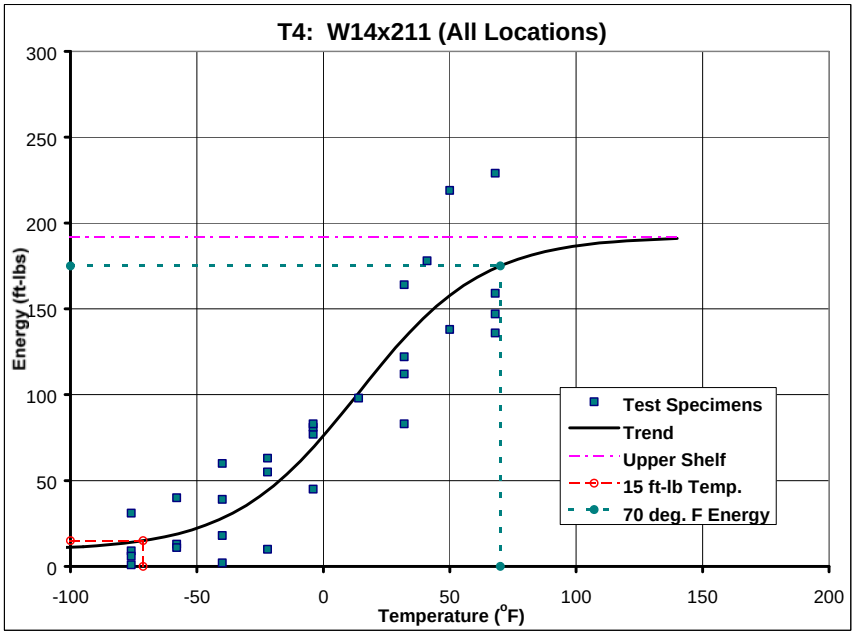

β_1=	101
β_2=	91
β_3=	0.020
β_4=	14

Shelf Energy	
Upper	Lower
192	9

Energy	Temp.
10	<-75
15	-71
20	-55
25	-45

Temp.	Energy*
60	170
70	175
80	180
90	185

* Round to nearest 5 ft-lbs

Figure D.15.4: All Charpy Impact Test Results for Member T4

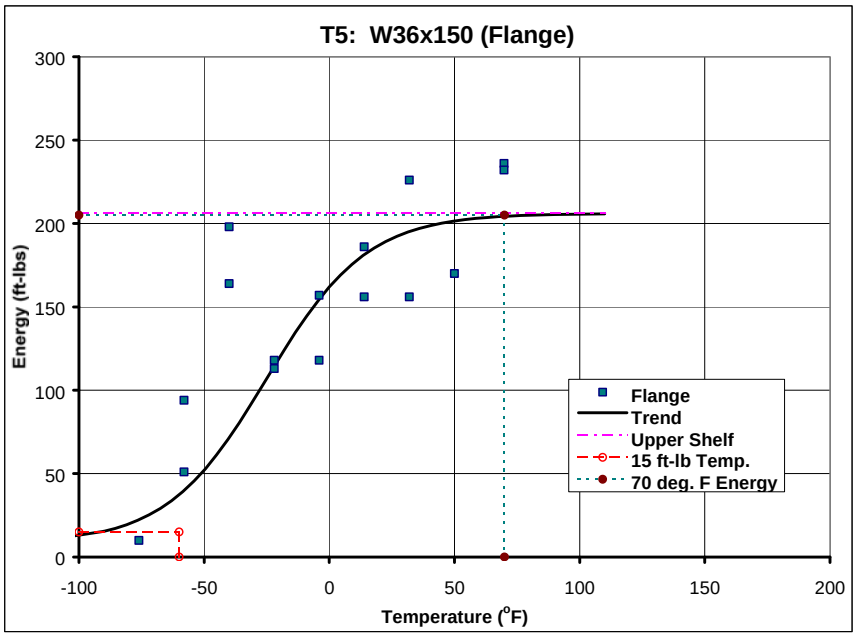

β_1=	107
β_2=	99
β_3=	0.025
β_4=	-25

Shelf Energy	
Upper	Lower
206	8

Energy	Temp.
10	-60
15	-60
20	-60
25	-60

Temp.	Energy
60	205
70	205
80	205
90	205

* Round to nearest 5 ft-lbs

Figure D.16.1: Flange Region Charpy Impact Test Results for Member T5

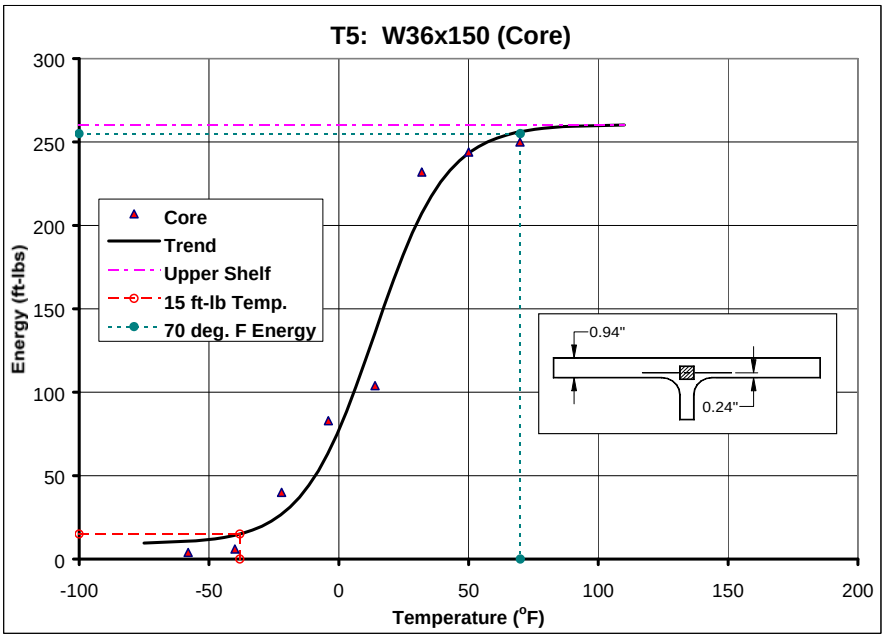

β_1=	135
β_2=	126
β_3=	0.036
β_4=	14

Shelf Energy	
Upper	Lower
260	9

Energy	Temp.
10	<-60
15	-38
20	-29
25	-24

Temp.	Energy*
60	250
70	255
80	260
90	260

* Round to nearest 5 ft-lbs

Figure D.16.2: Core Region Charpy Impact Test Results for Member T5

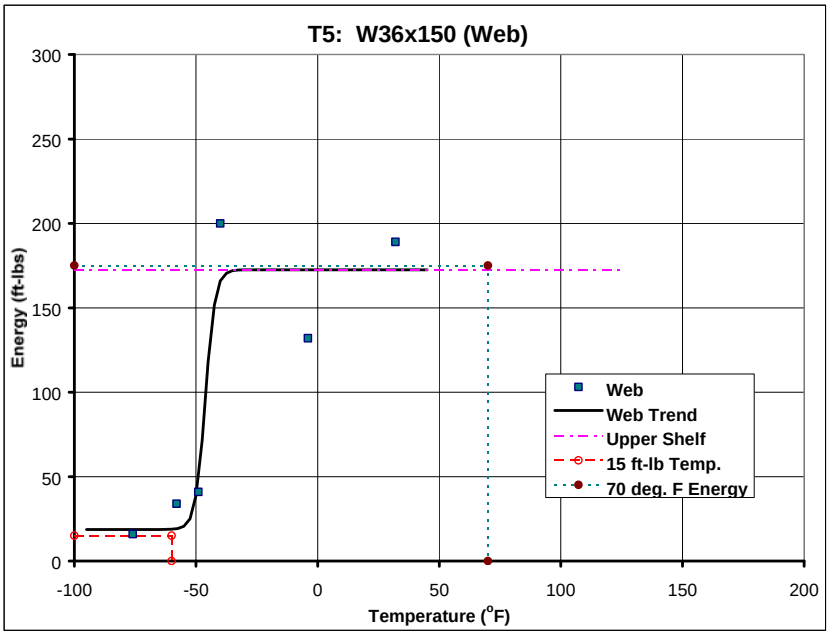

β_1=	96
β_2=	77
β_3=	0.25
β_4=	-46

Shelf Energy	
Upper	Lower
173	19

Energy	Temp.
10	#NUM!
15	-60
20	-56
25	-53

Temp.	Energy
60	175
70	175
80	175
90	175

* Round to nearest 5 ft-lbs

Figure D.16.3: Web Region Charpy Impact Test Results for Member T5

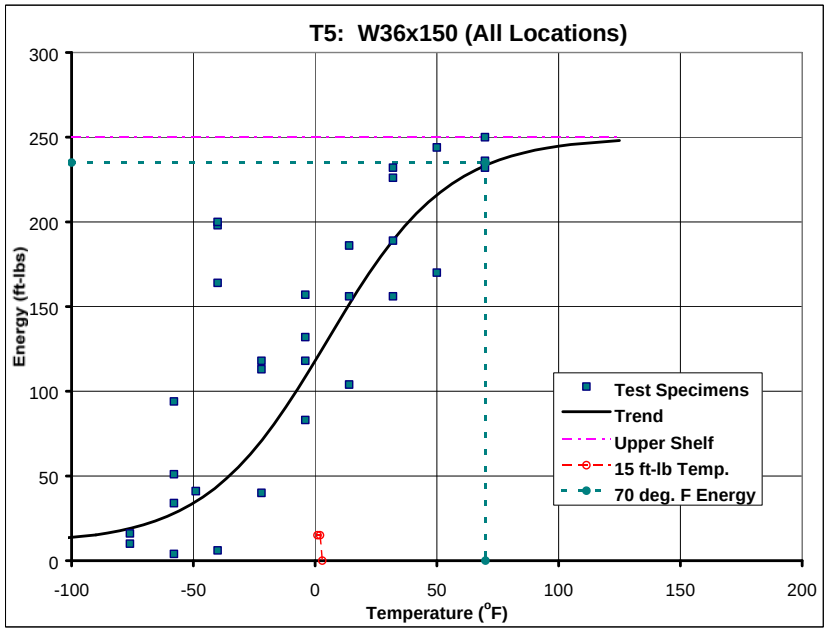

β_1=	130
β_2=	120
β_3=	0.02
β_4=	5

Shelf Energy	
Upper	Lower
250	10

Energy	Temp.
10	<-75
15	<-75
20	-73
25	-63

Temp.	Energy*
60	225
70	235
80	240
90	240

* Round to nearest 5 ft-lbs

Figure D.16.4: All Charpy Impact Test Results for Member T5

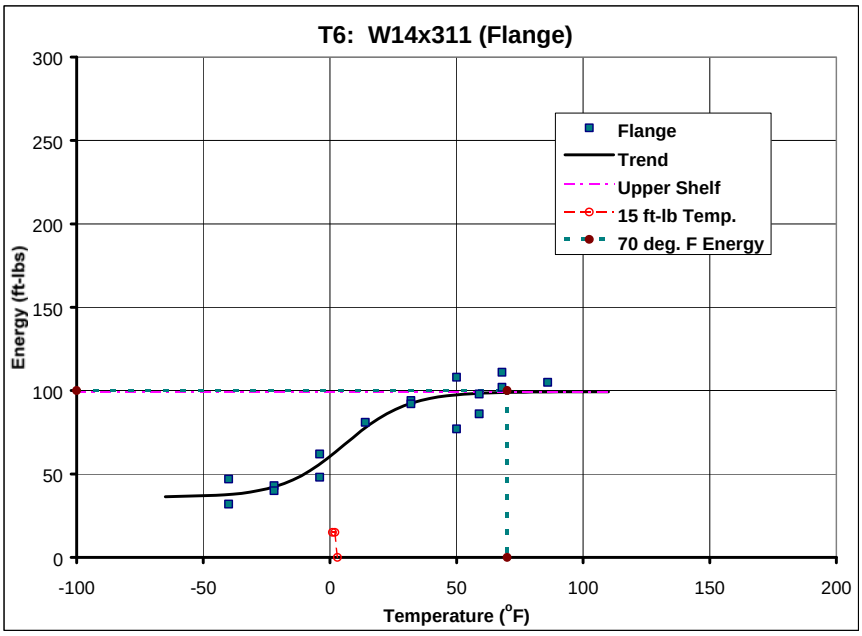

β_1=	68
β_2=	32
β_3=	0.040
β_4=	6

Shelf Energy	
Upper	Lower
99	36

Energy	Temp.
10	<-40
15	<-40
20	<-40
25	<-40

Temp.	Energy
60	100
70	100
80	100
90	100

* Round to nearest 5 ft-lbs

Figure D.17.1: Flange Region Charpy Impact Test Results for Member T6

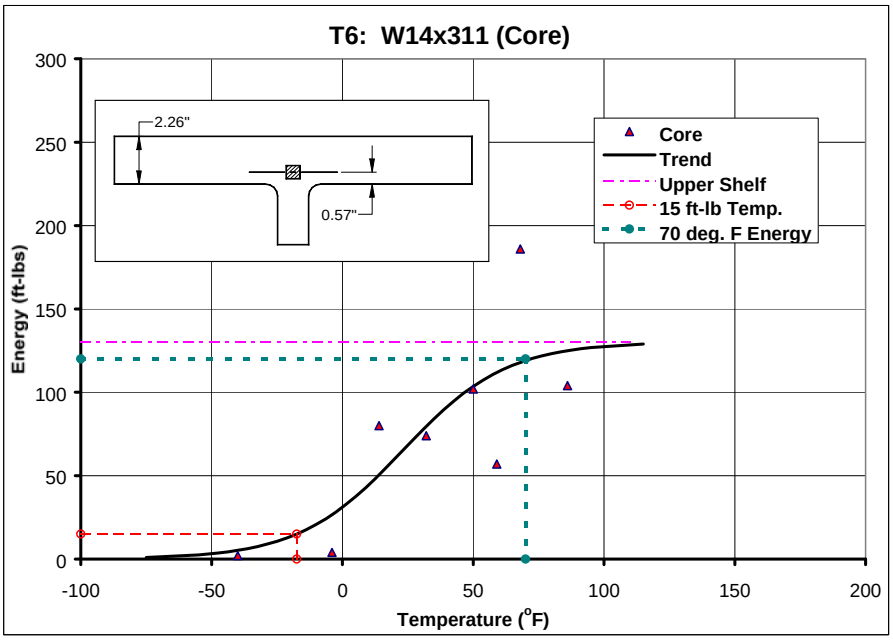

β_1=	65
β_2=	65
β_3=	0.025
β_4=	23

Shelf Energy	
Upper	Lower
130	0

Energy	Temp.
10	-26
15	-17
20	-11
25	-6

Temp.	Energy*
60	115
70	120
80	125
90	125

* Round to nearest 5 ft-lbs

Figure D.17.2: Core Region Charpy Impact Test Results for Member T6

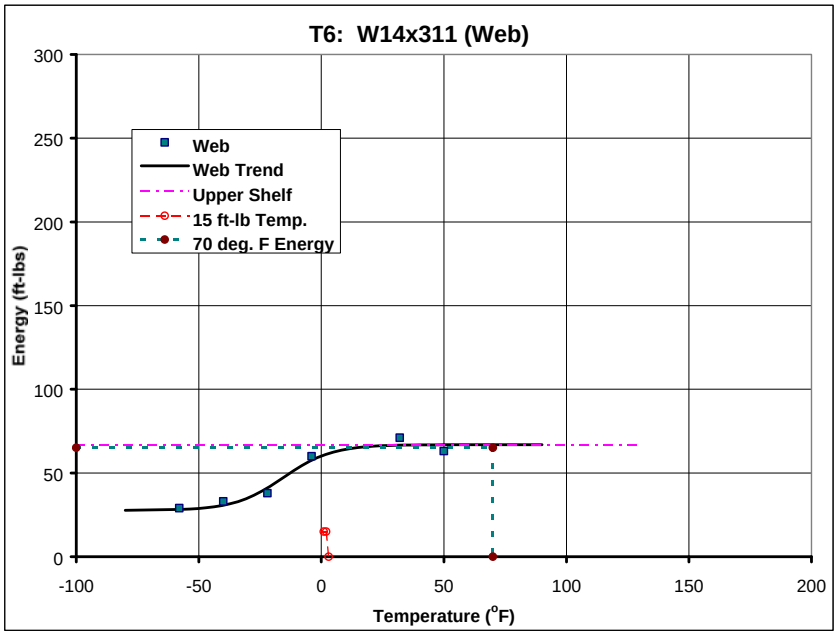

β_1=	47
β_2=	20
β_3=	0.050
β_4=	-15

Shelf Energy	
Upper	Lower
67	28

Energy	Temp.
10	<-60
15	<-60
20	<-60
25	<-60

Temp.	Energy
60	65
70	65
80	65
90	65

* Round to nearest 5 ft-lbs

Figure D.17.3: Web Region Charpy Impact Test Results for Member T6

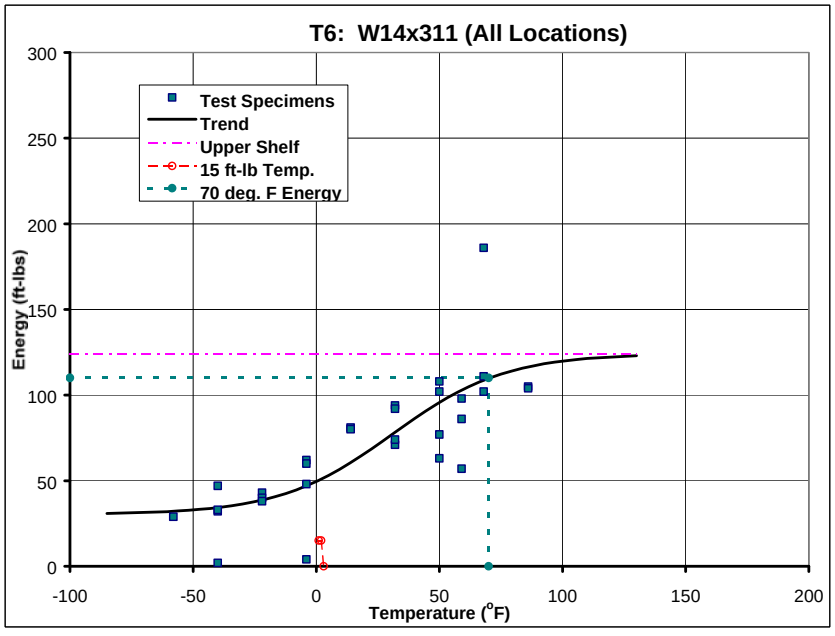

β_1=	77
β_2=	47
β_3=	0.022
β_4=	31

Shelf Energy	
Upper	Lower
124	30

Energy	Temp.
10	<-60
15	<-60
20	<-60
25	<-60

Temp.	Energy*
60	105
70	110
80	115
90	120

* Round to nearest 5 ft-lbs

Figure D.17.4: All Charpy Impact Test Results for Member T

References

ASTM Specification A6 “General Requirements for Rolled Steel Plates, Shapes, Sheet Piling, and Bars for Structural Use”.

ASTM Specification A370 “Standard Test Methods and Definitions for Mechanical Testing of Steel Products”.

ASTM Specification A572 “Standard Specification for High-Strength Low-Alloy Columbium-Vanadium Steels of Structural Quality”.

ASTM Specification E23 “Standard Test Methods for Notched Bar Impact Testing of Metallic Materials”.

Barsom, John M.; Korvink, Sjaan D. 1998. “Effects of Strain Hardening and Strain Aging on the K-region of Structural Shapes.” SAC Joint Venture, Sacramento, CA.

Beedle, Lynn S.; Tall, Lambert. 1959. “Basic Column Strength,” Fritz Laboratory Report No. 220D.34. Fritz Engineering Laboratory, Lehigh University. Bethlehem, PennsylvaniD.

Engestrom, Michael F. 1998. Fax.

Galambos, Theodore V.; Ravindra, Mayasandra K. 1978. “Properties of Steel for Use in LRFD,” Journal of the Structural Division, ASCE, Vol. 104, No. ST9, September, 1978.

“Guide to Stability Design of Metal Structures, 4th Edition.” 1988. B.7 SSRC Technical Memorandum No. 7: Tension Testing. John Wiley & Sons. p. 744.

Horne, M. R.; Morris, L. J. 1982. Plastic Design of Low-Rise Frames. MIT Press. Cambridge, Massachusetts. p. 2.

Salmon, Charles G.; Johnson, John E. 1990. Steel Structures: Design and Behavior, Emphasizing Load and Resistance Factor Design, Third Edition. HarperCollins Publishers Inc. p. 50-63.